Central Alberta: CO_2 Disposal Into Alberta Basin Aquifers - Phase II

Client Report

CENTRAL ALBERTA: CO_2 DISPOSAL INTO ALBERTA BASIN AQUIFERS - PHASE II

Hydrogeological and Mineralogical Characterization of Mannville Group Strata in the Lake Wabamun Area
&
Water-Rock Reactions due to CO_2 Injection into the Glauconitic Sandstone Aquifer

-by-
W.D. Gunter
S. Bachu
E.H. Perkins
J.R. Underschultz
B. Wiwchar
L.P. Yuan
M. Berhane
D. Cotterill

-at the-
Alberta Research Council
PO Box 8330
Edmonton, Alberta
Canada, T6H 5X2

C-1994-3

August, 1994

ARC Open File Report 1994-17

-funded by-
Alberta Energy
Environment Canada
CANMET
&
TransAlta Utilities Corporation

CENTRE DE L'ALBERTA: DISPOSITION DE CO_2 DANS LES AQUIFÈRES DU BASSIN ALBERTAIN - PHASE II

Caractérisation hydrogéologique et minéralogique des strates du groupe Mannville dans la région du lac Wabamun

&

Réactions eau-roche dues à l'injection du CO_2 dans l'aquifère de grès glauconitique

par

W.D. Gunter
S. Bachu
E.H. Perkins
J.R. Underschultz
B. Wiwchar
L.P. Yuan
M. Berhane
D. Cotterill

Alberta Research Council

C-1994-3

Août 1994

ARC Document Ouvert Rapport 1994-17

ACKNOWLEDGEMENT AND DISCLAIMER

The research project for which this report is submitted was funded in part from the Government of Alberta through the Alberta Office of Coal Research and Technology, Alberta Department of Energy.

This report and its contents, the project in respect of which it is submitted and the conclusions and recommendations arising from it do not necessarily reflect the view of the Government of Alberta, its officers, employees or agents; or the Board of Directors of the Alberta Office of Coal Research and Technology.

Neither the Government of Alberta, its officers, employees or agents nor the Board of Directors of the Alberta Office of Coal Research and Technology, its agents and consultants make any warranty, express or implied, representation or otherwise, in respect of this report or its contents.

The Government of Alberta, it officers, employees and agents and the Alberta Office of Coal Research and Technology, its agents and consultants are exempt, excluded and absolved from all liability for damage for injury, howsoever caused, to any person in connection with or arising out of the use by that person for any purpose of this report or its contents.

The partial funding by Natural Resources Canada, Environment Canada, Alberta Research Council and TransAlta Utilities Corporation is also acknowledged with thanks. Environment Canada's contribution was derived from PERD (The Federal Interdepartmental Program of Energy Research and Development). The foregoing clauses are also applicable to those agencies and companies.

The underlying work, conclusions and statements of this study are those of the authors and may not be in agreement with the views of the governments of Alberta and/or Canada, and/or TransAlta Utilities Corporation.

This report was prepared as an accounting of work conducted by the Alberta Research Council (ARC). Ever possible effort was made to ensure that the work conforms to accepted scientific practice. However, neither ARC, nor any of its employees, makes any warranty, express or implied, or assumes any legal liability or responsibility for the accuracy, completeness, or usefulness of any of the information, apparatus, product, or process disclosed, or represents that its use would not infringe privately owned rights. Reference herein to any specific commerical product, process, or service by trade name, trademark, manufacturer, or otherwise, does not necessarily constitute or imply its endorsement, recommendation, or favoring by the ARC. The views and opinions of the authors expressed herein do not necessarily state or reflect those of ARC.

EXECUTIVE SUMMARY

I. Greenhouse gas disposal in aquifers is an important option for Alberta.

In order to reduce emissions of CO_2 into the atmosphere, which could have adverse effects on the global climate, CO_2 can be captured at emission sources and injected into deep geological formations in the Alberta Sedimentary Basin where it is retained for geological time periods by a combination of stratigraphic, hydrodynamic and geochemical trapping mechanisms.

II. Desired aquifer characteristics to consider for CO_2 disposal candidates.

(i) Geologically, a deep aquifer should be chosen, capped by a regional aquitard, which, preferably, should also have trapping capabilities. This last requirement is particularly important for immiscible lighter-than-water CO_2.

(ii) From a physical point of view, the top of the aquifer must be located at more than 800 meters depth and the aquifer must be relatively thick to accommodate large quantities of CO_2.

(iii) From a geochemical point of view, a "basic" mineralogy must be present in the solid aquifer matrix to sequester or trap the CO_2 as bicarbonate ion in water or as a component of a solid, once the CO_2 is injected into the aquifer.

(iv) In terms of rock properties, the formation should have enough porosity and adequate permeability. Near-well permeability should be high for injection purposes, but regional scale permeability sould be low such that CO_2 residence time is high.

(v) From an economic and ecological point of view, deep formations suitable for CO_2 disposal have to be located in close vicinity to CO_2 emitting power plants.

III. A disposal aquifer adjacent to Alberta's main power stations has been identified.

Approximately two-thirds of Alberta's power generating capacity is located in the Lake Wabamun area west of Edmonton. As part of "proof-of-concept" ongoing research, the Mannville Group strata in the Lake Wabamun area (Tp. 50-52, R. 3-5W5M) were studied and the Glauconitic Sandstone was identified as the preferred aquifer satisfying most of the conditions required for deep disposal of CO_2.

(i) It is the most homogeneous of all Mannville Group units in the succession being approximately 14 meters thick.

(ii) Hydrostratigraphically it is confined by the shaley Ostracod Beds and Basal Grand Rapids aquitards at depths exceeding 1300 meters.

(iii) It has generally good porosity (12% on average).

(iv) It has low regional-scale permeability (10 md on average), which is needed for hydrodynamic entrapment, slow dispersion and high sweep ratio.

(v) It has high permeability in places (100 md), which is needed for avoiding high pressure buildup in the near-well region at the CO_2 injection sites.

(vi) It has a siliciclastic based mineralogy with clays present, which will contribute to the mineral trapping of CO_2 through geochemical reactions.

(vii) There is no hydrocarbon production from this unit, unlike the Ellerslie Member, thus avoiding unwarranted contamination of energy resources.

IV. CO_2-mineral-trapping by water-rock reactions can be important in aquifer disposal.

The CO_2-trapping capability of the Glauconitic Sandstone aquifer was assessed based on detailed mineralogical analysis of drill core, autoclave experiments and geochemical

modelling. Experiments on potential CO_2-trapping reactions in the Glauconitic Sandstone were carried out at 105°C and 90 bars CO_2 pressure for one month, but very little reaction was seen on this time scale. These experiments and field time scales were evaluated by geochemical modelling using rate data from the literature for the minerals making up the Glauconitic Sandstone. The modelling predicted that in the field, CO_2-trapping reactions take a minimum of 100 years to complete after the formation water has equilibrated at the temperature of the Glauconitic Sandstone aquifer (i.e. 54°C) and at the proposed injection pressure of the CO_2 (260 bars). Every square kilometer of the Glauconitic Sandstone aquifer could sequester approximately 0.5 megatons of CO_2 by these mineral-trapping reactions, once the CO_2-charged formation water has swept through.

V. Hydrodynamic or time traps are effective on the scale of sedimentary basins. Both the water-rock experiments and modelling indicate that geochemical trapping reactions of CO_2 are slow - on the order of tens to hundreds of years but fast enough to form effective CO_2 traps given the tens of thousands of years residence time of a packet of fluid in the deeper aquifers of the Alberta Basin where the regional-scale flow velocity of the formation waters is on the order of 1 to 10 cm/year. This order of magnitude difference in the two time scales ensures that CO_2-mineral trapping should be complete before the aquifer leaks to the surface. Thus given appropiate formation mineralogy (Gunter et al., 1993), mineral traps can replace stratigraphic traps ensuring that the injected CO_2 will be immobilized for ever in the subsurface. Sedimentary basins provide

the appropiate setting for mineral traps, hydrodynamic or time traps and stratigraphic traps to be operable and thus are ideal candidates for CO_2 storage in aquifers.

VI. The capacity for aquifer storage of CO_2 in the Alberta Basin is much greater than Alberta's total power plant emissions over the next 30 years.

Assuming that the CO_2-consuming mineral reactions go to completion, the maximum CO_2 disposal capacity of the Glauconitic Sandtone in the study area of 30x30 kilometers (consisting of 9 townships) is 450 megatons of CO_2. Assuming the properties of the aquifer extend beyond this arbitrarily defined area, for each additional township, 50 more megatons of CO_2 could be sequestered. A 500 megawatt coal-fired power plant would emit close to 15,000 tons/day of CO_2. Over the life of the power plant (approximately 30 years), 164 megatons of CO_2 would be produced. Ideally this could be trapped in the Glauconitic Sandstone aquifer within an area of four townships.

On a larger scale, total Alberta power plant emissions over a 30 year period are estimated at 2 gigatons of CO_2. A recent estimate by Bachu et al. (1994) of the storage capacity of the whole Alberta Sedimentary Basin is 20,000 megatons or 20 gigatons. This estimate is conservative as the Alberta Basin covers an area of 825,000 km^2 with a volume of approximately 2 million km^3. This figure is based on the following assumptions:

(i) For the basin as a whole, the total pore space of the aquifers suitable for CO_2 injection is about 1.25% of the basin's volume.

(ii) The effective sweep of the CO_2 will be on the order of 5% of the aquifer pore volume.

(iii) Only 1% of this remaining pore space would be accessible because these aquifers are distributed across the entire basin, and obviously are not going to be used in their entirety because of economic, technical and policy reasons.

On an even larger scale, this value of 20 gigatons of CO_2 storage capacity for aquifers in the Alberta Basin represents approximately 5% of total global estimates of 400+ gigatons. However we expect global estimates to increase as more detailed aquifer inventories, such as presented here, are completed.

VII The results of this geochemical hydrogeological evaluation should be used to identify well siting, injectivity, flow and trapping of CO_2 in the Glauconitic Sandstone aquifer.

An injection site could be selected based on surface and subsurface considerations, like distance from the CO_2-emitting power plants, location of existing oil and gas wells, access facilities, and rock properties (porosity, permeability and mineralogy). Once a site is selected, numerical simulations of CO_2 injection in the Glauconitic Sandstone could be performed taking into account the real geometry, rock properties and characteristics of formation water at the selected site based on the data presented here. A sensitivity analysis performed on variables such as rock porosity and permeability, and CO_2 injection rate and pressure, should indicate an optimum scenario for CO_2 disposal, and the expected CO_2 volumes to be disposed of over the lifetime of the operation. If the

Glauconitic Sandstone aquifer proves to be incapable of accepting high volumes of CO_2, then the Grand Rapids Formation may be considered for added capacity.

VIII. A Canada-wide inventory of sedimentary basins is needed.

In the future an inventory of other sedimentary basins across Canada, which could serve as disposal sites for CO_2, should be made. This should include depleted oil and gas reservoirs as well as aquifers. In the event that global policy dictates drastic reductions in CO_2 emissions, then Canada would be able to target their disposal options immediately to meet imposed annual quotas.

RÉSUMÉ EXÉCUTIF

I. La disposition en aquifère du gaz de serre est une option importante pour l'Alberta.

Afin de réduire les émissions de CO_2 dans l'atmosphère, lesquelles peuvent avoir des effets adverses sur le climat global, le CO_2 peut être capturé aux sources d'émission et injecté dans les formations géologiques profondes du bassin sédimentaire de l'Alberta où il est retenu pour des durées de temps géologique par une combinaison de mécanismes de piégeage stratigraphique, hydrodynamique et géochimique.

II. Caractéristiques désirables à considérer pour une aquifère candidate de disposition du CO_2.

(i) Géologiquement, l'aquifère profonde choisie devrait être coiffée par un aquitard régional qui, préférablement, devrait aussi avoir des capacités de piégeage. Cette dernière exigence est particulièrement importante pour le CO_2 immiscible plus léger que l'eau.

(ii) Du point de vue physique, le haut de l'aquifère doit être localisé à plus de 800 mètres de profondeur et celle-ci doit être relativement épaisse afin d'accommoder de larges quantités de CO_2.

(iii) Du point de vue géochimique, une minéralogie "basique" doit être présente dans la matrice solide de l'aquifère afin de séquestrer ou piéger le CO_2 sous forme d'ion bicarbonate dans l'eau, ou de composant d'un solide, une fois que le CO_2 a été injecté dans l'aquifère.

(iv) En termes de propriétés des roches, la formation devrait avoir une porosité suffisante et une perméabilité adéquate. La perméabilité près du puits devrait être élevée pour fin d'injection, mais elle devrait être basse à l'échelle régionale de telle sorte que le temps de résidence du CO_2 soit élevé.

(v) Du point de vue économique et écologique, les formations profondes appropriées pour la disposition du CO_2 doivent être localisées dans le proche voisinage des centrales émettrices de CO_2.

III. Une aquifère de disposition adjacente aux principales centrales de l'Alberta a été identifiée.

Approximativement les deux tiers de la capacité de génération d'électricité de l'Alberta sont situés dans la région du lac Wabamun à l'ouest d'Edmonton. Les strates du groupe Mannville dans la région du lac Wabamun (Tp.50-52, R. 3-5W5M) furent étudiées, comme partie de la "preuve de concept" de la présente recherche, et le grès glauconitique fut identifié comme étant l'aquifère préférée satisfaisant à la plupart des conditions requises de disposition en profondeur du CO_2.

(i) Elle est la plus homogène de toutes les unités dans la succession du groupe Mannville, avec approximativement 14 mètres d'épaisseur.

(ii) Hydrostratigraphiquement elle est confinée par les aquitards de shiste de "Ostracod Beds" et de "Basal Grand Rapids" à des profondeurs excédant 1300 mètres.

(iii) Elle a généralement une bonne porosité (12 % en moyenne).

(iv) Elle a une faible perméabilité à l'échelle régionale (10 md en moyenne), ce qui est nécessaire pour le piégeage hydrodynamique, une dispersion lente et un haut taux de balayage.

(v) Elle a une perméabilité locale élevée (100 md), ce qui est nécessaire pour éviter l'accumulation de haute pression dans la région près du puits aux sites d'injection du CO_2.

(vi) Elle a une minéralogie à base siliciclastique avec présence d'argiles, lesquelles vont contribuer au piégeage minéral du CO_2 par l'intermédiaire de réactions géochimiques.

(vii) Il n'y a pas de production d'hydrocarbone à partir de cette unité, au contraire du membre Ellerslie, évitant ainsi toute contamination indésirable des ressources énergétiques.

IV. Le piégeage minéral du CO_2 par réactions eau-roche peut être important en aquifère de disposition.

La capacité de piégeage de CO_2 de l'aquifère de grès glauconitique fut établie en se basant sur l'analyse minéralogique détaillée de carottes de sondage, sur des

expériences en autoclave et sur la modélisation géochimique. Les expériences de réactions potentielles de piégeage du CO_2 dans le grès glauconitique furent menées à 105°C et à 90 bars de pression de CO_2 pendant un mois, mais très peu de réaction fut observée à cette échelle de temps. Les échelles de temps pour ces expériences et pour le terrain furent évaluées par modélisation géochimique en utilisant les données, obtenues de la littérature, sur les taux des minéraux constituant le grès glauconitique. La modélisation a prédit que, sur le terrain, les réactions de piégeage du CO_2 prendront un minimum de 100 ans à compléter après que l'eau de formation s'est équilibrée à la température de l'aquifère de grès glauconitique (i.e. 54°C) et à la pression proposée d'injection du CO_2 (260 bars). Chaque kilomètre carré de l'aquifère de grès glauconitique pourrait séquestrer approximativement 0.5 mégatonnes de CO_2 par ces réactions de piégeage minéral, une fois que l'eau de la formation chargée en CO_2 est passée à travers.

V. Les pièges hydrodynamiques ou temporels sont efficaces à l'échelle des bassins sédimentaires.

Les expériences eau-roche et la modélisation ont toutes deux indiquer que les réactions de piégeage géochimique du CO_2 sont lentes - de l'ordre de dizaines à des centaines d'années, mais suffisamment rapides pour former des pièges efficaces de CO_2, donnant des dizaines de milliers d'années de temps de résidence d'une entité de fluide dans les aquifères les plus profondes du bassin albertain où la vitesse d'écoulement, à l'échelle régionale, des eaux de formation est de l'ordre de 1 à 10 cm/année. Cette différence d'ordre de grandeur des deux échelles de temps nous assure que le piégeage minéral du CO_2 devrait être complet avant que l'aquifère ne soude à la surface. Ainsi, étant donné une minéralogie de formation appropriée (Gunter et al., 1993), les pièges minéraux peuvent remplacer les pièges stratigraphiques, ce qui nous assure que le CO_2 injecté sera immobilisé pour toujours

va

sous la surface. Les bassins sédimentaires fournissent la mise en scène appropriée pour rendre praticable l'action des pièges minéraux, des pièges hydrodynamiques ou temporels et des pièges stratigraphiques et, ainsi, sont des candidats idéals pour l'emmagasinage du CO_2 dans les aquifères.

VI. La capacité d'emmagasinage du CO_2 en aquifère dans le bassin albertain est beaucoup plus grande que le total des émissions des centrales au cours des 30 prochaines années.

En assumant que les réactions minérales consumant le CO_2 se rendent à complétion, la capacité maximale de disposition du CO_2 du grès glauconitique dans la superficie étudiée de 30x30 kilomètres (comprenant 9 communes-'townships') est de 450 mégatonnes de CO_2. En assumant que les propriétés de l'aquifère s'étendent au-delà de cette région définie arbitrairement, pour chaque commune ('township') additionnelle, 50 mégatonnes de CO_2 de plus pourraient être séquestrées. Une centrale au charbon de 500 mégawatts émettrait près de 15,000 tonnes/jour de CO_2. Pendant la durée de vie de la centrale (approximativement 30 ans), 164 mégatonnes de CO_2 seraient produites. Idéalement ceci pourrait être piégé dans l'aquifère de grès glauconitique compris dans une superficie de quatre communes ('townships').

À plus grande échelle, sur une période de 30 ans, les émissions totales des centrales de l'Alberta sont estimées à 2 gigatonnes de CO_2. Une évaluation récente, par Bachu et al. (1994), de la capacité d'emmagasinage de tout le bassin sédimentaire albertain est de 20,000 mégatonnes ou 20 gigatonnes. Cet évaluation est conservatrice parce que le bassin albertain couvre une superficie de 825,000 km^2 avec un volume d'approximativement 2 million km^3. Ce chiffre est basé sur les assomptions suivantes:

(i) En prenant le bassin comme un tout, l'espace total en pores des aquifères approprié pour l'injection du CO_2 est d'environ 1.25% du volume du bassin.

(ii) Le balayage efficace du CO_2 sera de l'ordre de 5% du volume de pore de l'aquifère.

(iii) Seulement 1% de cet espace de pore qui reste serait accessible parce que ces aquifères sont distribuées à travers le bassin entier, et évidemment, ne seront pas utilisées dans leur entièreté à cause de raisons économiques, techniques et politiques.

À une échelle encore plus grande, cette valeur de 20 gigatonnes de capacité d'emmagasinage de CO_2 des aquifères dans le bassin albertain représente approximativement 5% des évaluations globales totales de 400 gigatonnes et plus. Cependant, nous nous attendons à ce que les évaluations globales augmentent à mesure que plus d'inventaires détaillés d'aquifère, tel que celui présenté ici, seront complétés.

VII. Les résultats de cette évaluation géochimique et hydrogéologique devraient être utilisés pour identifier l'emplacement de puits, l'injectivité, l'écoulement et le piégeage du CO_2 dans l'aquifère de grès glauconitique.

Un site d'injection pourrait être choisi en se basant sur des considérations de surface et de subsurface, comme la distance aux centrales émettrices de CO_2, la localisation des puits existants d'huile et de gaz, les facilités d'accès et les propriétés des roches (porosité, perméabilité et minéralogie). Une fois qu'un site a été choisi, des simulations numériques d'injection de CO_2 dans le grès glauconitique pourraient être exécutées en tenant compte de la géométrie réelle, des propriétés des roches et des caractéristiques de l'eau de formation au site choisi en se basant sur les données présentées ici. Une analyse de susceptibilité exécutée sur des variables telles que la porosité et la perméabilité de la roche et le taux et la pression d'injection du CO_2,

devrait indiquer un scénario optimum de disposition du CO_2, et les volumes attendus de CO_2 à éliminer au cours de la durée totale de l'opération. Si l'aquifère de grès glauconitique se montre incapable d'accepter de larges volumes de CO_2, alors la formation de "Grand Rapids" pourrait être considérée pour capacité ajoutée.

VIII. Un inventaire, à l'échelle du Canada, des bassins sédimentaires est nécessaire.

On suggère que soit fait au Canada, dans le futur, un inventaire des autres bassins sédimentaires qui pourraient servir comme sites de disposition du CO_2. Cet inventaire devrait inclure les réservoirs épuisés d'huile et de gaz ainsi que les aquifères. Dans l'éventualité qu'une politique globale dicte des réductions drastiques d'émissions de CO_2, le Canada serait alors capable de cibler ses options de disposition immédiatement afin de satisfaire aux contingents annuels imposés.

ACKNOWLEDGEMENTS

Wayne Nesbitt, University of Western Ontario, assisted us with collection of kinetic data and some of the rate calculations. Tom McCann, Stanley Industrial Consultants, kindly provided engineering advice as required. The authors wish to acknowledge the support provided by Michel Brulotte with data extraction from various data bases, by Daryl Wightman with the petrographic analysis of core samples, by John Zhou and Shauna Cameron with the XRD and SEM examination of the mineral mixes and powdered core and by Kelly Roberts and Campbell Kidston with data processing and manuscript preparation. The authors wish also to express their gratitude to the funding agencies and representatives on the management committee which made possible this research work: Alberta Office of Coal Research and Technology (D.E. Macdonald), CANMET (F.M. Mourits) , Environment Canada (V.R. Marawaha) and TransAlta Utilities Corporation (D. Drysdale).

TABLE OF CONTENTS

LIST OF TABLES

LIST OF FIGURES

INTRODUCTION

Carbon dioxide is a greenhouse gas that is considered to contribute to global climate warming, thus the emission of CO_2 and other greenhouse gases should actually be reduced. A general reduction of CO_2 emissions into the atmosphere can be achieved by a variety of means which can be broadly classified into: (1) improved/alternate energy uses, (2) CO_2 capture and utilization, and (3) CO_2 long term disposal. A very attractive and cost-effective solution is energy conservation, although it may require tough policy measures (Turkenburg, 1992). Another option is the use of renewable energy sources. Until such energy sources are developed and applied on a large scale, fossil energy resources will continue to be the primary energy source for many countries. Improving energy efficiency may lead to a lowering of the rate of CO_2 generation. However, it is questionable whether improving on energy use, conservation and alternate sources can solve the CO_2 problem quickly enough. While these are probably solutions for the long term, short and medium term solutions have to be found to deal with the problem of increasing CO_2 emissions.

The capture of CO_2 from power plants is the main operation prior to utilization or disposal. The CO_2 recovered from power plants may be used in a variety of industries, but their overall effect is negligible (Turkenburg, 1992; Herzog et al., 1992; Jack, 1992). Also, many of the CO_2 uses only delay for a very short time its release to the atmosphere. The

attempt to capture and transport CO_2 ultimately leads to production of more CO_2 than would be made otherwise (Battelle, 1991), therefore, long-term effective CO_2 disposal is essential for reducing greenhouse effects in the short and medium terms.

Generally, there are four types of possible CO_2 disposal: biological, mineral immobilization, deep ocean disposal and injection into geological formations. Deep ocean disposal is not a practical alternative for reducing CO_2 emissions from Alberta-based sources. The biological disposal starts from the idea that CO_2 emissions may be offset by CO_2 intake by forests. Nevertheless, this option suffers from a lack of credibility in the overall carbon and energy balance, and it is not clear how permanent the CO_2 storage is. Mineral immobilization of CO_2 is a possibility for Alberta and it can be achieved by the conversion into carbonates of calcium and/or magnesium rich brines found in close proximity of fossil fuel deposits (Battelle, 1991; Dunsmore, 1992). However, large amounts of base are needed, with considerable associated costs incurred (Battelle, 1991).

In Alberta, CO_2 can be injected into closed traps (depleted oil and gas reservoirs) and open traps (deep aquifers). The technology for CO_2 transport and injection is well established; already being used in Enhanced Oil Recovery (EOR). Moreover, the environmental problems are minimal, if any, and relate only to the possible escape of CO_2 along improperly completed or abandoned wells. However, the capacity of oil reservoirs for CO_2 disposal is limited (Herzog et al., 1992) and has the disadvantage that the CO_2

is rather quickly produced back to the surface with the oil (van der Haarst and van Nieuwland, 1989). EOR use as a CO_2 disposal method is the least costly and probably could be economical in Alberta (Bailey and MacDonald, 1993; Todd and Grand, 1993). The use of depleted and abandoned gas fields for CO_2 disposal, while promising (van der Haarst and van Nieuwland, 1989; Blok et al., 1989; van der Burgt et al., 1992), presents some practical problems (Herzog et al., 1992), the most important being proximity to power plants. The last land based CO_2 disposal option is into deep sedimentary formations, which cover large areas and in many cases are close to CO_2-emitting thermal power plants. Carbon dioxide is an ideal candidate for disposal into deep sedimentary formations because of its high density and high solubility in formation water at the relatively high pressures encountered. The disposal of CO_2 into deep aquifers probably represents the best short term approach and with the largest capacity available for CO_2 disposal, and may have the fewest risks of all large scale operations because of the hydrodynamic and geochemical trapping of CO_2 (Bachu et al., 1994; Gunter et al., 1993). In the longer term CO_2 emissions have to be reduced.

Previous work has indicated that it is desirable to inject CO_2 at depths greater than 800 m where CO_2 is in a dense supercritical state (van der Meer, 1992). High density of CO_2 is required to make the most efficient use of the pore space available. Regarding injectivity, high aquifer permeability is desirable near the injection well in order to avoid large pressure buildups and gradients (van der Meer, 1992), but generally low aquifer

permeability is needed for long term storage and hydrodynamic trapping (Koide et al., 1992; Bachu et al., 1994). With regard to aquifer storage capacity, high porosity is desirable, but the physical capacity can be increased if geochemical trapping by reactive minerals present in the aquifer rock matrix is possible (Gunter et al., 1993).

In Alberta, there are over 100 million tons of CO_2 emissions annually. Over 40 million tons is attributable to electrical power generation. The major power plants, comprising more than two thirds of the coal-based power generating capacity are located in the centre of the province. From transportation and logistical points of view, the most economical alternative for CO_2 disposal seems to be injection into a deep aquifer within close vicinity to these power plants. Excluding the power plant and the raw CO_2 capture system (capture costs can exceed $50/ton), the cost per ton of disposed CO_2 has been projected at $8 to $16 per ton (Stanley Industrial Consultants et al., 1993) when the disposal field is no more than 30 kilometers from the plant and the the disposal wells are 1000 to 2000 meters deep. Pipeline delivery pressure was set at 21MPa in order to provide 28MPa at aquifer depths. Over 85% of such costs are related to purification and pressurizing due to the high costs of compression; only 15% is related to pipeline and disposal well costs Trace impurities in the CO_2 can increase the compression costs because the density of the mixture is significantly reduced by the presence of impurities. This and the potential for corrosion by trace water are the reasons for the purification

stage.

Previous geochemical work (Gunter et al., 1993) has indicated that a siliciclastic formation with brackish formation water would be preferable for CO_2 injection over a carbonate one. As it happens, siliciclastic Cretaceous Mannville Group strata are found at depths greater than 800 m in central Alberta. They are overlain by thick Colorado Group shales, providing the regional-scale seal for protecting shallow groundwater resources. Carbonate aquifers with high salinity formation waters are found at greater depths; this makes the Mannville Group strata an ideal candidate for CO_2 disposal.

This study is a continuation of ongoing research into aquifer disposal of CO_2 in the Alberta basin, currently supported by the Alberta Office of Coal Research and Technology, Environment Canada, Natural Resources Canada and TransAlta Utilities Corporation. For the overall purpose of the study there is need for realistic aquifer characteristics in order to perform geochemical and fluid flow numerical modelling of CO_2 injection. Thus, based on the geological, geochemical and economic considerations discussed previously, it was decided to study, in detail, the pertinent characteristics of Mannville Group strata in the area defined by Tp 50-52, R 3-5, W5M where several major power plants are located (Fig. 1). More than 300 wells which penetrate the Mannville Group in the area were considered in the study. The following is a detailed geological,

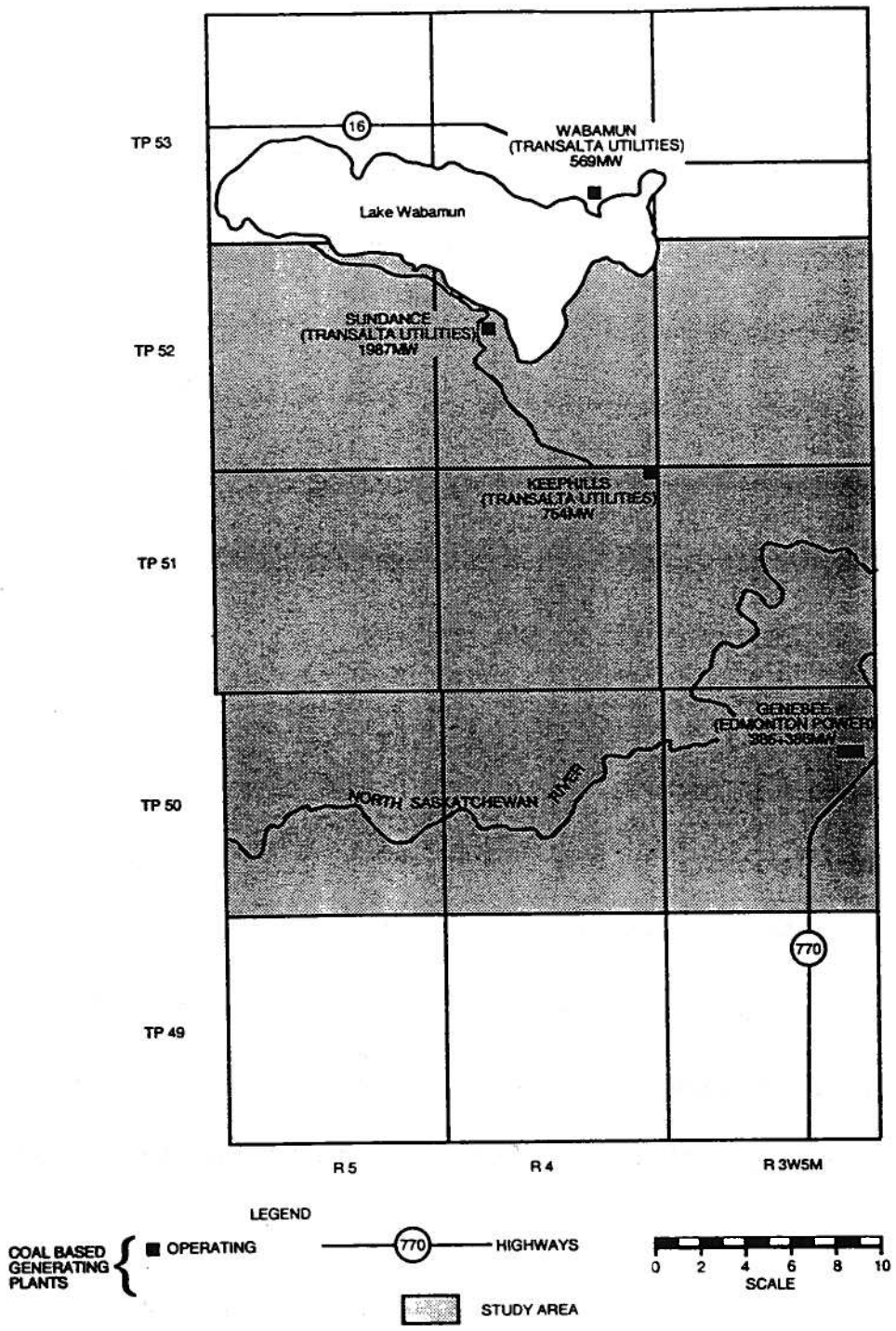

Figure 1. Location of major power plants in relation to the study area

hydrogeological and geochemical analysis of the siliciclastic Mannville Group strata in the area of interest (all the elevation and hydraulic head maps are referenced to the sea level). Figure 2 shows the topography of the study area (constructed from well data) and the distribution of wells with various types of data used in the analysis.

GEOLOGY

The stratigraphy of the sedimentary succession in the study area is comprised of siliciclastic Cambrian strata at the base, overlain by Devonian and Mississippian carbonates, evaporites and shales. These Paleozoic rocks are, in turn, unconformably overlain by a thick succession of Jurassic and Cretaceous siliciclastic sediments. The Mannville Group, the lowermost in the Cretaceous succession, was deposited on the sub-Cretaceous unconformity developed on subcropping Jurassic and Mississippian strata, and it is overlain by the Joli Fou Formation shales of the Colorado Group (Table 1). The Mannville Group is divided into Lower and Upper Mannville strata (Rudkin, 1964). The Lower Mannville succession consists of the basal Ellerslie Member and overlying Ostracod Beds. The Upper Mannville succession consists of the Glauconitic Sandstone and undifferentiated Grand Rapids Formation (Table 1). More than 300 wells penetrate the Mannville Group succession in the study area, but are unevenly distributed. With the exception of the Glauconitic Sandstone, the Mannville Group consists primarily of mudstones, siltstones and minor, thin sandstones. Figures 3 and 4 show dip and strike

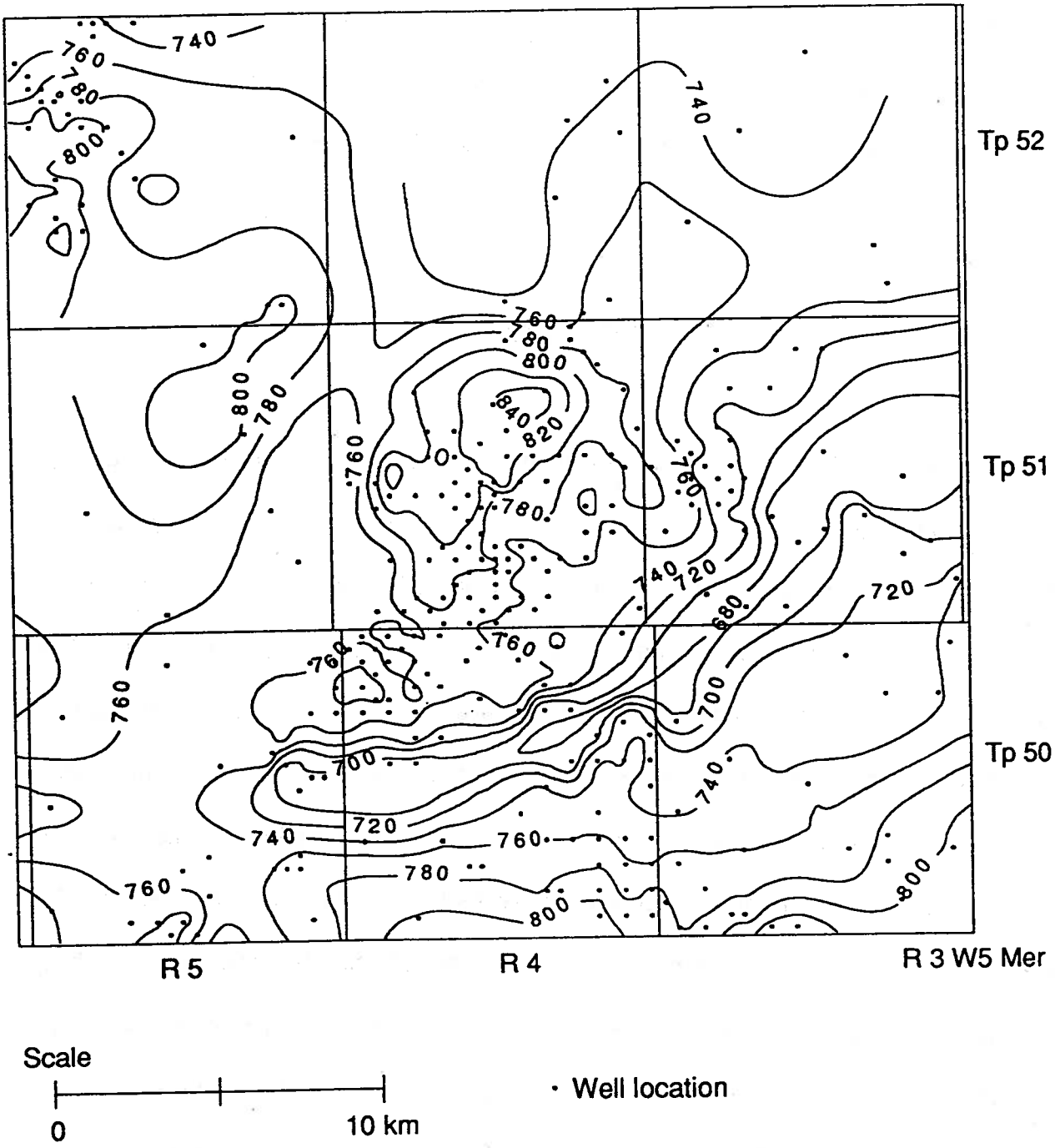

Figure 2: Topography and well distribution in the study area (contour interval: 20 m).

Table 1. Stratigraphic and hydrostratigraphic delineation and nomenclature of Mannville Group strata in the study area (Tp 50-52, R 3-5, W5M).

PERIOD	STRATIGRAPHY		LITHOLOGY	HYDROSTRATIGRAPHY
Cretaceous	Joli Fou Formation		Shale	aquitard
	Mannville Group	Grand Rapids Formation	Sandstone	aquifer
			Shale	aquitard
		Glauconitic Sandstone	Sandstone	aquifer
		Ostracod Beds	Sandstone/shale	aquifer/aquitard
		Ellerslie Member	Sandstone	aquifer
Jurassic	Nordegg Member		Carbonate	aquifer
Mississippian	Banff Formation		Carbonate/shale	aquifer/aquitard

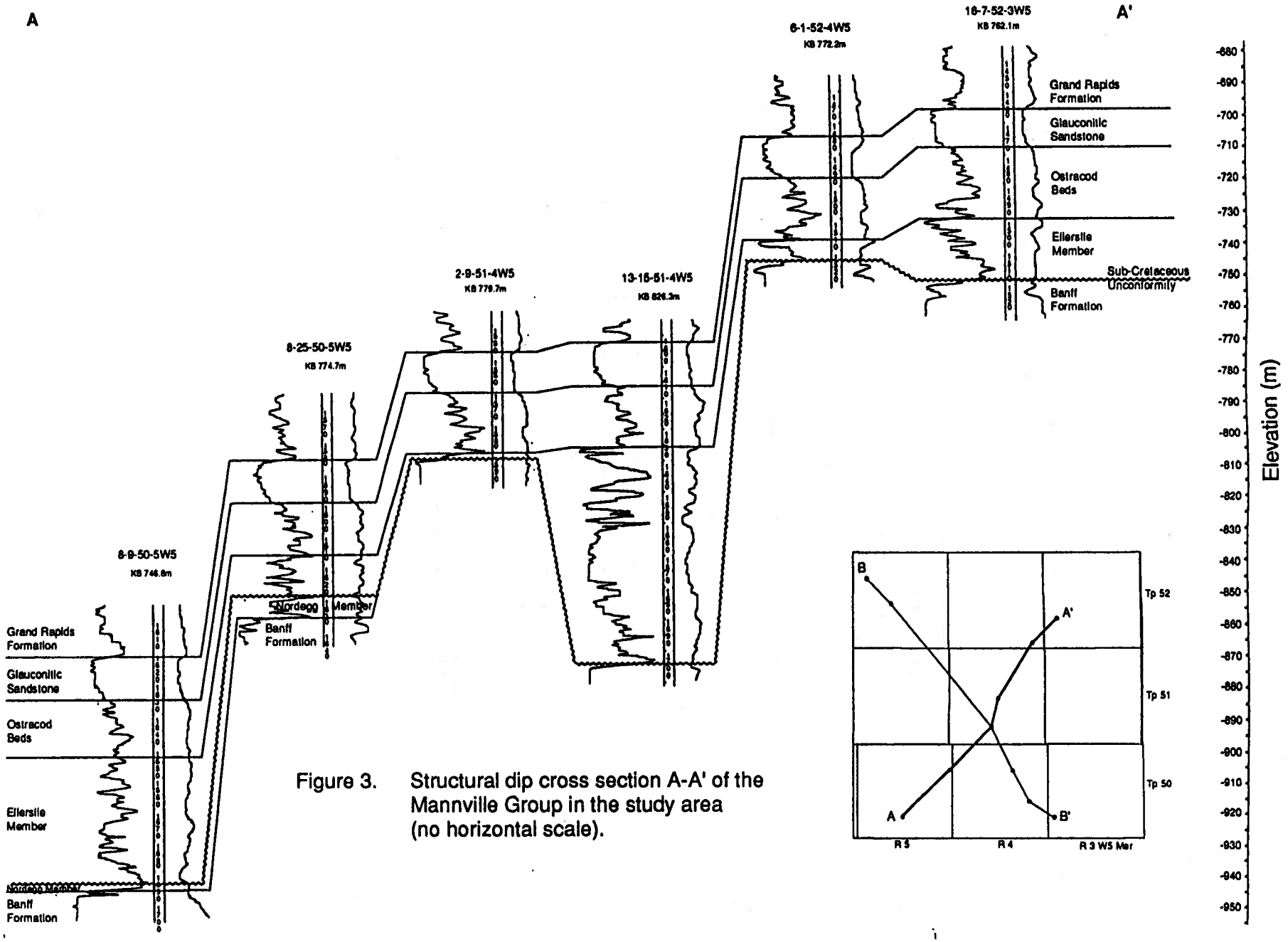

Figure 3. Structural dip cross section A-A' of the Mannville Group in the study area (no horizontal scale).

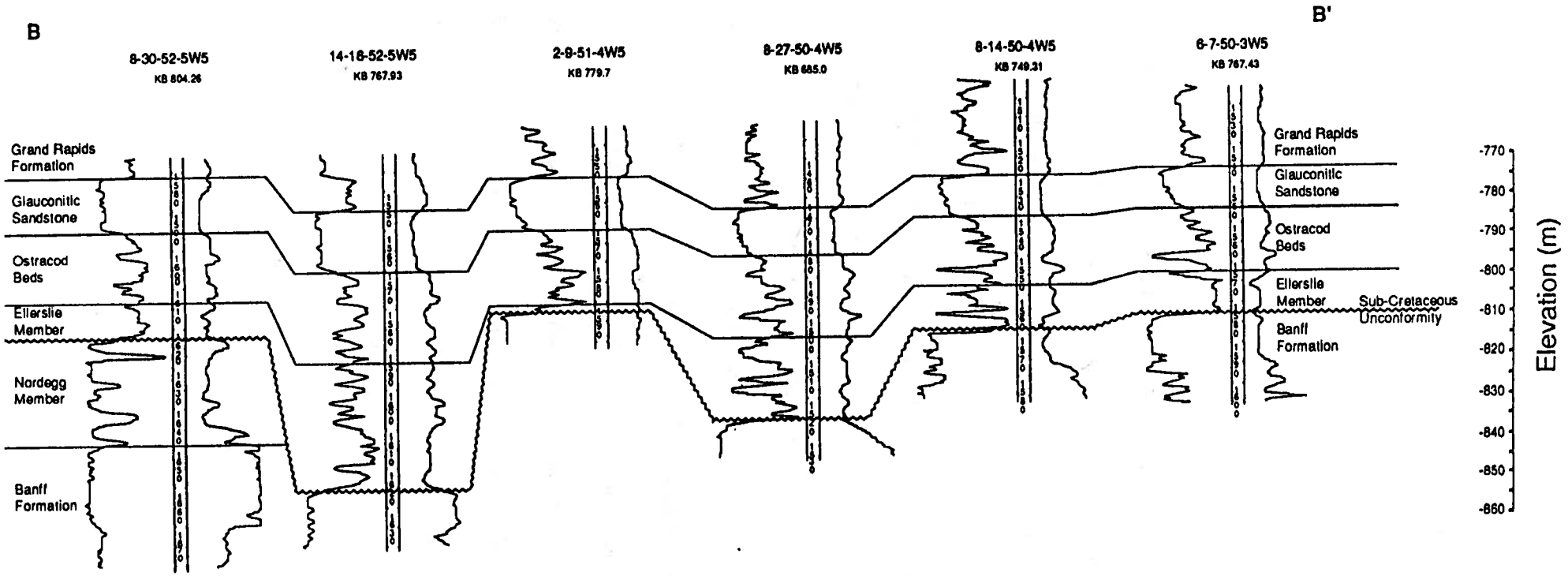

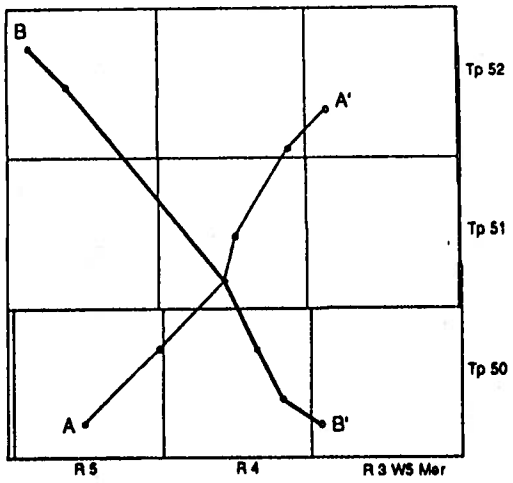

Figure 4. Structural strike cross section B-B' of the Mannville Group in the study area (no horizontal scale).

structural cross-sections, respectively, through the Mannville strata in the study area, with associated representative well logs.

SUB-CRETACEOUS UNCONFORMITY

Within the Alberta Basin, the regional sub-Cretaceous unconformity forms erosional ridge and valley systems onto which Cretaceous sediments were deposited. The study area is located within a part of this regional system called the Edmonton Embayment (Banerjee and Davies, 1988). In the study area, the sub-Cretaceous unconformity is divided into two areas by a central, northeast trending high. This high is flanked to the west by a broad, extensive valley and to the east by somewhat isolated, locally developed lows (Fig. 5). The geometry and continuity of the western valley is somewhat speculative due to sparse well control in the region. Prominent ridges consist primarily of resistant, sometimes porous limestones of the Mississippian Banff Formation, which are capped, in places, by isolated pods of cherty limestones of the Jurassic Nordegg Member. The ridge and valley topography accounts for most of the thickness variability within the Mannville Group. Topographic relief on the unconformity greatly influenced the sediment distribution patterns and facies architecture of the Ellerslie Member and, to a lesser degree, the Ostracod Beds and the Glauconitic Sandstone.

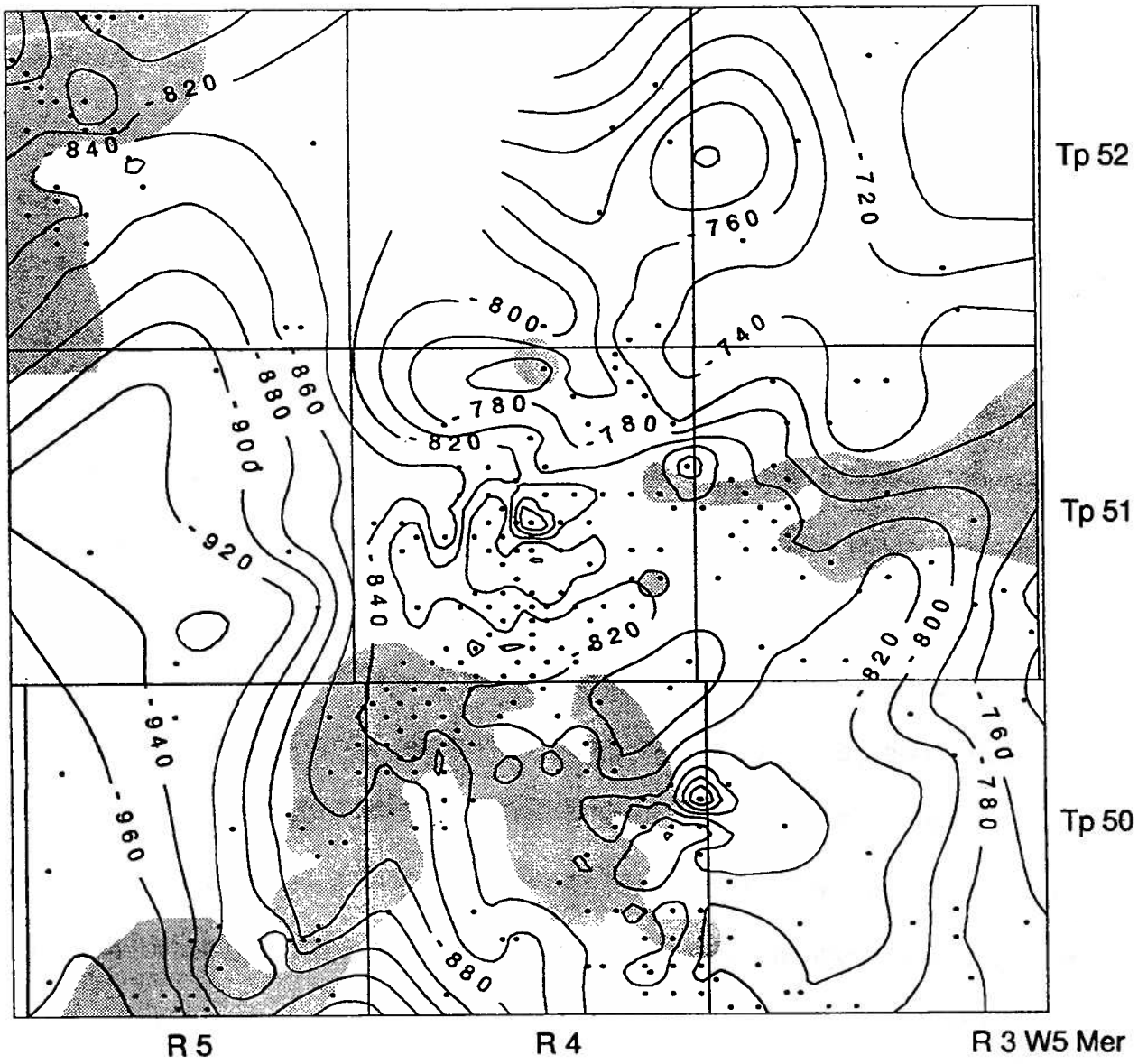

Figure 5: Structure top of the sub-Cretaceous unconformity (contour interval: 20 m). Shaded areas show where the Jurassic Nordegg Member is present on top of the Mississippian Banff Formation.

ELLERSLIE MEMBER

The Lower Mannville Ellerslie Member is the most variable in terms of thickness and lithology due to the irregular topography with karst features on which the unit was deposited. The unit varies from less than 10 m to greater than 60 m (Fig. 6). The top of the Ellerslie Member is often marked by a thin coal or very carbonaceous shale (generally less than 50 cm thick). Strata consist primarily of interbedded black mudstones, thin coals, and clean siltstones. The siltstones are commonly bioturbated at the base and rooted at the top. Thin, discontinuous, quartzose sandstones (less than 3 m thick) are found scattered throughout the area. These sandstones range from very fine to coarse grained and are clean to very argillaceous. Rare, granule to pebble sized, thin conglomerates (less than 3 m thick) were observed in one core. Very thin, dark brown limestones (less than 50 cm thick) composed primarily of bivalve shells, are commonly found near the top of the unit. The prominent ridge on the unconformity is reflected structurally on the top of the Ellerslie Member (Fig. 7). By the end of Ellerslie time, most of the topographic relief on the sub-Cretaceous unconformity had been infilled with sediments.

OSTRACOD BEDS

The Ellerslie Member is conformably overlain by the Ostracod Beds. Unlike the Ellerslie Member, the Ostracod Beds are relatively uniform in thickness and lithology; averaging approximately 18 m in thickness throughout the region (Fig. 8). Thickness variations,

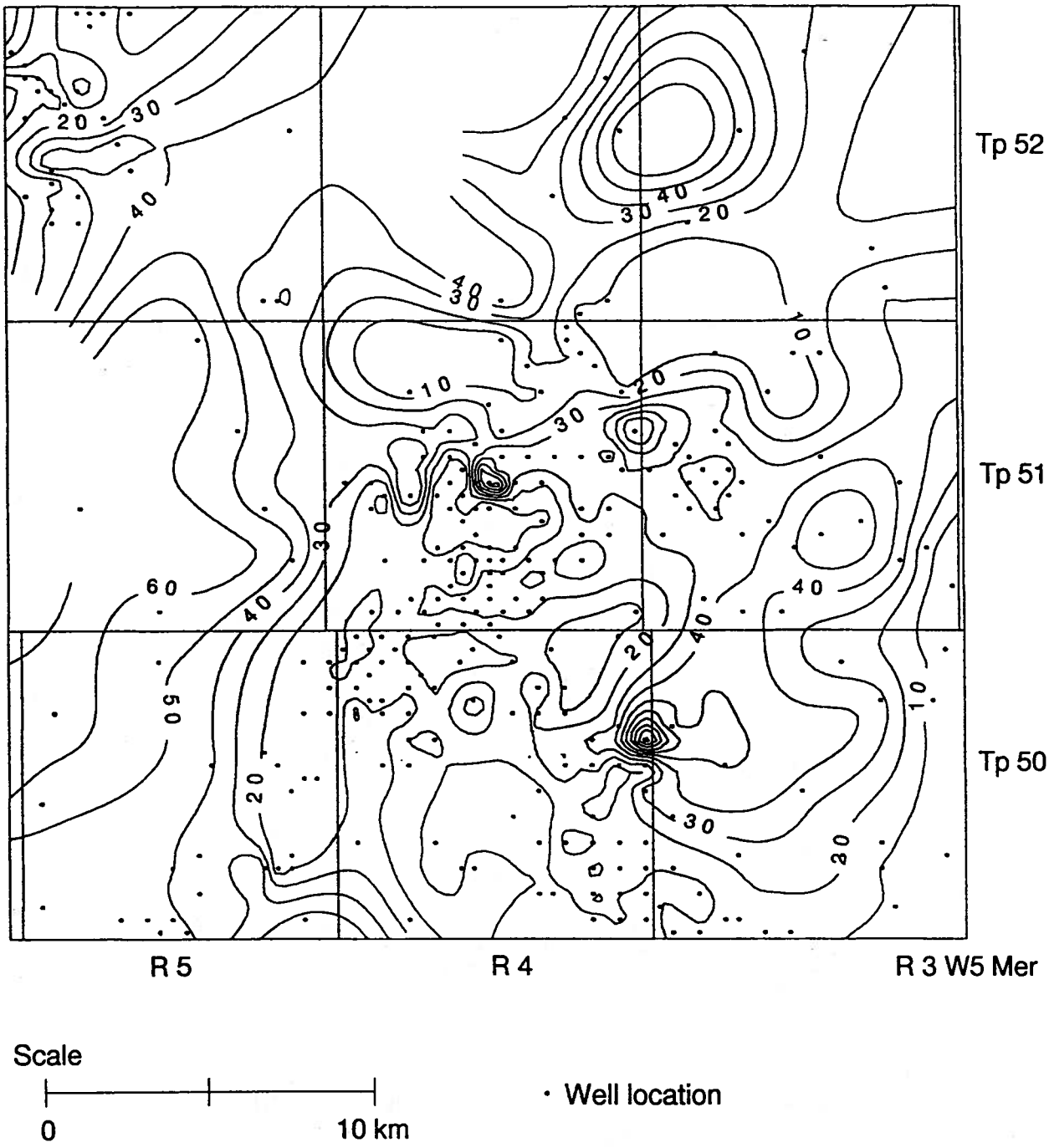

Figure 6: Isopach of the Ellerslie Member, Mannville Group (contour interval: 10 m).

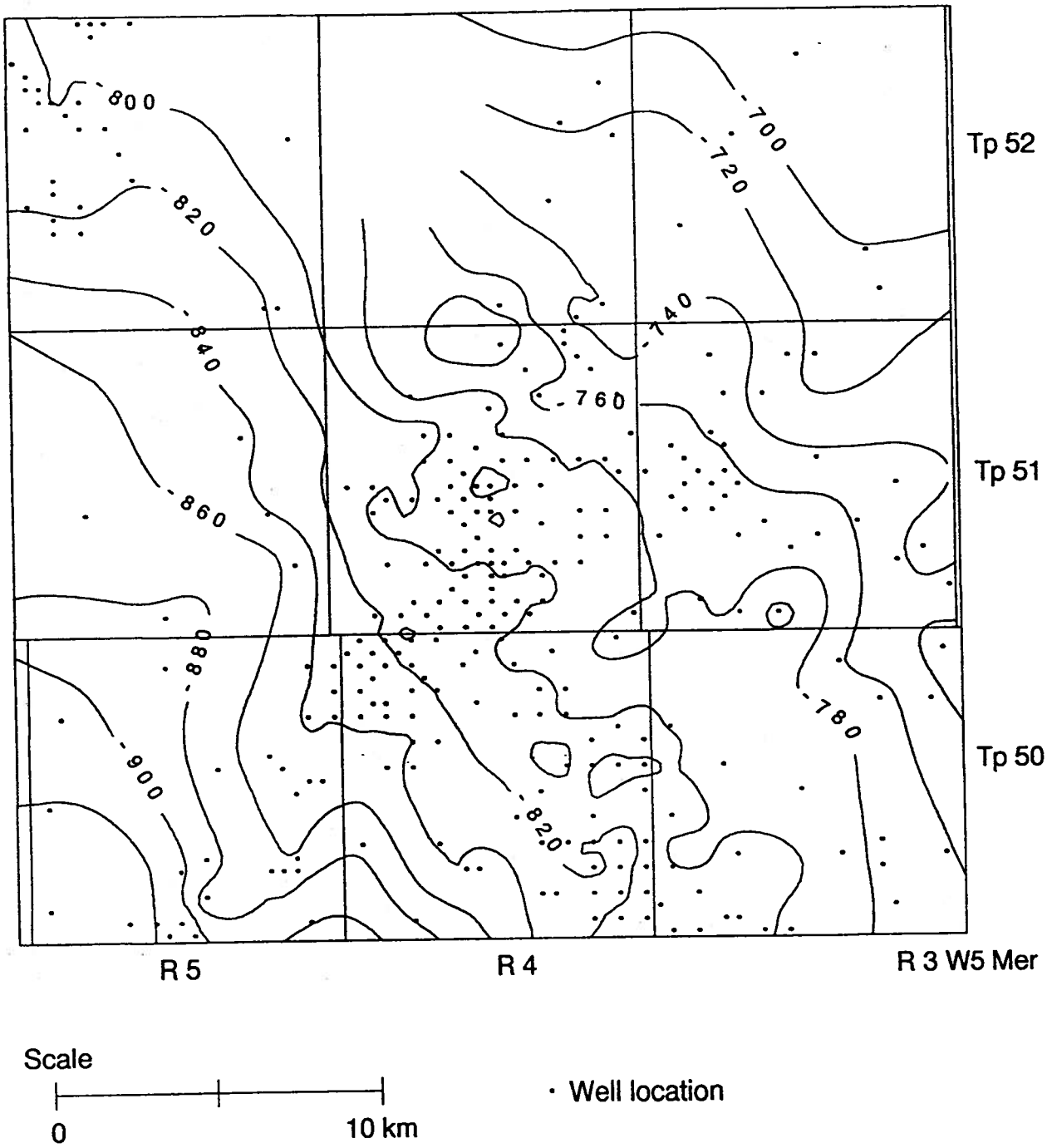

Figure 7: Structure top of the Ellerslie Member, Mannville Group (contour interval: 20 m).

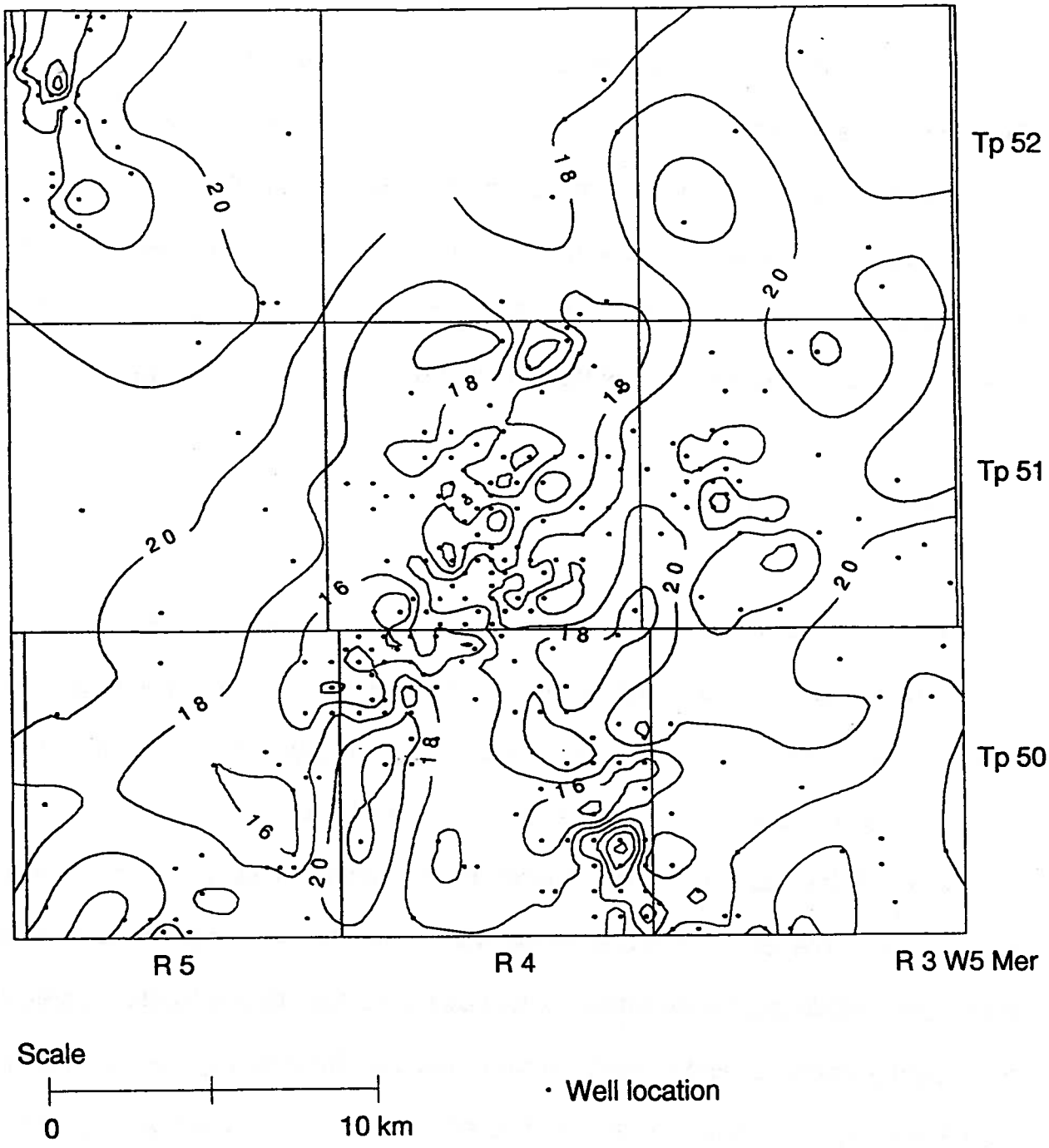

Figure 8: Isopach of Ostracod Beds, Mannville Group (contour interval: 2 m).

although subdued, mimic that of the Ellerslie Member. Ostracod strata thin over the highs and thicken along the flanks of the ridges of the sub-Cretaceous unconformity. The Ostracod Beds are dominated by black, bioturbated mudstones with abundant, thin, shelly beds (less than 15 cm). Some densely packed shell hashes form thin, porous limestone beds. The unit does contain thin, sporadic, commonly bioturbated, quartzose sandstones and siltstones. Structure on top of the Ostracod Beds (Fig. 9), although somewhat subdued, shows the same trend as that on the top of the Ellerslie Member.

GLAUCONITIC SANDSTONE

The Ostracod Beds are disconformably overlain by the Glauconitic Sandstone. The Glauconitic Sandstone consists of a laterally continuous, thick, clean, coarsening upward, lithic sandstone throughout the region. The sand averages about 14 m in thickness (Fig. 10). Unlike the Ostracod Beds and the Ellerslie Member, the thickness and orientation of the sand does not appear to be controlled by the sub-Cretaceous unconformity. The Glauconitic Sandstone, from bottom to top, is comprised of heavily bioturbated, argillaceous sand which grades upward into thin, stacked cycles of grey, fine to medium grained, salt and pepper, porous sandstone. Individual cycles (generally less than 3 m thick) are identified by a cross-bedded to massive sand base grading upwards into bioturbated sand at the top. The Glauconitic Sandstone is capped by a medium grained bioturbated sand which grades upwards into a white siltstone. The upper contact

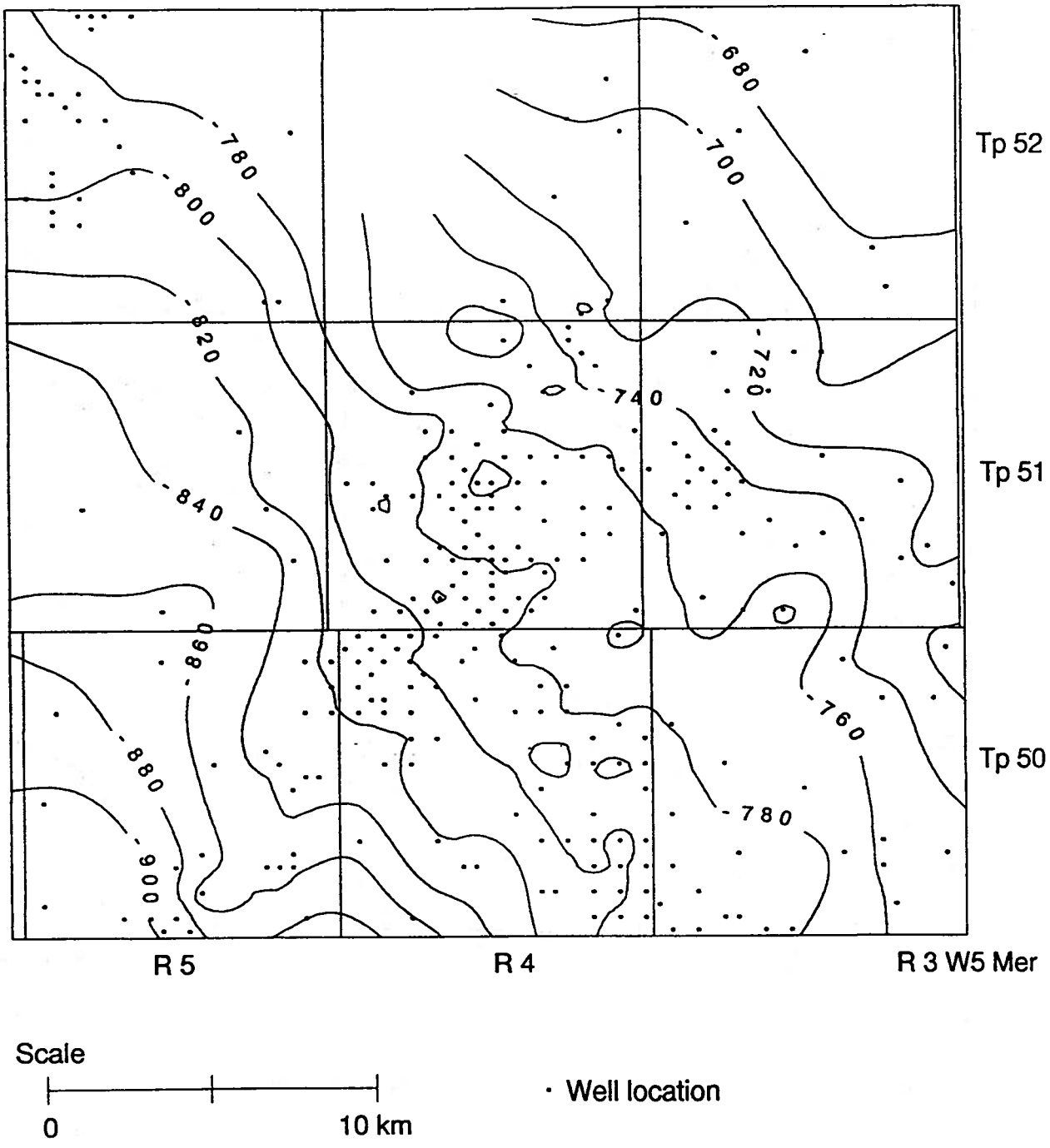

Figure 9: Structure top of Ostracod Beds, Mannville Group (contour interval: 20 m).

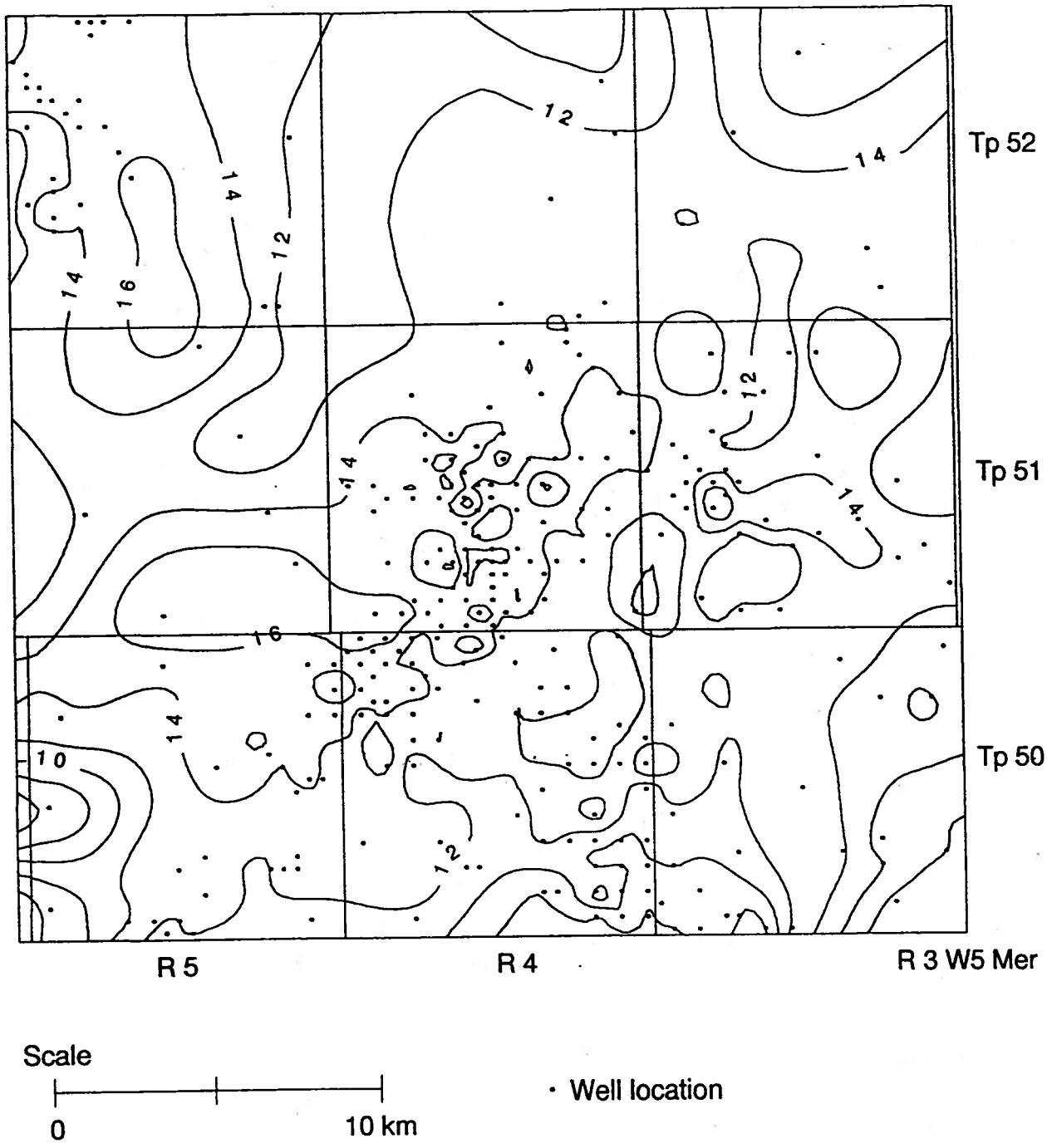

Figure 10: Isopach of Glauconitic Sandstone, Mannville Group (contour interval: 2 m).

is sharp and erosional. The structure top of the Glauconitic Sandstone (Fig. 11) reflects the general southwest dip of the basin in central Alberta.

GRAND RAPIDS FORMATION

The Grand Rapids Formation is the uppermost formation in the Mannville Group. Lithologically, it can be divided into a relatively continuous basal shale zone which grades into silts and sands which make up the upper part of the formation. The basal shale zone averages ~10 m in thickness within the study area (Fig. 12). Because of its uniform thickness, the structure on the top of the basal shale zone (Fig. 13) mimics that of the Glauconitic Sandstone, uniformly dipping to the southwest. The Grand Rapids Formation above the basal shale zone has a more variable isopach (Fig. 14), averaging approximately 120 m in thickness. This upper part contains thin interbedded silts, shales and sands with frequent thin coal zones. Although some channel sands exist, they tend to be thin and discontinuous, making them poor injection targets. The structure on the top of the Mannville Group (Fig. 15) dips to the southwest with an average slope of 7 m/km, which is high compared to the more regional-scale slope of Cretaceous strata elsewhere along strike.

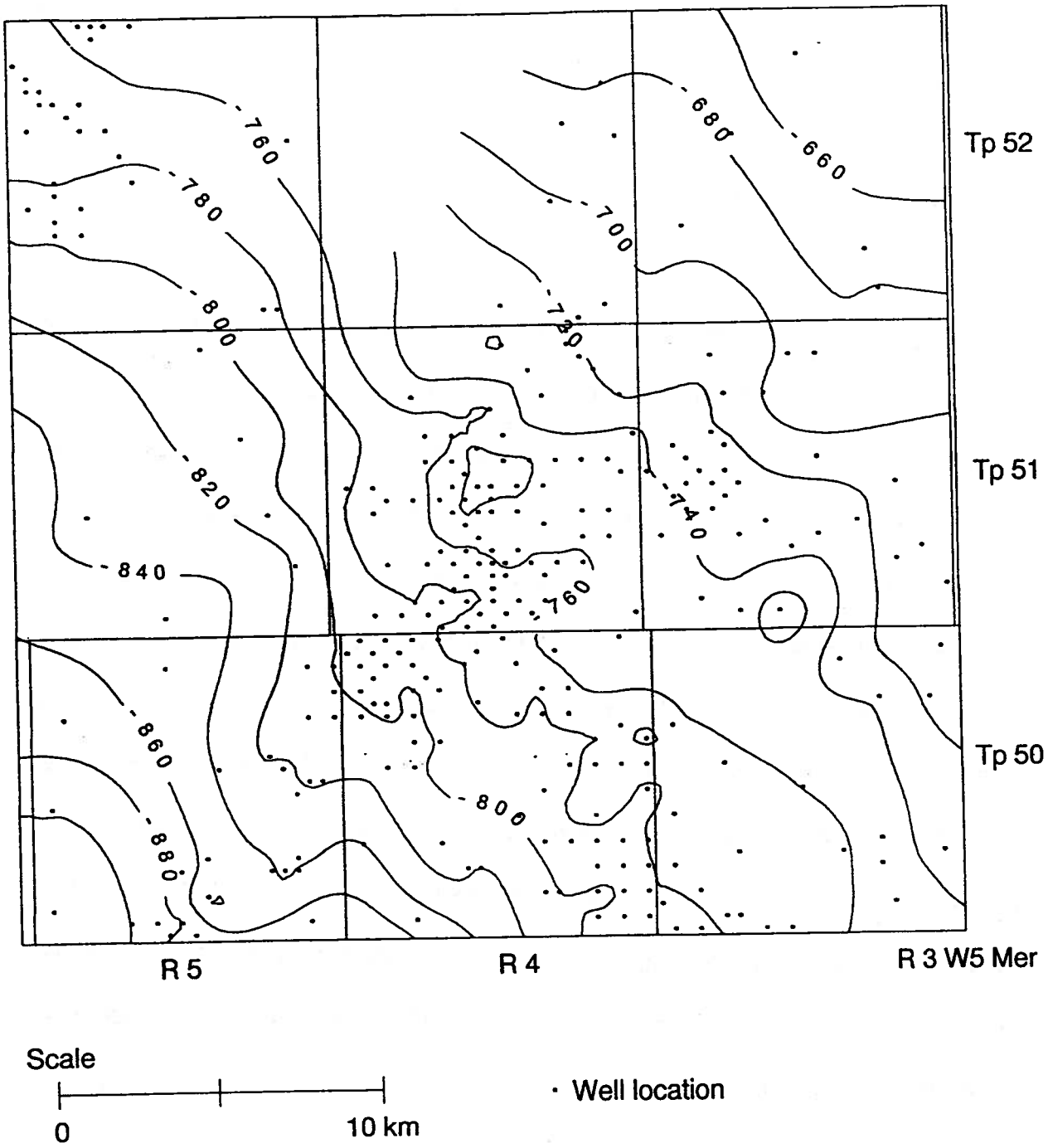

Figure 11: Structure top of the Glauconitic Sandstone, Mannville Group (contour interval: 20 m).

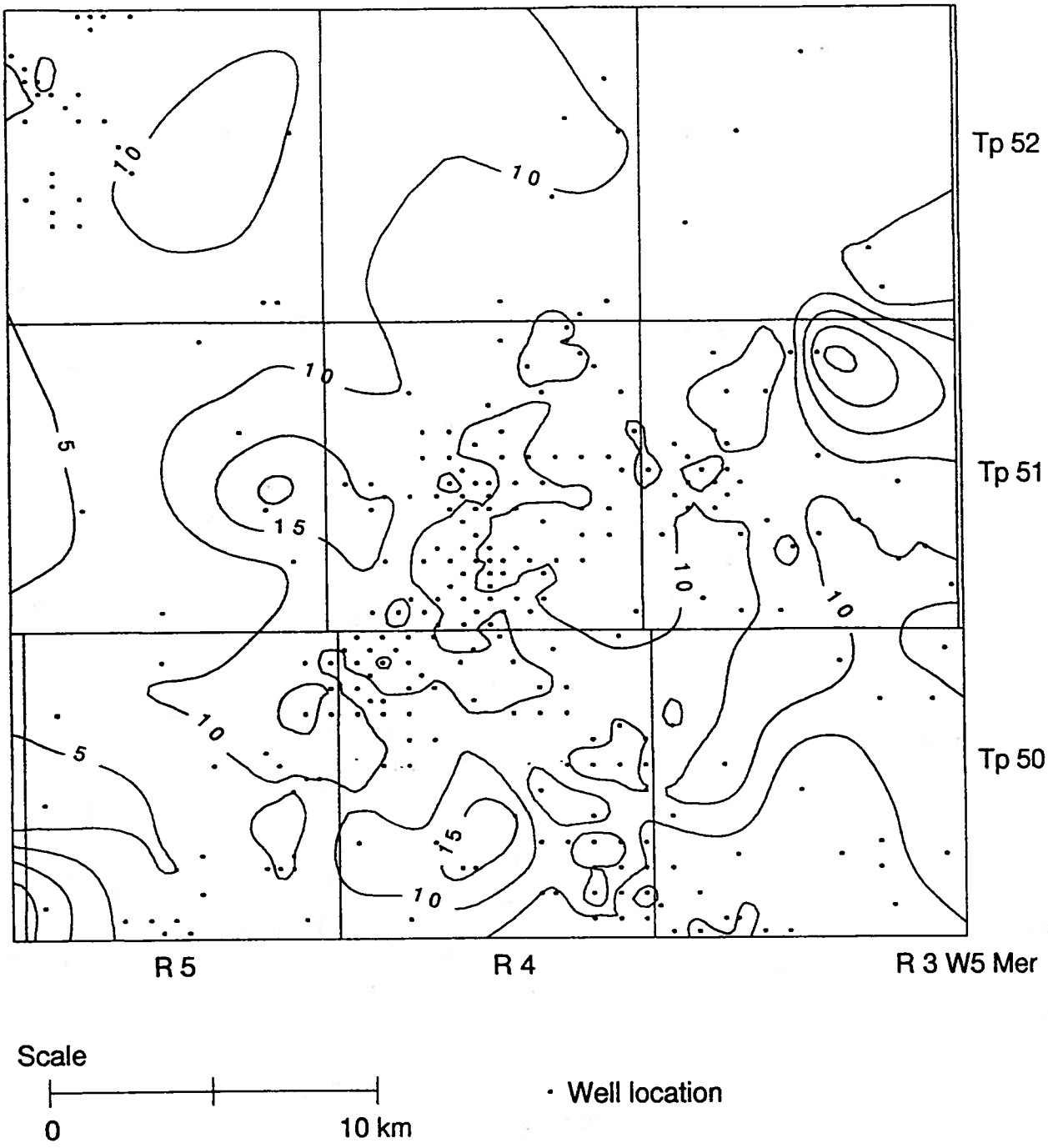

Figure 12: Isopach of basal shale zone, Grand Rapids Formation, Mannville Group (contour interval: 5 m).

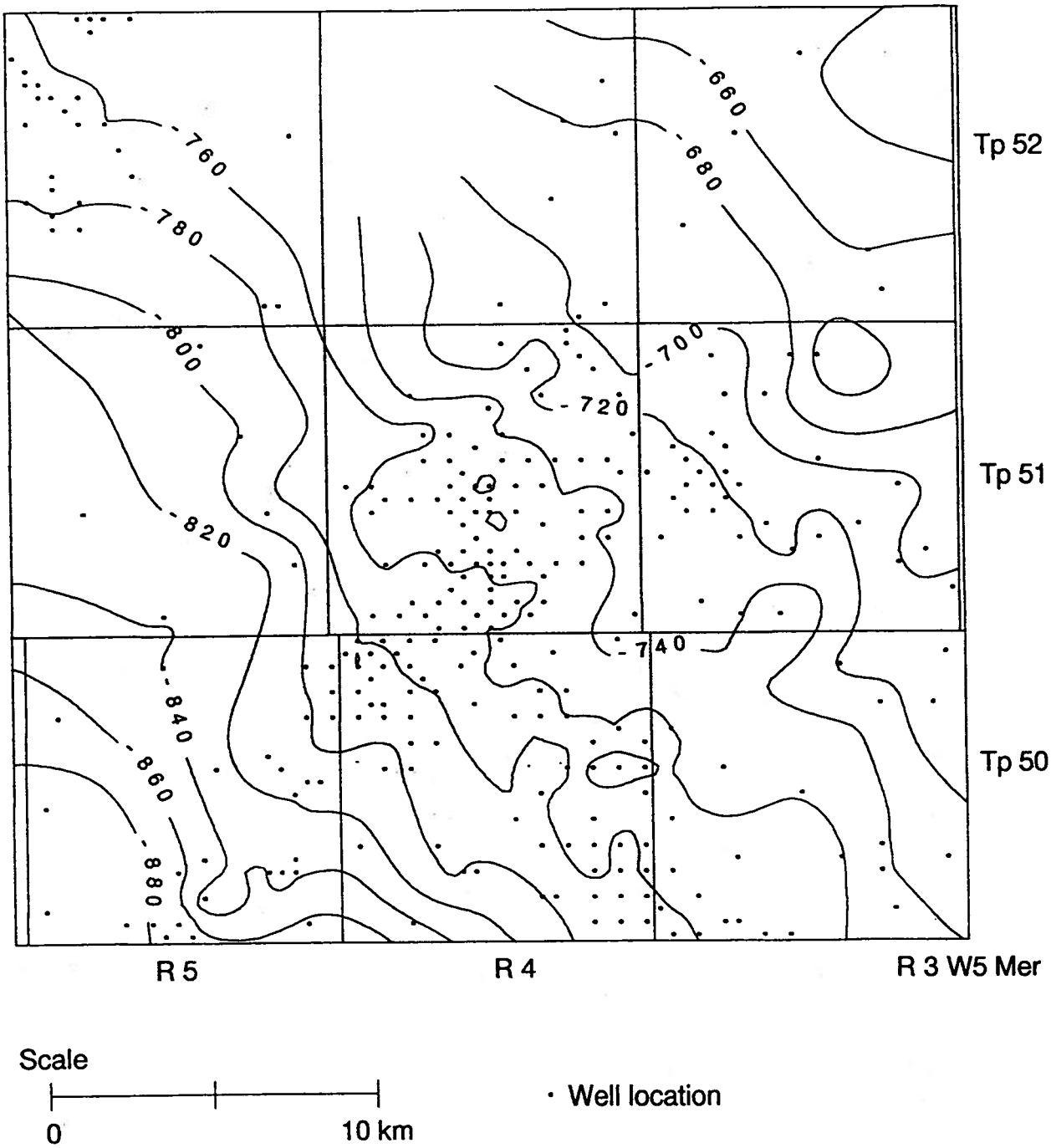

Figure 13: Structure top of the basal shale zone, Grand Rapids Formation, Mannville Group (contour interval: 20 m).

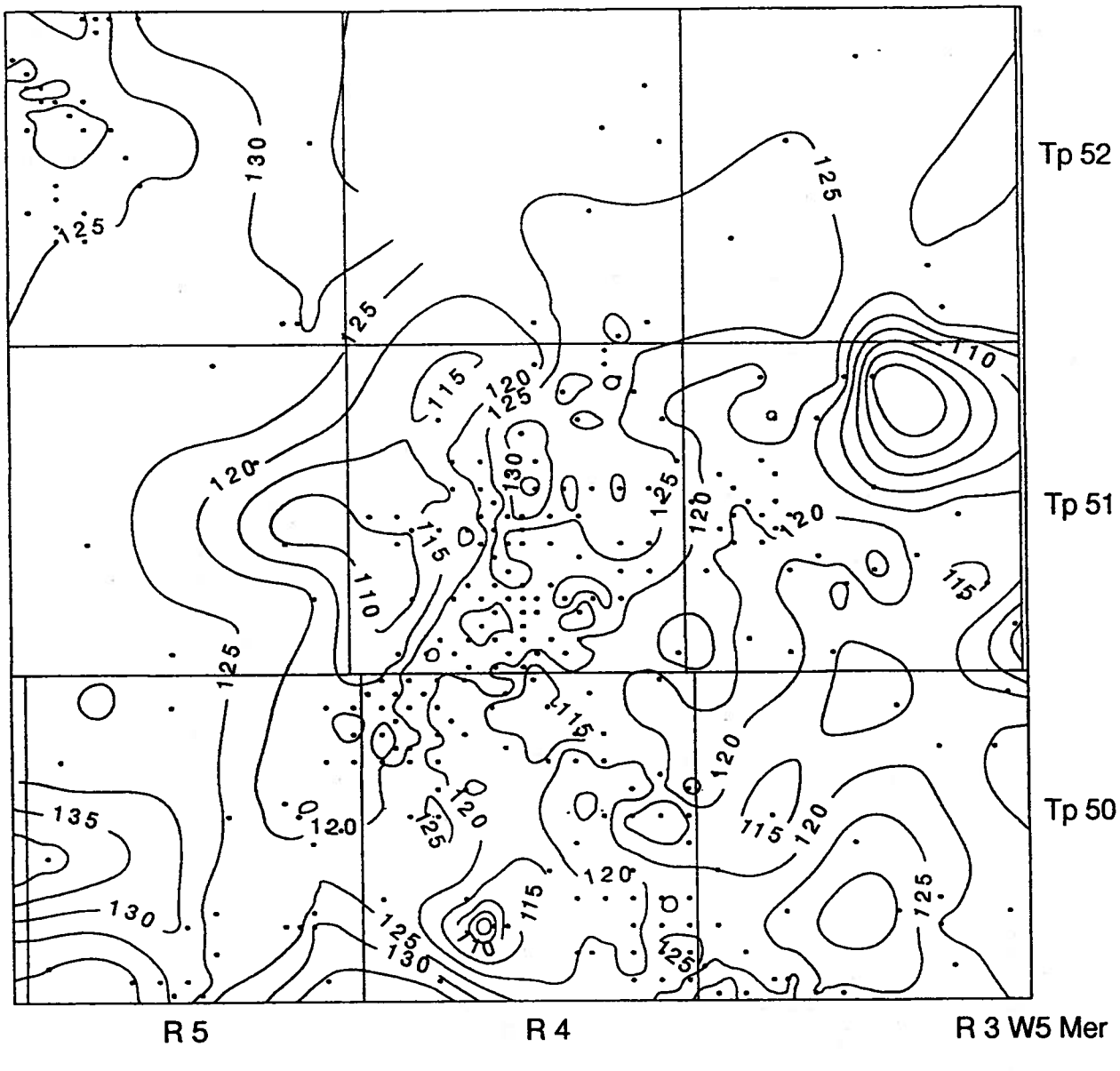

Figure 14: Isopach of the Grand Rapids Formation strata above the basal shale zone, Mannville Group (contour interval: 5 m).

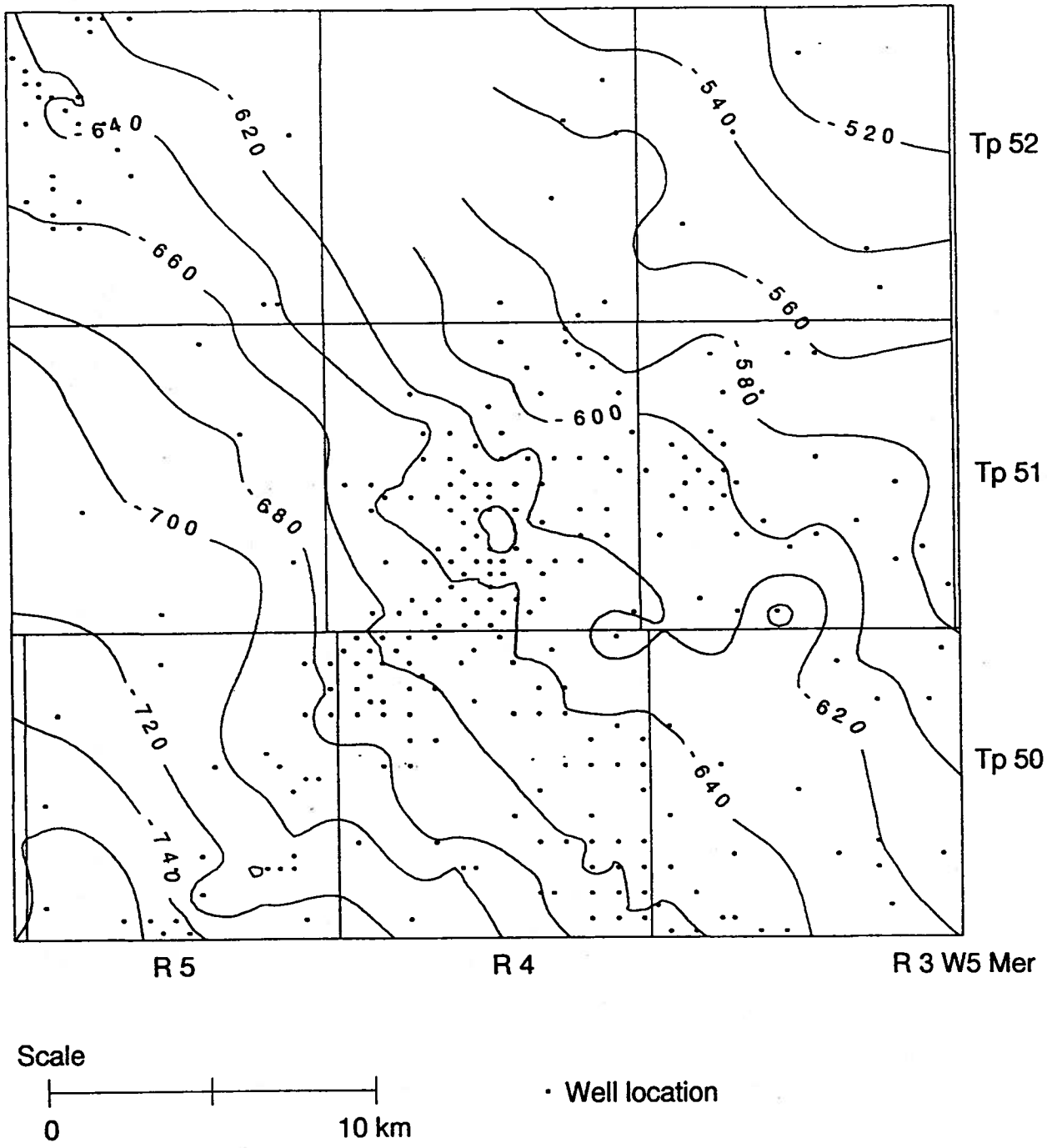

Figure 15: Structure top of Mannville Group (contour interval: 20 m).

ROCK PROPERTIES

As mentioned in the introduction, rock properties are important in establishing the ability of the injection-target aquifer to receive the proposed volumes of CO_2 and to retain them over long periods of time through geochemical and hydrodynamic trapping. The relevant rock properties for this study are mineralogy, porosity and permeability. The aspects of the mineralogy that need to be known are different than commonly described for the purpose of determining the provenance and environment of deposition of the formation or aquifer. To determine the reactivity of the formation or aquifer, the mineral compositions, mineral volume %, mineral suface areas, % of mineral surface areas exposed in pores (i.e. "reactive" surface area) must be measured or estimated in some fashion.

Although there are many wells with cored intervals in the study area, most of the cores are taken only over the Ellerslie Member and Ostracod Beds interval. Only two wells have core taken in the Glauconitic Sandstone and Grand Rapids interval. Thus, the results of the analysis of petrophysical and mineralogical rock characteristics for these units have a lesser degree of confidence than those for the Ellerslie Member and Ostracod Beds. Nevertheless, they are based on all the information available at this time and are representative as such.

PETROGRAPHY

A total of fifteen thin sections were produced for petrographic and XRD analyses from sandy parts of the Ellerslie Member, Ostracod Beds and Glauconitic Sandstone. Detailed thin sections descriptions are contained in Appendix I. Seven thin sections were taken from the Glauconitic Sandstone, one from the Ostracod Beds and seven from the Ellerslie Member. From these 15 samples, 7 were chosen for XRD analysis. The Results of the XRD analysis and traces of the XRD patterns are found in Appendix II. These two sets of observations form the basis for the descriptions and conclusions on the mineralogy which follow.

Quartz:Feldspar:Rock (Q:F:R) proportions, summarized in Table 2, show the Ellerslie Member to be the most diverse of the three units. Mineralogically, the Glauconitic Sandstone is shown to be relatively homogeneous and with the highest proportion of K-feldspar and clays (Table 3). The high proportion of clay in the Glauconitic Sandstone is due to the presence of glauconite which ranges in size from sand-size grains to clay-size-grains. Figure 16 shows the location and average mineralogy of the analyzed samples.

Table 2. Framework petrography (%) of Mannville Group rocks in the study area (the rock fragments are mainly sedimentary and include carbonates, cherts, siltstones, mudstones and glauconites).

SAMPLE #	DEPTH (m)	STRATIGRAPHY	QUARTZ	FELDSPAR	ROCK FRAG	SANDSTONE DESCRIPTION
Well Location	7-9-50-4w5					
DW 93-1	1602	Glauconitic	45	1	54	Fine to medium grained Litharenite
DW 93-2	1599.7	Glauconitic	43	2	55	Fine to medium grained Litharenite
DW 93-3	1597	Glauconitic	49	1	50	Fine to medium grained Litharenite
DW 93-4	1594.3	Glauconitic	55	4	41	Fine to medium grained Litharenite
	7-11-50-5w5					
DW 93-5	1615.4	Glauconitic	40	3	57	Fine to medium grained Litharenite
DW 93-6	1611	Glauconitic	47	2	51	Fine to medium grained Litharenite
DW 93-7	1605.7	Glauconitic	55	1	44	Fine to medium grained Litharenite
	16-20-52-5w5					
DW 93-8	1612.75	Ellerslie	30	1	69	Very fine to fine grained Extralitharenit
DW 93-9	1609.7	Ostracode	48	2	52	Very fine to fine grained Extra litharenite
	5-12-50-5w5					
DW 93-10	1660	Ellerslie	40	1	59	Interlaminated Coarse and Medium grained Litharenite
DW 93-11	1659.75	Ellerslie	15	0	85	Granule to very coarse grained Extra Litharenite
DW 93-12	1657.5	Ellerslie	35	0	65	Very fine to very coarse grained Litharenite
	6-11-51-4w5					
DW 93-13	1584	Ellerslie	75	1	24	Fine to medium grained Sublitharenite
DW 93-15	1559.5	Ellerslie	75	1	24	Fine grained Sublitharenite
	10-17-51-4w5					
DW 93-16	1635	Ellerslie	50	0	50	Interlaminated Medium and very fine grained Litharenite

Table 3. Framework and matrix mineralogy (%) of Mannville Group samples in the study area (quartz includes quartz, mudstone, siltstone and chert).
N.B. Dol, Cal, Sid and Kaol stand for dolomite, calcite, siderite and kaolinite, respectively.

SAMPLE #	DEPTH (m)	STRATIGRAPHY	QUARTZ	CARBONATES	PLAGIOCLASE	K-FELDS	GLAUCONITE	CLAYS
Well Location	7-9-50-4w5							
DW 93-1	1602	Glauconitic	90	tr. Dol	1	-	8	1 (Kaol)
DW 93-2	159.7	Glauconitic	90	2 Dol	-	2	5	1
DW 93-3	1597	Glauconitic	78	15 Dol	-	1	5	1
DW 93-4	1594.3	Glauconitic	86	3 (1cal,1dol,1Sld)	-	4	5	2 (Kaol)
	7-11-50-5w5							
DW 93-5	1615.4	Glauconitic	80	4 (2Cal,1Dol,1Sld)	2	3	10	1 (Kaol)
DW 93-6	1611	Glauconitic	86	tr. cal	-	2	10	2
DW 93-7	1605.7	Glauconitic	92	2 (2Cal, tr. Sld)	-	1	3	2 (Kaol)
	16-20-52-5w5							
DW 93-8	1612.75	Ellerslie	60	37 (20Cal, 17Dol)	-	1	-	2 (Kaol)
DW 93-9	1609.7	Ostracode	77	20 (10Cal, 10dol)	1	1	-	1 (Kaol)
	5-12-50-5w5				-			
DW 93-10	1660	Ellerslie	89	8 Sld	-	1	-	2
DW 93-11	1659.75	Ellerslie	85	13 Sld	-	-	-	2
DW 93-12	1657.5	Ellerslie	97	-	-	-	1	2
	6-11-51-4w5							
DW 93-13	1584	Ellerslie	97	-	-	1	-	2 (Kaol)
DW 93-15	1559.5	Ellerslie	88	10 (10 Dol, tr. Cal)	-	1	-	1
	10-17-51-4w5							
DW 93-16	1635	Ellerslie	95	-	-	-	-	5

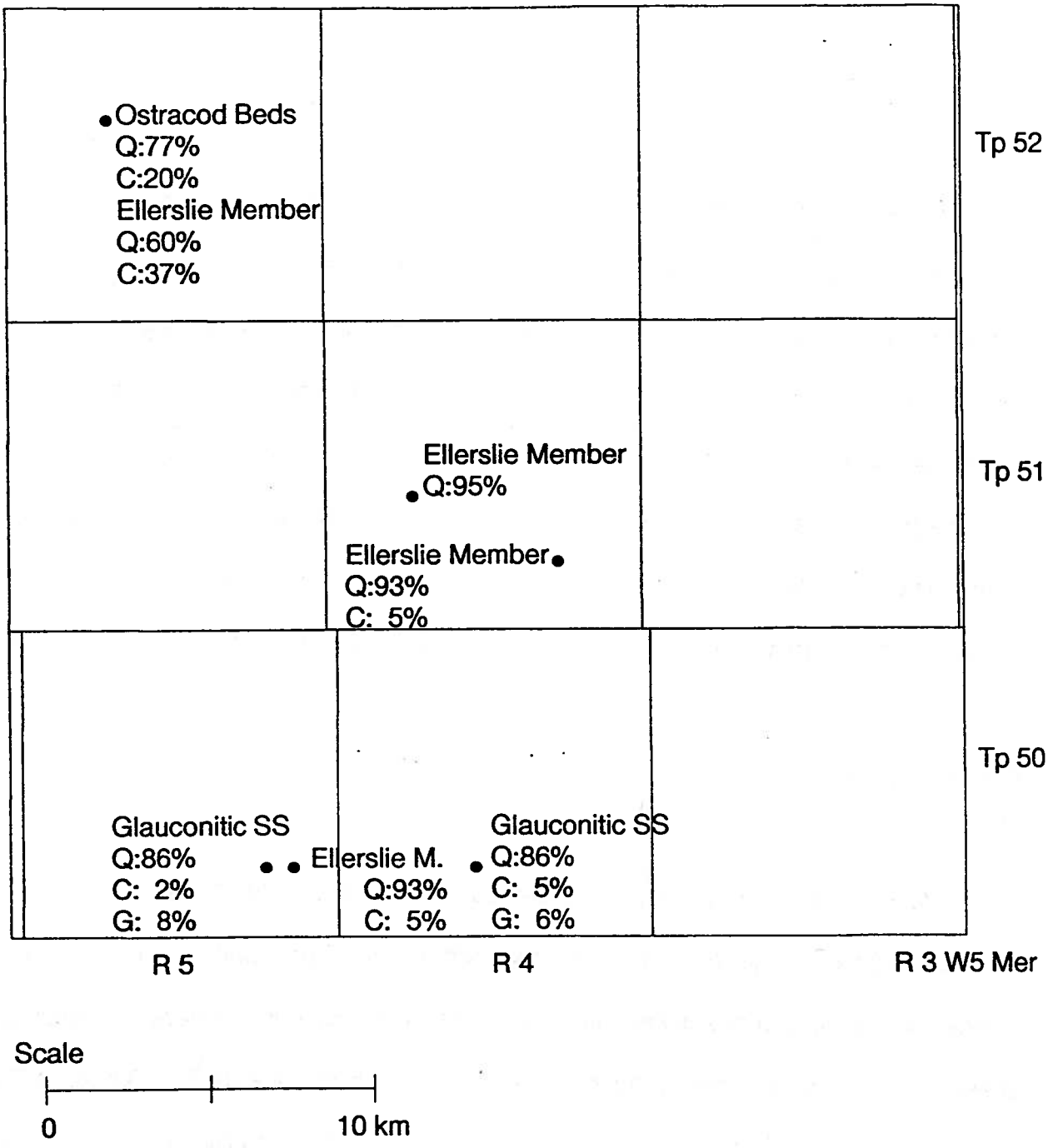

Figure 16: Location and average mineralogy of rock samples from the Mannville Group strata (Q, C and G stand for quartz, carbonate and glauconite, respectively).

Ellerslie Member

The Ellerslie Member contains thin, discontinuous sandstones ranging from immature to mature litharenites. Sandstones are generally very fine to very coarse grained, subangular to subrounded and are poor to well sorted; the thin sandstones tend to be porous. Matrix material consists of dolomite, calcite and some siderite cement, and kaolinite. Quartz:Feldspar:Rock-Fragments proportions, range from 15:0:85 to 75:1:24. Quartz consists primarily of monocrystalline grains with subordinate amounts of polycrystalline grains scattered throughout. Rock fragments consist of varying amounts of dolomite, calcite, chert, siltstone and mudstone. Plagioclase to K-feldspar ratio is generally 0:1.

Ostracod Beds

Similar to the Ellerslie Member, the Ostracod Beds contain thin, immature litharenites. The sandstones are generally fine grained, poorly sorted and porous. The sandstone matrix consists of abundant kaolinite and calcite and dolomite cement. Muscovite is present as a minor accessory mineral. The Q:F:R proportions for the Ostracod Beds sample are 48:2:52. The quartz grains are dominantly monocrystalline and rockfragments consist of dolomite, mudstone, chert and siltstone. The plagioclase to K-feldspar ratio is generally 1:1.

Glauconitic Sandstone

The Glauconitic Sandstone is classified as a mature to submature litharenite. The sandstone is fine to medium grained, subangular to subrounded, moderately well sorted and has good to very good porosity. Quartz:Feldspar:Rock-Fragments proportions range from 55:4:41 to 40:3:57. Monocystalline and polycrystalline quartz grains are generally very clean but a few samples contain traces of kaolinite coatings and dolomite and calcite crystal growth along grain contacts. Minor matrix materials include kaolinite and dolomitic cement. Rock fragments consist of chert, glauconite, mudstone and minor calcite and dolomite. The plagioclase to K-feldspar ratio ranges from 1:0 to 0:4.

POROSITY

Porosity data for the Mannville strata in the area of interest were obtained from core analyses. According to the relativist concept of measurement and scale (Baveye and Sposito, 1984), these data represent volume-averaged values corresponding to the plug scale. Thus, they do not reflect larger scale features such as fractures. Because of the large difference between the plug scale (cm) and formation scale in the study area (meters and tens of meters in thickness, tens of kilometres areally), there is need for a sequential scaling-up approach in order to arrive at representative values (Cushman, 1984). Accordingly, the plug-scale measurements in each well in each formation are scaled-up to the well scale, and then the well-averaged values are scaled-up to the study-

area scale. This approach implicitly takes into account the distances of the order of 10^{-1} m between measurements in the same well, and of the order of 10^{2} to 10^{4} m between measurements in different wells. Any scaling-up process inherently involves loss of detailed information from the lower scale, retaining, however, the main characteristics at the larger scale.

In the study area, examination of porosity distributions in all the wells with core analyses has shown that generally there is no vertical porosity trend in any unit. Figure 17 illustrates the porosity distribution in well 15-15-51-4W5M, covering the Ellerslie Member and Ostracod Beds interval, and in well 7-9-50-4W5M covering the Glauconitic Sandstone and Grand Rapids Formation interval. In the absence of any trend, their well-average value is given by the plug-average values weighted by the length of the representative interval indicated in the core analysis. This averaging is justified by the fact that porosity is a scalar property of a porous medium. The porosity variation at the scale of the study area was analyzed by stratigraphic unit using distribution maps and frequency plots. Only the Ellerslie Member and Ostracod Beds have enough well-scale data to allow this type of analysis. The areal distributions of well-scale porosity for these two units (Figs. 18 and 19, respectively) show no areal trend. Areas of high and low porosity are apparent in both units. The corresponding frequency plots (Fig. 20) show that these values are distributed normally (Ellerslie Member) or close to normal (Ostracod Beds). In this case, the study-area representative value is given by the median (50% frequency) value or arithmetic average of the well-scale porosity data. Only two wells have porosity data for

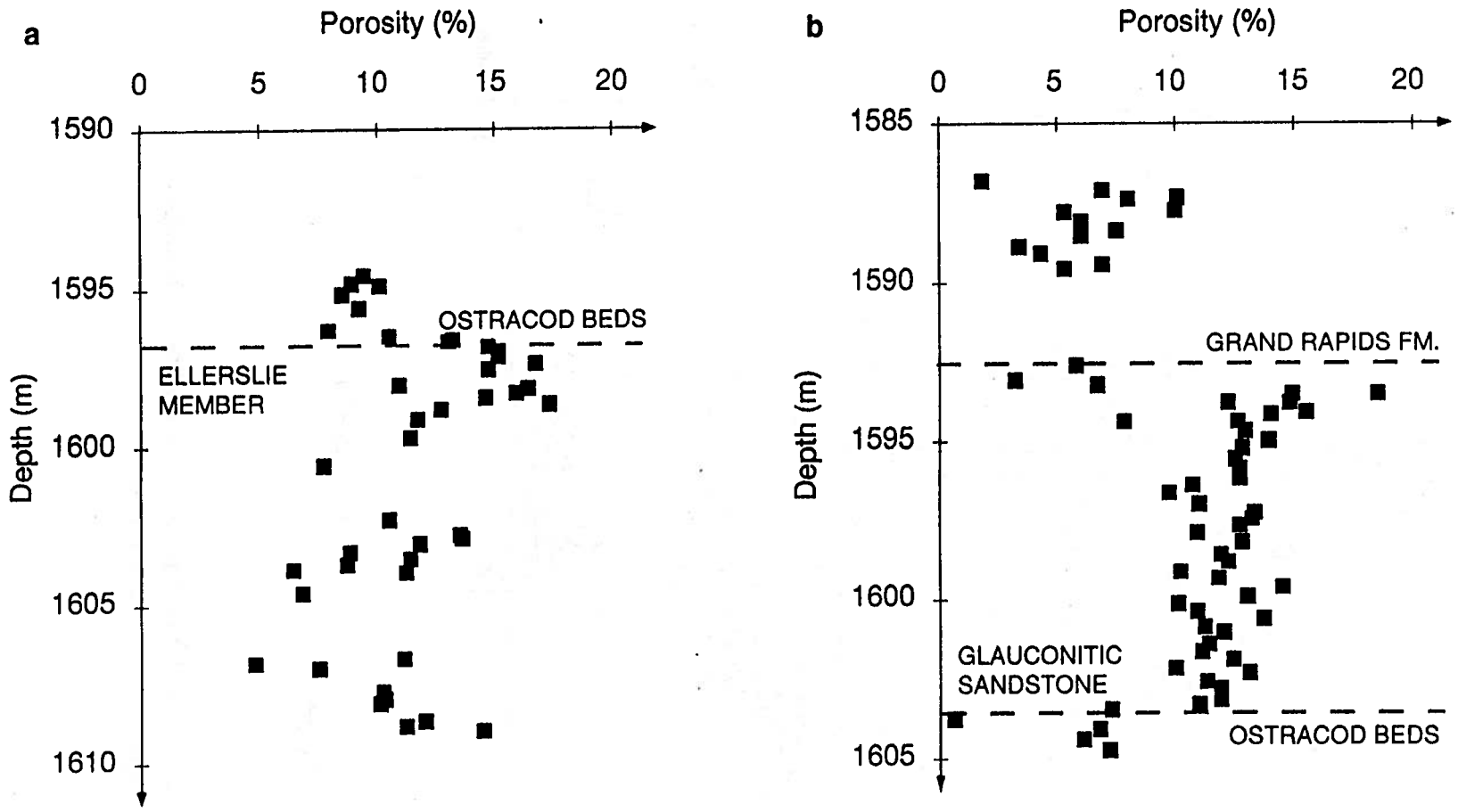

Figure 17: Vertical variation of porosity in: a) well 15-15-51-4-W5M, Ellerslie Member and Ostracod Beds; and b) well 7-9-50-4-W5M, Glauconitic Sandstone and Grand Rapids Formation.

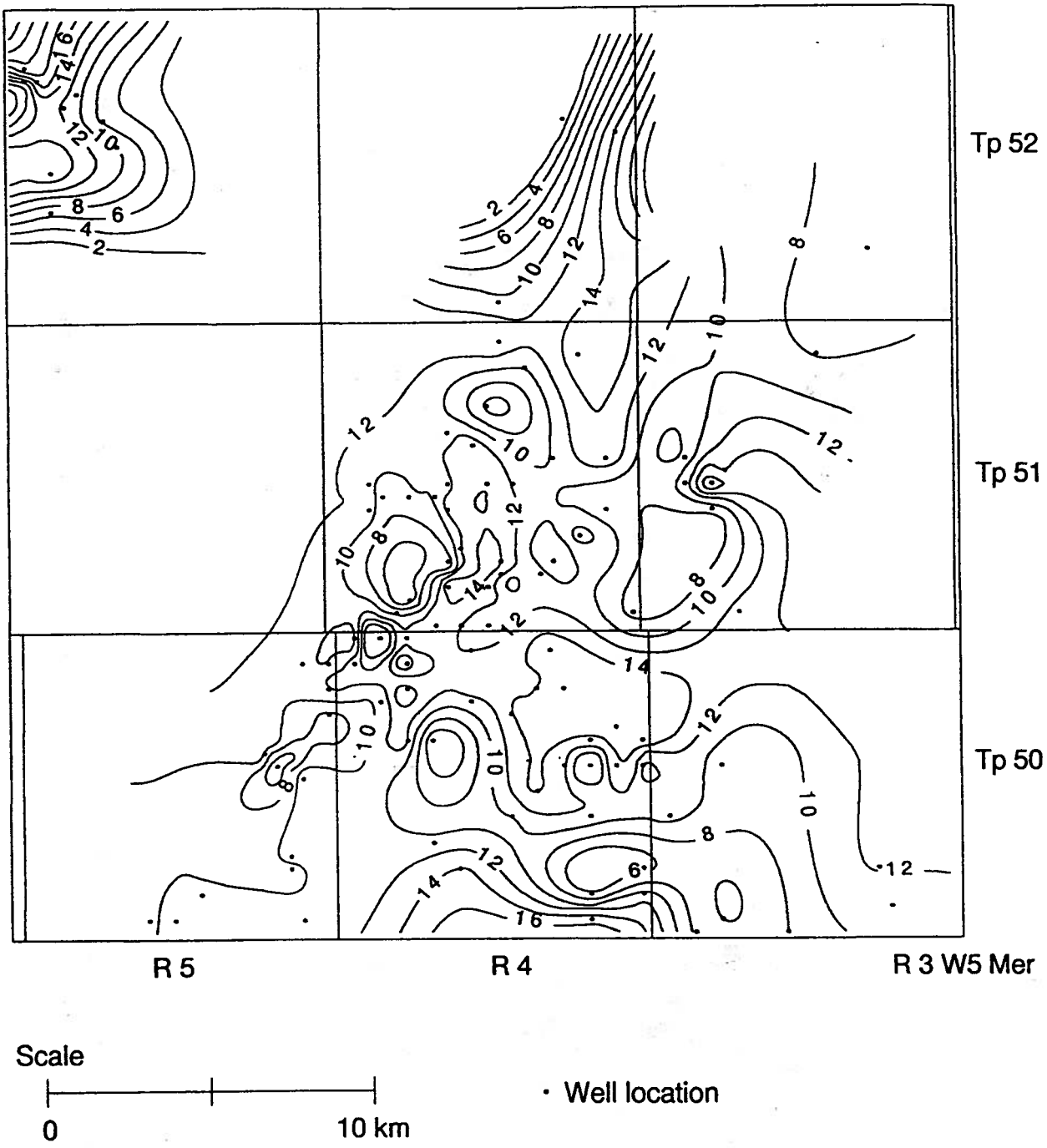

Figure 18: Areal distribution of well-average porosity in Ellerslie Member, Mannville Group (contour interval: 2%).

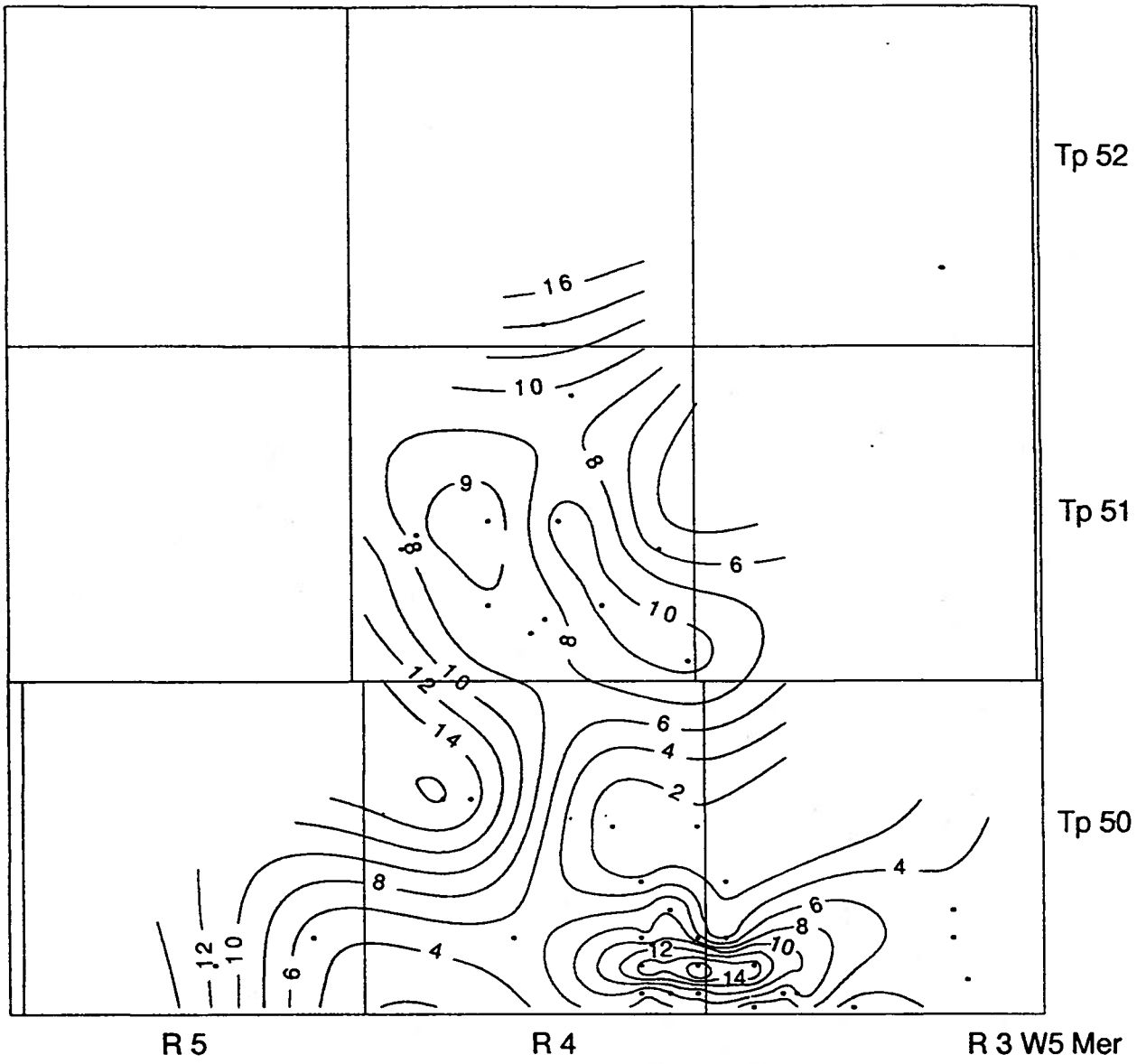

Figure 19: Areal distribution of well-average porosity in Ostracod Beds, Mannville Group (contour interval: 2%).

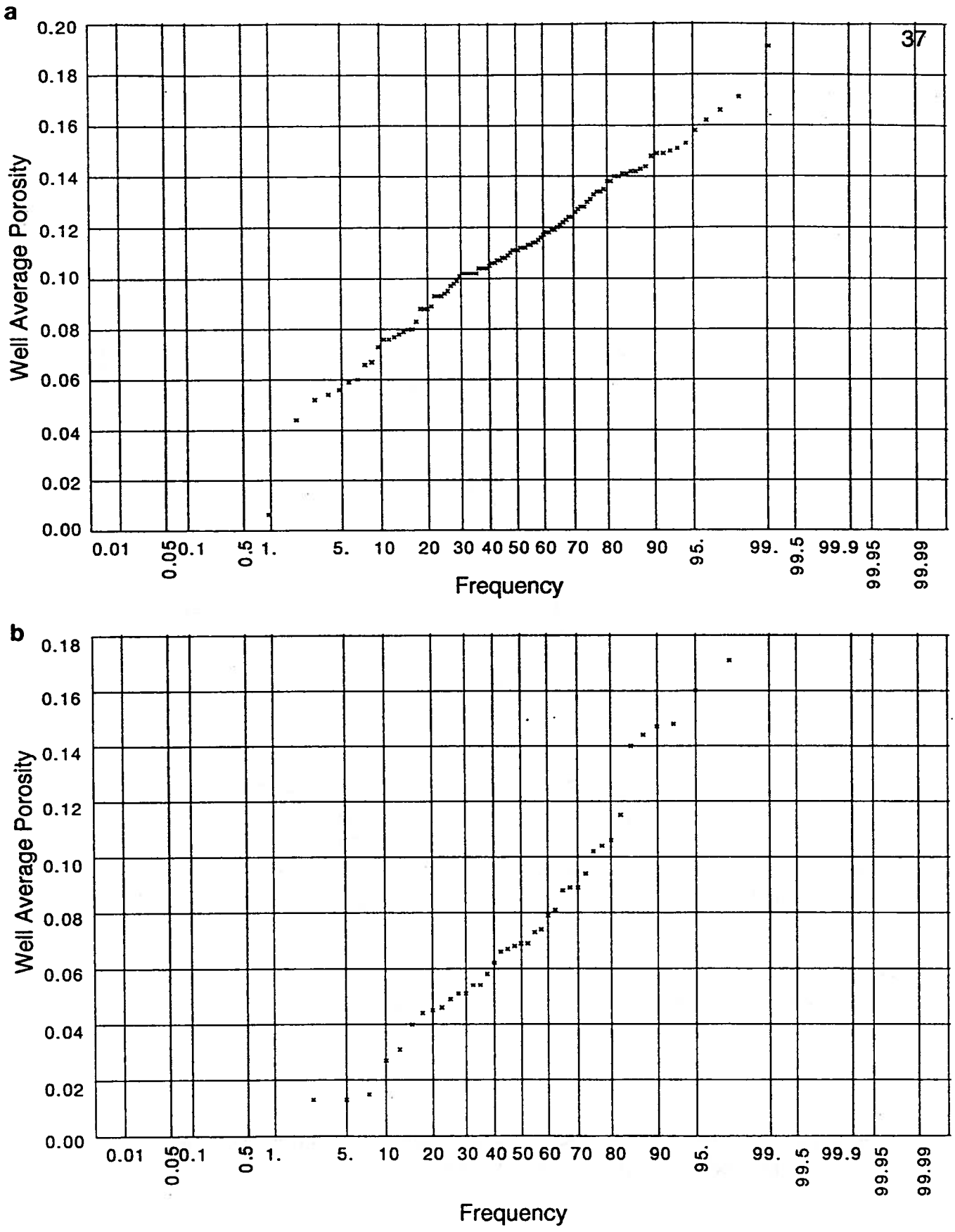

Figure 20: Frequency distribution of well-average porosity in:
a) Ellerslie Member, and b) Ostracod Beds, Mannville Group.

the Glauconitic Sandstone and the Grand Rapids Formation, whose respective averages are shown in Figure 21. Table 4 presents the stratigraphic distribution and variability of well-scale porosity of Mannville strata in the study area.

Unit	Number of wells	Well average porosity %		
		Minimum	Average	Maximum
Grand Rapids	2	5.6	6.1	6.6
Glauconitic Sandstone	2	11.8	11.9	12.0
Ostracod Beds	40	1.3	7.8	17.1
Ellerslie Member	105	0.6	11.1	19.0

Table 4. Stratigraphic distribution and variability of well-scale porosity of Mannville strata.

It can be seen from Table 4 and Figures 17 to 21 that the porosity of the Mannville strata is quite variable, but high on average, particularly for the succession below the basal shale zone of the Grand Rapids Formation. This means that areas of relatively high porosity can be found, which could probably accommodate large volumes of injected CO_2.

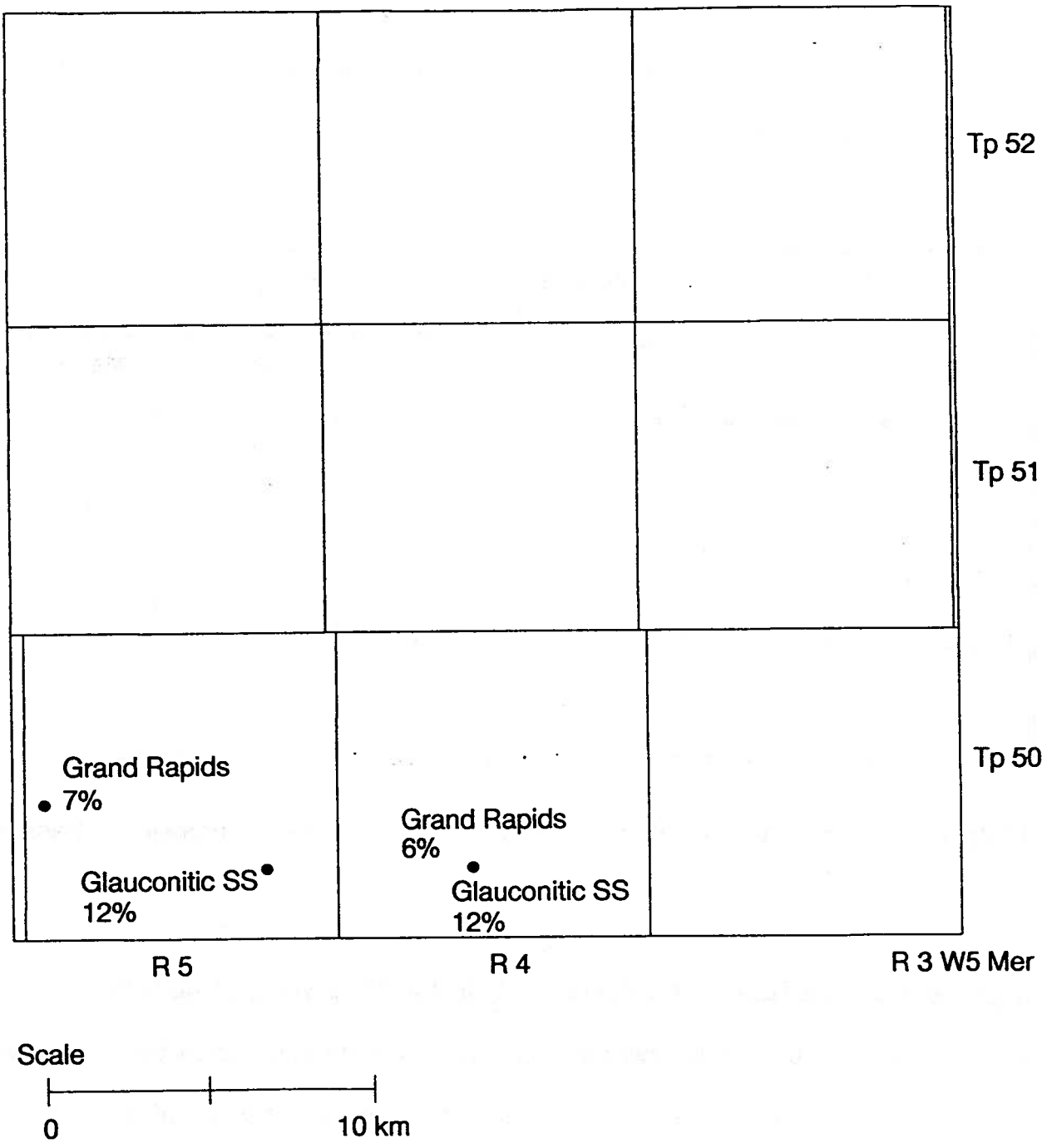

Figure 21: Well-average porosity in Glauconitic Sandstone and Grand Rapids Formation, Mannville Group.

PERMEABILITY

Rock permeability was measured in the study area both in core (plug scale) and drillstem tests (well scale). The core permeability data in all wells show generally no vertical trend (Fig. 22). No definitive conclusions could be drawn regarding the Glauconitic Sandstone and Grand Rapids Formation, for which core analyses are available in two wells only. Like porosity, the plug-scale permeability values need to be scaled up to the well scale. Unlike porosity, permeability is a non-additive quantity, therefore straight scaling-up is inappropriate. Depending on rock characteristics and stratification, various averaging methods can be used (see Dagan, 1989). Theoretical applications and numerical experiments using permeability data from the siliciclastic Wabiskaw aquifer in northeastern Alberta show that the well-scale permeability value k_{ef} is given by the generalized (or power) average:

$$K_{ef}^{w} = \frac{1}{n} \Sigma \, k_i^{w}$$

where k_i are n individual plug-scale permeability values and w is an empirical power found to be in the 0.8 to 0.9 range (Desbarats and Bachu, 1994). The well-scale permeability values along bedding were obtained for each unit in the Mannville Group by applying the above relation with w = 0.8 to the plug-scale maximum permeability values k_m measured in core. The areal distributions of well-scale permeability show no trend, while the frequency distributions for the Ellerslie Member and Ostracod Beds (Figs. 23 and 24,

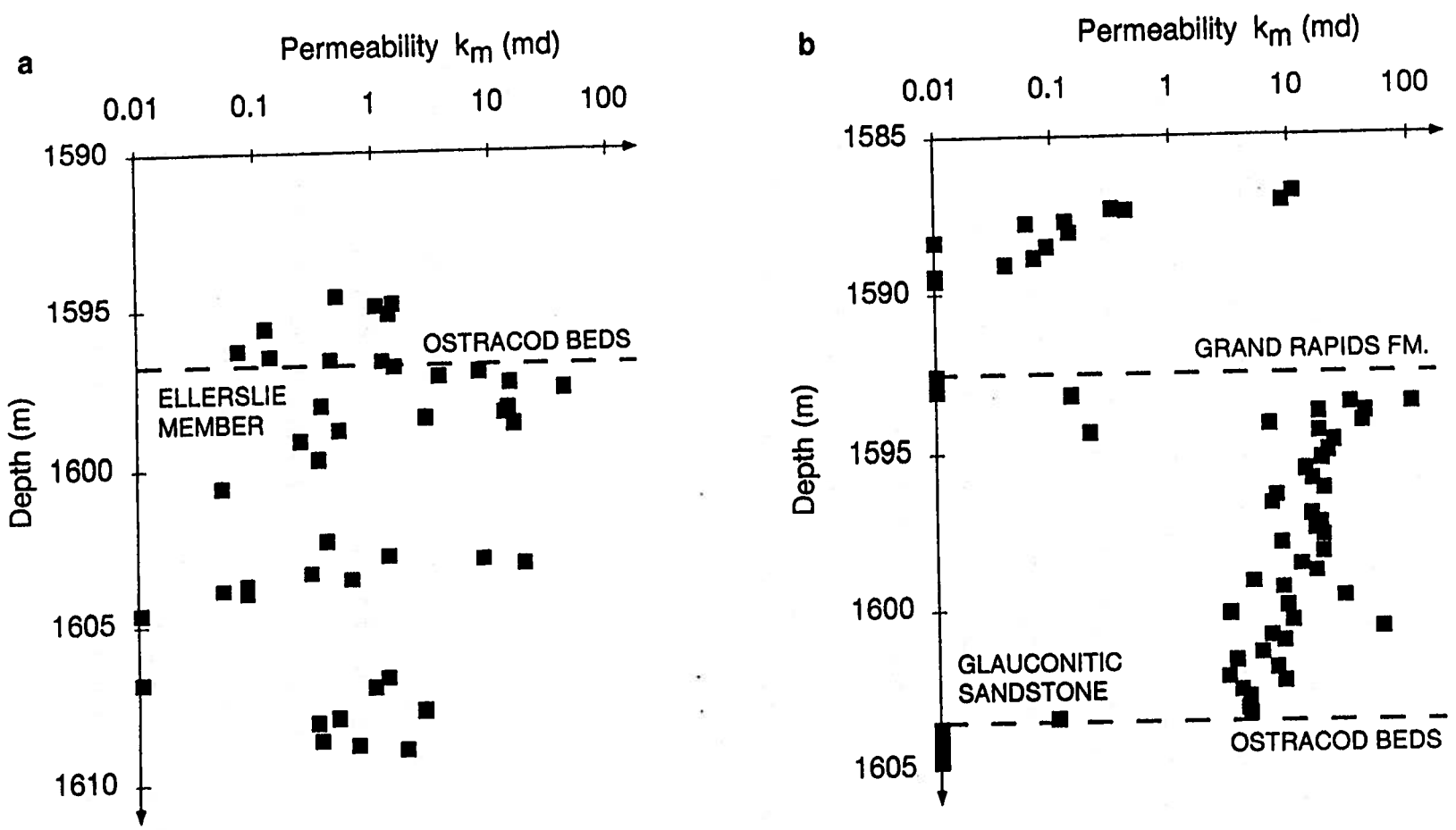

Figure 22: Vertical variation of maximum permeability k_m in: a) well 15-15-51-4W5M, Ellerslie Member and Ostracod Beds; and b) well 7-9-50-4W5M, Glauconitic Sandstone and Grand Rapids Formation.

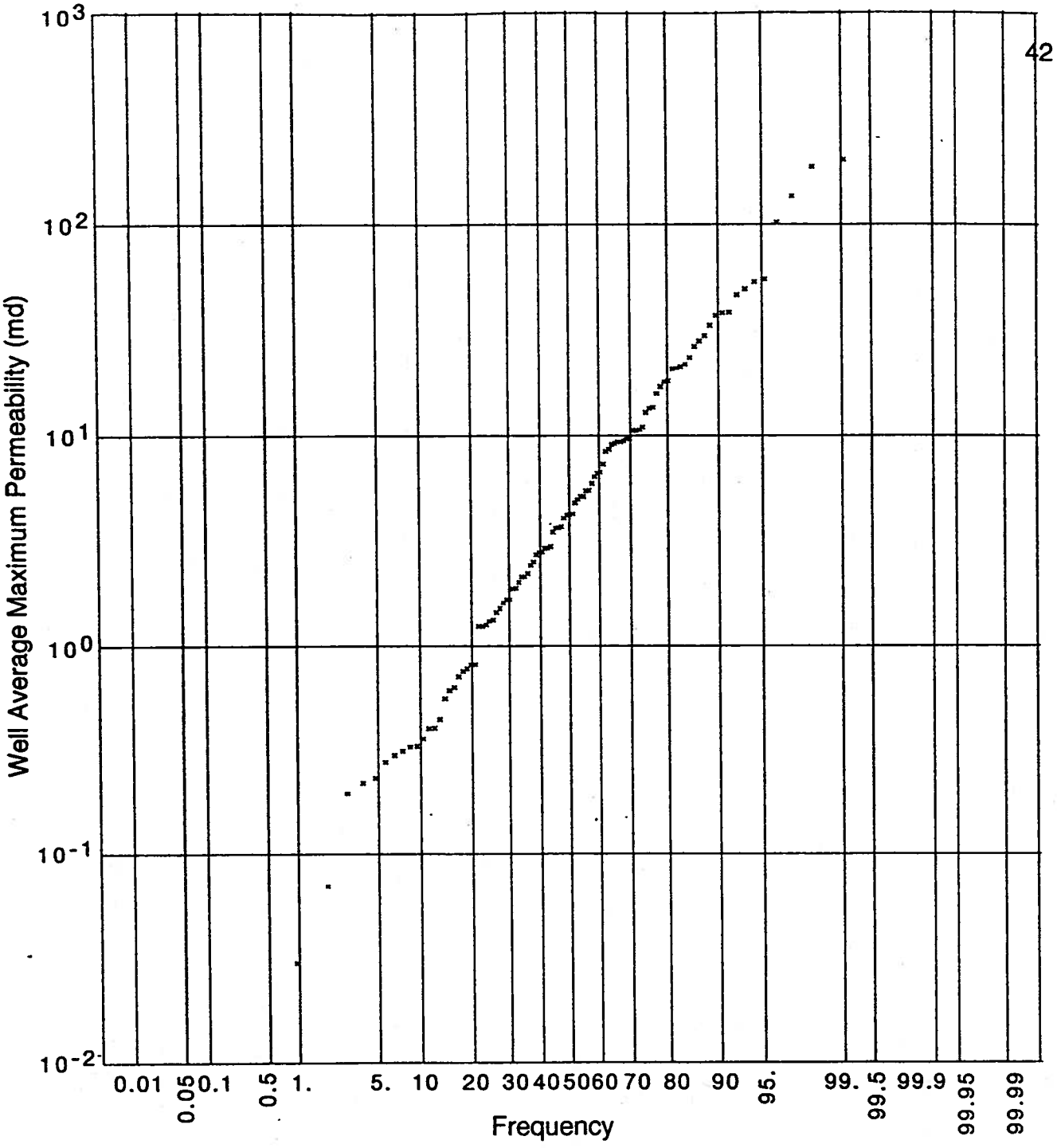

Figure 23: Frequency distribution of well-average maximum permeability k_m in the Ellerslie Member, Mannville Group.

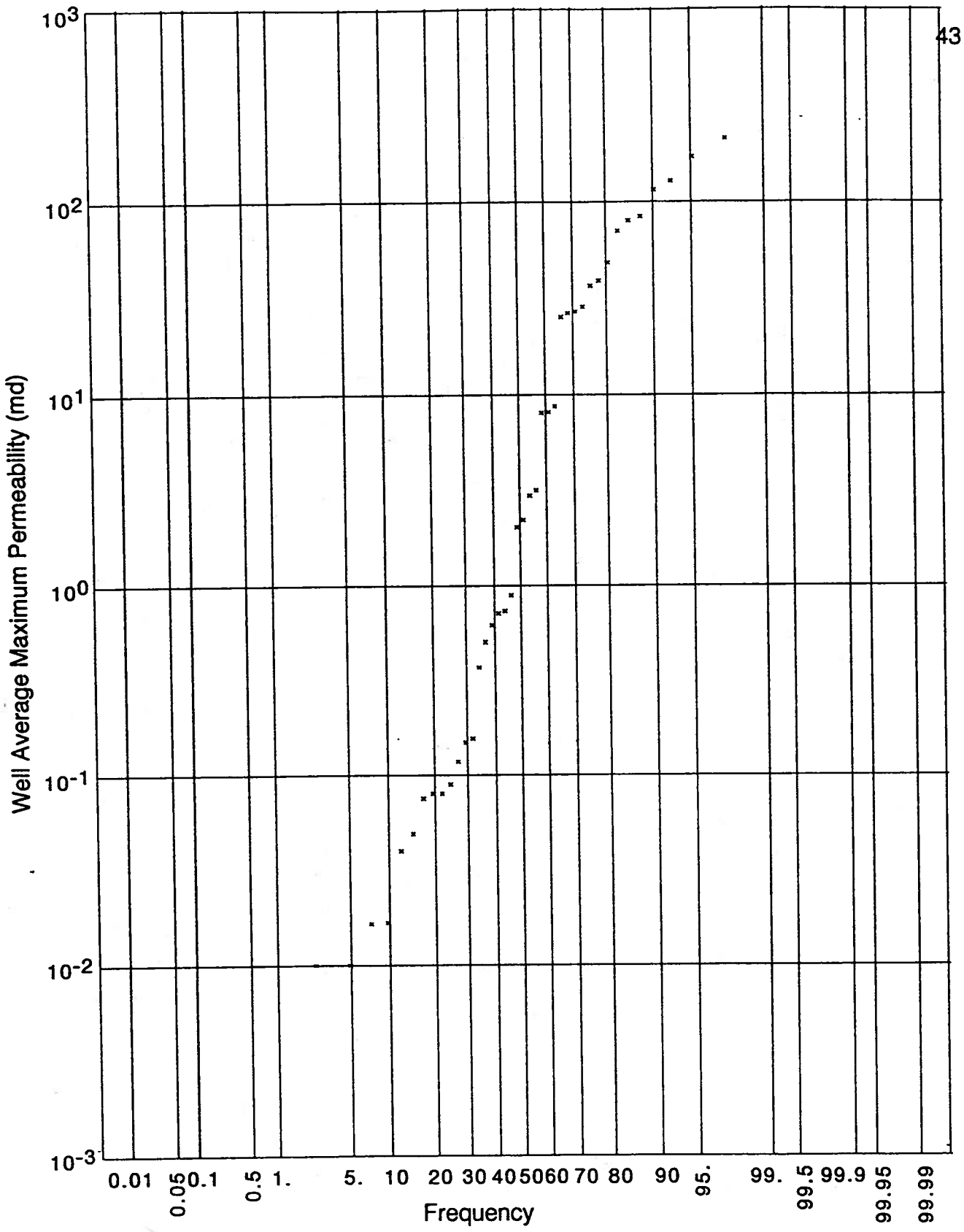

Figure 24: Frequency distribution of well-average maximum permeability k_m in Ostracod Beds, Mannville Group.

respectively) show that permeability is generally log-normally distributed. For such distributions, the representative value at the study-area scale is given by the geometric average of the well-scale values. Table 5 presents the stratigraphic distribution and variability of well-scale maximum permeability of Mannville strata in the study area.

Unit	Number of Wells	Maximum permeability k_m (md)		
		Minimum	Average	Maximum
Grand Rapids	2	0.01	0.10	1.00
Glauconitic Sandstone	2	13.40	14.15	14.95
Ostracod Beds	40	0.01	1.87	212.73
Ellerslie Member	105	0.03	4.06	201.93

Table 5. Stratigraphic distribution and variability of well-scale maximum permeability of Mannville strata, as obtained from core analyses.

Unlike for maximum permeability k_m (for flow along the bedding), there are less data regarding vertical permeability k_v (for flow normal to bedding). Thus, statistical averaging at the well scale is not representative and is meaningless. The vertical anisotropy of the Mannville strata was estimated using regression-analysis techniques applied to the plug-scale permeability measurements. Table 6 presents the results of this analysis for the Mannville strata, except for the Grand Rapids Formation, where not enough data were

available for statistical analysis. The coefficient of correlation R^2 of the linear regression k_v vs. k_m is also given in Table 6.

Unit	Number of data pairs k_m-k_v	Vertical Anisotropy	
		k_v/k_m	R^2
Grand Rapids	4	-	-
Glauconitic Sandstone	80	0.30	0.71
Ostracod Beds	93	0.24	0.51
Ellerslie Member	905	0.52	0.85

Table 6. Plug-scale vertical anisotropy of rock permeability in Mannville strata, obtained from core analyses.

As mentioned previously, permeability values measured in drillstem tests were also available in a number of wells. A much larger volume of rock is tested by a drillstem test, such that these permeability data already represent well-scale values. They are generally log normally distributed (Figs. 25, 26, and 27), such that the representative value for each unit is given by their respective geometric average. Table 7 presents the stratigraphic distribution and variability of permeability of Mannville strata in the study area, as measured in drillstem tests.

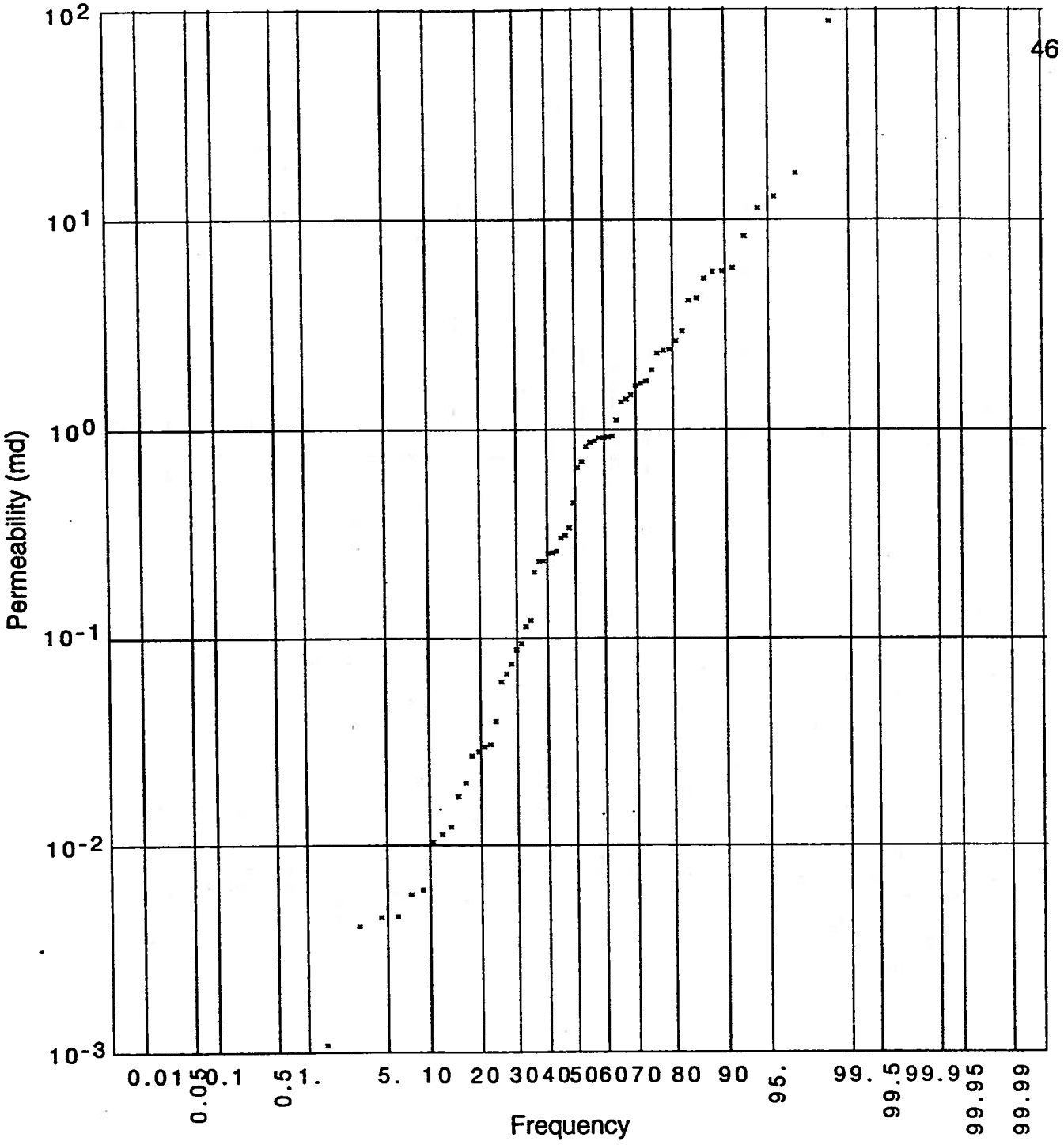

Figure 25: Frequency distribution of permeability in Ellerslie Member, Mannville Group, as measured in drillstem tests.

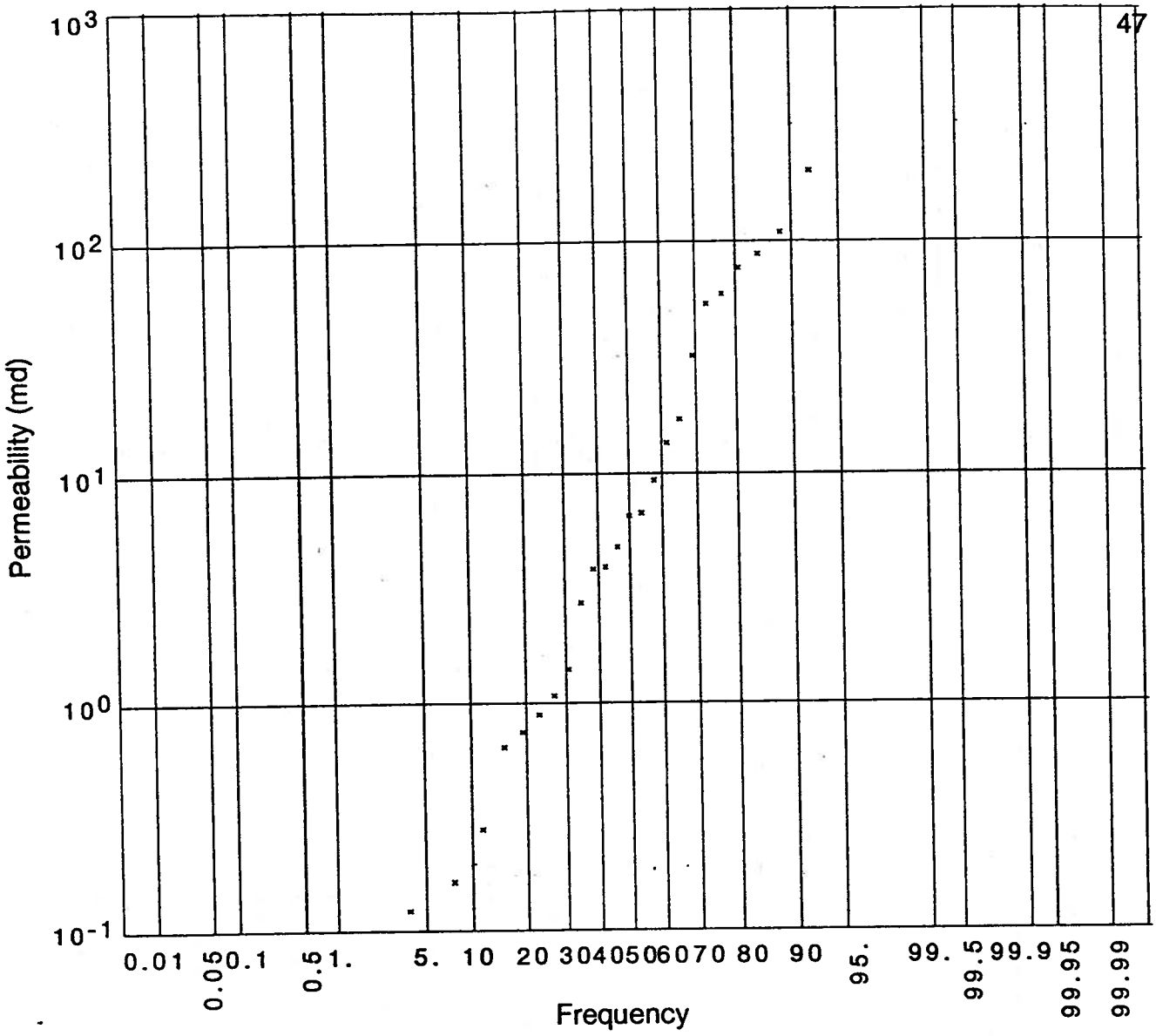

Figure 26: Frequency distribution of permeability in Ostracod Beds, Mannville Group, as measured in drillstem tests.

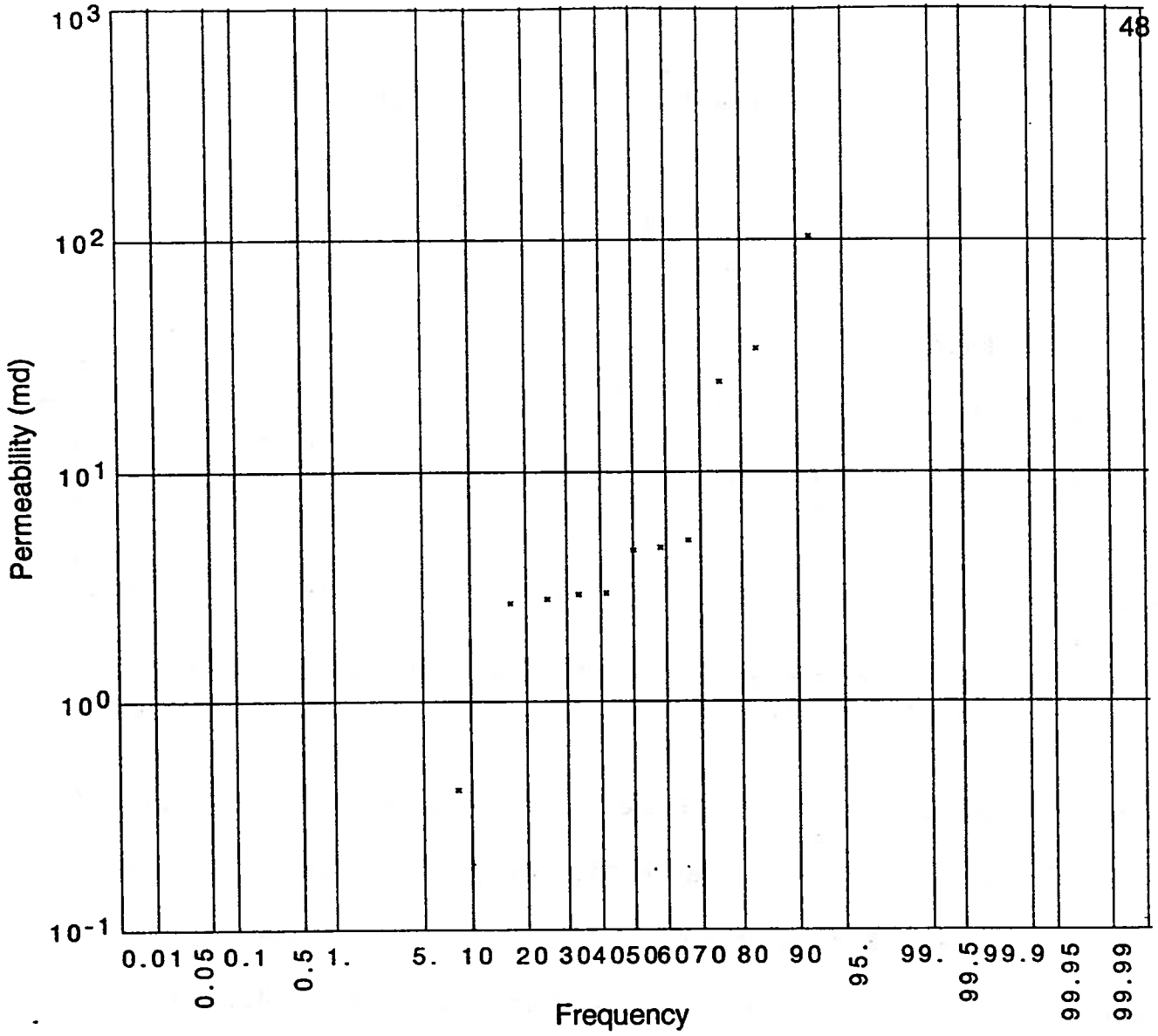

Figure 27: Frequency distribution of permeability in Glauconitic Sandstone, Mannville Group, as measured in drillstem tests.

Unit	Number of Wells	Permeability (md)		
		Minimum	Average	Maximum
Grand Rapids	4	0.93	6.35	78.9
Glauconitic Sandstone	11	0.41	5.80	103.9
Ostracod Beds	25	0.02	0.68	97.2
Ellerslie Member	66	0.01	0.34	88.1

Table 7. Stratigraphic distribution and variability of permeability of Mannville strata as measured in drillstem tests.

As mentioned previously, core analyses and drillstem tests sample different volumes of rocks (10^{-2} m vs. 10^{1}-10^{2} m), and are performed under different conditions (laboratory and in-situ, respectively). Thus, statistically they do not represent samples of the same population, even if the core analyses were scaled-up to the well scale. This is because the scaling-up is purely statistical, and cannot account for the permeability characteristics of rock not sampled. From this point of view, the permeability values obtained from drillstem tests are more representative. Also, for Glauconitic Sandstone, the statistical sample is significantly bigger (11 drillstem tests vs. 2 wells with core analyses). Nevertheless, both core analyses and drillstem tests for all Mannville Group strata indicate the same order of magnitude and variability for permeability values.

Representative values will be selected in the numerical study of Phase III, and a sensitivity analysis will be performed with regard to this essential flow parameter.

Figures 28 and 29 show the areal distribution of permeability measurements (in core and drillstem tests) taken in Glauconitic Sandstone and Grand Rapids Formation strata in the study area. Figures 23 to 29 and Tables 5 to 7 indicate that the Mannville strata in the area of interest have, on average, relatively low permeability (of the order of 10^0-10^1 md), although the variability is quite high, spanning up to 5 orders of magnitude. Although a few measurements from the Grand Rapids Formation indicate permeability values comparable to other Mannville Group units, it should be noted that these are from isolated, discontinuous sands and do not reflect the general character of the unit. The Glauconitic Sandstone strata seem to have on average higher permeability than the other units. This indicates that high permeability regions could be found for injecting CO_2, satisfying the need for high near-well permeability (van der Meer, 1992; Bachu et al., 1994). This will decrease the likelihood of high pressure gradients and pressure buildups at the well. On the other hand, the permeability of Mannville strata at the study-area scale is sufficiently low that the injected CO_2 will be hydrodynamically trapped by a long residence time (Bachu et al., 1994).

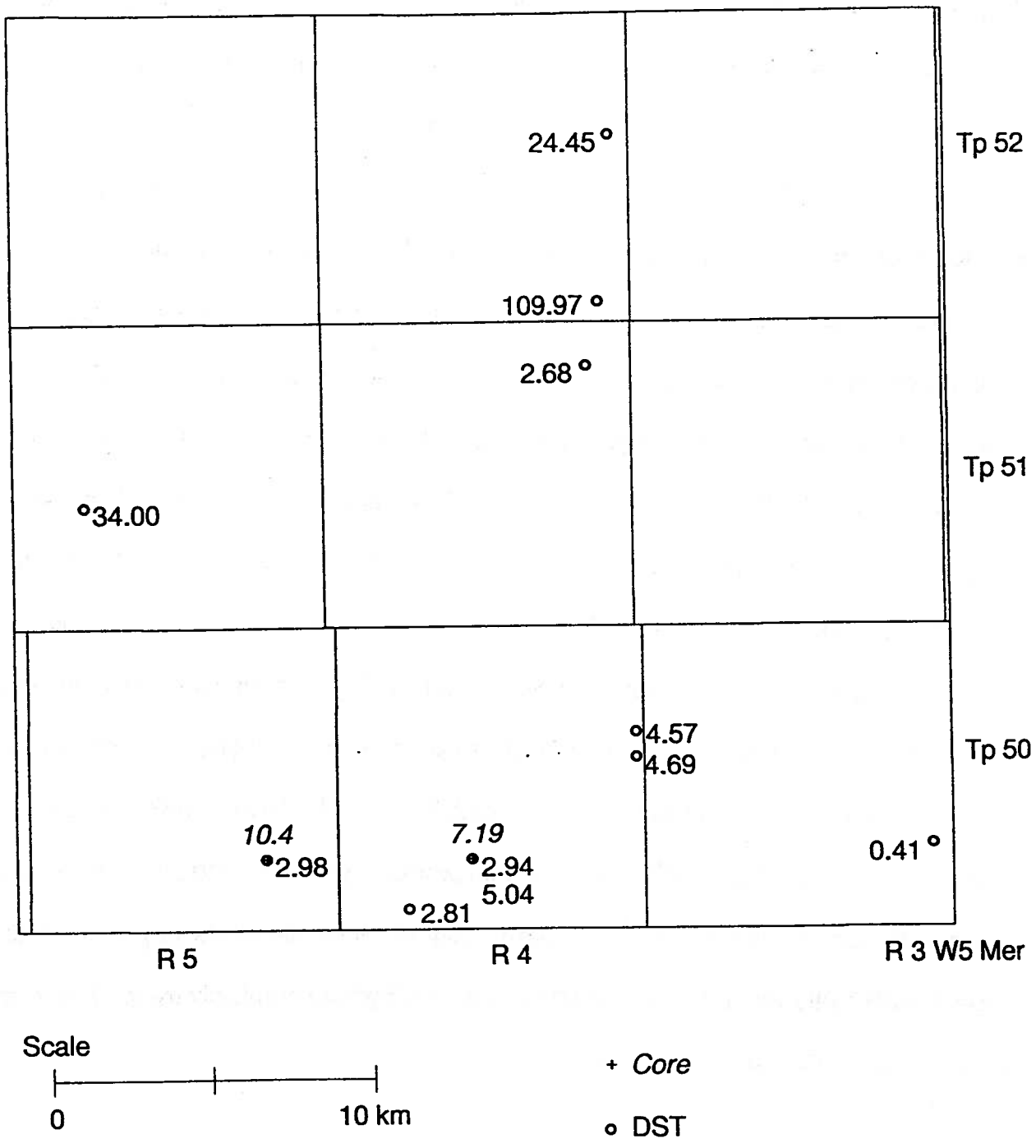

Figure 28: Areal distribution of permeability measurements in Glauconitic Sandstone strata, Mannville Group

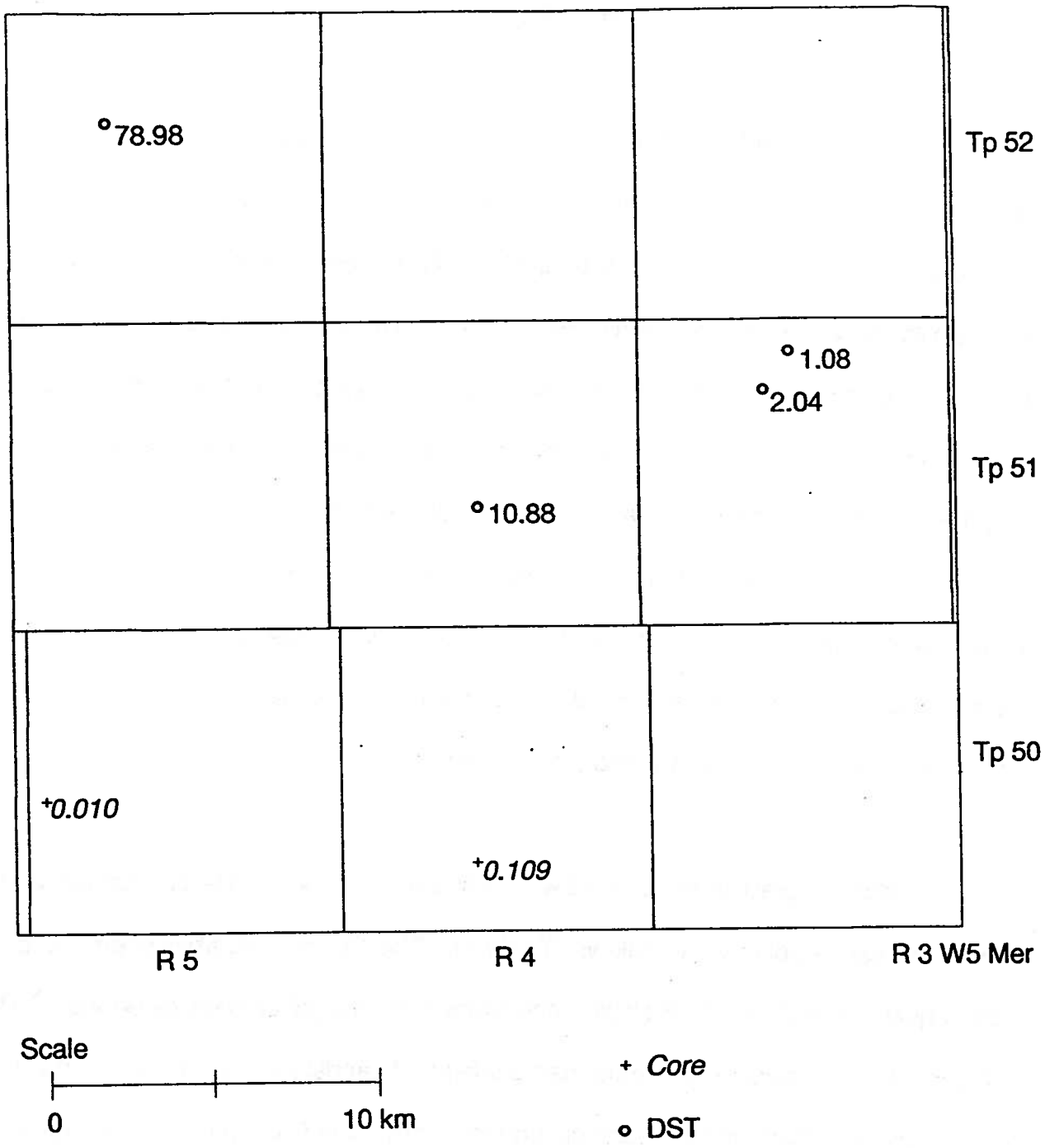

Figure 29: Areal distribution of permeability measurements in Grand Rapids Formation, Mannville Group

FORMATION WATERS

The hydrochemical, hydrodynamic and geothermal regime of formation waters has a significant impact on any deep injection operation, particularly for CO_2. This is because, from a geochemical point of view, the injected CO_2 will dissolve in the formation water and accelerate water-rock reactions. From a hydrodynamic point of view, the injection pressure, the pressure buildup and gradient near the injection well (near field) and the flow of CO_2 far from the injection well (far field) all depend on the natural pressure regime and flow of formation waters. Finally, geochemical reactions, CO_2 solubility and mobility, and generally the flow depend on temperature. Thus, in order to complete the assessment of the Mannville strata in the study area with respect to their potential and suitability for CO_2 disposal, there is need to characterize the geothermal, hydrochemical and hydrodynamic regimes of formation waters.

From a hydrostratigraphic point of view, the strata in the Mannville succession in the study area can be divided as follows (Table 1). The Ellerslie Member seems to be a good aquifer based on its lithology, rock properties and other data categories. The Ostracod Beds (a mixture of interbedded shales and sandstones) is an aquifer-aquitard (i.e. has varying characteristics associated with both). The Glauconitic Sandstone is an aquifer, while the basal shale zone of the Grand Rapids Formation is an aquitard. The remainder of the Grand Rapids Formation is probably an aquifer. The Mississippian Banff Formation and the localized remnants of the Jurassic Nordegg Member underlying the

Mannville Group strata are probably aquifers in contact with the Ellerslie aquifer. Figures 30 and 31 show, respectively, dip and strike hydrostratigraphic cross-sections through the Mannville Group strata in the area of interest.

GEOTHERMAL REGIME

The temperature of formation waters is not normally measured. However, at the end of drilling a number of temperature measurements are performed at the bottom of the well. These bottom hole temperature (BHT) measurements are then processed in order to obtain an estimate of the formation temperature. The wells reaching the Mannville strata in the area of interest penetrated the entire interval and continued into the underlying Mississippian Banff Formation carbonates where most of them end. BHT measurements were performed in 73 wells within the top 25 m of the Banff Formation. These BHT measurements were analyzed individually, culled for errors and processed using the Horner method in order to obtain the formation temperature (Chapman, et al., 1984; Bachu and Burwash, 1991). The average gradient was calculated in each well using a multiannual ground surface temperature of 5.6°C (Bachu and Burwash, 1991). This gradient was subsequently used to estimate the temperature difference between the well bottom and the elevation (or depth) in the respective well of each stratigraphic top of the Mannville Group strata. The average geothermal gradient in the area is 30°C/km. The estimates of formation temperature at the top of each unit were then mapped for analysis and further checking and culling. At the end of this iterative process, temperature

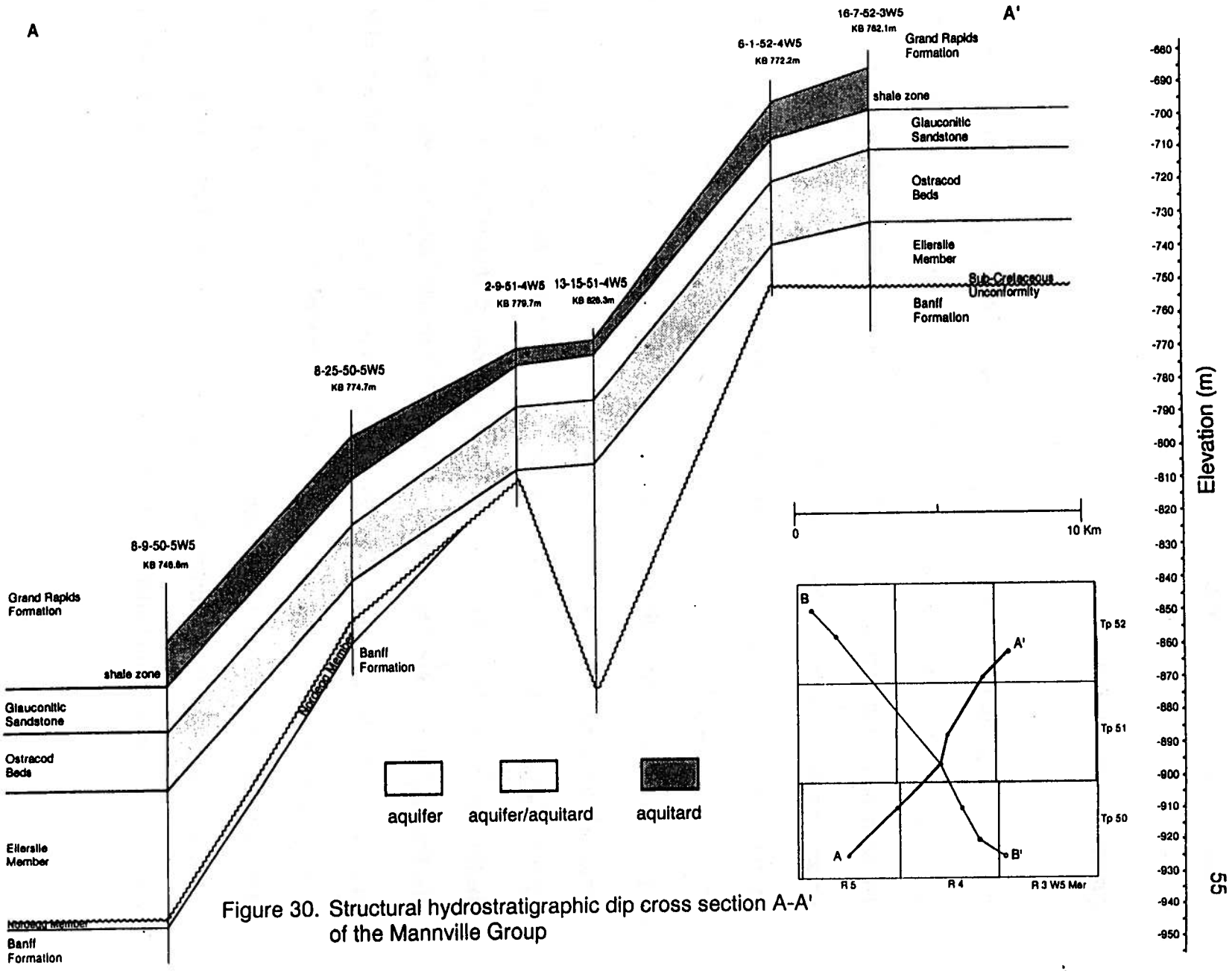

Figure 30. Structural hydrostratigraphic dip cross section A-A' of the Mannville Group

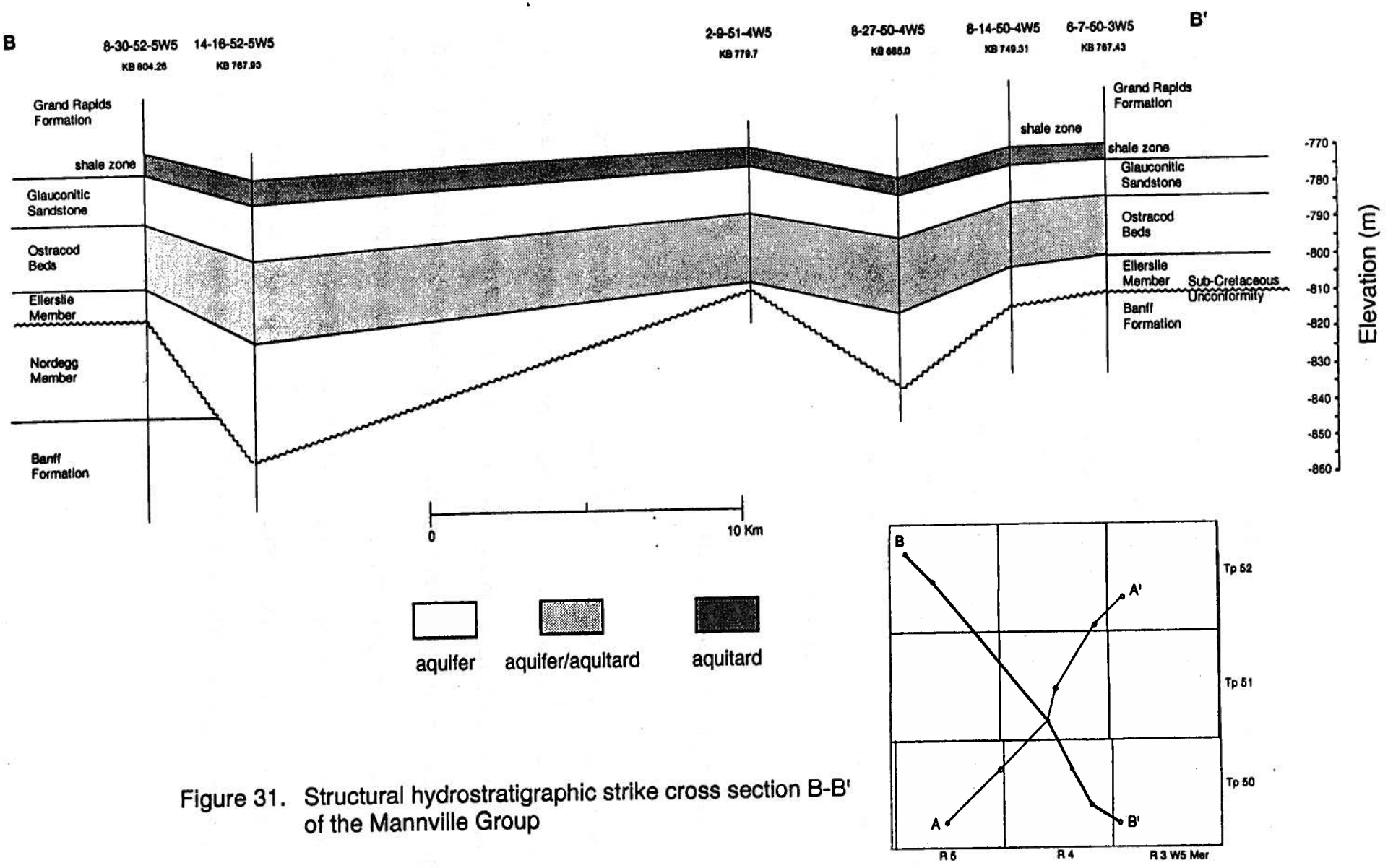

Figure 31. Structural hydrostratigraphic strike cross section B-B' of the Mannville Group

distribution maps were produced for the units of interest. Figure 32 shows the estimated temperature at the top of the Glauconitic Sandstone. The generally southwestward increase in temperature from approximately 50 to 58°C is consistent with a downdip increase in depth of approximately 240 m (estimated from Fig. 11). Apparent anomalies in the temperature distribution are most probably the result of inaccuracies in temperature measurement and in the Horner plot interpretation (low data quality). These inaccuracies cannot be detected and/or corrected with the available information. The main result, nevertheless, is that the formation temperature in the Glauconitic Sandstone is in the range of 50 to 58°C, and this should be used in any future modelling of geochemical and fluid flow modelling of CO_2 injection.

CHEMISTRY OF FORMATION WATER

The electronic data base of formation water analyses at the Alberta Geological Survey was searched for analyses in the Mannville Group within the study area. All the analyses were run through a standard automatic culling procedure for detection and rejection of incomplete and/or contaminated water analyses. The automatic cull takes into account the presence and values of OH, CO_3, Ca, Mg, Cl, SO_4, HCO_3, acceptable ranges of pH and density, and mixing. Further manual culling was applied to the analyses which passed the automatic culling. Twenty-four formation water analyses were left at the end of this process of checking and culling, of which four included minor and trace element

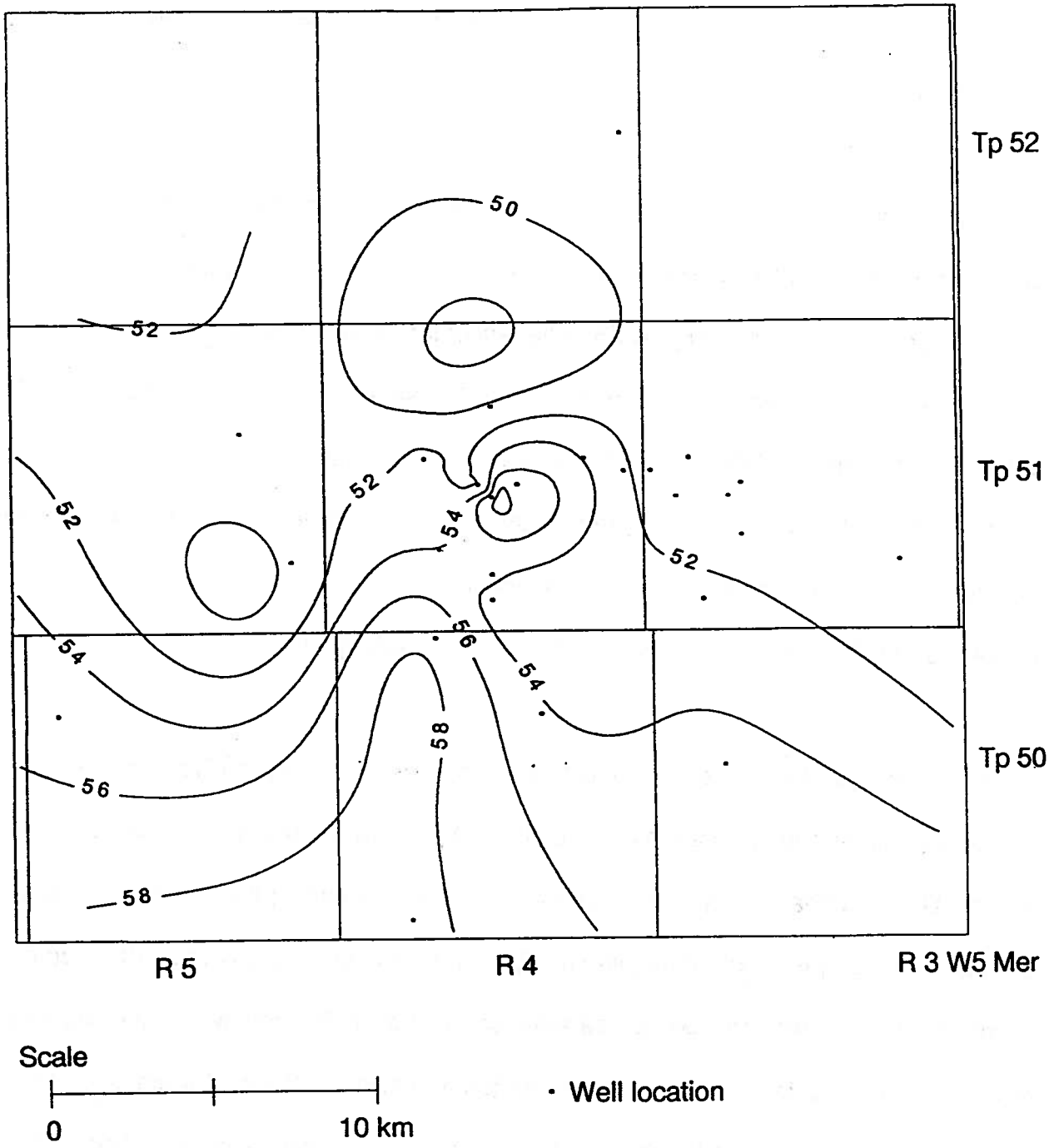

Figure 32: Distribution of estimated formation temperature at the top of the Glauconitic Sandstone, Mannville Group (contour interval: 2°C).

data. All the remaining analyses were allocated within the Mannville hydrostratigraphic succession.

There are only one formation water analysis each in the Grand Rapids Formation and Ostracod Beds, and three analyses in the Glauconitic Sandstone, whose distribution and chloride content is shown in Figure 33. The rest of formation water analyses are from the Ellerslie Member. Their distribution and chloride content is shown in Figure 34. The variation in the composition of formation water in the Mannville Group in the study area is poorly defined due to the few analyses available. Consequently, one representative detailed analysis will have to suffice for water-rock interaction studies and geochemical modelling of CO_2 injection, combined with some sensitivity modelling.

Because most analyses are so-called "standard" analyses in which "Na" is determined as the difference between anions and cations, they incorporate all analytical and other errors. Detailed analyses are required for geochemical studies; therefore, in addition to the four previously mentioned detailed analyses from within the study area, three detailed formation water analyses from areas adjacent to the study area were included in the study. All the detailed analyses are presented in Table 8. None of them is complete, with missing data including Li, Sr, NH_3, SiO_2, F, Br and I in various combinations. Some of these analyses were run through the geochemical equilibrium program SOLMINEQ.88 (Kharaka et al., 1988), with the analyses adjusted for CO_2 loss and calcite saturation at formation temperature. Of the seven, sample RCAH50-874A is recommended as

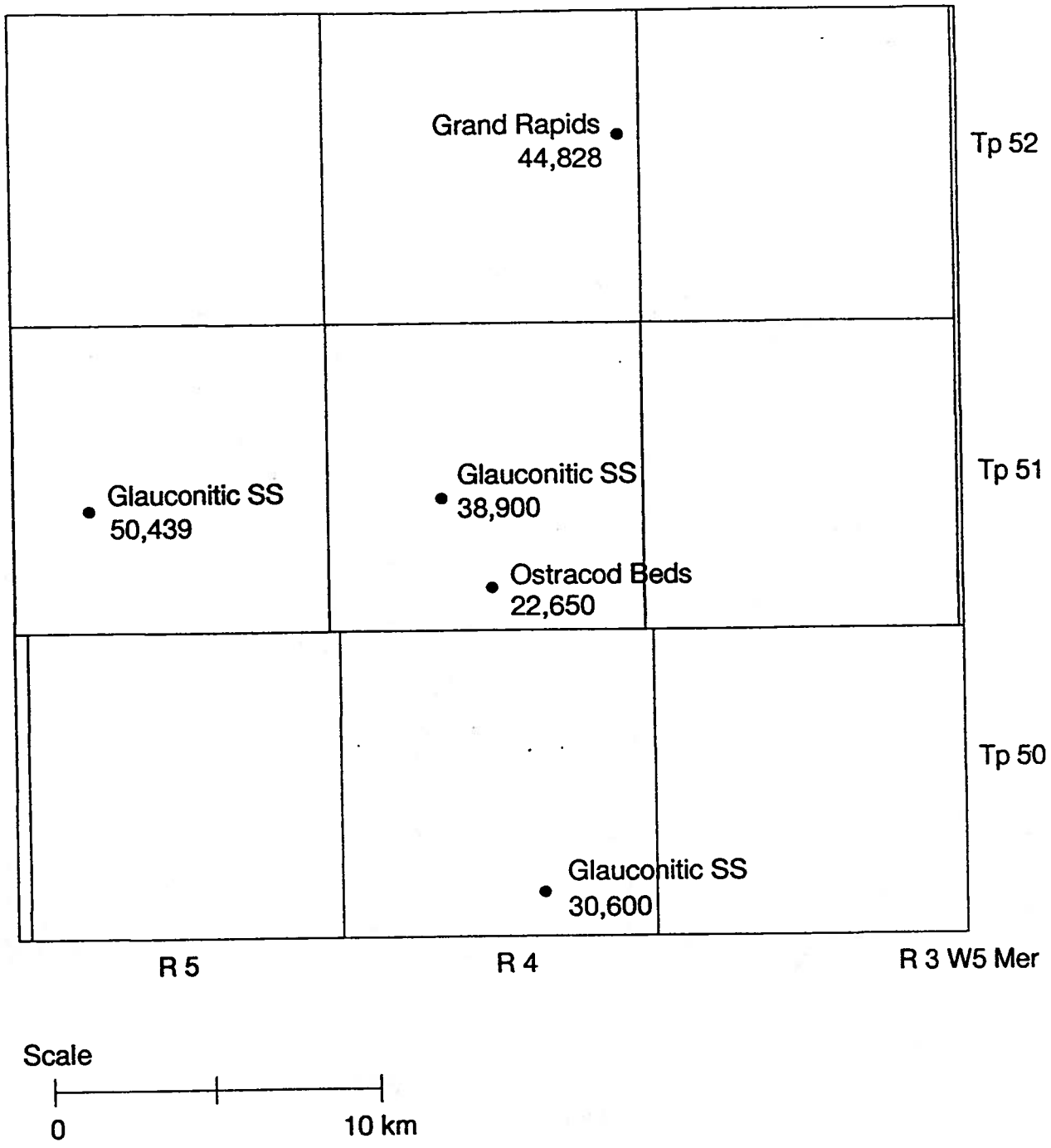

Figure 33: Distribution and chloride content of formation water analyses in Grand Rapids, Glauconitic Sandstone and Ostracod Beds, Mannville Group.

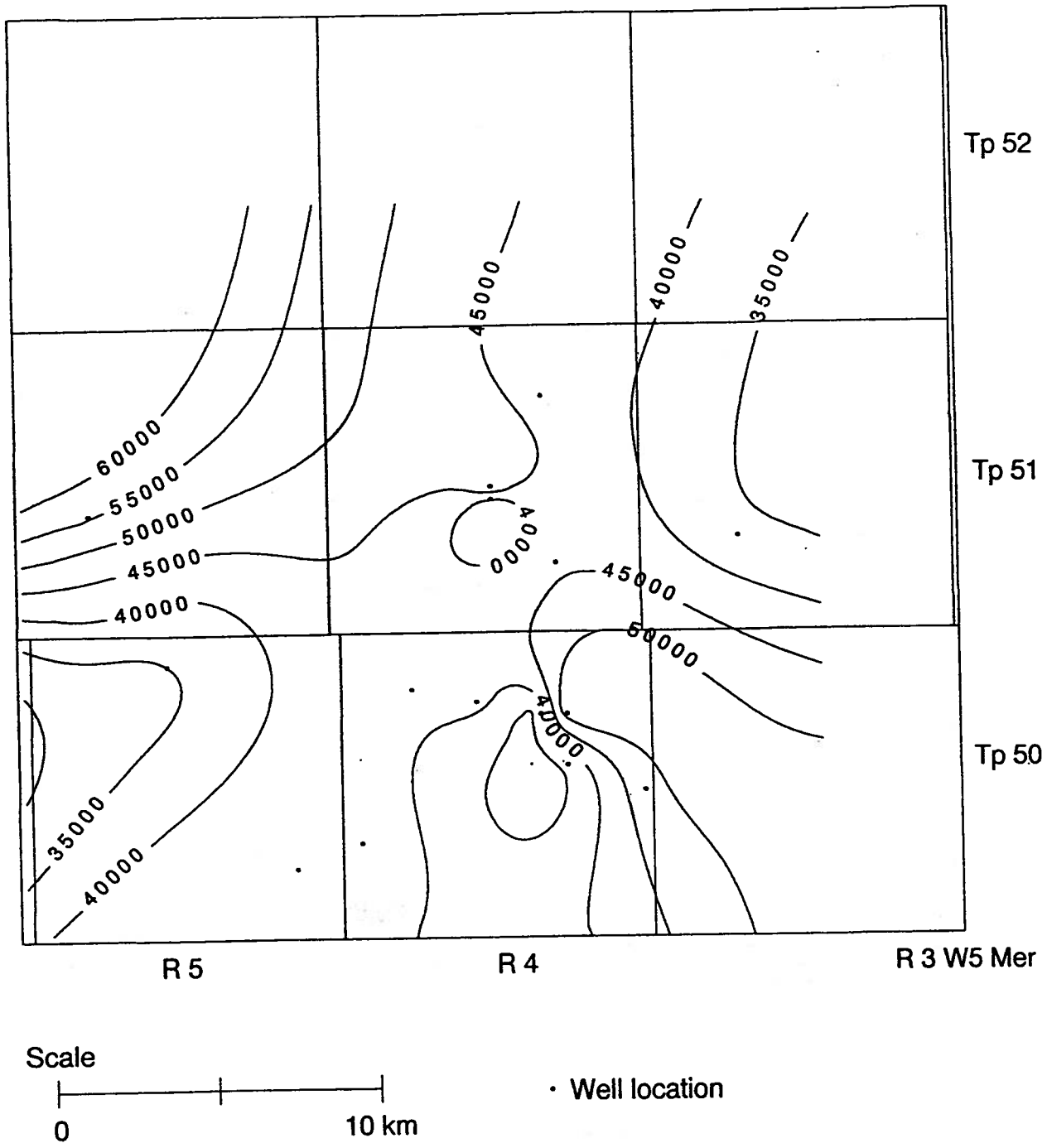

Figure 34: Distribution and chloride content of formation water analyses in the Ellerslie Member, Mannville Group (contour interval: 5000 mg/l).

Table 8. Chemical and physical properties of formation waters in Mannville Group strata within and adjacent to CO_2 disposal study area.

Sample Number	80792-1 (C-13) (Glauconitic)	RCAH50-874A	C-16	C-15	78181-1 (Ellerslie)	78188-2 (Ellerslie)	78192-1 (Ellerslie)
Location	12-16-51-4-W5	6-18-51-2-W5	5-30-49-3-W5	16-20-49-3-W5	6-23-50-4-W5	6-26-50-4-W5	8-27-50-4-W5
Depth (m)	1571.00-1578.00	1507.54-1516.68	1640	1609	1508.50-1512.00	1481.00-1483.00	1502.00-1505.00
Source	-	DST 2	-	-	-	-	-
Recovery	-	274.3 m gc sw 30.4 m oc mud	-	-	-	-	-
Li	12	17	11	12	-	-	-
Na	24800	28800	22600	25900	22800	30653	23379
K	489	690	354	330	885	687	292
Mg	207	578	236	390	219	655	193
Ca	510	2970	888	1350	518	1853	727
Sr	88	215	151	264	-	-	-
Ba	7	3.4	72	395	18.5	2.9	31.5
Cu	-	0.13	-	-	-	0.09	1.6
Ag	-	0.57	-	-	0.3	0.02	0.01
Zn	0.05	-	0.06	0.07	0.01	0.12	0.56
Pb	-	1.1	-	-	0.27	0.32	0.25
Fe	20.19	0.23	0.21	36.74	-	0.33	0.11
Mn	0.21	0.44	1.03	0.99	0.20	0.62	0.32
Al	-	0.54	-	-	0.94	2.16	0.78

Sample Number	80792-1 (C-13) (Glauconitic)	RCAH50-874A	C-16	C-15	78181-1 (Ellersile)	78188-2 (Ellersile)	78192-1 (Ellersile)
B	7	7.8	7	5	5.7	9.4	5.1
PO_4	-	6.2	-	-	5.9	13.9	7.1
NH_3	-	74.8	-	-	-	-	-
SiO_2	-	6.9	-	-	3.0	7.9	3.2
F	-	3.2	-	-	-	-	-
Cl	38900	51600	37200	42700	36557	51528	37639
Br	153	182	129	137	-	-	-
I	-	8	-	-	-	-	-
SO_4	36	366	17	10	79	211	15
HCO_3	1630*	198	790*	725*	280	390	252
Organic acids (total)	-	-	496.1*	377.8*	-	-	-
Total solids (calc.)	66739	85577	62812	72479	60354	84738	62009
pH (laboratory)	6.9	7.20	7.7	7.1	8.0	7.8	7.86
pH (formation temp., °C)	5.84 (65°C)	6.26 (44°C)	5.87 (67°C)	5.80 (65°C)	-	-	-
Density	1.043	1.0616	1.041	1.048	1.0411	1.0570	1.0437
ΔG_{dif}(calcite satn. at formation temperature)							
Anhydrite [$CaSO_4$]	-4.3	-1.8	-4.4	-4.5			

Sample Number	80792-1 (C-13) (Glauconitic)	RCAH50-874A	C-16	C-15	78181-1 (Ellersile)	78188-2 (Ellersile)	78192-1 (Ellersile)
Barite [$BaSO_4$]	-0.8	0.6	0.3	1.1			
Dolomite [$CaMg(CO_3)_2$]	2.3	1.4	2.0	2.1			
Halite [NaCl]	-3.1	-2.6	-3.2	-3.0			
Strontianite [$SrCO_3$]	-0.9	-1.2	-0.9	-0.8			
Siderite [$FeCO_3$]	1.0	-3.1	-2.5	0.7			
Quartz [SiO_2]	-	0.0	-	-			

- = Not determined or below detection

* See Connolly et al. (1990a,b) for equivalent titrated alkalinity, carbonate alkalinity and individual organic acids

representative for geochemical modelling of CO_2 disposal even though it lies just outside the study area. For this sample, quartz was in equilibrium and the ΔG_{diff} of fluorite was 0.52. This suggests that missing values for SiO_2 and F could be set, respectively, to quartz and fluorite saturation at formation temperature. The value for Al is almost certainly too high, but a more correct value can be calculated for equilibrium with whichever is the dominant clay mineral.

HYDRODYNAMIC REGIME

The flow of formation waters in mature sedimentary basins like Alberta is driven generally by topography and buoyancy in regional, intermediate and local flow systems. The small size of the study area (3 x 3 townships) does not allow the identification of any particular flow system. However, thick Colorado shales (tens to a few hundred m) separate the Mannville Group from the ground relief, such that most probably no local topographic influences are present. Regional-scale studies of the flow of formation waters north of the study area (Hitchon, et al., 1990; Bachu and Underschultz, 1993) indicate that the flow in the Mannville Group is generally part of either regional or intermediate-scale flow systems which discharge farther to the east close to the basin edge. The relatively low values and range of both salinity and temperature variations indicate that buoyancy effects caused by density differences are likely to be negligible. Pressure cannot be directly used in the study of flow of formation waters in sloping aquifers because of

hydrostatic effects which normally lead to a pressure increase with depth. In this case, distributions of hydraulic heads, defined as:

$$H = p/\rho_o g + z$$

can be used to study the hydrodynamic regime of formation waters. In the above relation, p is pressure, ρ_o is freshwater density, g is the gravitational constant and z is elevation with respect to the sea level.

The pressure in deep strata is measured using drillstem tests. After extraction from the Alberta Geological Survey Well Data Base, the individual tests were submitted to a process of individual checking and culling, given the relatively low quality of these tests. After allocation of pressure data in the stratigraphic succession and calculation of hydraulic heads, potentiometric surfaces were produced for the units with sufficient data. Most drillstem tests were performed in the Ellerslie Member, which is also a producing unit. The potentiometric surface for this unit (Fig. 35) shows flow generally from south-southeast toward the north, from highs in the 1000 m range to lows in the 600 m range. This flow direction is different from the regional-scale southwest-northeast flow direction in the basin, and most probably is due to as yet unidentified effects at a larger scale than the study area. The drop in hydraulic head is also quite large, leading to high hydraulic gradients in the 15 m/km range. The potentiometric surfaces for the top of the Banff Formation and for the Ostracod Beds (not shown) feature the same characteristics. Most

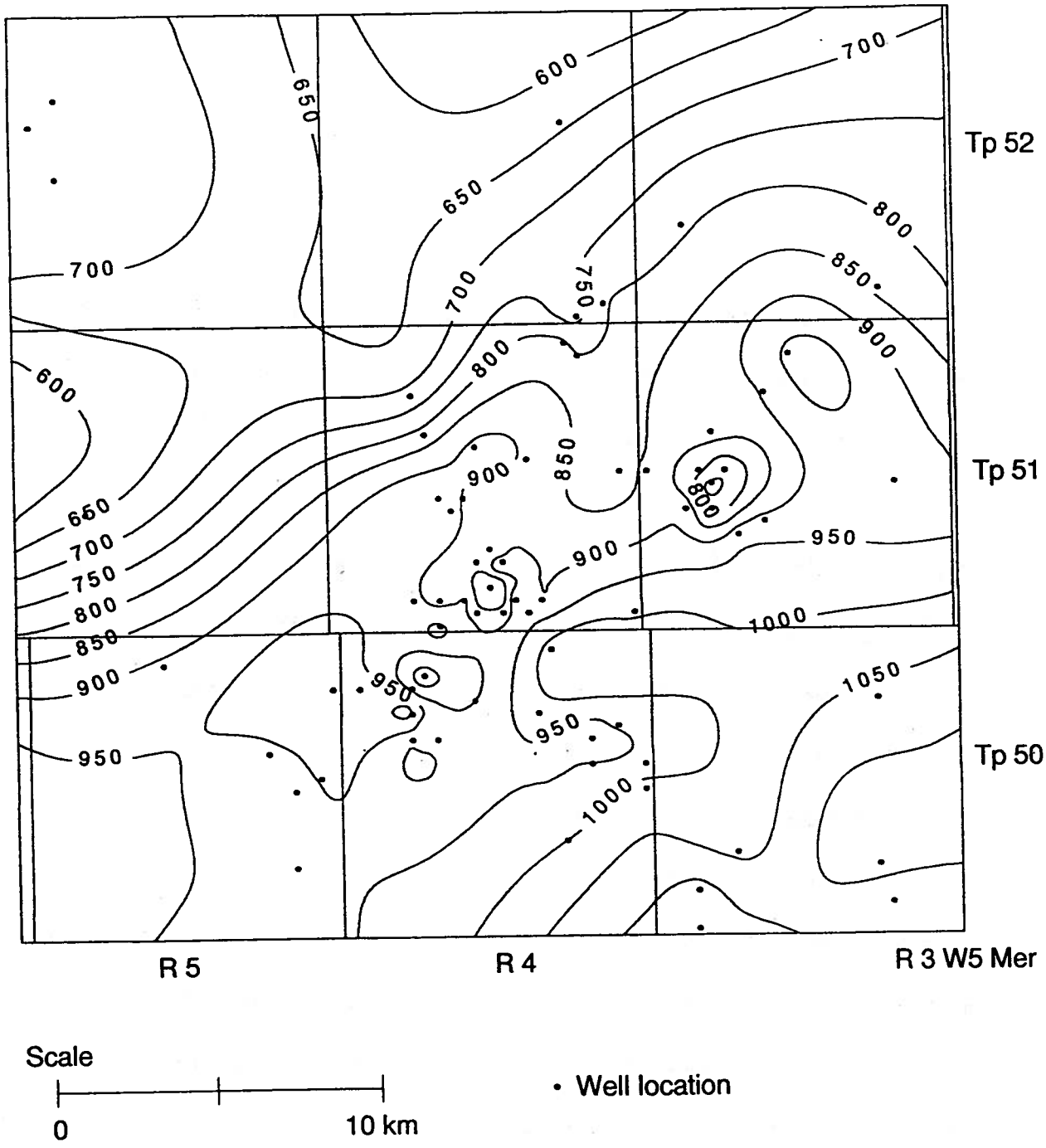

Figure 35: Distribution of freshwater hydraulic head in the Ellerslie Member, Mannville Group (contour interval: 50 m).

of the drillstem tests in the Ostracod Beds are in the lower part of this unit, adjacent to the Ellerslie Member. The commonality in features of the three individual potentiometric surfaces indicates that, hydraulically, the top of the Banff Formation, the Ellerslie Member, and at least the lower part of the Ostracod Beds, form a single aquifer, regardless of their individual rock properties. The flow is part of either a regional or an intermediate-scale flow system which can be identified only at a scale larger than the study area.

The potentiometric surface for the Glauconitic Sandstone (Fig. 36) is quite different from the one for the underlying units. The hydraulic heads are much lower and vary in a much smaller range (550 to 590 m), with corresponding hydraulic gradients of 3 m/km or less. The flow direction is generally to the northeast. Five drillstem tests in the Grand Rapids Formation show hydraulic heads in the 560 to 580 m range similar to the ones in the Glauconitic Sandstone. The marked difference in strength and pattern between the flow of formation water in the Glauconitic Sandstone and in the underlying units indicates that the upper part of the Ostracod Beds form a good, strong aquitard separating the two flow systems. The Glauconitic Sandstone and Grand Rapids aquifers, although separated by an intervening shale layer, exhibit similar hydraulic heads which indicate that either the shale layer is a weak aquitard, or it is discontinuous somewhere upstream of the study area, allowing hydraulic contact between the two aquifers.

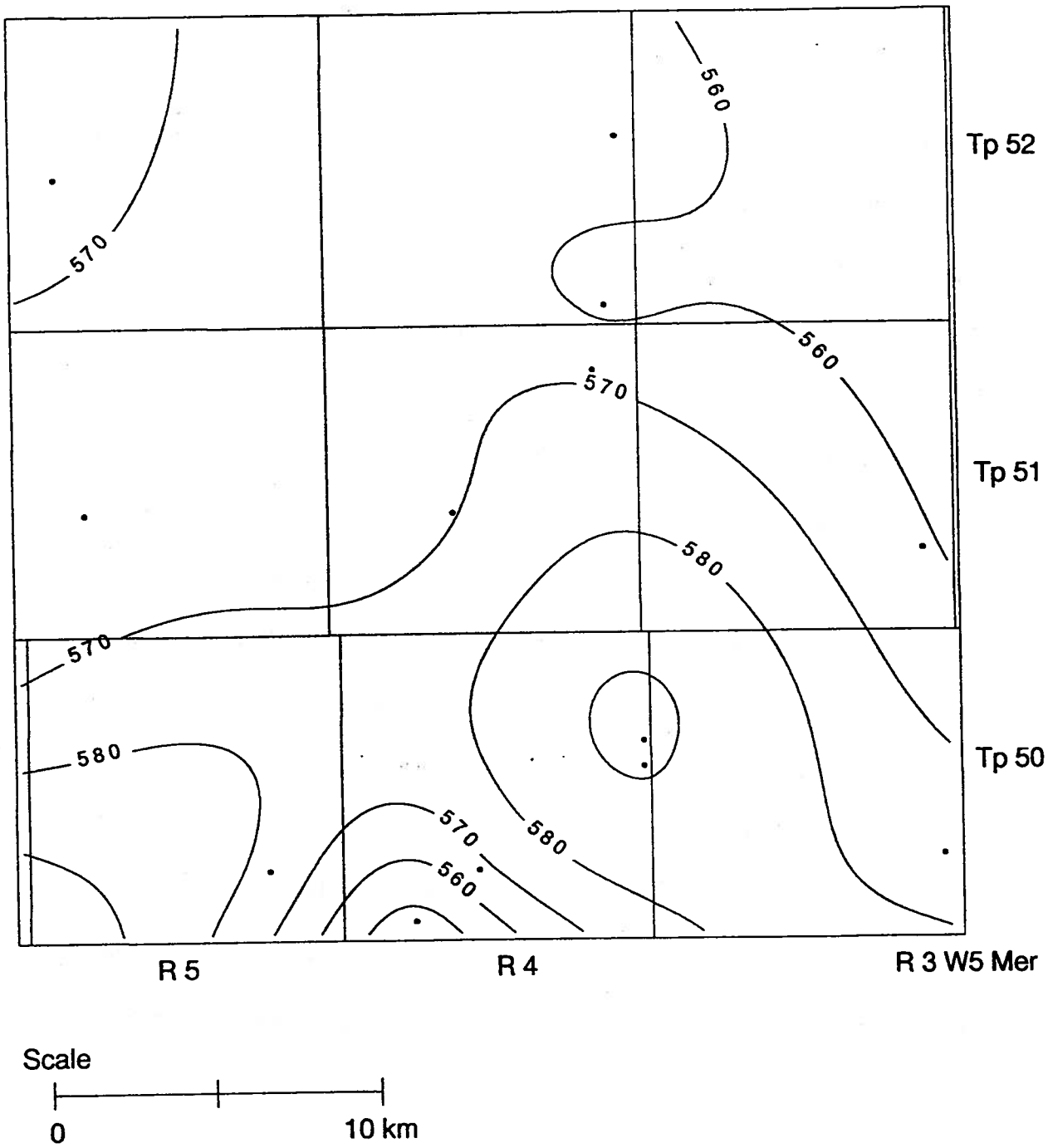

Figure 36: Distribution of fresh water hydraulic head in the Glauconitic Sandstone, Mannville Group (contour interval: 10 m).

CO_2-WATER-ROCK EXPERIMENTS

EXPERIMENTAL PROCEDURES

A set of four autoclave experiments was performed to validate results obtained with the geochemical model. These experiments follow the earlier series of experiments (reported in Phase I - Gunter et al., 1993) performed at room temperature during which very little reaction was observed. Although the geochemical model (PATHUBC) predicted that carbon dioxide would be consumed with carbonate mineral precipitation under certain conditions, the kinetics of reaction at room temperature were much too slow to observe any significant changes experimentally. These later experiments were therefore performed at 105 °C to enhance the kinetics of reaction.

During characterization of the stratigraphy of the study area, the Glauconitic Sandstone was identified as a good potential candidate for disposal. This formation lies just above the siliciclastic Ellerslie sand which was used as a baseline in the previous autoclave experiments. Drill core from this Glauconitic Sandstone formation was used in these later experiments. Also, the salinity of the formation water used in these experiments was significantly higher than in the earlier experiments. Analysis of formation waters in the study area showed a range of compositions. The higher salinity of the water used in these later experiments along with the higher temperature result in lower aqueous carbon dioxide concentrations compared with the earlier experiments.

Drill core from the Glauconitic Sandstone (7-9-50-4W5, samples DW 93-1, -4, -5, and -7) was ground to a fine powder. Relatively pure mineral specimens from Ward's Natural Science Ltd. were also ground to fine powder. The powdered drill core and mineral powders were characterized by XRD and SEM. A synthetic brackish formation water was prepared according to the following recipe based on analysis of RCAH50-874A (see Table 8) from the Mannville group strata within the CO_2 disposal study area:

1.2420 M sodium chloride

0.0176 M potassium chloride

0.0741 M calcium chloride

0.0238 M magnesium chloride

0.0032 M sodium bicarbonate

0.0038 M sodium sulphate

0.0044 M ammonium chloride

0.0025 M strontium chloride

The pH of the water was adjusted to 6.5 with HCl, as the above mixture was slightly super-saturated with calcite.

Mixtures of 10 g of the powdered drill core from the Glauconitic Sandstone spiked with powdered:

1. albite (30 g) (Na-feldspar) (experiment 4711)
2. biotite (30 g) (experiment 4714)
3. labradorite (30 g) (Ca-Na-feldspar) (experiment 4712)
4. control (30 g of Glauconitic Sandstone alone) (experiment 4713)

were placed into 300 ml autoclaves along with 150 g of the synthetic formation water and sealed. The control experiment consisting of the Glauconitic Sandstone alone was prepared to evaluate the reaction rate of the actual reservoir mineralogy under the experimental conditions. Selected pure minerals were combined with the reservoir material to force the desired CO_2-trapping reactions to proceed at a higher rate. Because the sandstone was relatively poor in glauconite, one of the experiments was spiked with biotite (as a suitable source of glauconite could not be located). The composition of the biotite was $(K_{1.74}Na_{0.13})(Fe_{1.38}Mg_{3.89}Mn_{0.03}Ti_{0.22})(Si_{5.83}Al_{1.8})\ O_{20}\ (F_{1.88})$.

Each autoclave was fitted with two ports in the head at the top to facilitate aqueous sampling. One port was affixed with a dip tube which extended to within 1.5 cm of the bottom of the autoclave, and the other with a 2 cm diameter sintered stainless steel filter, with a nominal pore size of 0.5 microns. Autoclaves were flushed with carbon dioxide, and then approximately 0.45 moles (20 g) of carbon dioxide were transferred into each sealed autoclave quantitatively. They were placed in an oil bath at approximately 105 °C. Additional formation water was then quantitatively added to the autoclave (with a syringe pump) to increase the carbon dioxide partial pressure to approximately 90 bars (similar

to the previous experiments). An additional 70 ml to 85 ml of water were added to each autoclave in this way. The autoclaves were inverted daily to mix the contents, as the magnetic stirrers used in the earlier experiments were found to be ineffective through the oil bath.

The autoclave contents were allowed to react for approximately four weeks. During this time the pressures were constantly monitored. The pressure in the autoclaves remained constant over this period and ranged from 90 to 96 bars.

At the end of this time the aqueous contents were sampled. The sampling procedure differed from the earlier experiments because of the higher temperature of these experiments. The autoclave was removed from the oil bath and inverted. A sample tube was pressurized to the autoclave pressure (about 90 bars) with nitrogen and connected at the autoclave head to the port with the filter element. The outlet end of the sample tube was connected to a back pressure regulator (BPR) set to maintain 90 bars pressure. Carbon dioxide was injected at 90 bars through the dip tube into the autoclave, displacing the aqueous sample through the filter, into the sample tube. At the same time the nitrogen was displaced from the sample tube through the BPR to atmosphere. After the contents of the sample tube were flushed about three times, the sample tube was isolated by closing valves at either end. Injection of the carbon dioxide continued into the autoclave, displacing water through a by-pass line along side the sample tube, and through the BPR. This was done until all of the water was displaced from the autoclave.

The replacement of the water, under pressure, ensured that no minerals precipitated as a result of the de-gassing that occurs as a result of depressurization at the end of the experiment. This entire sampling procedure was performed in such a short time that the autoclave contents did not cool significantly (because of the relatively large mass of the autoclave). After cooling and de-pressurization, the autoclaves were opened. All but about 10 g of water (which filled the porosity of the sand mixture) were displaced from the autoclave by the carbon dioxide. The sand was rinsed with de-ionized water, dried and analyzed by XRD and SEM to determine the extent of reaction.

The carbon dioxide was collected quantitatively from the sample tube by slowly depressurizing into a Brooks Gas Meter. The remaining aqueous sample was analyzed for cations (by ICP), alkalinity, chloride and sulphate (by IC).

PRODUCT EXAMINATION

The solid products from the autoclave experiments were examined by X-Ray Diffraction (XRD) and Scanning Electron Microscopy (SEM), and compared to the starting materials. The XRD patterns are shown in Appendix 3. The mineral compositions (from XRD) of the starting materials and post-run products are shown qualitatively in Table 9.

The glauconitic sandstone used as a base for all of the experiments consisted of predominantly quartz with traces of kaolinite, halite and a 10 A clay mineral. The trace

Table 9. XRD Mineralogy of Reaction Products from Autoclave Experiments

Sample ID	Albite High 3.18Å	Magnetite 2.53Å	10Å	Halite 2.82Å	Kaolinite 7.14Å	Labradorite 3.16Å	Pyrite 1.63Å	Quartz 3.33Å
4711 Pre	76.7%			4.2%				19.1%
4711 Post	72.0%			4.0%				24.0%
4712 Pre*				1.1%		78.7%		20.2%
4712 Post		2.7%		3.4%	0.3%	46.2%		47.4%
4713 Pre				0.5%	0.7%			98.8%
4713 Post			0.8%		0.9%			98.3%
4714 Pre			36.2%				5.0%	58.8%
4714 Post			41.4%				6.0%	52.6%
Dw 93 - 1,4,5,7			0.8%	0.9%	1.1%			97.2%

Percentages of minerals are based on relative peak intensities.

Two pre-experiment mixtures were prepared, one was used as the autoclave charge and the other was used for XRD analysis.

* The recorded relative change in the %s of labradorite and quartz between pre- and post-experiment in experiment 4712 is an artifact due to peak splitting of the major XRD peak of labradorite (see Appendix III), and should be ignored.

components of this sand did not consistently appear in XRD patterns of the pre-run mixtures; even for experiment 4713 which was the glauconitic sand alone. This can be attributed to non-random packing of the XRD specimen. Minor variations in the intensity of these XRD peaks after autoclave treatment are therefore not considered significant.

There were no new major reaction products observed in any of the autoclave experiments. No carbonate minerals were detected by XRD or SEM in any of the reaction products. The most notable difference was the presence of a trace of magnetite observed in the products of experiment 4712 (labradorite + sand). The presence of magnetite in the post-run sample was also confirmed by SEM. Some minor differences in relative peak intensity before and after autoclave treatment can again be attributed to non-randomness of the packing of the XRD specimen.

There were no differences between the starting materials and products from experiments 4711 (albite + sand) or 4714 (biotite + sand). There were only some minor variations in the relative intensities of some peaks.

Figures 37 to 40 contain SEM photographs of pre and post-run specimens. There was minimal evidence of hydrothermal alteration in the experiments. Photo #010 in Figure 38 shows a few iron oxide crystals in the products from experiment 4712 (labradorite + sand), which were not present in the starting materials. This confirms the observed magnetite peak in the XRD spectrum of the reaction products. Otherwise there were

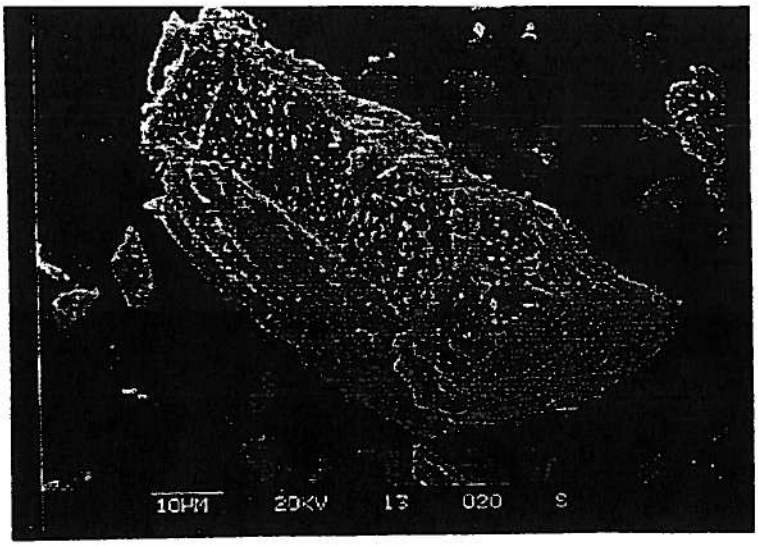

Pre-Run
An Albite grain

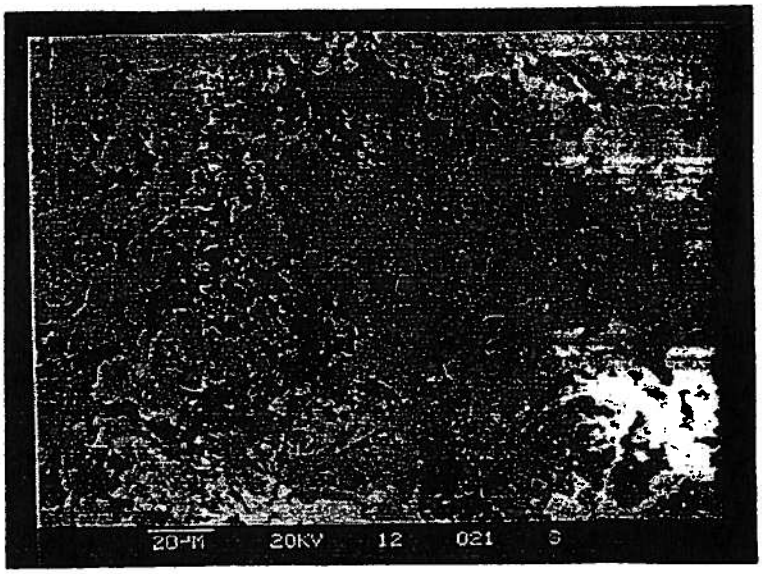

Post-Run
An albite grain covered with fines. There are no obvious dissolution features present. Some iron oxide crystals are visible.

Figure 37: **SEM of Solids from** Autoclave Experiment 4711 (Albite plus Sand).

Pre-Run
Surface of a calcium feldspar

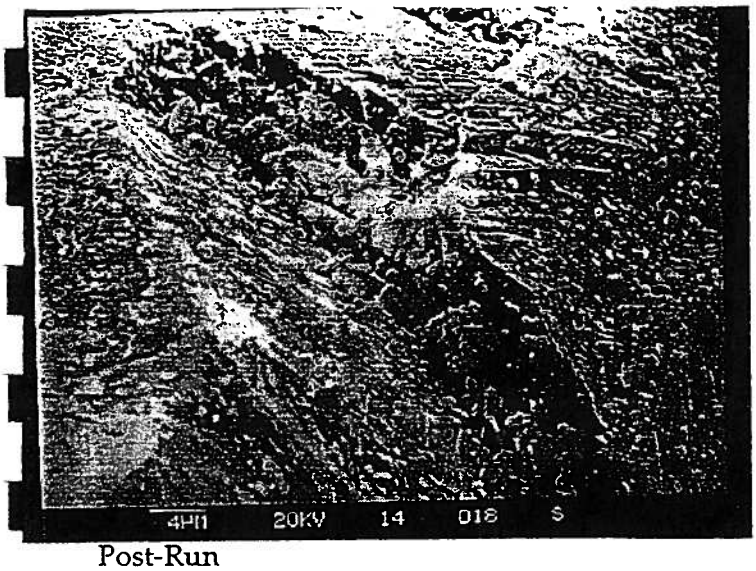

Pre-Run
Natural leaching texture on the surface of a feldspar grain

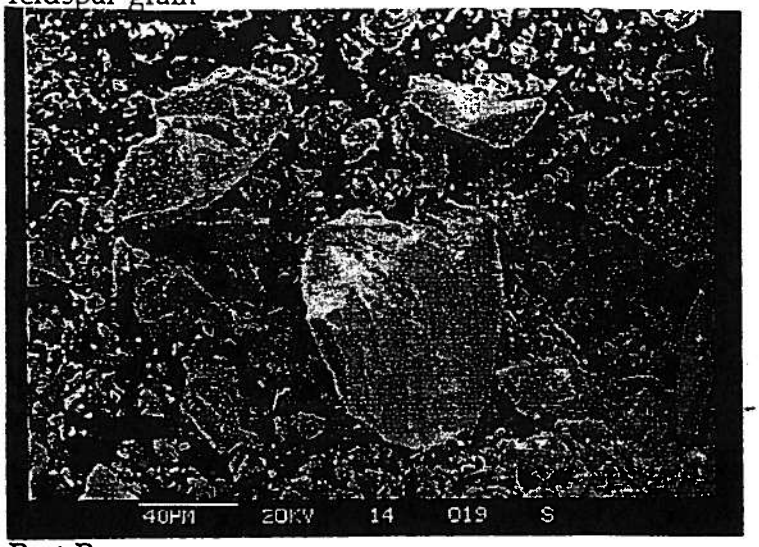

Post-Run
Newly formed iron oxide crystals confirmed with EDX

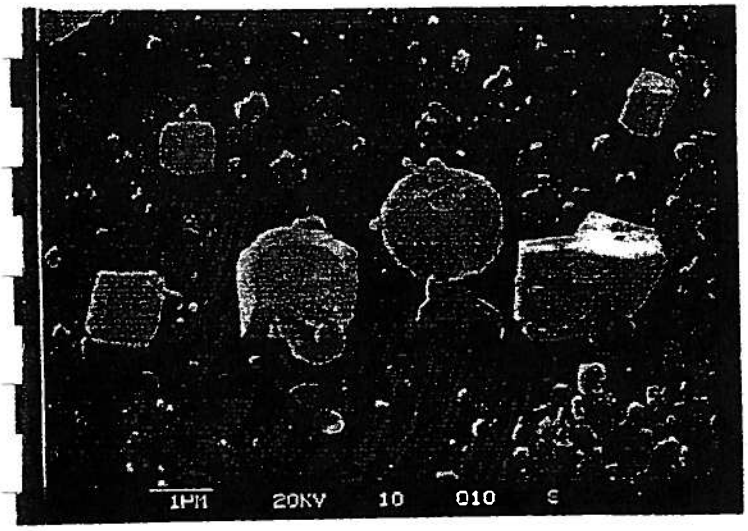

Post-Run
Feldspar surface coated with fines

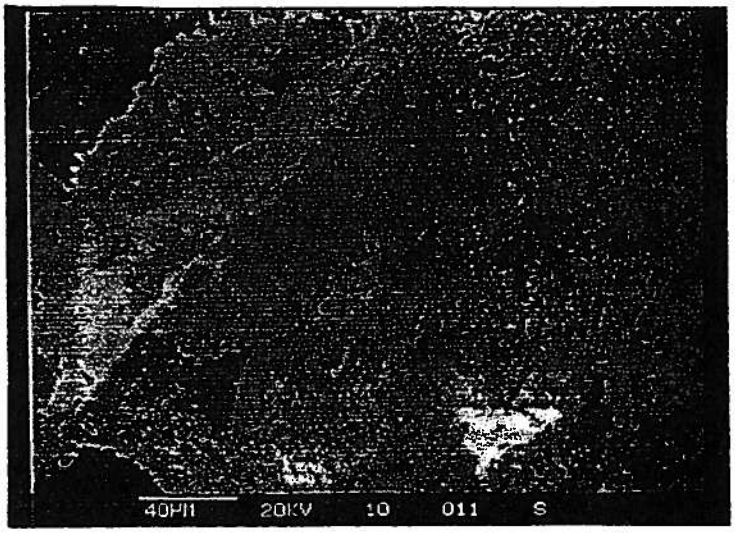

Post-Run
Clean surface of a feldspar grain with no dissolution features

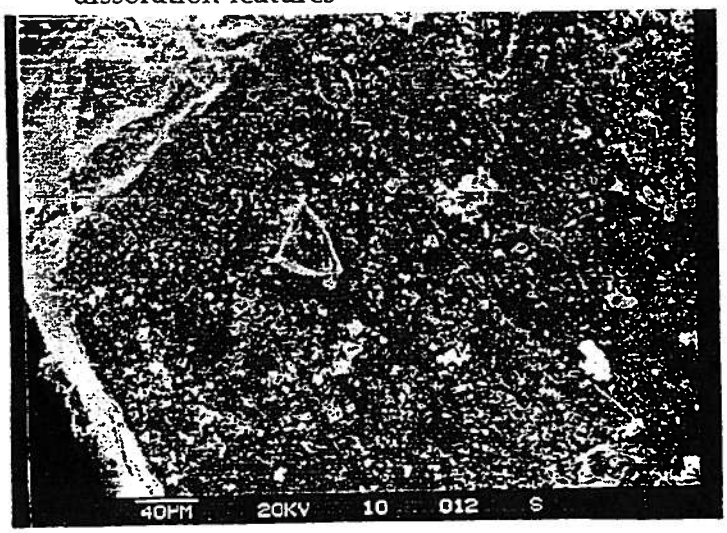

Figure 38: SEM of Solids from Autoclave Experiment 4712 (Labradorite plus Sand)

Pre-Run

Specimen covers a wide distribution of particle size and consists of predominantly quartz. Photos 015, 016 and 017 are of the finest fraction, mainly kaolinite.

Post-Run

Photos 007, 008 and 009 show high and low magnification views of products from the autoclave. There are no visible signs of reaction

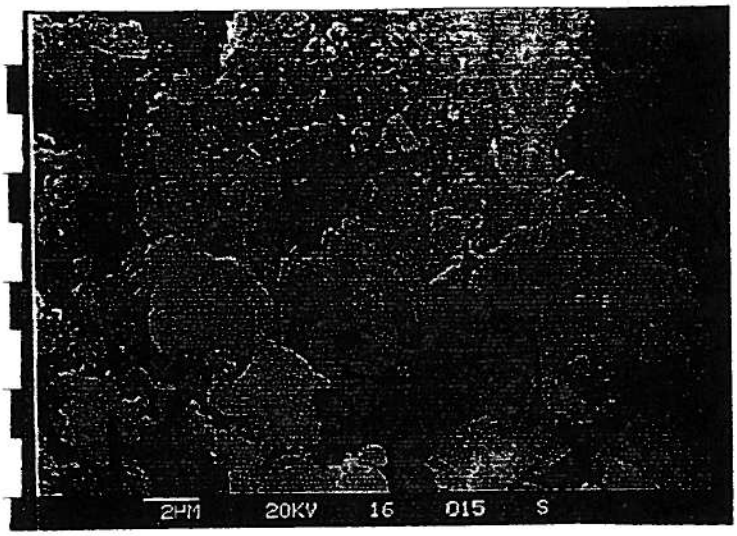

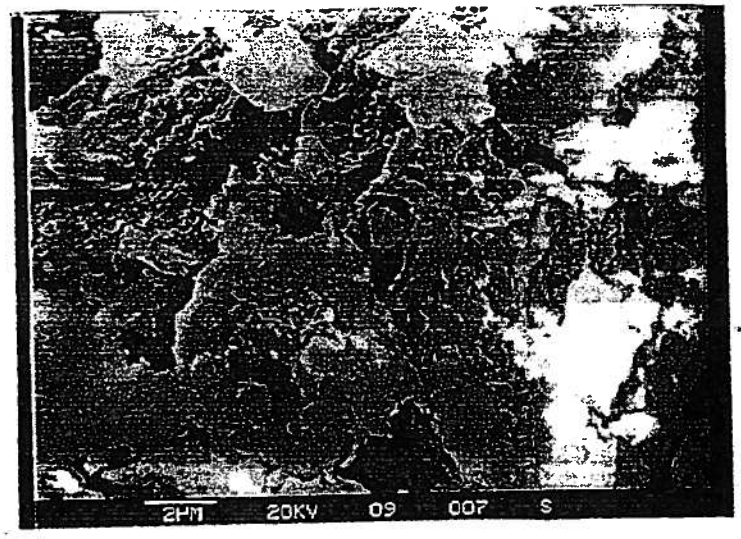

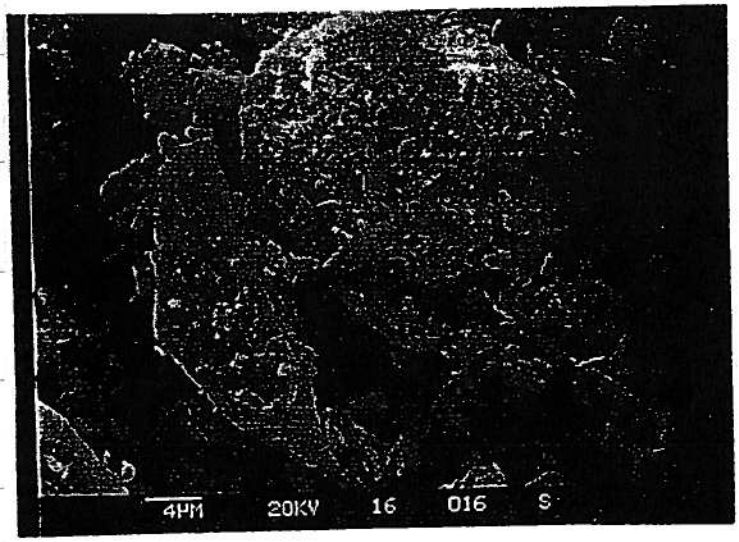

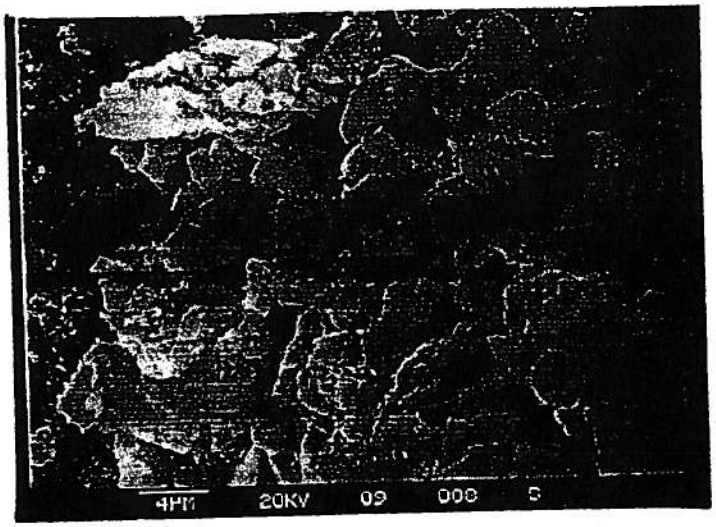

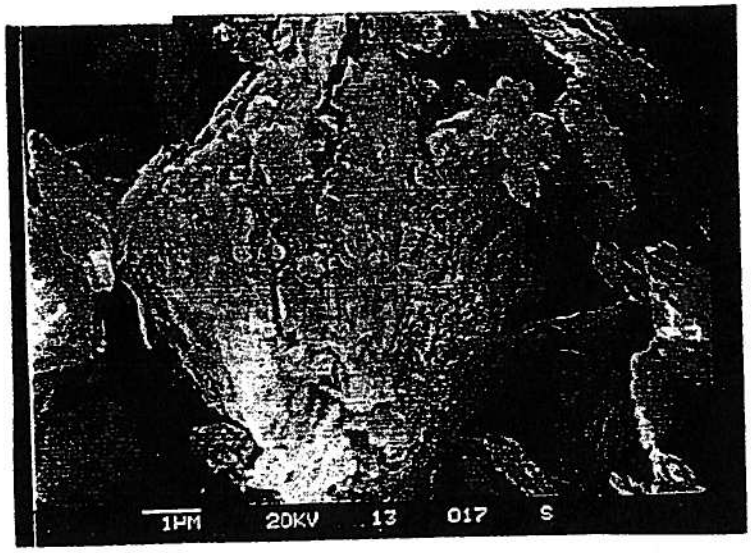

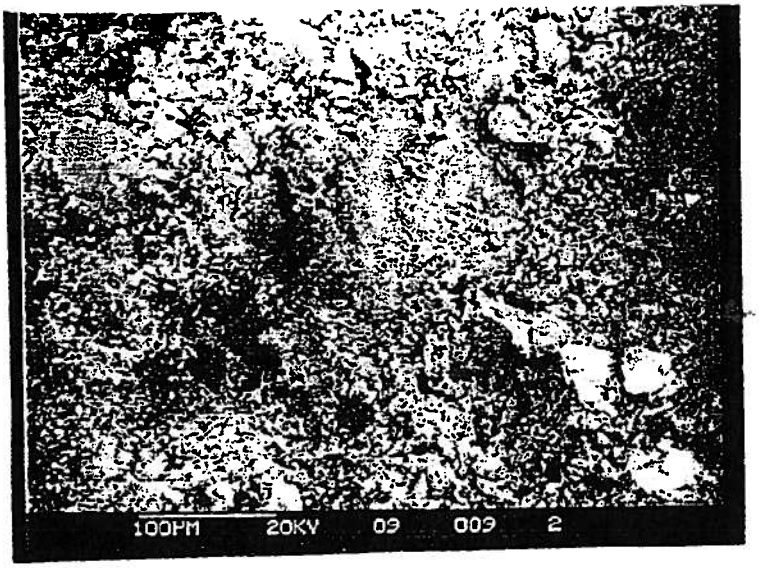

Figure 39: SEM of Solids from Autoclave Experiment 4713 (Sand Only).

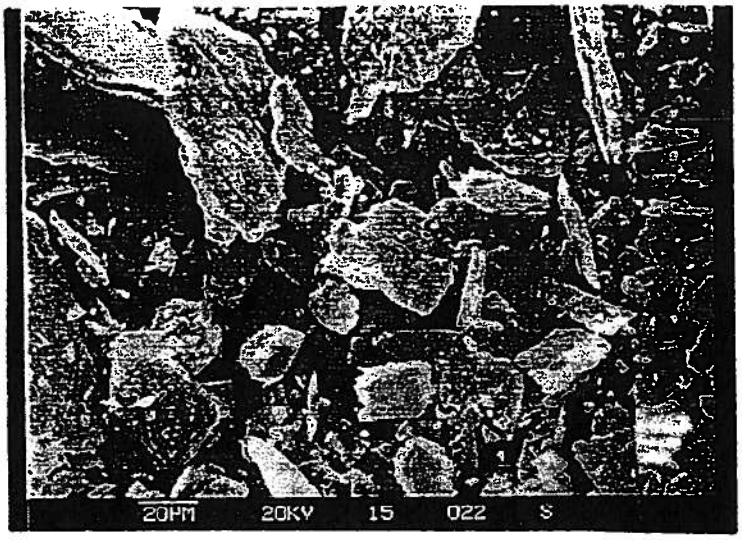

Pre-Run
A general view of the mica (biotite) shows the size distribution of these particles.

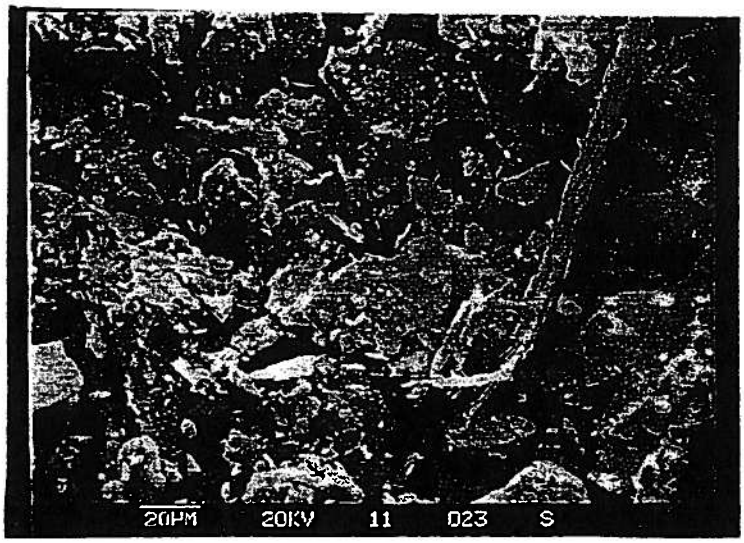

Post-Run
A general view of the post-run mica at similar magnification showing no obvious sign of alteration.

Figure 40: SEM of Solids from Autoclave Experiment 4714 (Biotite and Sand).

no noticeable differences. Photo # 019 in Figure 38, shows a leaching feature on a labradorite crystal. This is a natural leaching feature present in the pre-run as well as the post-run material. No other dissolution textures or grain alterations were evident in any of the other specimens.

Table 10 contains the analysis of the waters from each of the autoclave experiments. The salinity of the pre-run water was significantly higher than the water used in the earlier autoclave experiments at room temperature. The sodium chloride molality of the starting water was 1.25, compared to 0.05 for the earlier experiments. Also, the starting water was saturated with calcite at room temperature (3000 ppm Ca) compared to 5 ppm in the starting water from the previous experiments at 25 °C. The water analysis was therefore not as sensitive to changes in this experiment as in the earlier experiments.

The sodium and chloride values vary around the pre-run composition, and variations are probably due to normal analytical error. Likewise, calcium, magnesium and potassium levels varied only slightly from starting conditions. The magnesium level in experiment 4714 (biotite + sand) was elevated slightly from the starting conditions because of the magnesium component present in the biotite. This resulted in the solution being slightly supersaturated with dolomite at the experimental temperature and P_{CO2} (calculated by SOLMINEQ). However, the presence of any carbonate mineral was not noted in the reaction products.

Aquifer Disposal of Carbon Dioxide Autoclave Experiments at 105 C							
Analysis of Post Run Waters							
Concentration			Pre-Run	4711	4712	4713	4714
mg/L				albite	labradorite	control	biotite
sodium			28814	30035	29748	29443	28919
potassium			690	869	875	900	1007
calcium			2970	3019	3053	3063	3143
magnesium			578	533	536	550	645
silicon				77.9	73.3	48	65.1
aluminum				0	0	0	1
sulphur				122	211	133	123
iron				242	191	222	148
nickel				11.3	31.1	42.3	12.3
manganese				7.3	10.1	9.5	14.3
chromium				0.1	0.2	0.5	0.4
phosphorus				0	0.2	0	0.1
alkalinity(HCO3)			198	990	984	1030	1610
chloride			51600	53100	48800	50000	48900
sulphate			366	550	650	690	640
pH			6.5	6.34	6.31	6.41	6.64
CO2 (molal)				0.65	0.43	0.75	0.54

Table 10. Water chemistry of the formation water in the autoclave experiments.

The alkalinity of the post-run waters increased from approximately 200 ppm in the starting water to about 1000 ppm in experiments 4711, 4712, and 4713 (albite, labradorite, and control). This cannot be explained simply by the imposition of 90 bars of carbon dioxide pressure. Addition of CO_2 will not change the alkalinity. The increase in bicarbonate alkalinity by a factor of five can only be explained through dissolution of basic aluminum silicate minerals by reaction with protons supplied by the addition of the CO_2. The alkalinity increased to about 1600 ppm in the biotite experiment. As in the earlier experiments at 25 °C, the buffering of the solutions due to the silicate mineralogy allows more carbon dioxide to be taken up in the aqueous phase than that predicted from the solubility of CO_2 alone.

The pH of the post-run waters did not change much from the starting conditions. The carbon dioxide dissolved in the water is expected to decrease the pH, however because of buffering by reactions with the silicate mineralogy, the pH was not shifted noticeably. The pH varied in all experiments from 6.3 to 6.6 compared to the starting pH of 6.5.

Sulphur and sulphate concentrations increased during the experiments, probably due to the dissolution of a sulphate mineral such as gypsum (calcium sulphate). A small amount of such a mineral could be present in the glauconitic sandstone below the detection limit of the XRD.

Silica levels increased in all experiments. Increased iron in the water from all the autoclaves reflects dissolution of the glauconite from the reservoir sand.

SUMMARY OF REACTIVITY

None of the spiked mixtures, or the control showed significant reaction or precipitation of new mineral phases. Some reaction was observed in the earlier experiments (as reported in Phase I - Gunter et al, 1993), but they did not proceed to a significant extent due to the slow kinetics at room temperature. Increasing the temperature to 105 °C was expected to increase the kinetic rates sufficiently to observe considerably more reaction than in the earlier experiments. Additionally, the higher salinity of the synthetic formation water used in these higher temperature experiments should tend to enhance the kinetics. Although little reaction was observed by either XRD or SEM, the increased alkalinity of the produced waters indicates that water-rock reactions are proceeding slowly.

The use of an oil bath to maintain the autoclaves at temperature precluded continuous stirring of the autoclave contents. The stir bars were ineffective over the increased thickness of the bath, and the contents had to be manually mixed by inverting the autoclaves daily. The pore fluids in contact with the mineral phases were therefore mixed with the bulk solution only by diffusion, except for occasional mixing by hand. This would have adverse effects on reaction rates.

While the higher temperature and increased salinity tend to increase reaction rates, they also were responsible for significantly reduced dissolved carbon dioxide in solution. SOLMINEQ calculations for the starting waters from the two series of experiments indicate that at similar carbon dioxide partial pressures of approximately 90 bars, the solubility of the carbon dioxide in a brackish formation water at room temperature was 3.0 moles/kg compared to 0.8 moles of carbon dioxide/kg of the higher salinity formation water at 105 °C. Reduction of the solubility of carbon dioxide in solution would lower the the potential amount of carbonate minerals which could precipitate.

Consequently, based on experiments, complete reaction and mineral trapping of CO_2 would take, at a minimum, in the order of years, after the injected CO_2 had dissolved in the formation water. Geochemical modelling must be used to estimate the longer reaction times required.

MODELLING RATES OF CO_2-WATER-ROCK REACTION

In Phase I (Gunter et al., 1993), only relative linear rates of reaction were used to model the CO_2-trapping reactions. In this past year, our geochemical modelling capability has been significantly enhanced by having the option now to use absolute time rate equations in our geochemical computer models. Application of absolute time rate modelling over periods of 100s and 1000s of years is in its infancy but extremely important in evaluating environmental hazards and their solutions. Consequently below we have tried to define our physical and chemical representation of the system we are modeling at some length. It is hoped that this attention to detail will allow the reader to fairly assess our conclusions.

A RATE EQUATION TO DESCRIBE WATER-ROCK INTERACTION

Most data for mineral reaction kinetics is based on the dissolution reaction of the mineral in water. In this report, we are specifically concerned with the reaction rates for silicate and carbonate minerals. In the laboratory, far from equilibrium, silicate dissolution appears to take place in two stages; an initial short rapid parabolic kinetics (i.e. where the concentration in solution builds up in direct proportion to the square root of time) which decays with time to linear kinetics. Holdren and Berner (1979) have attributed the non-linear kinetics exhibited by plagioclase to the dissolution of ultrafine particles which are artifacts produced during grinding of the sample. In the field the bulk of the dissolution

is expected to follow a linear rate law with the dissolution occuring at crystal defects, sites of excess surface energy.

In addition, far from equilibrium, the rate of silicate mineral dissolution appears to vary between "distinct" pH regions; acidic, neutral and basic. Knauss and Wollery (1989) used a rate law of the form:

$$R_+ = R_{acid} + R_{neutral} + R_{base} = (k_{a+}[H^+]^x + k_{n+} + k_{b+}[OH^-]^y)$$

(where the "k"s are the rate constants, "$[a_i]$" represents the activity of the designated aqueous species and x, y are the order of the reaction) to fit their experimental data for muscovite dissolution over the pH range of 1.4 to 11.8. In addition, Sverdrup and Warfvinge (1988) consider additional rate terms dependent on the activities of the aqueous neutral forms of both weak organic (i.e. CH_3COOH) and weak inorganic (i.e. H_2CO_3) acids as important in silicate hydrolysis. For example:

$$R_{CD+} = k_{CD+}[P_{CO2}]^z$$

describes the linear dependency of the rate constant on CO_2 pressure. Plummer et al. (1978) and Chou et al. (1989) found a similar dependence on pH and CO_2 for carbonate mineral dissolution.

Some aqueous species inhibit the reaction of carbonate and silicate minerals in water. The inhibiting effects of phosphate (Burton and Walther, 1990) and Mg^{++} (above a minimum concentration) on carbonate mineral precipitation are well known. In addition to these ions, Na^{+}, K^{+}, Ca^{++} and most notably Al^{+++} can inhibit silicate dissolution (Sverdrup and Warfvinge, 1988) by blocking the reactive sites of dissolution. There are several ways to take account of this in the formulation of the rate equation. One is by including the activity of these ions in the denominator of all the rate terms affected (to act as rate reduction factors) as Sverdrup and Warfvinge (1993) have done. This is the more preferable solution. However in most cases, the existing data is too sketchy to do this. The other method is to include the inhibiting effects in the surface area term.

The rate of reaction depends directly on the amount of surface of the mineral (i.e. surface area = A) in contact with the aqueous phase. A number of authors (e.g. Talman and Nesbitt, 1988, White and Peterson, 1990; Anbeek, 1993) distinguish between "reactive" and "non-reactive" surface area. Reactive surface area (A^{*})is simply that portion of the mineral surface (e.g. possibly related to dislocation density) which is rate controlling in the precipitation or dissolution of the mineral. The total rate of dissolution (R_{+} where "+" indicates dissolution and "-" indicates precipitation) for a mineral is simply:

$$R_{+} = \Sigma_{i}(A^{*}k_{+}[a]^{x})$$

where the Σ_i indicates summation over all the kinetic terms. The total reaction rate is simple the sum of the total rate of dissolution and the total rate of precipitation:

$$R = R_+ + R_-$$

For elementary reactions (see Lasaga, 1981), this expression can be reduced to an equation solely in terms of the dissolution rate constants and the saturation quotient, Ω (see Appendix IV for a detailed derivation and definitions):

$$R = (1-\Omega^n)^m \Sigma_i (A^{\circ} k_+ [a]^x)$$

The term $(1-\Omega^n)$ forces the total rate to approach zero as equilibrium is approached; a necessary requirement of equilibrium. This equation was used in our geochemical modelling code PATHARC to analyze probable water-rock interaction in high CO_2 pressure environments.

RATE CONSTANT DATA

Sverdrup and Warfvinge (1988) have classified minerals into five groups based on their dissolution kinetics in a weathering environment. The most rapidly dissolving group (with rate constants between 10^{-5} to 10^{-8} moles/m^2s) are the carbonate minerals (i.e. calcite, aragonite, dolomite, magnesite and brucite). The silicates are split into three weathering

groups: fast with rate constants between 10^{-9} to $10^{-10.5}$ moles/m^2s (i.e. anorthite, nepheline, jadeite, leucite, spodumene, pyroxenes such as forsterite, diopside, wollastonite, hedenbergite, bronzite, amphiboles such as hornblende and glaucophane, chlorites, garnets and epidotes), intermediate between $10^{-10.5}$ to 10^{-12} moles/m^2s (i.e. pyroxenes such as enstatite, hypersthene, and augite, amphiboles such as tremolite, actinolite and anthophyllite, and sepentines such as chrysotile and talc) and slow between 10^{-12} to 10^{-13} moles/m^2s (i.e. feldspars such as albite, orthoclase, and plagioclase, clay minerals like gibbsite and kaolinite, and micas such as muscovite and biotite). The "non-reactive" or "inert group" with the smallest rate constants (10^{-14} to 10^{-16} moles/m^2s) have quartz, rutile and zircon as representatives.

Often there was rate data available from a variety of sources especially for the k_{n+}s and choices were required. Although the activities of the ions (i.e. $[H^+]$, $[OH^-]$, $[P_{CO2}]$) associated with k_{a+}, k_{b+} and k_{CO2+} respectively (in the rate equation) nominally were raised to the power of one, in certain cases, the power was less than one at 25°C but approached unity at higher temperatures. The largest effect of CO_2 on the rate was for the carbonate minerals. The effects of CO_2 concentration on silicate minerals was thought to be controlled through the proton because H_2CO_3 is a weak acid; and was modeled as such. Also k_{b+} would not be important in CO_2 disposal as the high pressures of CO_2 would force the formation water to remain on the acid side of the pH.

Specific rate data was gathered to be able to model the mineral reactions in the Glauconitic Sandstone aquifer. The mineralogy of the Glauconitic Sandstone aquifer is dominated by quartz with accessory K-feldspar, plagioclase, glauconite, kaolinite, calcite, dolomite and siderite (see Table 3). Rate data for quartz was examined from three sources (Appendix V). Rimstidt and Barnes (1980) data was chosen as it was in close agreement with Knaus and Wollery (1988). Sverdrup's (1990) value for k_{n+} was simply too large to be credible. K-feldspar rate data was also examined from three sources, and was in fair agreement. The data of Helgeson et al. (1984) was chosen because it represented a larger temperature range than the others. Plagioclase is composed of a solid solution of albite and anorthite. Albite rate data was examined from five sources and was in general agreement. Sverdrup's (1990) data was used because it was more complete. Pure anorthite reacts more rapidly then pure albite. However when present in a solid solution in a plagioclase such as labradorite, the overall rates are much closer to those of albite. Consequently Sverdrup's (1990) 25°C data was chosen, but the general activation energy of 55 kilojoules/mole for silicate dissolution kinetics from Walther and Wood (1983) was used to calculate the rates at higher temperatures. Data for glauconite was poor. Glauconite is a member of the mica family. An iron-rich biotite was chosen to proxy for glauconite, taking the 25°C data from Acker and Bricker, 1992 and using an activation energy of 58.6 kilojoules/mole taken from Fleer and Johnston's compilation of rate data. Kaolinite was taken from Sverdrup (1990) in agreement with Carroll and Walther's (1988, 1990) experiments. The carbonates, calcite and dolomite were taken from Plummer et al. (1978) and Busenburg and Plummer (1982) because the

data covered a temperature range but was in general agreement with that of Chou et al. (1989)at 25°C. No data was found for siderite, so it was assumed to have the same rate constants as dolomite. The rate data chosen for the carbonates is not as critical as the silicates because the carbonate minerals react orders of magnitude faster and are nearly always very close to equilibrium where processes take place over a longer period of time.

SENSITIVITY ANALYSIS

The final rate equations used in PATHARC was of the same form for each mineral

$$R = R_{neutral} + R_{acid} + R_{CarbonDioxide} = A^{*}(k_{n+} + k_{a+}[H^{+}]^{x} + k_{CD+}[P_{CO2}]^{z})(1-\Omega^{n})^{m}$$

where n=neutral, a=acid and CD = CO_2, $R_{Carbon\ Dioxide}$ was set to zero for the silicate minerals, and the powers, x, z, n and m were set equal to 1. Consequently the only uncertainities left are found in the rate constants (i.e.the "k"s), and the reactive surface areas (i.e. the "A^{*}"s). The uncertainities in the "k"s have been discussed above and are set at approximately 1 log unit. The reactive surface area, "A^{*}", was set equal to the geometrical surface area, "A". The geometry of the individual mineral grains was considered as constant volume spheres. For this geometry the rate is inversely proportional to the radius of the sphere. That is if you double the radius of the grain for a constant mass of a mineral, the rate of reaction will be halved. The uncertainity is difficult to estimate. Differences between geometrical surface area and BET are

commonly an order-of-magnitude (Sverdrup, 1990) with the additional area found by the BET method being attributed to surface roughness. However the corrrelation of these two natural surface areas to reactive surface area is not simple, and is a complicated function of grain size (Anbeek, 1993). White and Peterson (1990) suggest that reactive surface areas are one to three orders-of-magnitude lower than physical surface areas. Consequently using geometrical surface areas yields a conservative estimate of "A"; with an uncertainity set at one order-of-magnitude for most cases. Therefore, if these arguments are correct, the total uncertainity in our calculations would be two orders-of-magnitude in absolute time.

COMPUTER MODELS AND INITIAL CONDITIONS

Modelling of water-rock reactions were carried out at 25°C and 100 bars of CO_2 pressure, under laboratory systems conditions of 105°C and 90 bars of CO_2 pressure and at aquifer temperature of 54°C at injection pressures of 260 bars of CO_2 on stoichiometric end member mineralogies (i.e. pure Na-, K-, Ca-, Fe- and Mg- minerals) using the mass transfer geochemical computer code PATHARC and SOLMINEQ88 (Kharaka et al., 1988). PATHARC is a highly modified and improved version of PATHUBC (Perkins, 1980). PATHUBC was used extensively for the geochemical modelling in the Phase I report (Gunter et al., 1993). PATHUBC calculates the path of water-rock reaction for a given set of reactants as a function of the progress variable, 'XI' which is proportional to the log of time. 'XI' is used to define the molar amount of reactant phases added to the

aqueous phase per step. This effectively results in a constant surface area, far from equilibrium kinetics, essentially a constant relative linear kinetic rate law. The relative reaction rate for each reactant are defined by a user specified factor with the default of one normally being used. In PATHARC, "XI" is replaced by absolute time by using absolute rate equations for each reactant mineral. The surface area of each phase is specified at the start of each run by specifying the grain radius. The modelling does not take into account the effects of solid solution on the size of each of the mineral stability fields, even though feldspars, zeolites and clays generally do form solid solutions in the same mineral group. The reason for this assumption is simplicity; the thermodynamic data for solid solution minerals is non-existant or poor, and the numerical methods for calculating dynamic equilibrium for solid solution minerals are intractable.

The initial conditions necessary to run PATHARC include the formation water chemistry, the mass (specified in grams) of each of the formation minerals in equilibrium with the formation water (equilibrium phases) and the mass (specified in grams), grain size (specified in millimeters), and kinetic parameters for each reactant phase. Reactant phases are those phases not in equilibrium with the formation fluid. (In the previous report, carbon dioxide gas was treated as a reactant phase.) As time progresses, the reactants dissolve into the formation water, thus modifying the formation water composition. The change in formation water composition may be buffered by the precipitation (or dissolution) of the equilibrium phases or by the formation of new equilibrium phases. Often an equilibrium phase is formed but later completely reacts out,

with none left in the system. PATHARC terminates when equilibrium has been achieved with all of the reactant phase(s) and/or when all of the reactant phase(s) have reacted out.

The formation water chemistry was chosen to represent the Glauconitic Sandstone aquifer as described in Table 8 (sample RCAH50-874A). The equilibrium phases used for the initial conditions were based upon the observed formation mineralogy, but modified to obtain the necessary *end member composition* constraints. The amount of equilibrium minerals present is calculated from the porosity. Assuming an average porosity of 12% for the Glauconitic Sandstone aquifer and an average rock density of 2.5, there are approximately 18,000 grams of rock per 1000 grams of water. Even if the porosity is doubled to 20%, the weight of rock would only be reduced to 10,000 grams. For the former case, the presence of 5 wt% of a mineral phase would account for 900 grams of that phase being contacted by 1000 grams of water.

In these calculation, equilibrium of the aqueous phase with the injected CO_2 is maintained at all times (i.e. CO_2 is an equilibrium phase in the context of the modelling). It is assumed that the solution of injected CO_2 in the formation water is fast relative to the mineral reactions with the formation water.

Glauconite is an iron bearing sheet silicate present in the formation. Unfortunately, thermodynamic data is not available for it, and annite (an iron endmember of biotite) was used in the modelling as a proxy.

TEST RUN OF PATHARC

In the Phase I report (Gunter et al, 1993) based on modelling using PATHUBC, it was concluded that **reactions with basic aluminosilicate minerals (i.e. feldspars, chlorites, biotites, glauconites) would sequester injected CO_2 in two forms, either as bicarbonate ions dissolved in the formation water or by precipitating a carbonate mineral. Which mechanism occurred depended on the dominant cation released by the aluminosilicate minerals. If the dominant cation was Na^+ or K^+, then the concentration of bicarbonate built up in the aqueous phase forming a bicarbonate brine. Bicarbonate concentration was not constrained because of the high solubility of sodium and potassium carbonate minerals. If the dominate cation was Ca^{++}, Mg^{++} or Fe^{++}, the concentration of bicarbonate would not build up due to the low solubility of calcite, dolomite and siderite which precipitated.** In this report, the results of the modelling with PATHARC have not changed greatly with regard to the minerals dissolved and precipitated (There are differences in the figures presented in the two reports, however this is due to a different (more appropriate) formation fluid composition, more detailed formation mineralogy and the addition of kinetic rate equations

for the reactant phases). **Our goal here is to evaluate the time it takes for these reactions to occur so that eventually the mineral-time trapping of the injected CO_2 in the aquifer can be mapped out in detail in 3 dimensional space.**

Albite dissolution in the Glauconitic Sandstone aquifer formation water was numerically simulated to test both the neutral (k_{n+}) and the acidic (k_{a+}) rate constants, and the results are shown in Figure 41 a, b, c, and d. One hundred grams of albite were dissolved in a 1000 grams of water at 25°C and 100 bars of CO_2 pressure. The starting pH of the formation water was adjusted from 7.2 to 3.14 using SOLMINEQ88 to reflect the equilibration of 100 bars of CO_2 pressure. At the low temperature of 25°C, amorphous silica controls the level of dissolved silica in the solution; quartz is metastable. To achieve this, the precipitation of quartz was suppressed in PATHARC. The grain diameter for albite used was 10 microns which is equivalent to a total surface area of 22 square meters of albite/1000 grams H_2O. By the time all the albite had reacted out, the pH shifts from 3.14 to 5.02 and the total bicarbonate concentration had risen 100 times to 0.2molal (Figure 41 a). The final bicarbonate concentration is only controlled by the amount of albite reacting out. If 500 grams of albite were reacted out, the final bicarbonate concentration would be in excess of 1 molal. Significant amounts of amorphous silica precipitated and the solution silica levels were elevated. Because of the high dissolved silica levels, pyrophyllite precipitated out instead of kaolinite. A small amount of calcite and dolomite precipitated due to the high calcium and magnesium

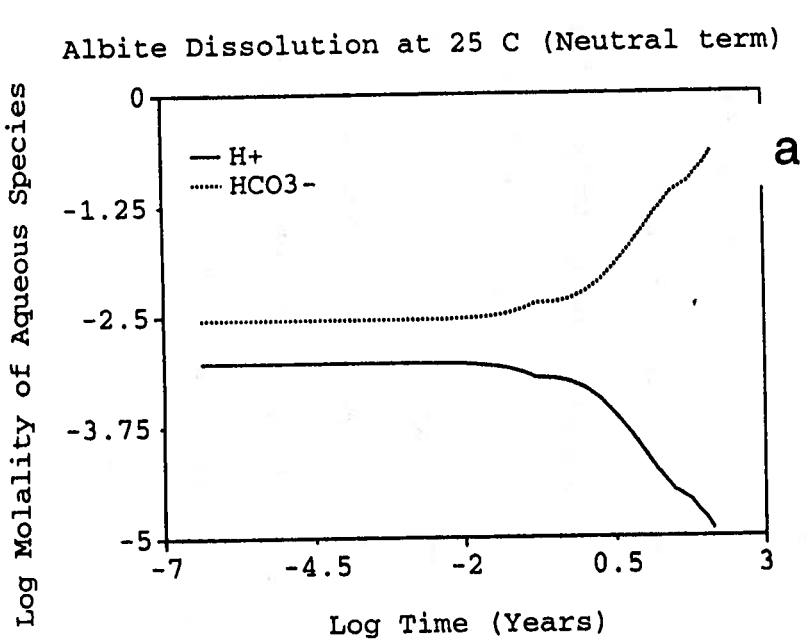

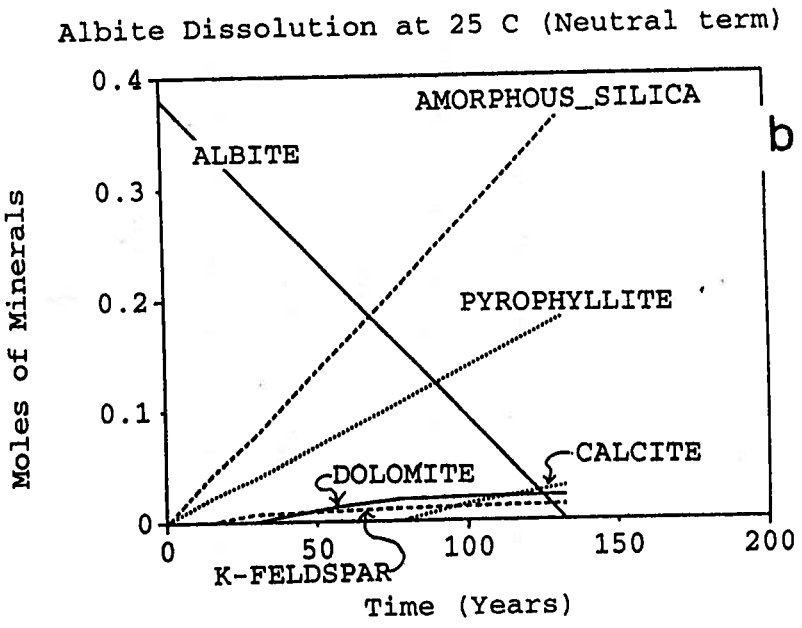

Figure 41. PATHARC geochemical modelling of **albite dissolution** at 25°C &100 bars CO_2 pressure

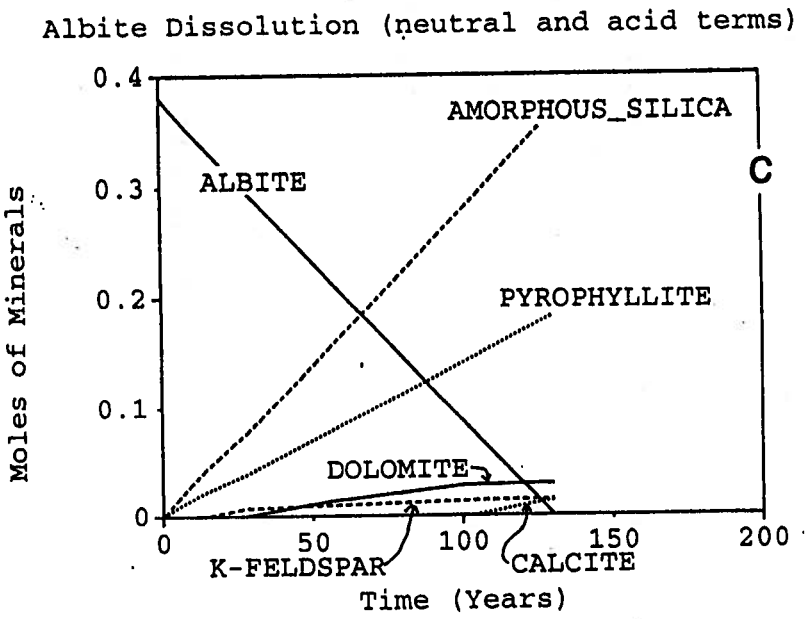

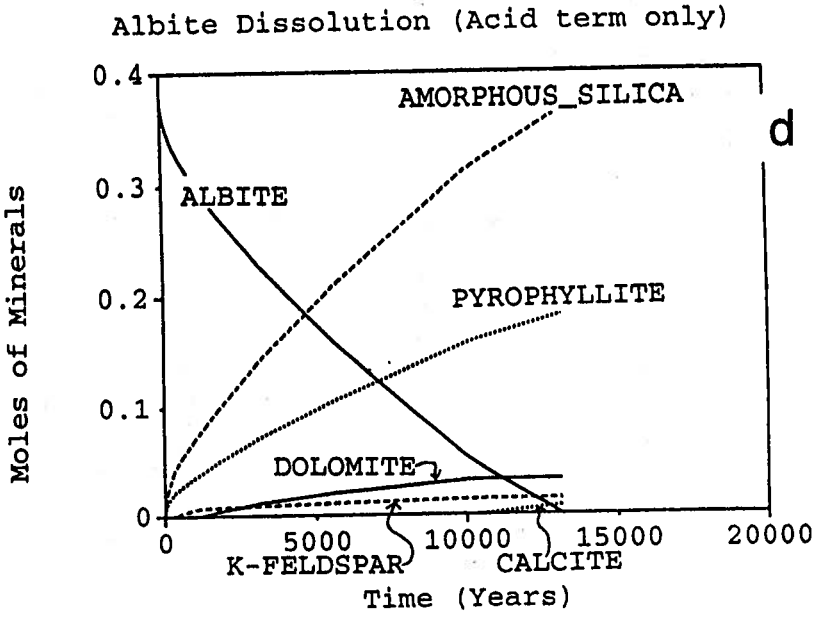

concentrations in the formation water. Small amounts of potassium feldspar precipitated because of the initial potassium in the formation fluid and the increased silica levels. The results are shown in Figure 41 b.

If only the effect of the proton on the rate constant is considered, it takes 13,000 years for 100 grams of albite to completely react out (Figure 41 d). When only the neutral rate constant is considered, the time is reduced to 130 years (Figure 41 b). When both the neutral and acid rate constant terms are used together, the effect of the acid rate constant is only seen in the beginning when the pH is low (Figure 41 c).

The effects of considering the different rate terms were duplicated by hand calculations. The hand calculation times were similar to the results calculated by PATHARC, well within the errors introducted by the simplifing assumptions introduced for hand calculations.

MODELLING OF THE AUTOCLAVE EXPERIMENTS

The grain size from the SEM pictures of the starting materials ranged from 2 mm to 1 micron. An average grain diameter of 100 microns was used in the modelling. The conditions of all the autoclave experiments were 105°C and 90 bars CO_2 pressure. Raising the Glauconitic Sand formation water to this temperature and pressure, causes the pH of the formation water to shift from 7.2 at 25°C to 3.47 as calculated by SOLMINEQ88. The mineralogy and grams of minerals standardized to 1000 grams of

water are tabulated in Table 11. All of the four autoclave experiments, contained a significant amount of the Glauconitic Sandstone powder as starting material.

The control experiment consists of 100% Glauconitic Sandstone in the formation water. PATHARC predicts that equilibrium with the formation water would take 40 years to achieve in the autoclave (Figure 42). As would be expected, the fastest reaction is the disappearance of calcite. This is shown in Figure 42 b (normal time scale) and 42 c (log time scale). It takes 6 years to react out the annite which is accompanied by the growth of siderite and kaolinite (Figure 42 a and b). This rapid growth of siderite is driven by the release of iron from the annite (biotite). Albite and K-feldspar completely react out between 30 and 40 years. As they react out, muscovite forms, in part from kaolinite. Although it is not shown on these figures because of the large amount present, quartz forms almost continuously during the reaction.

All of these reactions are too slow to be monitored in the autoclave experiment. This is not the case for the change in the formation water composition. The increase in the alkalinity by a factor of 5 to 10, observed in the experiments, is predicted to occur in less than a day by PATHARC (Figure 42 d). After this rapid initial change, only some minor changes are predicted to occur over the next 40 years, but they would be much too small to measure reliably.

Table 11: Mineral Weight in Grams/1000 Grams of Water

		Minerals Identified											
Expt.	Total Mineral Wt/1000 Grams H_2O	Albite	Biotite	Labradorite	Quartz	K-Feldspar	Plagioclase	Glauconite	Kaolinite	Calcite	Dolomite	Siderite	Porosity
4711	267	200	---	---	58	1.4	0.7	3.3	1.4	0.7	0.7	0.7	---
4714	267	---	200	---	58	1.4	0.7	3.3	1.4	0.7	0.7	0.7	---
4712	267	---	---	200	58	1.4	0.7	3.3	1.4	0.7	0.7	0.7	---
4713	200	---	---	---	174	4	2	10	4	2	2	2	---
Aquifer	18,333	---	---	---	15,950	367	183	917	367	183	183	183	12%
	PATHARC Minerals	Albite	Annite	Anorthite & Albite	Alpha-Quartz	K-Feldspar	Albite	Annite	Kaolinite	Calcite	Dolomite	Siderite	

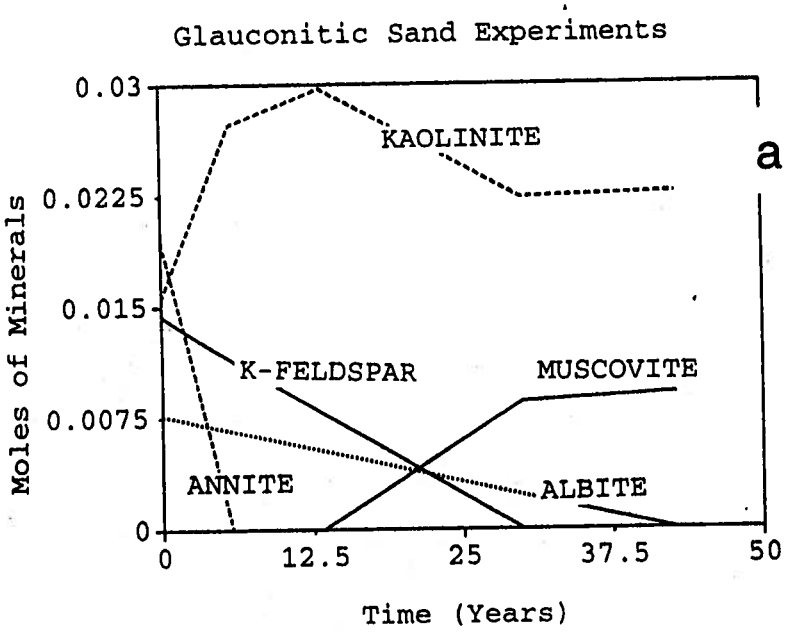

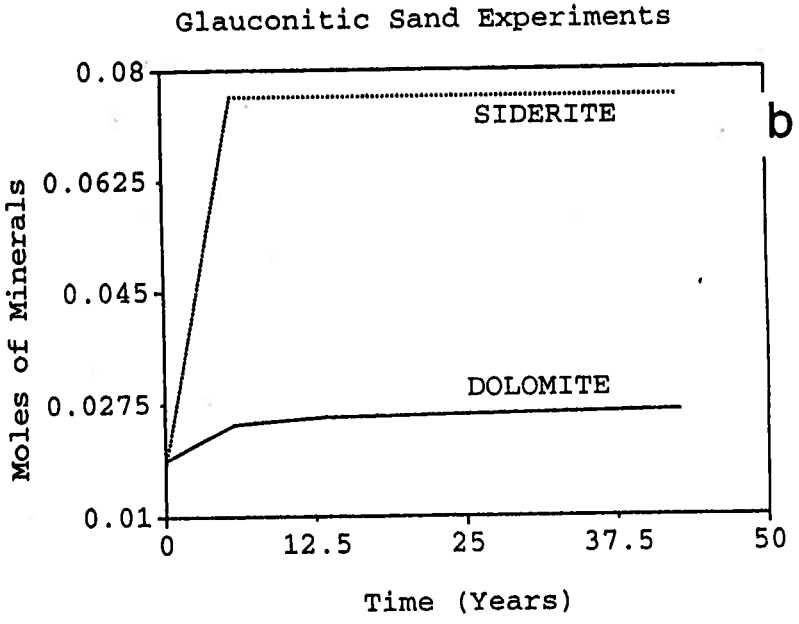

Figure 42. PATHARC geochemical modelling of Glauconitic Sand **control** autoclave experiment at 105°C & 90 bars CO_2

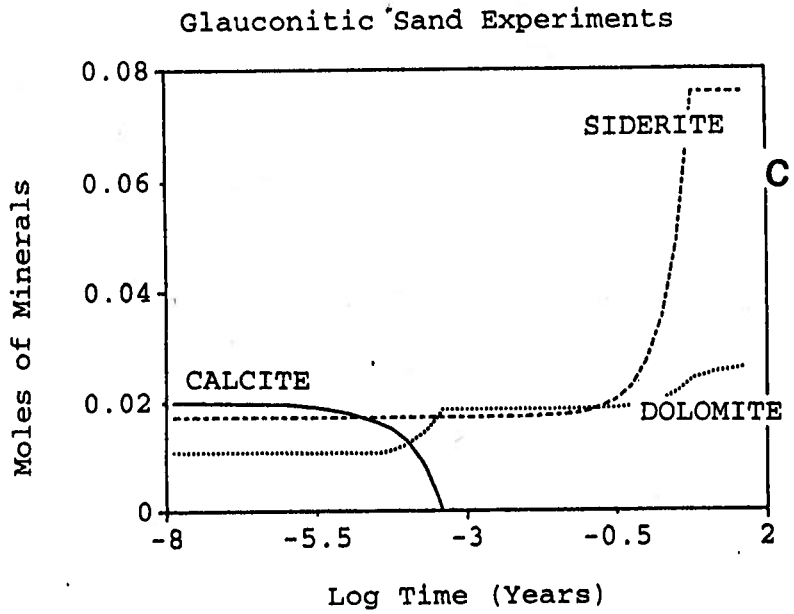

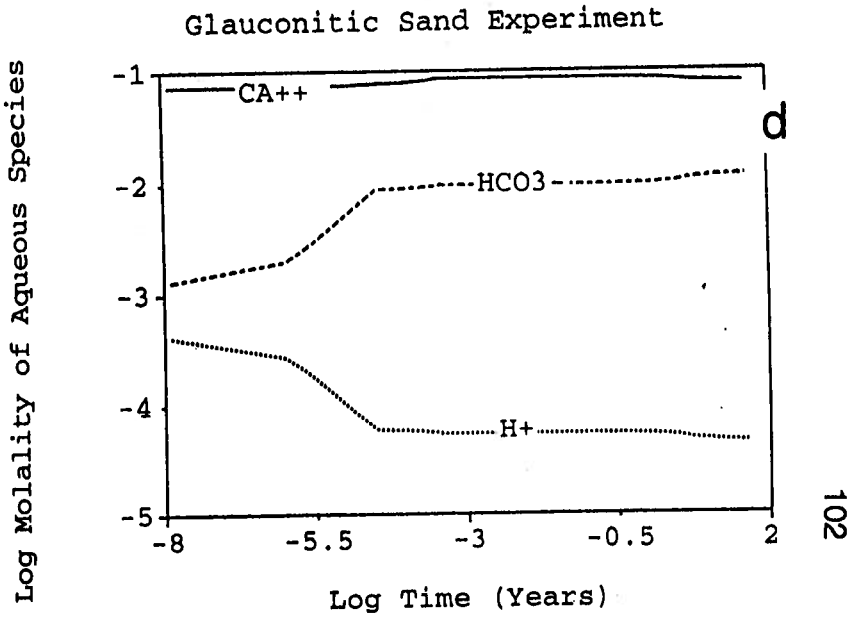

In the control experiment, the large amount of quartz (approximately 87% of the solid charge) masked changes to the other mineral phases when they were examined by XRD and SEM at the conclusion of the experiment. It was hoped that by spiking the glauconitic sandstone powder with large amounts of basic aluminosilicate minerals, the increased surface area would allow enough reaction to take place so that a change in the amount of the solids could be detected. Unfortunately this was not the case. The reasons for this can be examined using PATHARC.

Figure 43 details the calculated results when the experiment is spiked with albite. However it still takes over 40 years to react out all the albite and almost 60 years to reach complete equilibrium (In one month, only 60 milligrams of albite would react out - around 0.25% of the total). The effect of adding albite is to modify the reactions. As for the base case, kaolinite is synthesized at the expense of the albite. Slightly more muscovite is formed until the Na^+ concentration builds up high enough in solution to stabilize Na-smectite; and then the kaolinite breaks down completely and muscovite formation slows down. As in the control experiment, calcite reacts out completely and rapidly (so quickly that it can not be seen on Figure 43 c. However, after a number of years it begins to form and quickly becomes the dominate carbonate mineral.

In the labradorite spike experiment, labradorite was represented by the two feldspar end members, albite and anorthite, in a 40 : 60 ratio. The resulting mineralogy is similar as for the albite spiked experiment, with anorthite reacting out completely about 5 years

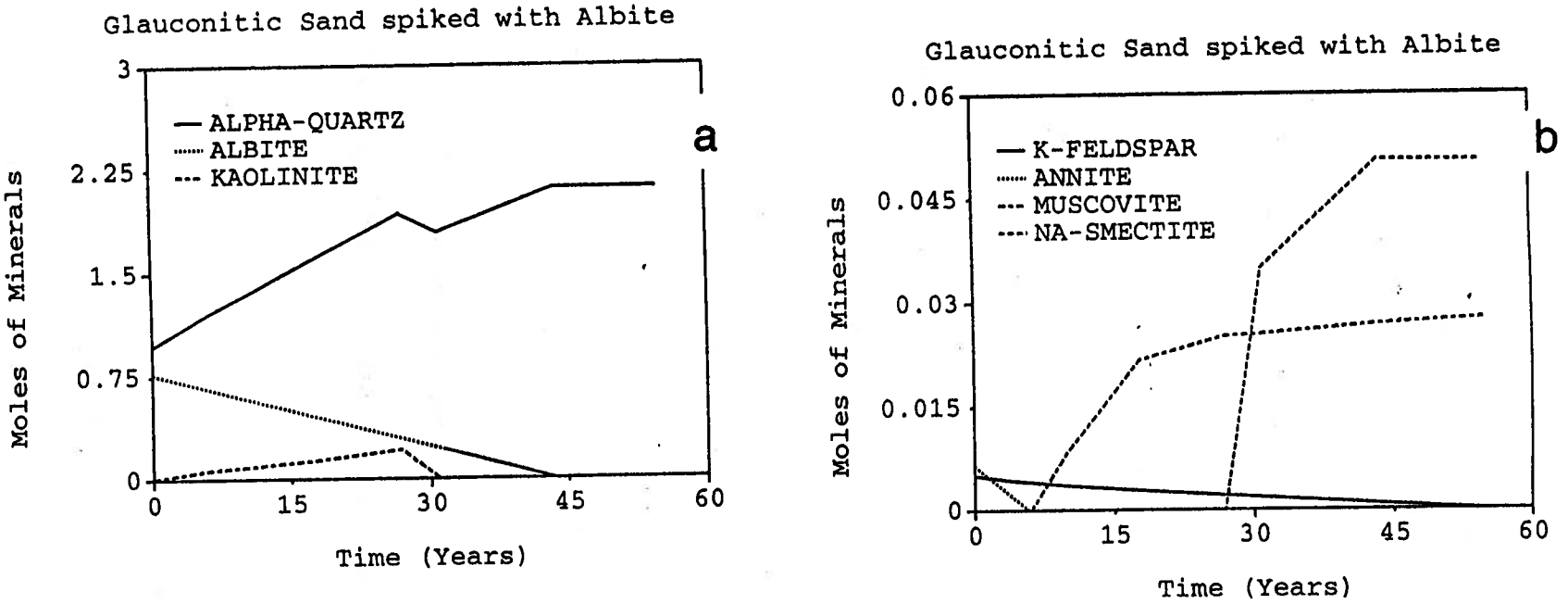

Figure 43. PATHARC modelling of Glauconitic Sand **spiked with albite** autoclave experiment at 105°C & 90 bars CO_2

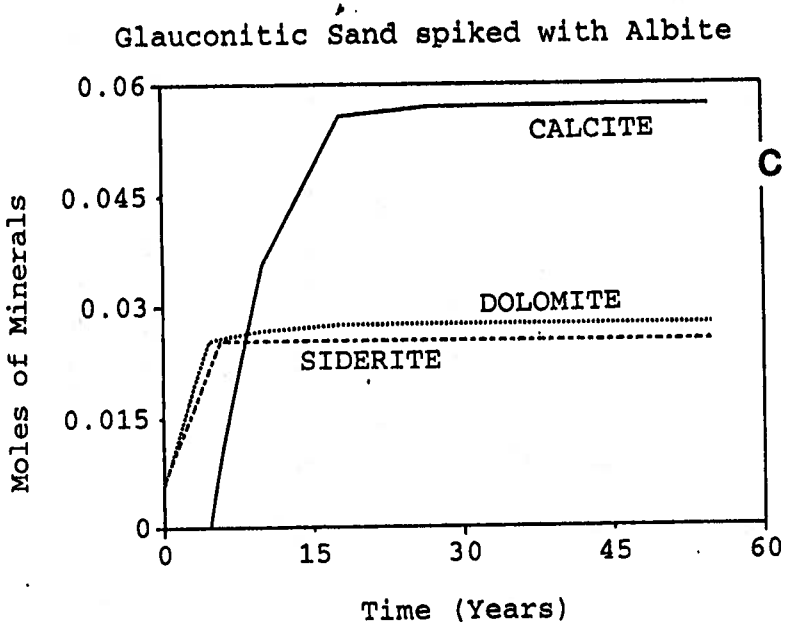

before the albite (i.e. 38 versus 45 years). As documented in Figure 44, the major differences are the large amount of calcite synthesized due to the breakdown of anorthite, which also stabilizes and encourages the formation of kaolinite. Figure 44 d shows the expected change in pH and in the molalities of calcium ion, magnesium ion and bicarbonate ion as a function of log time (log time was used in order to see the changes). The significant changes in pH and bicarbonate alkalinity exhibited in Figure 42 have already occured by 10^{-4} years and consequently are not recorded in Figure 44 d.

In the biotite spike experiment, the biotite (annite) is predicted to dissappear in 6 years. In one month, 400 mg of biotite would break down to form carbonate minerals and muscovite and result in an a maximum increase in Mg^{++} in solution of approximately 300 ppm if none of the Mg^{++} was taken up by the carbonates (This cannot be seen in the modelling because an iron analogue of biotite (i.e. annite) was used to represent biotite in PATHARC and no Mg^{++} was released). This would correlate with the increase in Mg^{++} recorded in the formation water at the end of the biotite spike experiment. In the modelling, the most significant result of the annite dissolution is to increase the amount of quartz, muscovite and siderite signficantly (Figure 45). The potassium feldspar reacts quite slowly and does not come to equilibrium till slightly over 2000 years, however, the majority of the reactions occur in the first 10 to 100 years.

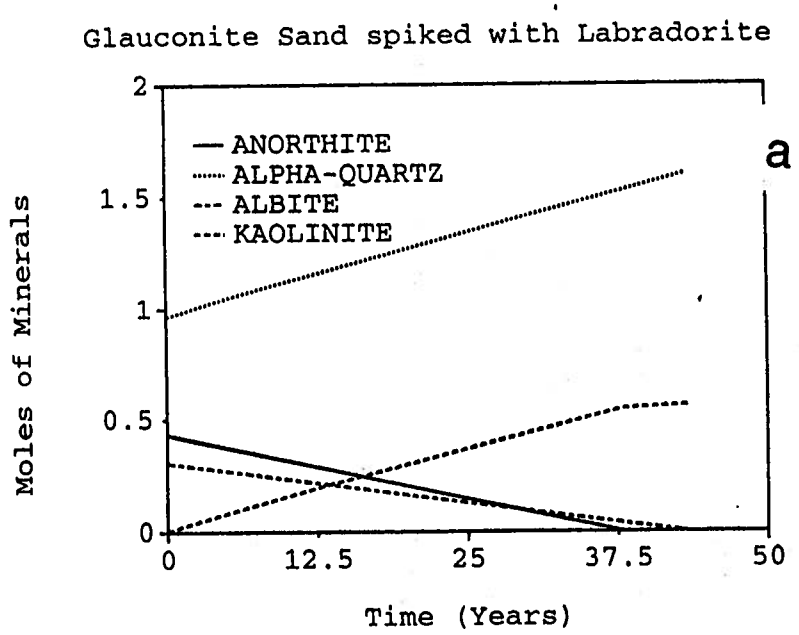

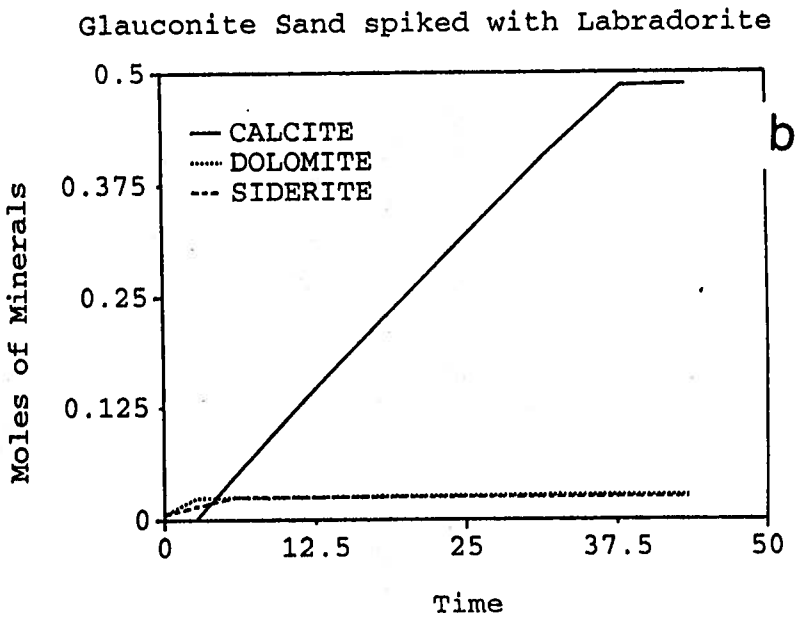

Figure 44. PATHARC modelling of Glauconitic Sand **spiked with labradorite** autoclave experiment at 105°C & 90 bars CO_2

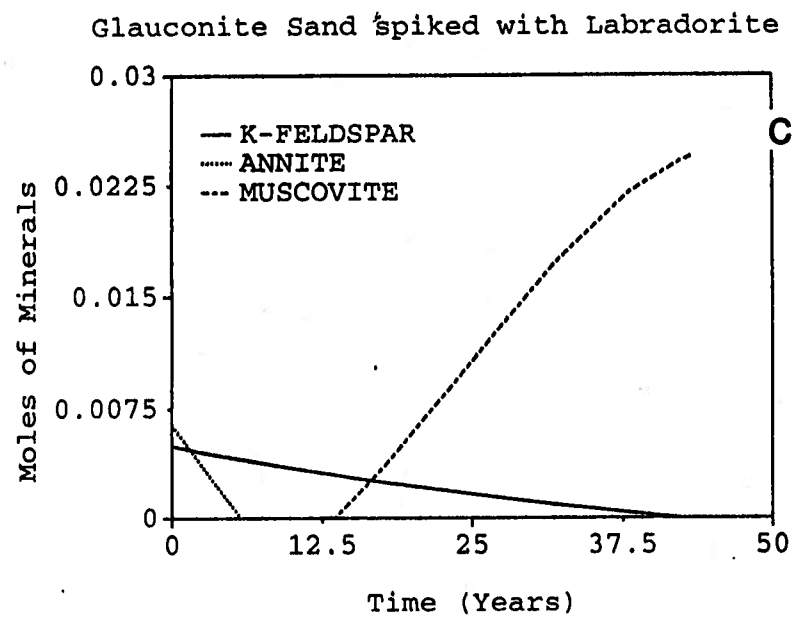

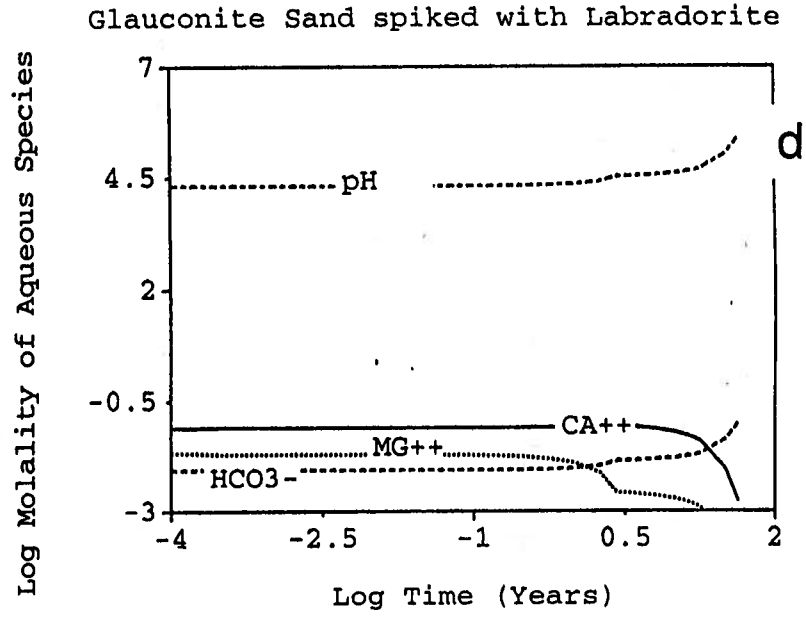

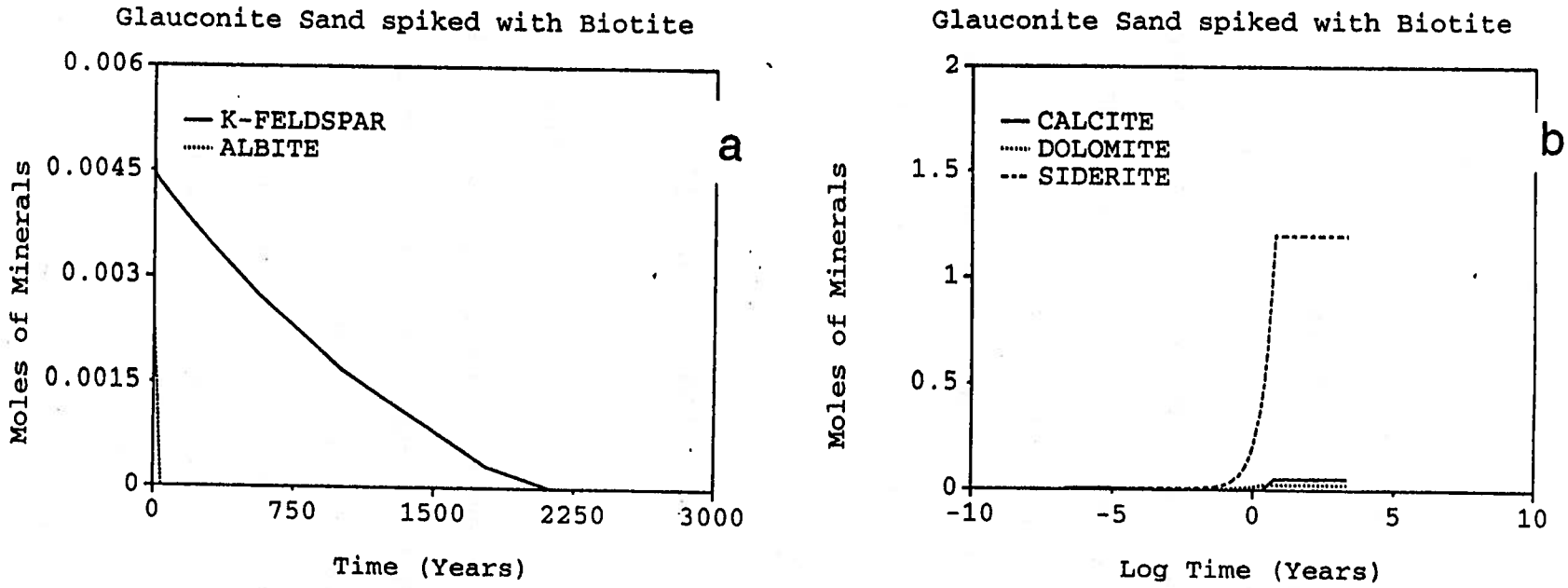

Figure 45. PATHARC modelling of Glauconitic Sand **spiked with biotite** autoclave experiment at 105°C & 90 bars CO_2

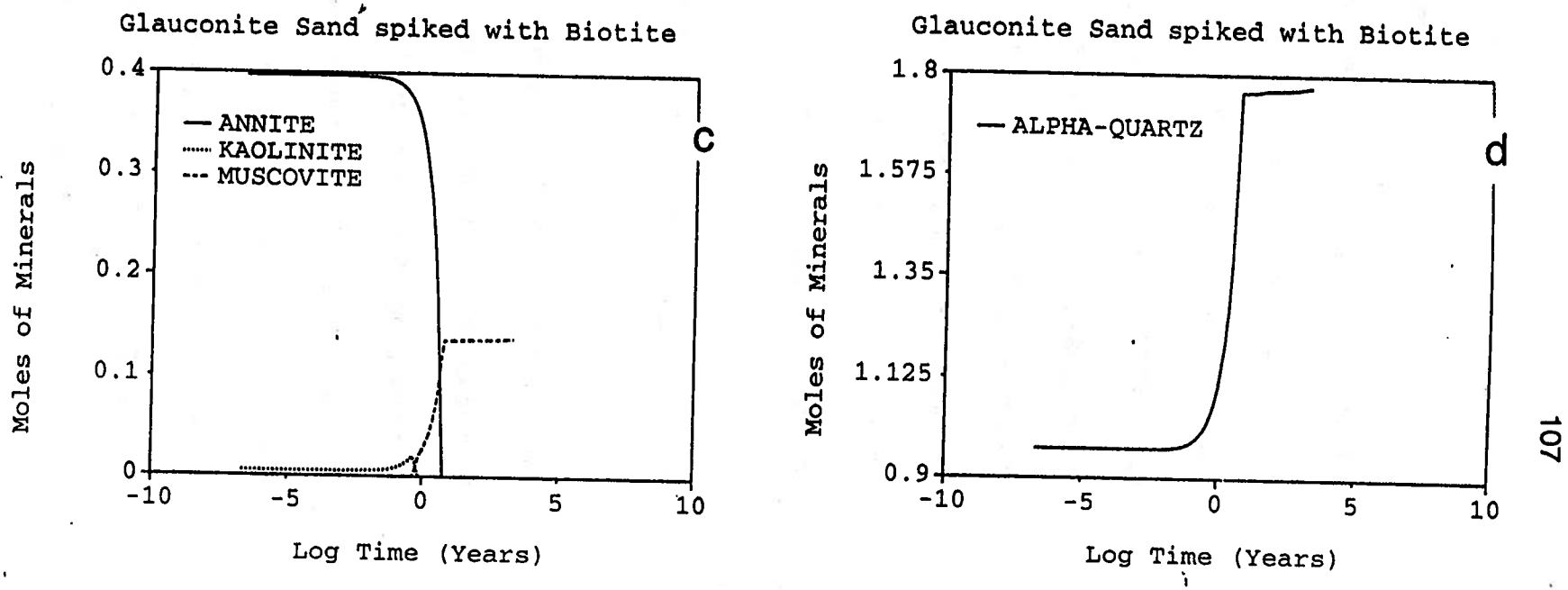

In summary, when using a "reactive" grain diameter of 100 microns the modelling agrees with the experimental observations; **experiment durations of one month are too short to observe any significant changes in the relative amounts of the minerals** with the analytical techniques used. However rapid changes in the composition of the aqueous phase were reasonably predicted. If a "reactive" grain size of 10 microns was used, significant amounts of mineral reaction would be predicted to occur in one month - which was not observed in the experiments. Higher temperatures must be used if significant amounts of reaction in a reasonable period of time are expected. The agreement between the modelling and the experiments with respect to the rates of reactions gives confidence in the use of PATHARC in the modelling of geochemical reactions in the aquifer if a "reactive" grain size of 100 microns is used.

MODELLING REACTIONS IN THE GLAUCONITIC SANDSTONE AQUIFER

The Glauconitic sandstone aquifer is a medium to fine grained litharenite (Table 2) located at average depth of approximately 700 meters (with respect to sealevel) and at an average temperature of 54°C in the study area. Framework grain size ranges in diameter from 0.125 to 0.5 mm while the clays and carbonates average about 0.008mm in diameter. The average mineralogy was taken from Table 3 as 87% quartz, 2% K-feldspar, 1% plagioclase, 5% glauconite, 2% kaolinite, 1% calcite, 1% dolomite and 1% siderite. The average porosity is 12%. For this porosity, a liter of water will contact over 18,000 grams of minerals (see Table 11). Fluid pressure in the aquifer was calculated

to be 13 MPa. Injection pressure of CO_2 was set at 26MPa or 80% of fracture pressure. Heating the formation water from 25 to 54°C and equilibrating it with 26MPa CO_2 pressure shifts the pH from 7.2 to 2.88 as calculated by SOLMINEQ88.

An average grain diameter of 100 microns (as for the autoclave experiments) was used to model the kinetics of the water-rock reactions in the aquifer during injection of CO_2. As discussed previously, the injected CO_2 will be assumed to be in equilibrium with the fluid at all times, and that the driving force for reactions will be the kinetically controlled dissolution of the silicate minerals. Figures 46 a and b show the change in the moles of minerals as a function time. Figure 46c shows the change in pH and log molality of calcium, iron and bicarbonate as a function of time, while Figure 46d shows the same aqueous species as a function of log time (in order to see the complete range of changes).

Under these conditions (Figure 46), PATHARC predicts that the glauconite (i.e. annite in the model) and kaolinite will react out completely in 100 and 80 years, respectively. Albite (sodium feldspar) reacts out in about 540 years while potassium feldspar comes to equilibrium with the formation fluid in about 820 years. The destruction of glauconite (annite), kaolinite and albite, with the partial destruction of potassium feldspar results in muscovite and signficant amounts of siderite being formed. Quartz is also formed, but has not been shown on the figures for reasons of scale. There is very little change in the amount of either calcite or dolomite. The amount of siderite formed is 5.4 moles thus 5.4

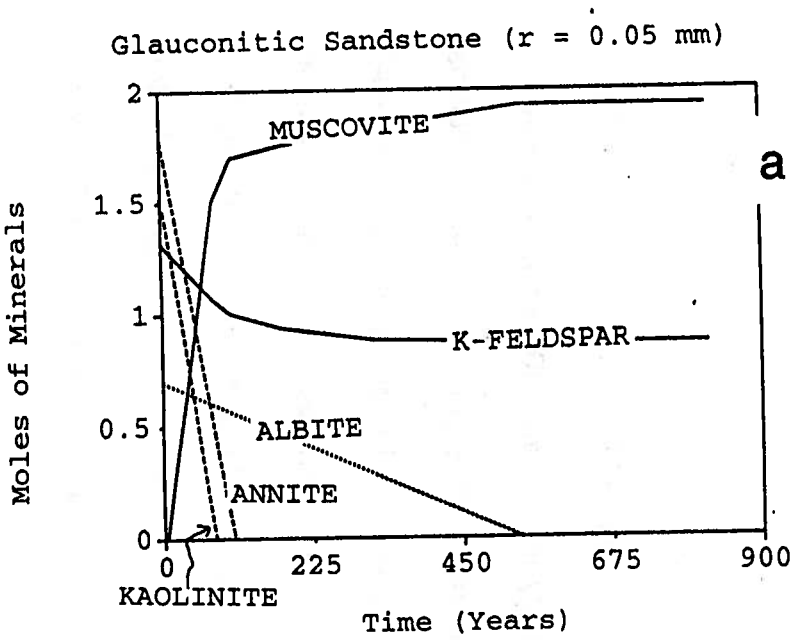

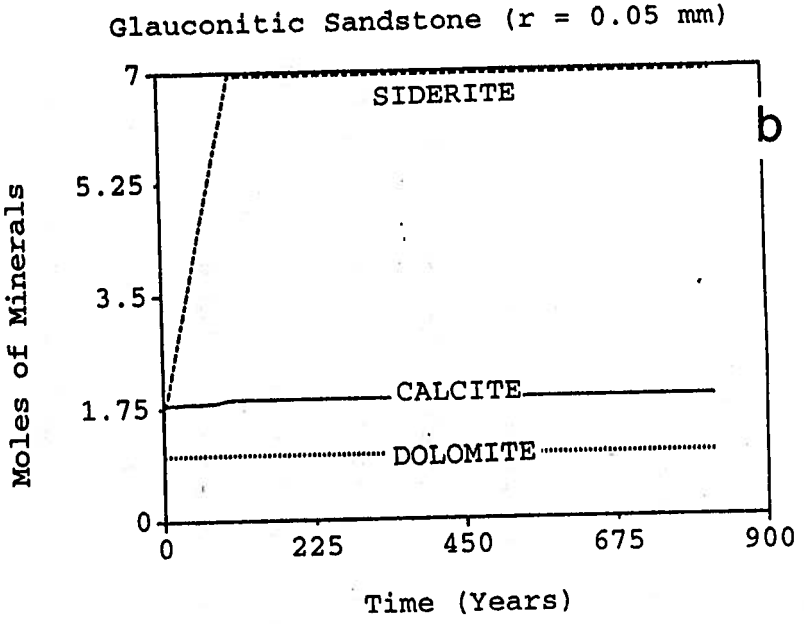

Figure 46. PATHARC geochemical modelling of Glauconitic Sand **aquifer** at 54°C & 260 bars CO_2

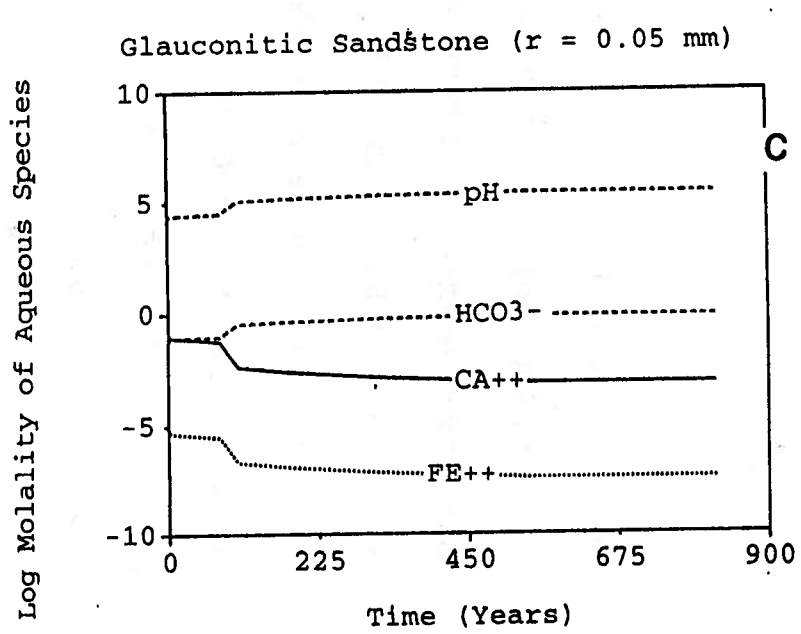

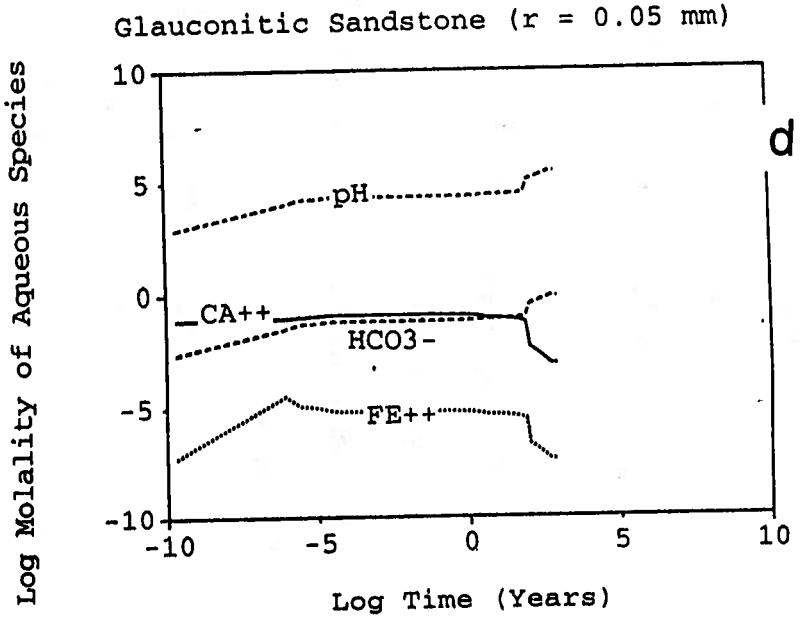

moles of CO_2 have been trapped. The reaction of albite traps additional CO_2 by forming bicarbonate ions from carbonic acid (which is buffered by the presence of CO_2 gas). Complete equilibrium is achieved within 820 years at which point the bicarbonate concentration is 0.8 molal at a pH of 5.4. **Therefore, the total CO_2 trapped is 6.2 moles relative to a stationary one kilogram of formation fluid in the aquifer.**

If an average grain diameter of 10 microns is used in the modelling, total equilibrium with a 260 bar CO_2 pressure is achieved in 82 years; glauconite destruction is complete in 10 years and albite in 54 years (Figure 47). As expected, the time of reaction is reduced 10 fold, but the final pH, bicarbonate concentrations, amounts of minerals destroyed and formed would not change; the same reactions would occur. Both the experiments and modelling indicate that the geochemical trapping reactions are slow - on the order of tens to hundreds of years but fast enough to form effective CO_2 traps given the thousands of years residence time in the aquifer.

Using the average thickness (14 meters) of the Glauconitic Sandstone aquifer, and average porosity (12%) and the average mineralogy (5% glauconite, 3% feldspar), one square kilometer of the aquifer could sequester approximately 0.5 megatons of CO_2 by mineral reactions when the aquifer reached geochemical equilbrium with the injected CO_2.

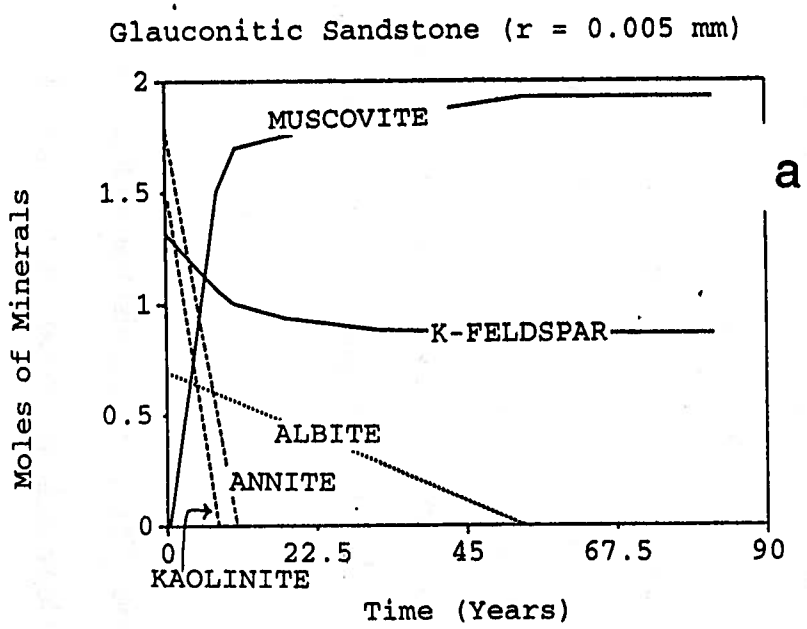

Figure 47. PATHARC geochemical modelling of Glauconitic Sand **aquifer** at 54°C & 260 bars CO_2

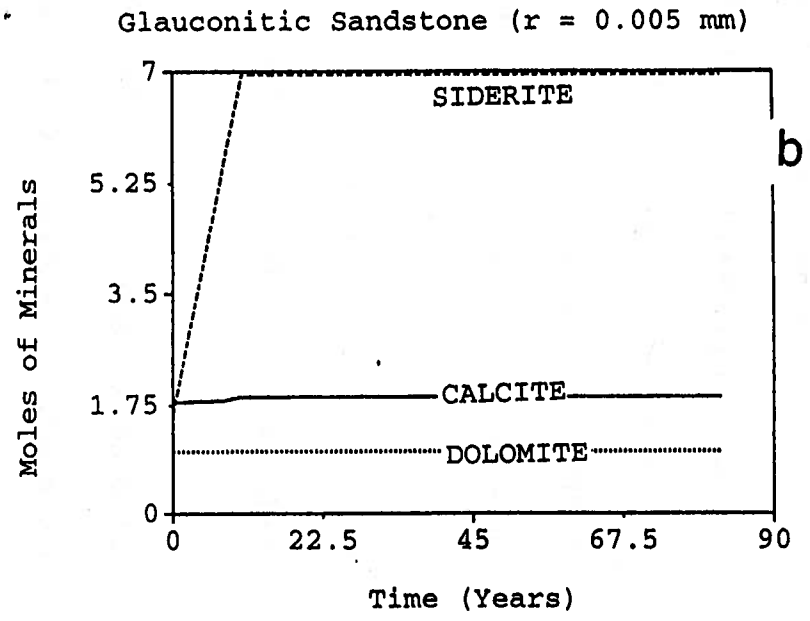

SUMMARY AND CONCLUSIONS

In order to reduce emissions of CO_2 into the atmosphere, which could have adverse effects on the global climate, CO_2 can be captured at emission sources and injected into deep geological formations where it is retained for geological time periods by a combination of stratigraphic, hydrodynamic and geochemical trapping mechanisms. Approximately two-thirds of Alberta's power generating capacity is located in the Lake Wabamun area west of Edmonton. As part of "proof-of-concept" ongoing research, the Mannville Group strata in the Lake Wabamun area (Tp. 50-52, R. 3-5W5M) were studied with the purpose of identifying an aquifer satisfying most of the conditions required for deep disposal of CO_2:

(i) Geologically, a deep aquifer should be chosen, capped by a regional aquitard, which, preferably, should also have trapping capabilities. This last requirement is particularly important for immiscible lighter-than-water CO_2.

(ii) From a physical point of view, the top of the aquifer must be located at more than 800 meters depth and the aquifer must be relatively thick to accommodate large quantities of CO_2.

(iii) From a geochemical point of view, a "basic" mineralogy must be present in the solid aquifer matrix to sequester or trap the CO_2 as bicarbonate ion in water or as a component of a solid, once the CO_2 is injected into the aquifer.

(iv) In terms of rock properties, the formation should have enough porosity and adequate permeability. Near-well permeability should be high for injection

purposes, but regional scale permeability sould be low such that CO_2 residence time is high.

(v) From an economic and ecological point of view, deep formations suitable for CO_2 disposal have to be located in close vicinity to CO_2 emitting power plants.

Information from more than 300 wells drilled in the area was used in defining and characterizing the geology, lithology, mineralogy, porosity and permeability of the rocks in the Mannville stratigraphic interval (which occurs at depths greater than 1300 meters). Bottom hole temperature measurements, formation water analyses and drillstem tests were used to characterize the hydrogeological regime of formation waters. The results of this hydrogeological evaluation should be used in future site-specific studies of CO_2 injectivity, trapping and flow in the selected aquifer.

The Mannville Group strata in the area of interest consist of the Ellerslie Member, Ostracod Beds, Glauconitic Sandstone and Grand Rapids Formation. The strata generally dip to the southwest with a slope of 7 m/km. The mainly siltstone and sandstone Ellerslie Member was deposited on the sub-Cretaceous unconformity, which explains its variable thickness from less than 10 m to more than 60 m. The predominantly mudstone Ostracod Beds conformably overlies the Ellerslie Member, averaging 18 m in thickness. The Glauconitic Sandstone is formed of sandstones approximately 14 m thick. It is overlain by a continuous basal shale zone of the Grand Rapids Formation which averages

10 m in thickness. The rest of the Grand Rapids Formation, comprised of interbedded sands and shales, averages approximately 120 m in thickness.

There is neither a vertical nor an areal trend in porosity and permeability distributions in the Mannville Group strata in the area of interest, although there are regions of locally high and low values. Only two wells contain core analyses for the Grand Rapids Formation and the Glauconitic Sandstone, while for the Ostracod Beds and the Ellerslie Member there are enough data for a more meaningful analysis. The porosity of the Glauconitic Sandstone and the Ellerslie Member is high on average (12%). The permeability of Mannville strata is generally low, of the order of 5 to 10 md on average. However, local permeabilities as high as 100 to 200 md have been measured both in core and drillstem tests.

Hydrostratigraphically, the Ellerslie Member and the lower portion of the Ostracod Beds form an aquifer, overlain by the aquitard comprised of the remainder of the Ostracod Beds. The overlying Glauconitic Sandstone and Grand Rapids aquifers are separated by the intervening aquitard formed by the basal shale layer of Grand Rapids Formation. The composition of formation water in the Mannville Group in the study area varies as much within units as it does from unit to unit and place to place. Salinities range from approximately 25,000 to 50,000 mg/l. The flow of formation water in the Ellerslie aquifer is generally from south-southeast toward the north, driven by a drop in hydraulic head from approximately 1000 to 600 m. The flow in the Glauconitic Sandstone aquifer is

different, with hydraulic heads varying in the 550 to 590 m range and flow direction generally to the northeast. Hydraulic heads in the Grand Rapids aquifer are in the same range as in the Glauconitic Sandstone aquifer. Geothermal gradients in the area are around 30°C/km. Temperatures in the Glauconitic Sandstone aquifer vary in the 50 to 60°C range because of the southwestward dip of the strata.

From the analysis of rock properties and hydrogeology of formation water in the Mannville Group strata in the study area (Tp. 50-52, R. 3-5W5M) it seems that the preferred aquifer for CO_2 disposal should be the Glauconitic Sandstone for the following reasons:

(i) It is the most homogeneous of all Mannville Group units in the succession.

(ii) Hydrostratigraphically it is confined by the shaley Ostracod Beds and Basal Grand Rapids aquitards.

(iii) It has generally good porosity (12% on average).

(iv) It has low regional-scale permeability (10 md on average), which is needed for hydrodynamic entrapment, slow dispersion and high sweep ratio.

(v) It has high permeability in places (100 md), which is needed for avoiding high pressure buildup in the near-well region at sites of CO_2 injection.

(vi) It has a siliciclastic based mineralogy with clays present, which will contribute to the mineral trapping of CO_2 through geochemical reactions.

(vii) There is no hydrocarbon production from this unit, unlike the Ellerslie Member, thus avoiding unwarranted contamination of energy resources.

The CO_2-trapping capability of the Glauconitic Sandstone aquifer was assessed based on detailed mineralogical analysis of drill core, autoclave experiments and geochemical modelling. Basic aluminosilicate minerals identified in the Glauconitic Sandstone aquifer, which could contribute to the trapping capacity of the aquifer, were feldspars and glauconite. Experiments on potential CO_2-trapping reactions in the Glauconitic Sandstone were carried out at 105°C and 90 bars CO_2 pressure for one month, but very little reaction was seen on this time scale. These experiments and field time scales were evaluated by geochemical modelling using rate data from the literature for the minerals making up the Glauconitic Sandstone. The geochemical model PATHARC predicted times from 6 to 40 years for the experiments to come to equilibrium. Extending the modelling to the field, CO_2-trapping reactions take a minimum of 100 years to complete after the formation water has equilibrated at the temperature of the Glauconitic Sandstone aquifer (i.e. 54°C) and at the proposed injection pressure of the CO_2 (260 bars). Every square kilometer of the Glauconitic Sandstone aquifer could sequester approximately 0.5 megatons of CO_2 by these mineral-trapping reactions, once the CO_2-charged formation water has swept through.

Both the experiments and modelling indicate that geochemical trapping reactions of CO_2 are slow - on the order of tens to hundreds of years but fast enough to form effective CO_2 traps given the tens of thousands of years residence time of a packet of fluid in the deeper aquifers of the Alberta Basin where the regional-scale flow velocity of the formation waters is on the order of 1 to 10 cm/year. The order of magnitude difference

in the two time scales ensures that CO_2-mineral trapping should be complete before the aquifer leaks to the surface. Thus given appropiate formation mineralogy (Gunter et al., 1993), mineral traps can replace stratigraphic traps ensuring that the injected CO_2 will be immobilized for ever in the subsurface. Sedimentary basins provide the appropiate setting for mineral traps, hydrodynamic or time traps and stratigraphic traps to be operable and thus are ideal candidates for CO_2 storage in aquifers.

Assuming that the CO_2-consuming mineral reactions go to completion, the maximum CO_2 disposal capacity of the Glauconitic Sandtone in the study area of 30x30 kilometers (consisting of 9 townships) is 450 megatons of CO_2. Assuming the properties of the aquifer extend beyond this arbitrarily defined area, for each additional township, 50 more megatons of CO_2 could be sequestered. A 500 megawatt coal-fired power plant would emit close to 15,000 tons/day of CO_2. Over the life of the power plant (approximately 30 years), 164 megatons of CO_2 would be produced. Ideally this could be trapped in the Glauconitic Sandstone aquifer within an area of four townships.

On a larger scale, a recent estimate by the authors (Bachu et al., 1994) of the storage capacity of the whole Alberta Sedimentary Basin is 20,000 megatons or 20 gigatons. This estimate is conservative as the Alberta Basin covers an area of 825,000 km^2 with a volume of approximately 2 million km^3. This figure is based on the following assumptions:

(i) For the basin as a whole, the total pore space of the aquifers suitable for CO_2 injection is about 1.25% of the basin's volume.

(ii) The effective sweep of the CO_2 will be on the order of 5% of the aquifer pore volume.

(iii) Only 1% of this remaining pore space would be accessible because these aquifers are distributed across the entire basin, and obviously are not going to be used in their entirety because of economic, technical and policy reasons.

On an even larger scale, this value of 20 gigatons of CO_2 storage capacity for aquifers in the Alberta Basin represents approximately 5% of total global estimates of 400+ gigatons. However we expect global estimates to increase as more detailed aquifer inventories, such as presented here, are completed.

In Phase III of the study, if approved, an injection site will be selected based on surface and subsurface considerations, like distance from the CO_2-emitting power plants, location of existing oil and gas wells, access facilities, and rock properties (porosity, permeability and mineralogy). Once a site is selected, numerical simulations of CO_2 injection in the Glauconitic Sandstone will be performed taking into account the real geometry, rock properties and characteristics of formation water at the selected site based on the data presented here. A sensitivity analysis performed on variables such as rock porosity and permeability, and CO_2 injection rate and pressure, should indicate an optimum scenario for CO_2 disposal, and the expected CO_2 volumes to be disposed of over the lifetime of

the operation. If the Glauconitic Sandstone aquifer proves to be incapable of accepting high volumes of CO_2, then the Grand Rapids Formation may be considered for added capacity.

In the future an inventory of other sedimentary basins across Canada, which could serve as disposal sites for CO_2, should be made. This should include depleted oil and gas reservoirs as well as aquifers. In the event that global policy dictates drastic reductions in CO_2 emissions, then Canada would be able to execute their disposal options immediately to meet imposed annual quotas.

REFERENCES

Anbeek, C. 1993. The effect of natural weathering on dissolution rates. Geochim. Cosmochim., v. 57, p. 4963-4975.

Acker, J.G. and Bricker, O.P. 1992. The influence of pH on biotite dissolution and alterration kinetics at low temperature. Geochim. Cosmochim., v. 56, p. 3073-3092.

Bachu, S. and Burwash, R.A. 1991. Regional-scale analysis of the geothermal regime in the Western Canada Sedimentary Basin. Geothermics, v. 20 (5/6), p. 387-407.

Bachu, S. and Underschultz, J.R. 1993. Hydrogeology of formation waters, northeastern Alberta basin. American Association of Petroleum Geologists Bulletin, v. 77 (10), p. 1745-1768.

Bachu, S., Gunter, W.D. and Perkins, E.H. 1994. Aquifer disposal of CO_2: hydrodynamic and mineral trapping. Energy Conversion and Management, v. 35, p. 269-279.

Bailey, R.T. and McDonald, M.M. 1993. CO_2 capture and use for EOR in Westem Canada 1. General overview. Energy Conversion and Management, v.35, p1145-1150.

Banerjee, I. and Davies, E.H. 1988. An integrated lithostratigraphic and palynostratigraphic study of the Ostracod Zone and adjacent strata in the Edmonton Embayment, central Alberta. *In* D.P. James and D.A. Leckie (eds.): Sequences, Stratigraphy, Sedimentology: Surface and Subsurface; Canadian Society of Petroleum Geologists, Memoir 15, p. 261-274.

Battelle, 1991. R&D status of carbon dioxide separation, disposal, and utilization technologies. Client Report.

Baveye, P. and Sposito, G. 1984. The operational significance of the continuum hypothesis in the theory of water movement through soils and aquifers: Water Resources Research, v. 20, p. 521-562.

Blok, K., Hendriks, C.A. and Turkenburg, W.C. 1989. The role of carbon dioxide removal in the reduction of the greenhouse effect. *In* Proceedings of an Experts' Seminar on Energy Technologies for Reducing Emissions of Greenhouse Gases. OECD/IEA, Paris 2, p. 135-155.

Busenburg, E. and Clemency, C.V. 1976. The dissolution kinetics of feldspars at 25°C and 1 atm CO_2 partial pressure. Geochim. Cosmochim. v. 40, p. 41-49.

Busenberg, E. and Plummer, L.N. 1982. The kinetics of dissolution of dolomite in CO_2-H_2O systems at 1.5 to 65°C and 0 to 1 atm P_{CO2}. Am. J. Sci. v. 282, p. 45-78.

Burton, E.A. and Walter, L.M. 1990. The role of pH in phosphate inhibition of calcite and aragonite precipitation in seawater. Geochim. Cosmochim., v. 54, p. 797-808.

Carroll-Webb, S.A. and Walther, J.V. 1988. A surface complex model for the pH-dependence of corundum and kaolinite dissolution rates. Geochim. Cosmochim. v. 52, p. 2609-2623.

Carroll, S.A. and Walther, J.V. 1990. Kaolinite dissolution at 25, 60 and 80°C. Am. J. Sci. v. 290, p. 797-810.

Chapman, D.S., Keho, T.H., Bauer, M.S. and Picard, M.D. 1984. Heat flow in the Uinta Basin determined from bottom hole temperature (BHT) data. Geophysics, v. 49, p. 453-466.

Chou, L. and Wollast, R. 1984. Study of the weathering of albite at room temperature and pressure with a fluidized bed reactor. Geochim. Cosmochim., v. 48, p. 2205-2217.

Chou, L. and Wollast, R. 1985. Steady-state kinetics and dissolution mechanisms of albite. Am. J. Sci., v. 285, p. 963-993.

Chou, L., Garrels, R.M. and Wollast, R. 1989 A comparitive study of the kinetics and mechanisms of dissolution of carbonate minerals. Chem. Geol. v. 78, p. 269-282.

Cushman, J.H. 1984. On unifying the concepts of scale, instrumentation and stochastics in the development of multiphase transport theory. Water Resources Research, v. 20, p. 1668-1676.

Dagan, G. 1989. Flow and transport in porous formations. Berlin and Heidelberg, Spring-Verlag, 465 p.

Desbarats, A.J. and Bachu, S. 1994. Geostatistical analysis of aquifer heterogeneity from the core scale to the basin scale. Water Resources Research, *In press.*

Dunsmore, H.E. 1992. A geological perspective on global warming and the possibility of carbon dioxide removal as calcium carbonate mineral. Energy Conversion and Management v. 33, p. 565-572.

Fleer, V.N. and Johnston, R.M. 1986. A compilation of solubility and dissolution kinetics data on minerals in granitic and gabbroic systems. Atomic Energy of Canada Limited technical report TR-328-2, 170p.

Gunter, W.D., Perkins, E.H., Bachu, S., Law, D., Wiwchar, B., Zhou, Z., and McCann, T.J. 1993. Aquifer disposal of CO_2-rich gases in the vicinity of the Sundance and Genesee power plants. Phase I: Injectivity, chemical reactions and proof of concept. Alberta Research Council Open File Report 1994-16 (OSHR C-1993-5).

Gunter, W.D., Perkins, E.H., and McCann, T.J. 1993. Aquifer disposal of CO_2-rich gases: Reaction design for added capacity. Energy Conversion and Management 34, p. 941-948.

Helgeson, H.C., Murphy, W.M. and Aagaard, P. 1984 Thermodynamic and kinetic constraints on reaction rates among minerals and aqueous solutions. II. Rate constants, effective surface area, and the hydrolysis of feldspar. Geochim.Cosmochim. Acta, v. 48, p. 2405-2432.

Herzog, H.J, Drake, E.M. and Tester, J.W. 1992. The capture and sequestration of power plant CO_2. ACS 204th National Meeting, ACS Division of Fuel Chemistry Preprints, Washington, D.C., August 23-28, v. 37, p. 1068-1075.

Hitchon, B., Bachu, S. and Underschultz, J. 1990. Regional subsurface hydrogeology, Peace River Arch area, Alberta and British Columbia. *In* Geology of the Peace River Arch (S.C. O'Connell and J.S. Bell, eds.). Bulletin of Canadian Petroleum Geology, v. 38(A), p. 196-217.

Holdren, G.R. and Berner, R.A. 1979 Mechanism of feldspar weathering - I. Experimental studies. Geochim. Cosmochim. v. 43, p. 1161-1171.

Jack, A.R. 1992. CO_2 removal and disposal. *In* Proceedings of the "International Conference on Coal, the Environment and Development: Technologies to Reduce Greenhouse Gas Emissions". Paris, OECD/IEA, p.527-537.

Kharaka, Y.K., Gunter, W.D., Aggarwal, P.K., Perkins, E.H. and DeBraal, J.D. 1988. SOLMINEQ.88: A computer program for geochemical modelling of water-rock interactions. U.S. Geological Survey, Water Resource Investigation Report 88-4227.

Koide, H., Tazaki, Y., Noguchi, Y., Nakayama, S., Lijima, M., Ito, K., and Shindo, Y. 1992. Subterranean containment and long-term storage of carbon dioxide in unused aquifers and in depleted natural gas reservoirs. Energy Conversion and Management v. 33, p. 619-626.

Knauss, K.G. and Wollery, T.J. 1986. Dependence of albite dissolution kinetics on pH and time at 25°C and 70°C. Geochim. Cosmochim. v. 50, p. 2481-2497.

Knauss, K.G. and Wollery, T.J. 1988. The dissolution kinetics of quartz as a function of pH and time at 70°C. Geochim. Cosmochim. v. 52, p. 43-53.

Knauss, K.G. and Wollery, T.J. 1989. Muscovite dissolution kinetics as a function of pH and time at 70°C. Geochim. Cosmochim. v. 53, p. 1493-1501.

Lasaga, A.C. 1981. Rate laws of chemical reactions. Chapter 1. *In* A.C. Lasaga and R.J. Kirkpatrick (eds): Kinetics of geochemical processes. Mineralogical Society of America's Reviews in Mineralogy v. 8, p. 1-68.

Lasaga, A.C. 1984. Chemical kinetics of water-rock interaction. J. Geophys. Research v. 89, p. 4009-4025.

Lin, F.C. and Clemency, C.V. 1981.The kinetics of dissolution of muscovites at 25°C and 1 atm CO_2 partial pressure. Geochim. Cosmochim. v. 45, p. 571-576.

Nagy, K.L., Steefel, C.I. Blum, A.E. and Lasaga, A.C. 1990. Dissolution and precipitation kinetics of kaolinite: Initial results at 80°C with application to porosity evolution in a sandstone. *In* I.D. Meshri and P.J. Ortoleva (eds): Prediction of reservoir quality through chemical modeling. AAPG Memoir 49, p. 85-101.

Nagy, K.L. and Lasaga, A.C. 1992. Dissolution and precipitation kinetics of gibbsite at 80°C and pH 3: The dependence on solution saturation state. Geochim. Cosmochim. v. 56, p. 3093-3112.

Perkins, E.H. 1980. A reinvestigation of the theoretical basis for the calculation of mass transfer in geochemical processes involving aqueous solutions. MSc thesis, University of British Columbia, Vancouver.

Plummer, L.N., Parkhurst, D.L. and Wigley 1978. The kinetics of calcite dissolution in CO_2-water systems at 5°to 60°C and 0.0 to 1.0 atm CO_2. Amer. J. Sci. v. 278, p. 179-216.

Rimstidt, J.D. and Barnes, H.L. 1980. The kinetics of silica-water reactions. Geochim. Cosmochim. Acta, v. 44, p. 1683 - 1699.

Rudkin, R.A. 1964. Lower Cretaceous. *In* R.A. McCrossan and R.P. Glaister (eds.): Geological History of Western Canada; Alberta Society of Petroleum Geologists, p. 156-168.

Stanley Industrial Consultants, Alberta Research Council and Mahoney Exploration Ltd. 1993, Carbon dioxide disposal: An examination of aquifers for the disposal of CO_2

arising from power generation using fossil fuel. International Energy Agency Report IEA/93/OE14, 120p.

Sverdrup, H.U. 1990. The kinetics of base cation release due to chemical weathering. Lund University Press, 245p.

Sverdrup, H.U. and Warfvinge, P. 1988. Weathering of primary silicate minerals in the natural soil environment in relation to a chemical weathering model. Water, Air, Soil Poll. v. 38, p. 387-408

Sverdrup, H.U. and Warfvinge, P. 1993. Calculating field weathering rates using a mechanistic geochemical model PROFILE. App. Geochem. v. 8, p. 273-284.

Talman, S.J. and Nesbitt, H.W. 1988. Dissolution of populations of ultrafine grains with applications in feldspars. Geochim. Cosmochim., v. 52, p. 1467-1471.

Todd, M.R. and Grand, G.W. 1993. CO_2 capture and use for EOR in Western Canada 3. Enhanced oil recovery using carbon dioxide. Energy Conversion and Management, v.35, p1157-1164.

Turkenburg, W. 1992. CO_2 removal; some conclusions. Energy Conversion and Management v. 33, p. 819-823.

van der Burgt, M.J., Cantle, J. and Boutkan, V.K. 1992. Carbon dioxide disposal from coal-based IGCC's in depleted gas fields. Energy Conversion and Management v. 33, p. 611-618.

van der Haarst, A.C. and van Nieuwland, A.J.F.M. 1989. Disposal of carbon dioxide in depleted natural gas reservoirs. Climate and Energy: The feasibility of Controlling CO_2 Emissions. Kluwer Academic Publishers, Dordrecht - Boston, p. 178-188.

van der Meer, L.G.H. 1992. Investigations regarding the storage of carbon dioxide in aquifers in the Netherlands. Energy Conversion and Management v. 33, p. 611-618.

White, A.F. and Peterson, M.L. 1990. Role of reactive-surface-area characterization in geochemical models. Chapter 35 *in* D.C. Melchor and R.L. Bassett (eds): Chemical modeling of aqueous systems II, ACS Symp. Ser. 416, p. 461-475.

Wood, B.J. and Walther, J.V. 1983. Rates of hydrothermal reactions. Science v. 222, p. 413-415.

APPENDIX I

Thin Section Descriptions

Visual examination of 15 thin section samples for CO2 injection study
N.B. Sedimentary Rock Fragments (SRF) includes chert , glauconite and carbonates.

WELL 7-9-50-4w4

Sample DW 93-1 depth = 5256' Unit - Glauconitic

Fine to medium grained sandstone.
Subangular to subrounded, fairly sorted, loosely packed, fairly clean with moderate porosity

Framework grains:	Quartz	45% (Both Monocrystaline and Polycrystaline)
	Feldspar	1%
	Rock Frags	54% (major component is SRF with minor MRF) SRF includes Chert(15%), Glauconite(5-10%) some Carbonates (Dolomite)

Grains don't show clay coating, mainly grain to grain contact.

Matrix is composed of clay and dolomite

Accessory Heavy mineral (Zircon?)

Classification: Mature Litharenite

WELL 7-9-50-4w4

Sample DW 93-2 depth = 5248.5' Unit - Glauconitic

Fine to medium grained sandstone.
Subangular, fairly sorted, loosely packed, clean with very good porosity

Framework grains:	Quartz	43% (Mainly Monocrystaline with some Polycrystaline)
	Feldspar	2%
	Rock Frags	55% (major component is SRF with minor MRF) SRF includes Chert(15%), Glauconite(5-10%) some Carbonates (Dolomite)

Mainly grain to grain contact, but some grains are clay coated,

Matrix is composed of clay and dolomite

Classification: Submature Litharenite

WELL 7-9-50-4w4

Sample DW 93-3 depth = 5239.5' Unit - Glauconitic

Fine to medium grained sandstone.
Subangular to subrounded, fairly sorted, loosely packed, clean with very good porosity

Framework grains:	Quartz	49% (mainly Monocrystaline with some Polycrystaline)
	Feldspar	1% K-Feldspar (altered)
	Rock Frags	50% (major component is SRF with minor MRF) SRF includes Chert(20%), Glauconite(5%) Carbonates (Fe. Dolomite) 15%

Mainly grain to grain contact with carbonate crystal growth along grain contacts, virtually no grain coatings.

Matrix is composed of clay and dolomite

Classification: Mature Litharenite

WELL 7-9-50-4w4

Sample DW 93-4 depth = 5230.5' Unit - Glauconitic

Fine to medium grained sandstone.
Subangular to subrounded, fairly well sorted, loosely packed, clean with very good porosity

Framework grains:	Quartz	55% (Mainly Monocrystaline with some Polycrystaline)
	Feldspar	4% K-Feldspar (partly altered)
	Rock Frags	41% (major component is SRF with minor MRF) SRF includes mudstone (15%), Chert(10%), Glauconite(5%), Carbonates (Calcite partly dolomitized) 5%.

Mainly grain to grain contact with virtually no grain coatings

Matrix is composed of some clay and partly dolomitized calcite

Classification: Submature Litharenite

WELL 7-11-50-5w5

Sample DW 93-5 depth = 5300' Unit - Glauconitic

Fine to medium grained sandstone.
Subangular, fairly sorted, fairly packed, fairly porous

Framework grains:	Quartz	40%	(mainly Monocrystaline with abundant Polycrystaline)
	Feldspar	3%	K-Feldspar (Partly altered)
	Rock Frags	57%	(major component is SRF with minor MRF) SRF includes Chert(15-20%), Glauconite(10%) mudstone (5%), Carbonates (Calcite partly dolomitized) 5%

Grains are clay coated.

Accessories Muscovite

Matrix is composed of abundant clay and partly dolomitized calcite some organic matter present.

Classification: Immature Litharenite

WELL 7-11-50-5w5

Sample DW 93-6 depth = 5248.5' Unit - Glauconitic

Fine to medium grained sandstone.
Subangular, fairly sorted, fairly packed with good porosity

Framework grains:	Quartz	47%	(Mainly Monocrystaline with some Polycrystaline)
	Feldspar	2%	K-Feldspar (partly altered)
	Rock Frags	51%	(major component is SRF with minor MRF) SRF includes mudstone (20%), Chert(15%), Glauconite(10%). some Carbonates (Calcite & Dolomite)

Matrix is composed of abundant clay and some authigenic calcite crystals in the pores and along grain contacts

Classification: Submature Litharenite

WELL 7-11-50-5w5

Sample DW 93-7 depth = 5268' Unit - Glauconitic

Fine to medium grained sandstone.
Subangular to subrounded, fairly sorted, loosely packed, very porous and fairly clean

Framework grains:	Quartz	55%	(mainly Monocrystaline with abundant Polycrystaline
	Feldspar	1%	
	Rock Frags	44%	(major component is SRF with minor MRF) SRF includes Chert(15%), Glauconite(2-3%) mudstone (10%), mud clasts etc.

Matrix is composed of some Clay and some authigenic calcite.

Classification: Immature Litharenite

WELL 16-20-52-5w5

Sample DW 93-8 depth = 1612.75m Unit - Ellerslie

Very fine to fine grained, finely laminated sandstone.
Subangular, fairly sorted, loosely packed, fairly porous

Framework grains:	Quartz	30%	(Mainly Monocrystaline with some Polycrystaline
	Feldspar	1%	
	Rock Frags	69%	(mainly SRF with some MRF) SRF includes Carbonates (40%) mudstone (15%), Chert(10%)

Matrix is composed of abundant clay and carbonates (calcite and dolomite)
Some bitumen present in pores?

Classification: Immature Extra litharenite

WELL 16-20-52-5w5

Sample DW 93-9 depth = 1609.7m Unit - Ostracod

Finely laminated, fine grained sandstone.
Subangular to subrounded, poorly sorted, fairly packed,fairly porous

Framework grains:	Quartz	48%	(mainly Monocrystaline with abundant Polycrystaline
	Feldspar	2%	
	Rock Frags	52%	(mainly SRF) SRF includes Carbonates (Calcite and Dolomite 15%), Chert(10%), mudstone (10%), siltstone (10%)

Matrix is composed of abundant clay and carbonate cement
Some bitumen present in pores?

Classification: Immature Litharenite

WELL 16-20-52-5w5

Sample DW 93-10 depth = 1660m Unit - Ellerslie

Coarse grained sand interlaminated with medium grained sandstone.
Subangular, bimodally sorted, loosely packed, fairly porous

Framework grains:	Quartz	40%	(Mainly Monocrystaline with some Polycrystaline
	Feldspar	1%	
	Rock Frags	59%	SRF SRF includes mudstone (25%), Chert(25%) siltstone (10%)

Matrix is composed of abundant clay and carbonate cement (Siderite?)
Some bitumen present in pores

Classification: Immature Litharenite

WELL 7-11-50-5w5

Sample DW 93-11 depth = 1659.75m Unit - Ellerslie

Very coarse grained sandstone to granule
Subangular to subrounded, bimodally sorted, very loosely packed, very porous

Framework grains:	Quartz	15%	(mainly Monocrystaline with abundant Polycrystaline
	Feldspar	--	
	Rock Frags	85%	SRF
			SRF includes Chert(20%), siltstone (20%) mudstone (35%), sandstone (10%)

Matrix is composed of abundant clay and carbonate cement (Siderite).

Classification: Immature Extra litharenite

WELL 16-20-52-5w5

Sample DW 93-12 depth = 1657.5m Unit - Ellerslie

Grain size ranging from very fine grained to very coarse grained sandstone, but generally very coarse sandstone.
Subangular to subrounded, very poorly sorted, loosely packed, very porous

Framework grains:	Quartz	35%	(Mainly Monocrystaline with some Polycrystaline
	Feldspar	--	
	Rock Frags	65%	SRF
			SRF includes mudstone (40%), Chert(15%) siltstone (5%) sandstone (<5%) and traces of glauconite

Most grains are clay coated.

Matrix is composed of abundant clay
Some organic matter (bitumen?) present in pores

Classification: Immature Litharenite

WELL 6-11-51-4w5

Sample DW 93-13 depth = 1584m Unit - Ellerslie

Grain size ranging from silt to medium grained sandstone.
Subangular to subrounded,poorly sorted, loosely packed, low porosity

Framework grains: Quartz 70-75% (mainly Monocrystaline
Feldspar 1%
Rock Frags 25-30% SRF
SRF includes Chert(15%), siltstone (10%)
mudstone (5%)

Matrix is composed of some clay and very fine silt.

Classification: Immature Litharenite to Sublitharenite

WELL 6-11-51-4w5

Sample DW 93-15 depth = 1559.5m Unit - Ellerslie

Fine grained sandstone.
Subangular to subrounded, well sorted, fairly packed, very porous

Framework grains: Quartz 70-75% (Mainly Monocrystaline with some Polycrystaline
Feldspar 1% K-Feldspar
Rock Frags 25-30% SRF
SRF includes mudstone (5%), siltstone (10%)

Carbonates dominantly dolomite (10%)
Most calcites are partly dolomitized

Most grains are clay coated

Matrix is composed of some clay and authigenic carbonates (mostly dolomite and some calcite crystals growing in pores).

Classification: Mature Litharenite

WELL 6-11-51-4w5

Sample DW 93-16 depth = 1635m Unit - Ellerslie

Very fine grained sand interlaminated with medium grained sandstone.
Subangular to subrounded, bimodally sorted, loosely packed with poor porosity

Framework grains:	Quartz	50%	(mainly Monocrystaline
	Feldspar	--	
	Rock Frags	50%	SRF
			SRF includes Chert(20%), siltstone (20%) mudstone (10%)

Almost all the fine grained sands are quartz
Most grains are clay coated

Matrix is composed of abundant clay.

Classification: Immature Litharenite

APPENDIX II

XRD Traces of Manville Powdered Core

CARBON DIOXIDE AQUIFER DISPOSAL: XRD RESULTS*

DW 93-1

Quartz	Kaolinite	10Å
98.9%	0.8%	0.3%

DW 93-4

Quartz	K+ Feldspar	Kaolinite	Siderite
95.9%	2.0%	1.3%	0.8%

DW 93-5

Quartz	Feldspar	10Å	Kaolinite
93.7%	4.7%	0.8%	0.8%

DW 93-7

Quartz	Feldspar	10Å	Kaolinite	Siderite
94.8%	2.2%	1.2%	1.2%	0.6%

DW 93-8

Quartz	Calcite	Dolomite	Kaolinite	10Å	Pyrite
78.8%	9.9%	6.7%	2.0%	1.4%	1.2%

DW 93-9

Quartz	Calcite	Dolomite	Kaolinite
79.7%	16.4%	3.7%	0.2%

DW 93-13

Quartz	Kaolinite
97.4%	2.6%

* Relative peak intensity, not weight percent

Jade: Peak Listing — Thu Nov 04 1993 @3:55pm

File: DW931BP.MDI> D:\CO2\DW931BP.MDI: DW 93-1 Back Pack

Scan Parameters:		Search Parameters:
Radiation = CU_1.540598	||	Filter length(pts) = 15
Scan Range = 2 - 65.99	||	Noise level(sigmas) = 4.5
Step Size = .03	||	Intensity cutoff(%) = .5-100
Count Time = 1 sec.	||	2-Theta Zero (degs) = 0

	Peak-Position		Centroid-Position		Peak & Area are without Bkgrd					
#	2Theta	d	2Theta	d	Bkgrd	Peak	I%	Area	I%	FWHM*
1:	12.526	7.0607	12.506	7.0720	68	123	1.0	1059	0.8	0.232
2:	19.910	4.4558	19.921	4.4533	57	159	1.3	2419	1.8	0.411
3:	21.017	4.2236	20.979	4.2312	62	2541	20.5	22824	16.9	0.243
4:	26.749	3.3301	26.738	3.3315	99	12403	100.0	135230	100.0	0.294
5:	34.732	2.5808	34.779	2.5774	58	109	0.9	1870	1.4	0.463
6:	36.678	2.4482	36.664	2.4491	75	885	7.1	8955	6.6	0.273
7:	39.618	2.2730	39.602	2.2739	66	1222	9.9	11914	8.8	0.263
8:	40.428	2.2293	40.409	2.2303	70	492	4.0	4554	3.4	0.250
9:	42.590	2.1211	42.584	2.1213	62	820	6.6	7526	5.6	0.248
10:	45.891	1.9759	45.898	1.9756	46	740	6.0	7770	5.7	0.283
11:	50.242	1.8145	50.262	1.8138	43	1714	13.8	17456	12.9	0.275
12:	55.010	1.6680	55.018	1.6677	55	454	3.7	5530	4.1	0.329
13:	60.054	1.5393	60.088	1.5385	66	3644	29.4	25477	18.8	0.189
14:	61.732	1.5015	61.742	1.5013	64	85	0.7	821	0.6	0.261
15:	64.133	1.4509	64.158	1.4504	49	350	2.8	2866	2.1	0.221

* Intensity values are based on counts per second.

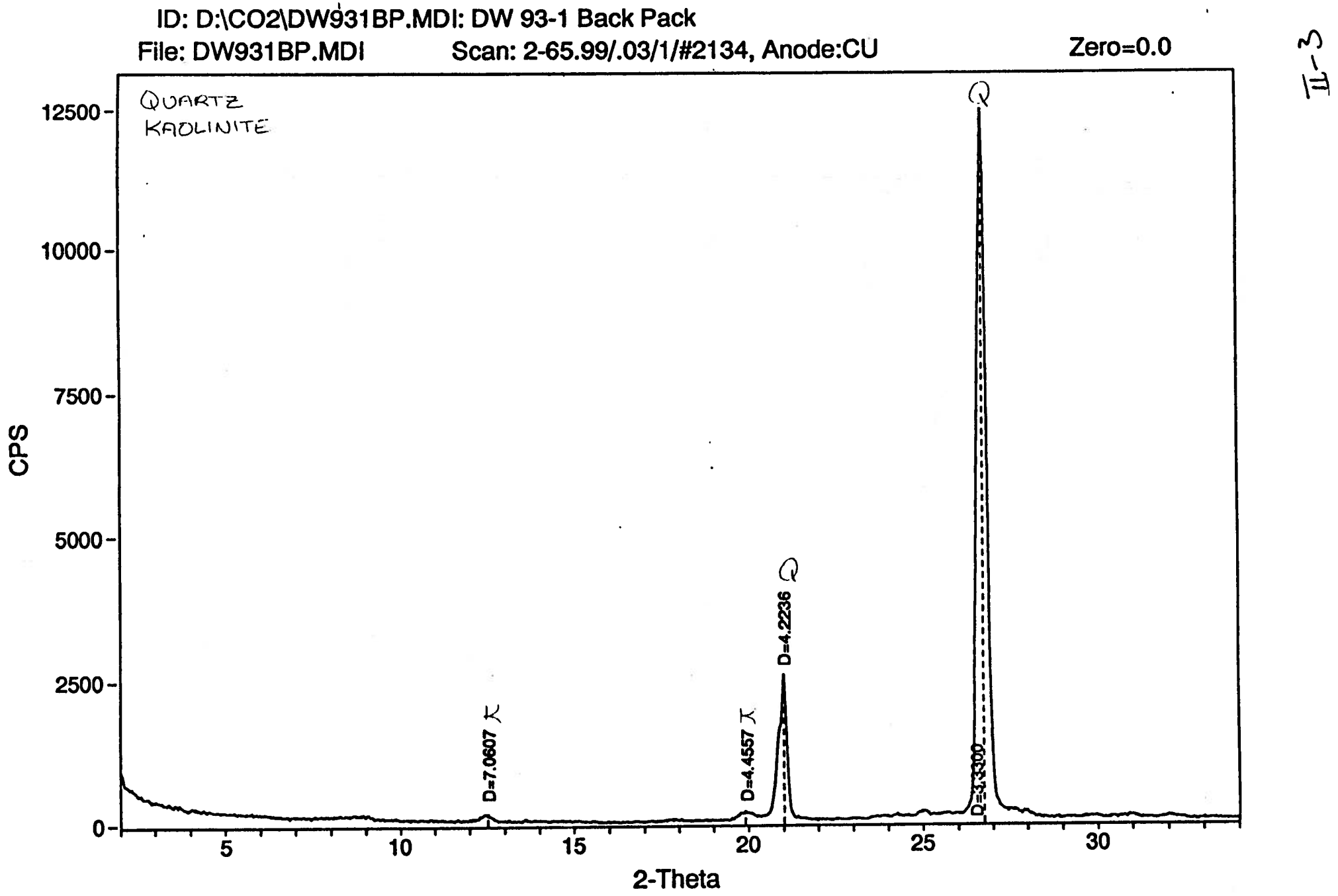
ID: D:\CO2\DW931BP.MDI: DW 93-1 Back Pack
File: DW931BP.MDI
Scan: 2-65.99/.03/1/#2134, Anode:CU
Zero=0.0
QUARTZ
KAOLINITE
CPS
12500
10000
7500
5000
2500
0
5
10
15
20
25
30
2-Theta
D=7.0607 K
D=4.4557 K
D=4.2236 Q
D=3.3300 Q
Q

ID: D:\CO2\DW931BP.MDI: DW 93-1 Back Pack
File: DW931BP.MDI Scan: 2-65.99/.03/1/#2134, Anode:CU Zero=0.0

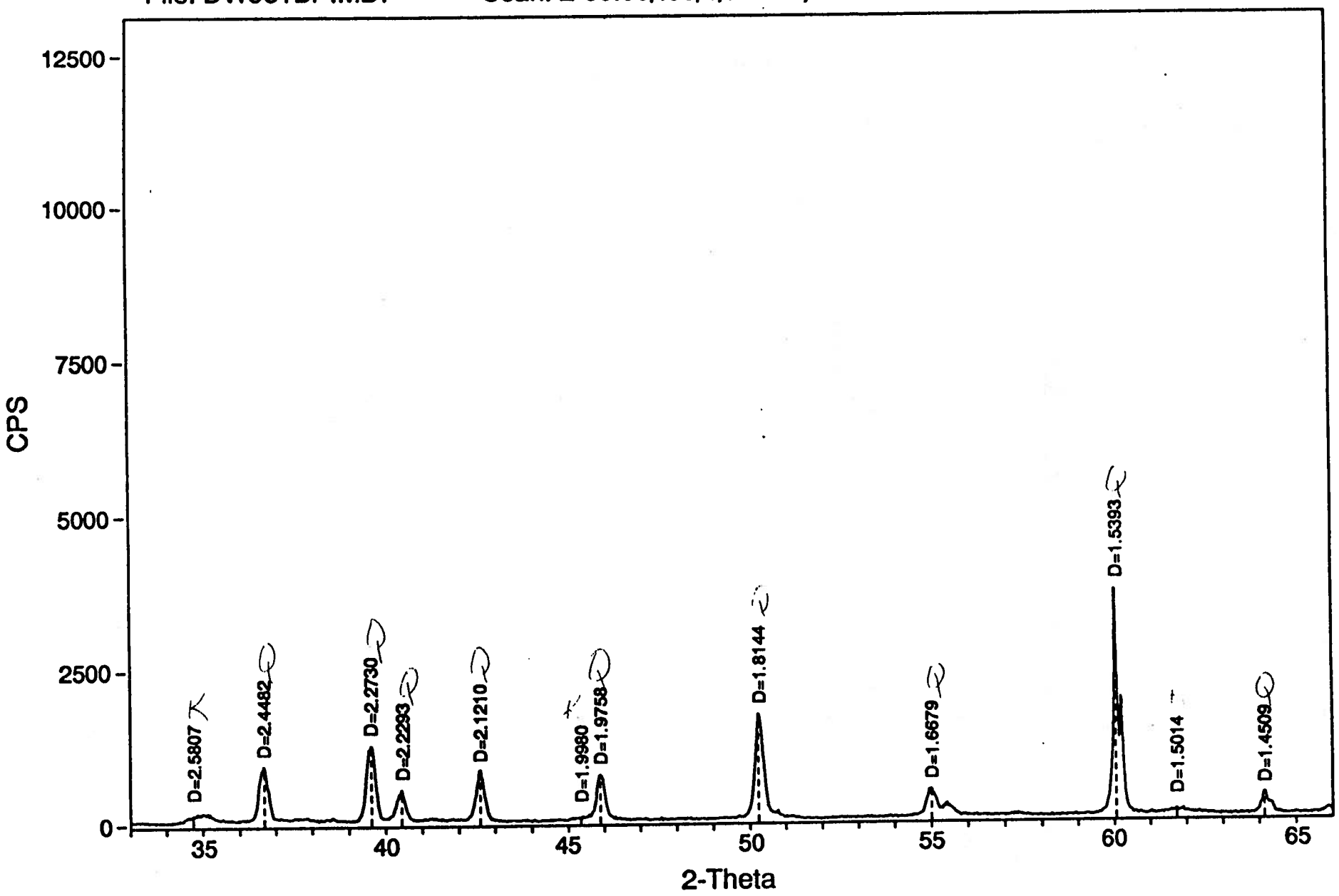

Jade: Peak Listing — Thu Nov 04 1993 @3:49pm

File: DW934BP.SAV> D:\CO2\DW934BP.MDI: DW 93-4 Back Pack

Scan Parameters:		Search Parameters:
Radiation = CU_1.540598	||	Filter length(pts) = 15
Scan Range = 2 - 65.99	||	Noise level(sigmas) = 4.5
Step Size = .03	||	Intensity cutoff(%) = .5-100
Count Time = 1 sec.	||	2-Theta Zero (degs) = 0

	Peak-Position		Centroid-Position		Peak & Area are without Bkgrd					
#	2Theta	d	2Theta	d	Bkgrd	Peak	I%	Area	I%	FWHM*
1:	12.408	7.1279	12.394	7.1358	74	192	1.0	2070	1.3	0.291
2:	19.878	4.4629	19.868	4.4652	70	101	0.5	1022	0.6	0.273
3:	20.899	4.2470	20.891	4.2488	82	3556	18.8	26737	16.7	0.203
4:	26.691	3.3372	26.692	3.3371	66	18873	100.0	160348	100.0	0.229
5:	27.739	3.2134	27.725	3.2151	58	190	1.0	4895	3.1	0.696
6:	32.088	2.7872	32.067	2.7890	65	150	0.8	1334	0.8	0.240
7:	35.029	2.5596	35.011	2.5608	62	138	0.7	1906	1.2	0.373
8:	36.617	2.4521	36.597	2.4534	69	1026	5.4	8315	5.2	0.219
9:	39.502	2.2794	39.515	2.2787	64	947	5.0	7986	5.0	0.228
10:	40.339	2.2341	40.329	2.2346	66	691	3.7	5702	3.6	0.223
11:	42.499	2.1254	42.495	2.1256	61	1389	7.4	11284	7.0	0.219
12:	45.857	1.9772	45.836	1.9781	48	544	2.9	5572	3.5	0.277
13:	50.211	1.8155	50.216	1.8154	45	2526	13.4	24057	15.0	0.257
14:	54.922	1.6704	54.949	1.6697	55	641	3.4	6037	3.8	0.254
15:	59.992	1.5408	60.012	1.5403	60	1134	6.0	11454	7.1	0.273
16:	64.101	1.4516	64.112	1.4513	46	260	1.4	2348	1.5	0.244

* Intensity values are based on counts per second.

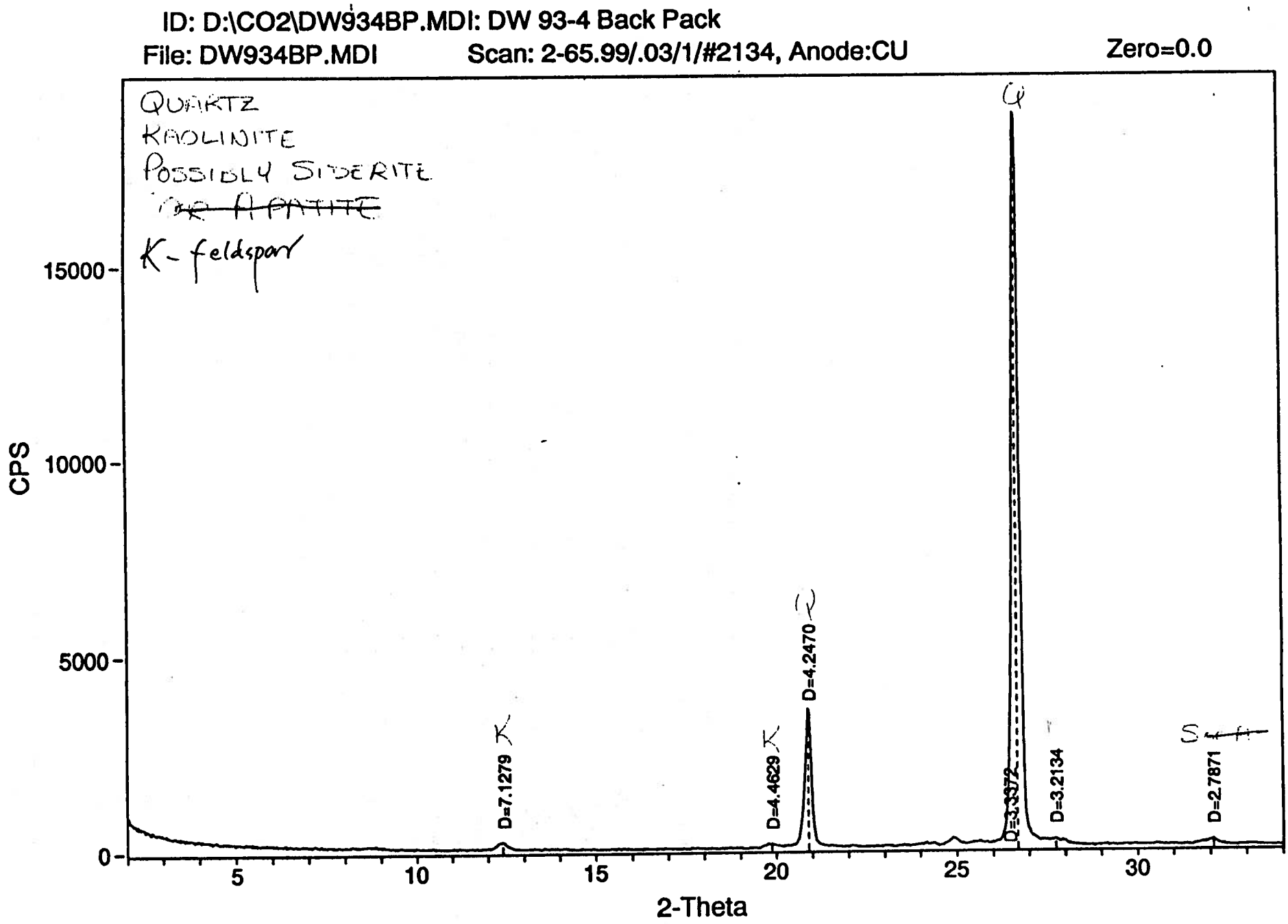
ID: D:\CO2\DW934BP.MDI: DW 93-4 Back Pack
File: DW934BP.MDI
Scan: 2-65.99/.03/1/#2134, Anode:CU
Zero=0.0
QUARTZ
KAOLINITE
POSSIBLY SIDERITE
~~OR APATITE~~
K-feldspar
CPS
15000
10000
5000
0
5
10
15
20
25
30
2-Theta
D=7.1279
D=4.4629
D=4.2470
D=3.3372
D=3.2134
D=2.7871
K
K
Q
Q
S

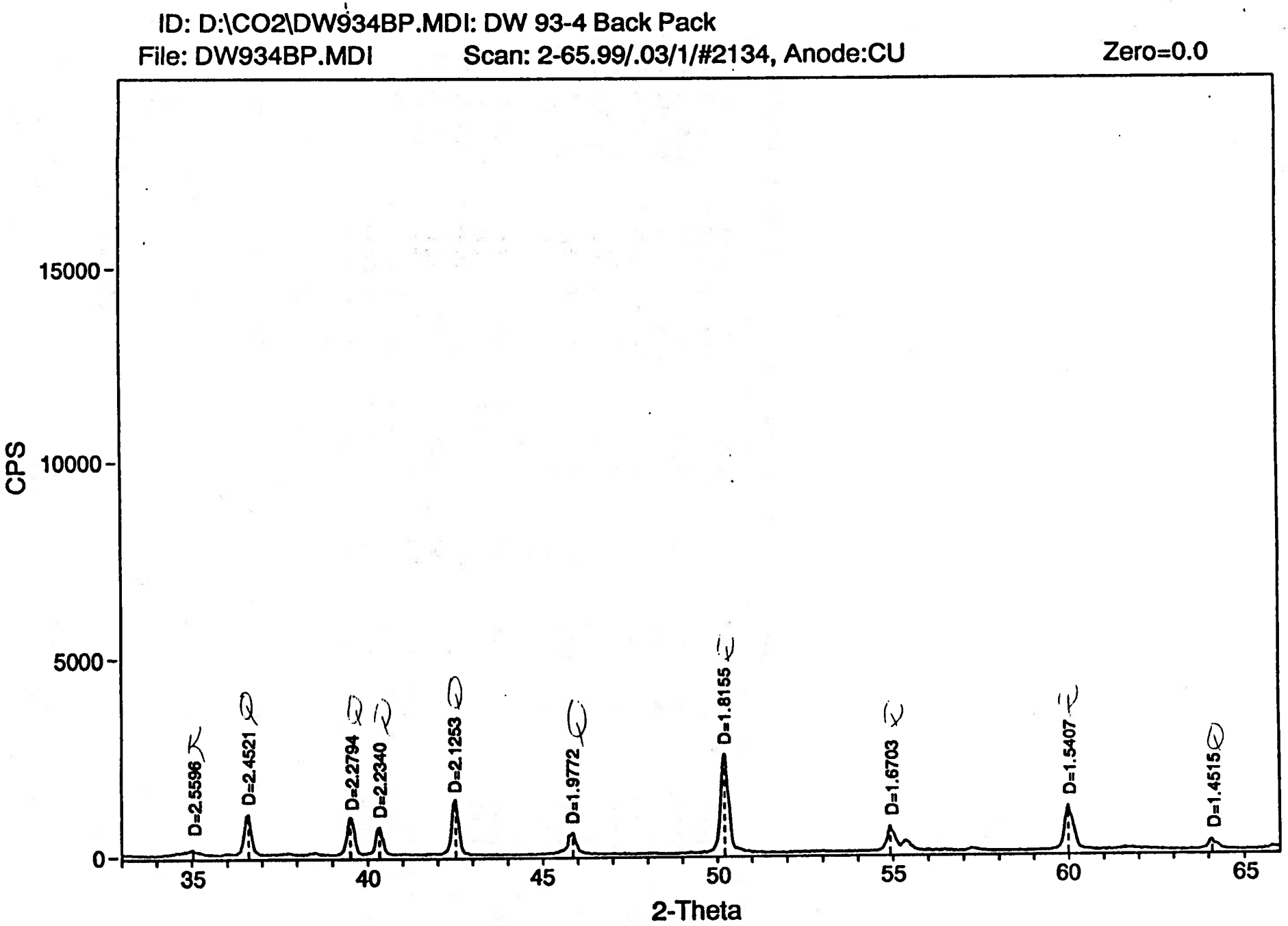
ID: D:\CO2\DW934BP.MDI: DW 93-4 Back Pack
File: DW934BP.MDI
Scan: 2-65.99/.03/1/#2134, Anode:CU
Zero=0.0
CPS
15000
10000
5000
0
35
40
45
50
55
60
65
2-Theta
D=2.5596
D=2.4521
D=2.2794
D=2.2340
D=2.1253
D=1.9772
D=1.8155
D=1.6703
D=1.5407
D=1.4515

Jade: Peak Listing — Thu Nov 04 1993 @3:49pm

File: DW935BP.SAV> D:\CO2\DW935BP.MDI: DW 93-5 Back Pack

Scan Parameters:		Search Parameters:
Radiation = CU_1.540598		Filter length(pts) = 15
Scan Range = 2 - 65.99		Noise level(sigmas) = 4.5
Step Size = .03		Intensity cutoff(%) = .5-100
Count Time = 1 sec.		2-Theta Zero (degs) = -.14

	Peak-Position		Centroid-Position		Peak & Area are without Bkgrd					
#	2Theta	d	2Theta	d	Bkgrd	Peak	I%	Area	I%	FWHM*
1:	8.821	10.0172	8.810	10.0295	95	85	0.7	861	0.8	0.273
2:	19.946	4.4478	19.911	4.4555	55	171	1.5	3114	3.0	0.492
3:	20.935	4.2399	20.891	4.2487	57	1989	17.1	19842	18.9	0.269
4:	26.670	3.3397	26.670	3.3398	94	11598	100.0	105042	100.0	0.245
5:	27.991	3.1851	27.992	3.1850	96	341	2.9	5245	5.0	0.415
6:	30.872	2.8941	30.863	2.8950	71	62	0.5	821	0.8	0.358
7:	35.009	2.5610	34.979	2.5631	61	197	1.7	3426	3.3	0.470
8:	36.571	2.4551	36.581	2.4544	66	836	7.2	7391	7.0	0.239
9:	37.649	2.3872	37.645	2.3875	59	61	0.5	979	0.9	0.433
10:	39.511	2.2790	39.518	2.2786	58	821	7.1	6705	6.4	0.221
11:	40.322	2.2349	40.338	2.2341	61	535	4.6	4967	4.7	0.251
12:	42.481	2.1262	42.491	2.1257	61	595	5.1	5535	5.3	0.251
13:	45.840	1.9779	45.834	1.9782	47	671	5.8	6198	5.9	0.249
14:	50.163	1.8172	50.183	1.8164	43	1729	14.9	17811	17.0	0.278
15:	54.902	1.6710	54.926	1.6703	57	472	4.1	5542	5.3	0.317
16:	59.973	1.5412	59.999	1.5406	62	1219	10.5	13039	12.4	0.289
17:	61.682	1.5026	61.705	1.5021	63	88	0.8	1219	1.2	0.374
18:	64.024	1.4531	64.054	1.4525	54	186	1.6	1972	1.9	0.286

* Intensity values are based on counts per second.

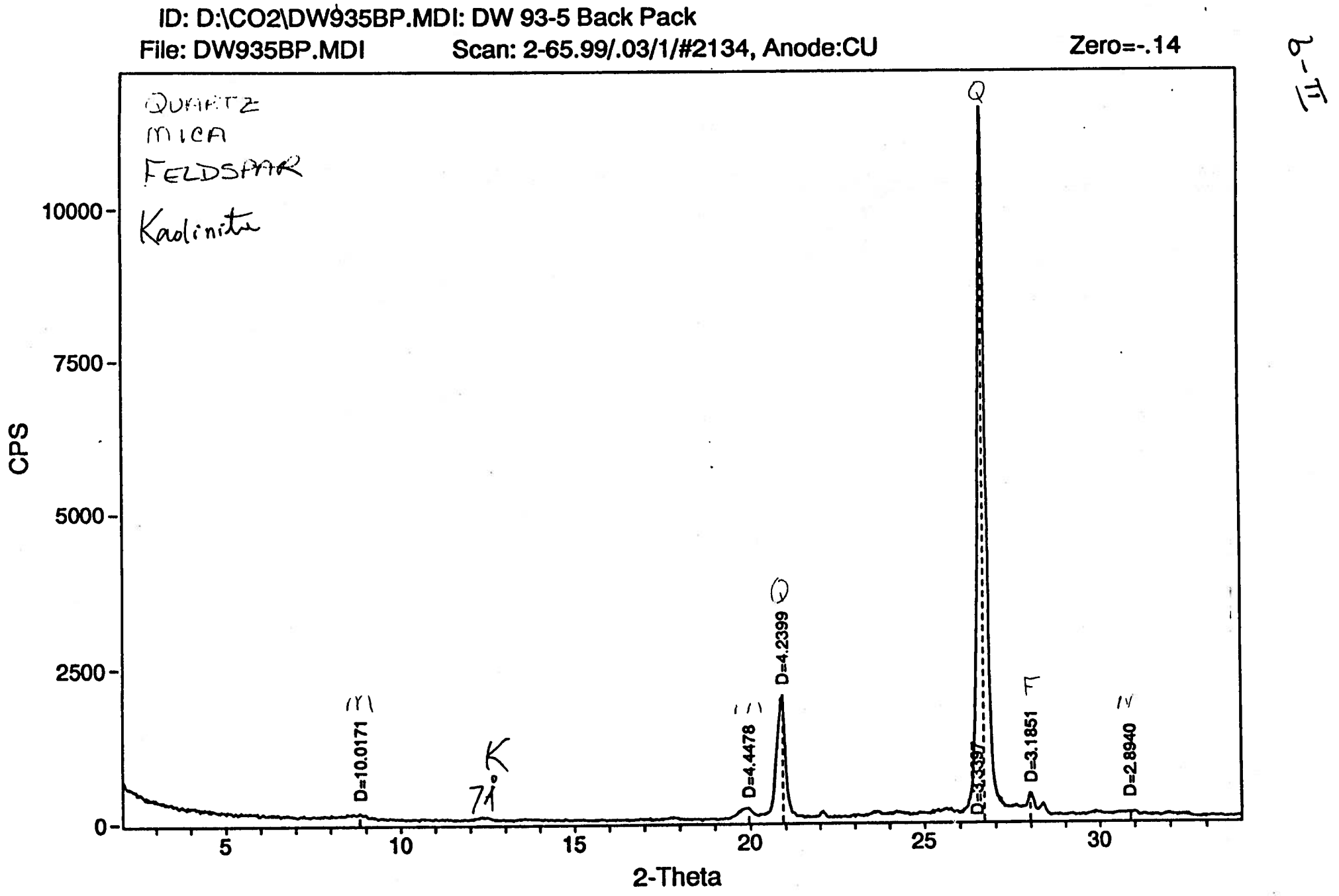
ID: D:\CO2\DW935BP.MDI: DW 93-5 Back Pack
File: DW935BP.MDI
Scan: 2-65.99/.03/1/#2134, Anode:CU
Zero=-.14
QUARTZ
MICA
FELDSPAR
Kaolinite
CPS
10000
7500
5000
2500
0
5
10
15
20
25
30
2-Theta
D=10.0171
D=4.4478
D=4.2399
D=3.3397
D=3.1851
D=2.8940
Q
K
T
M

ID: D:\CO2\DW935BP.MDI: DW 93-5 Back Pack
File: DW935BP.MDI Scan: 2-65.99/.03/1/#2134, Anode:CU Zero=-.14

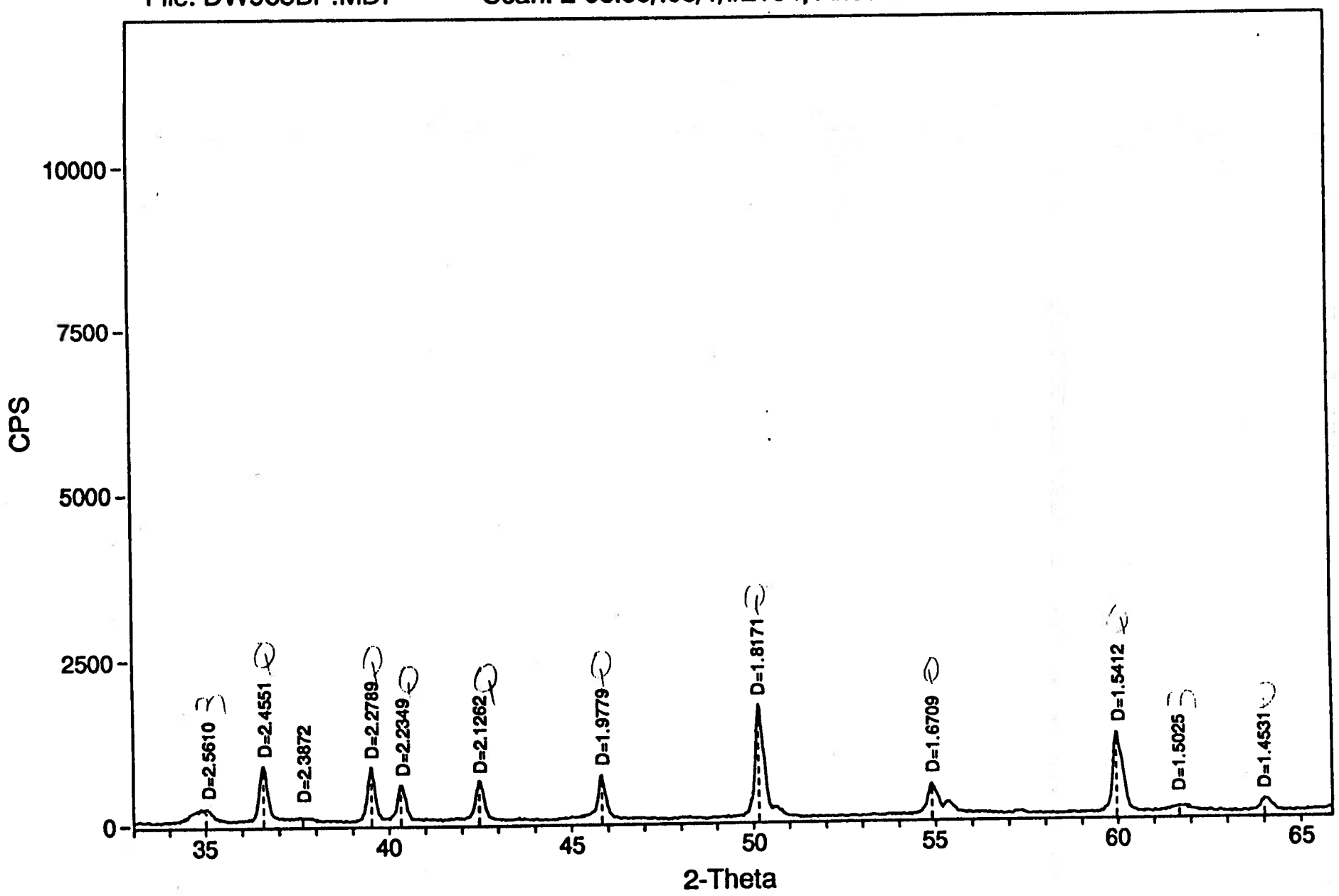

Jade: Peak Listing — Thu Nov 04 1993 @3:50pm

File: DW937BP.SAV> D:\CO2\DW937BP.MDI: DW 93-7 Back Pack

Scan Parameters:		Search Parameters:
Radiation = CU_1.540598		Filter length(pts) = 15
Scan Range = 2 - 65.99		Noise level(sigmas) = 4.5
Step Size = .03		Intensity cutoff(%) = .5-100
Count Time = 1 sec.		2-Theta Zero (degs) = 0

	Peak-Position		Centroid-Position		Peak & Area are without Bkgrd					
#	2Theta	d	2Theta	d	Bkgrd	Peak	I%	Area	I%	FWHM*
1:	12.470	7.0927	12.462	7.0969	78	140	1.0	1496	1.2	0.289
2:	19.853	4.4685	19.885	4.4614	70	151	1.1	1708	1.4	0.305
3:	20.986	4.2298	20.947	4.2376	67	2514	18.3	23727	19.6	0.255
4:	24.954	3.5655	24.962	3.5643	128	115	0.8	673	0.6	0.158
5:	26.750	3.3300	26.744	3.3307	105	13762	100.0	121264	100.0	0.238
6:	27.862	3.1995	27.876	3.1980	111	232	1.7	2810	2.3	0.327
7:	32.091	2.7869	32.101	2.7861	55	82	0.6	741	0.6	0.244
8:	35.089	2.5554	35.062	2.5572	67	175	1.3	2601	2.1	0.401
9:	36.651	2.4499	36.662	2.4492	76	1377	10.0	11189	9.2	0.219
10:	39.590	2.2746	39.587	2.2747	65	865	6.3	7107	5.9	0.222
11:	40.400	2.2308	40.399	2.2309	64	484	3.5	4341	3.6	0.242
12:	42.561	2.1224	42.567	2.1221	56	770	5.6	7061	5.8	0.248
13:	45.891	1.9759	45.897	1.9756	47	630	4.6	6369	5.3	0.273
14:	50.270	1.8135	50.272	1.8135	46	1586	11.5	15600	12.9	0.266
15:	54.982	1.6687	55.006	1.6681	61	1268	9.2	12710	10.5	0.271
16:	60.081	1.5387	60.090	1.5385	61	1484	10.8	14554	12.0	0.265
17:	61.760	1.5009	61.766	1.5007	57	61	0.4	899	0.7	0.398
18:	64.132	1.4509	64.149	1.4506	50	253	1.8	2364	1.9	0.252

* Intensity values are based on counts per second.

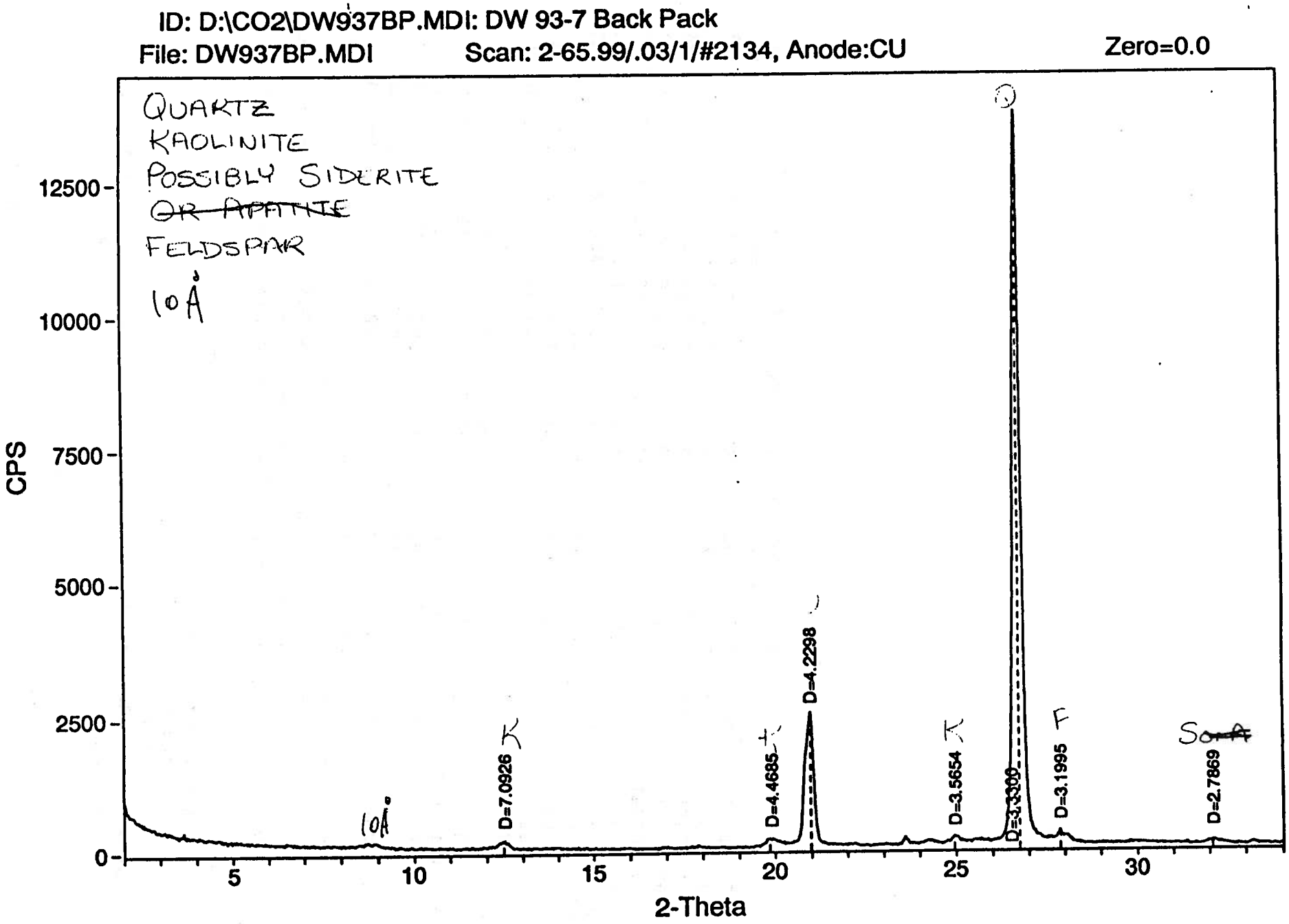
ID: D:\CO2\DW937BP.MDI: DW 93-7 Back Pack
File: DW937BP.MDI
Scan: 2-65.99/.03/1/#2134, Anode:CU
Zero=0.0
QUARTZ
KAOLINITE
POSSIBLY SIDERITE
~~OR APATITE~~
FELDSPAR
10Å
CPS
12500
10000
7500
5000
2500
0
5
10
15
20
25
30
2-Theta
10Å
D=7.0926
D=4.4685
D=4.2298
D=3.5654
D=3.3300
D=3.1995
D=2.7869
K
K
F

21-TL

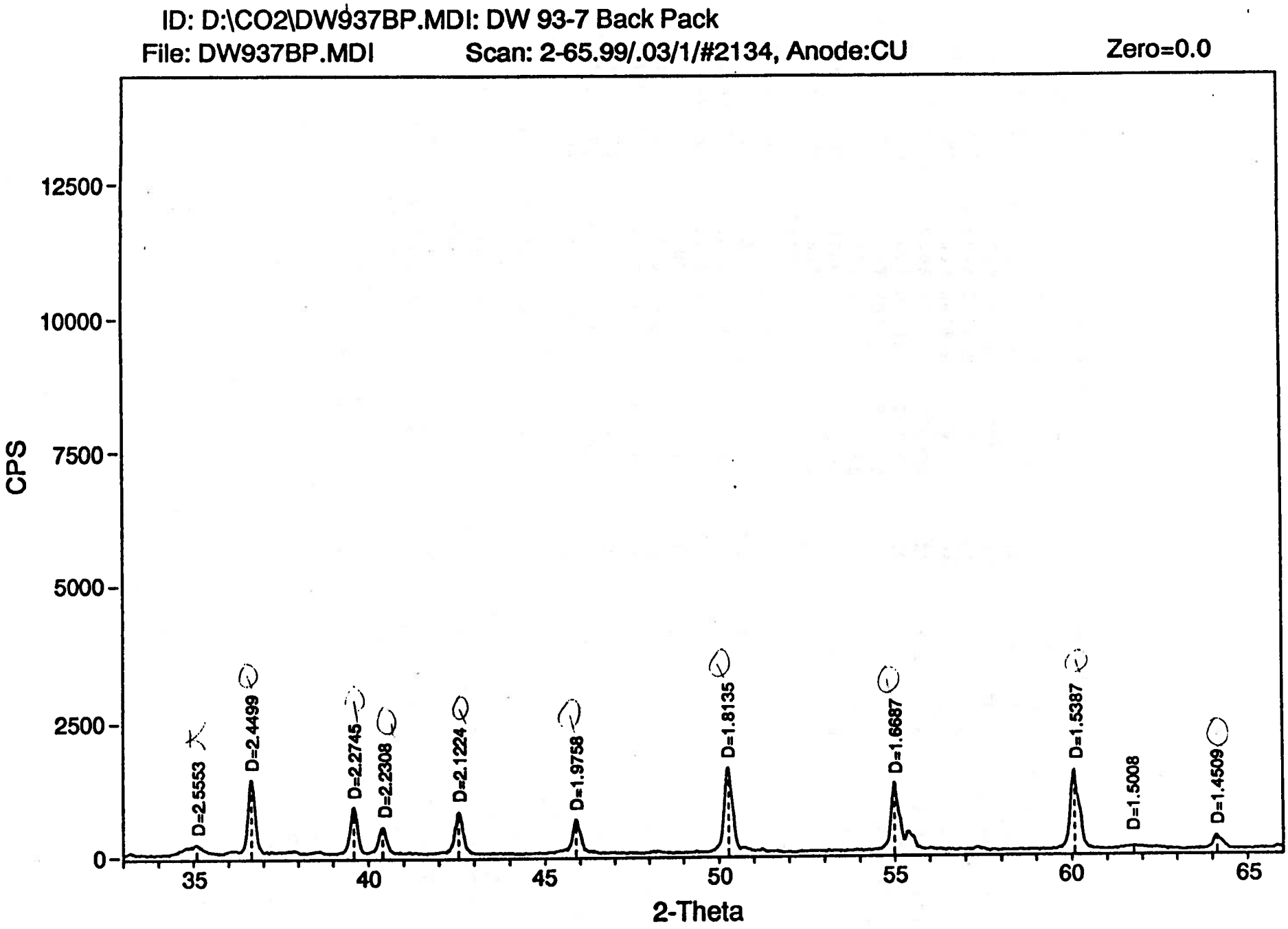
ID: D:\CO2\DW937BP.MDI: DW 93-7 Back Pack
File: DW937BP.MDI
Scan: 2-65.99/.03/1/#2134, Anode:CU
Zero=0.0
CPS
12500
10000
7500
5000
2500
0
35
40
45
50
55
60
65
2-Theta
D=2.5553
D=2.4499
D=2.2745
D=2.2308
D=2.1224
D=1.9758
D=1.8135
D=1.6687
D=1.5387
D=1.5008
D=1.4509

Jade: Peak Listing — Thu Nov 04 1993 @3:51pm

File: DW938BP.SAV> D:\CO2\DW938BP.MDI: DW 93-8 Back Pack

Scan Parameters:		Search Parameters:	
Radiation	= CU_1.540598	Filter length(pts)	= 15
Scan Range	= 2 - 65.99	Noise level(sigmas)	= 4.5
Step Size	= .03	Intensity cutoff(%)	= .5-100
Count Time	= 1 sec.	2-Theta Zero (degs)	= -.08

	Peak-Position		Centroid-Position		Peak & Area are without Bkgrd					
#	2Theta	d	2Theta	d	Bkgrd	Peak	I%	Area	I%	FWHM*
1:	8.849	9.9850	8.836	9.9994	118	149	1.5	1391	1.7	0.252
2:	12.361	7.1550	12.359	7.1559	74	190	2.0	1980	2.5	0.281
3:	17.819	4.9738	17.809	4.9765	49	85	0.9	862	1.1	0.274
4:	19.889	4.4605	19.884	4.4615	57	203	2.1	3161	4.0	0.420
5:	20.881	4.2507	20.884	4.2501	61	1413	14.6	15317	19.2	0.293
6:	24.929	3.5689	24.925	3.5694	115	191	2.0	1402	1.8	0.198
7:	26.671	3.3397	26.675	3.3392	107	9656	100.0	79850	100.0	0.223
8:	29.489	3.0266	29.485	3.0270	91	1081	11.2	10023	12.6	0.250
9:	30.990	2.8834	30.985	2.8838	79	710	7.4	6790	8.5	0.258
10:	33.089	2.7051	33.091	2.7049	54	163	1.7	1203	1.5	0.199
11:	35.009	2.5610	34.995	2.5620	72	239	2.5	4041	5.1	0.457
12:	36.032	2.4906	36.037	2.4902	62	180	1.9	1886	2.4	0.283
13:	36.600	2.4533	36.600	2.4532	84	876	9.1	7006	8.8	0.216
14:	37.440	2.4001	37.434	2.4005	76	124	1.3	2260	2.8	0.492
15:	38.580	2.3318	38.577	2.3320	69	69	0.7	404	0.5	0.158
16:	39.511	2.2789	39.516	2.2787	64	888	9.2	7469	9.4	0.227
17:	40.322	2.2349	40.331	2.2345	65	302	3.1	2935	3.7	0.262
18:	41.160	2.1914	41.149	2.1919	72	203	2.1	2001	2.5	0.266
19:	42.510	2.1249	42.507	2.1250	60	439	4.5	4172	5.2	0.257
20:	43.262	2.0896	43.269	2.0893	61	149	1.5	1134	1.4	0.205
21:	44.971	2.0141	44.985	2.0135	52	95	1.0	1039	1.3	0.295
22:	45.784	1.9802	45.798	1.9797	55	312	3.2	3753	4.7	0.325
23:	47.552	1.9106	47.546	1.9109	57	158	1.6	2108	2.6	0.360
24:	48.632	1.8707	48.644	1.8703	56	182	1.9	1567	2.0	0.232
25:	50.162	1.8172	50.189	1.8163	51	1219	12.6	11024	13.8	0.244
26:	51.092	1.7863	51.096	1.7861	48	180	1.9	2058	2.6	0.309
27:	54.931	1.6702	54.951	1.6696	57	277	2.9	3404	4.3	0.332
28:	56.281	1.6333	56.280	1.6333	64	136	1.4	2141	2.7	0.425
29:	57.511	1.6012	57.508	1.6013	63	84	0.9	787	1.0	0.253
30:	59.973	1.5412	59.999	1.5406	70	980	10.1	10168	12.7	0.280
31:	61.800	1.5000	61.785	1.5003	66	98	1.0	1505	1.9	0.415
32:	64.055	1.4525	64.079	1.4520	59	149	1.5	1171	1.5	0.212

* Intensity values are based on counts per second.

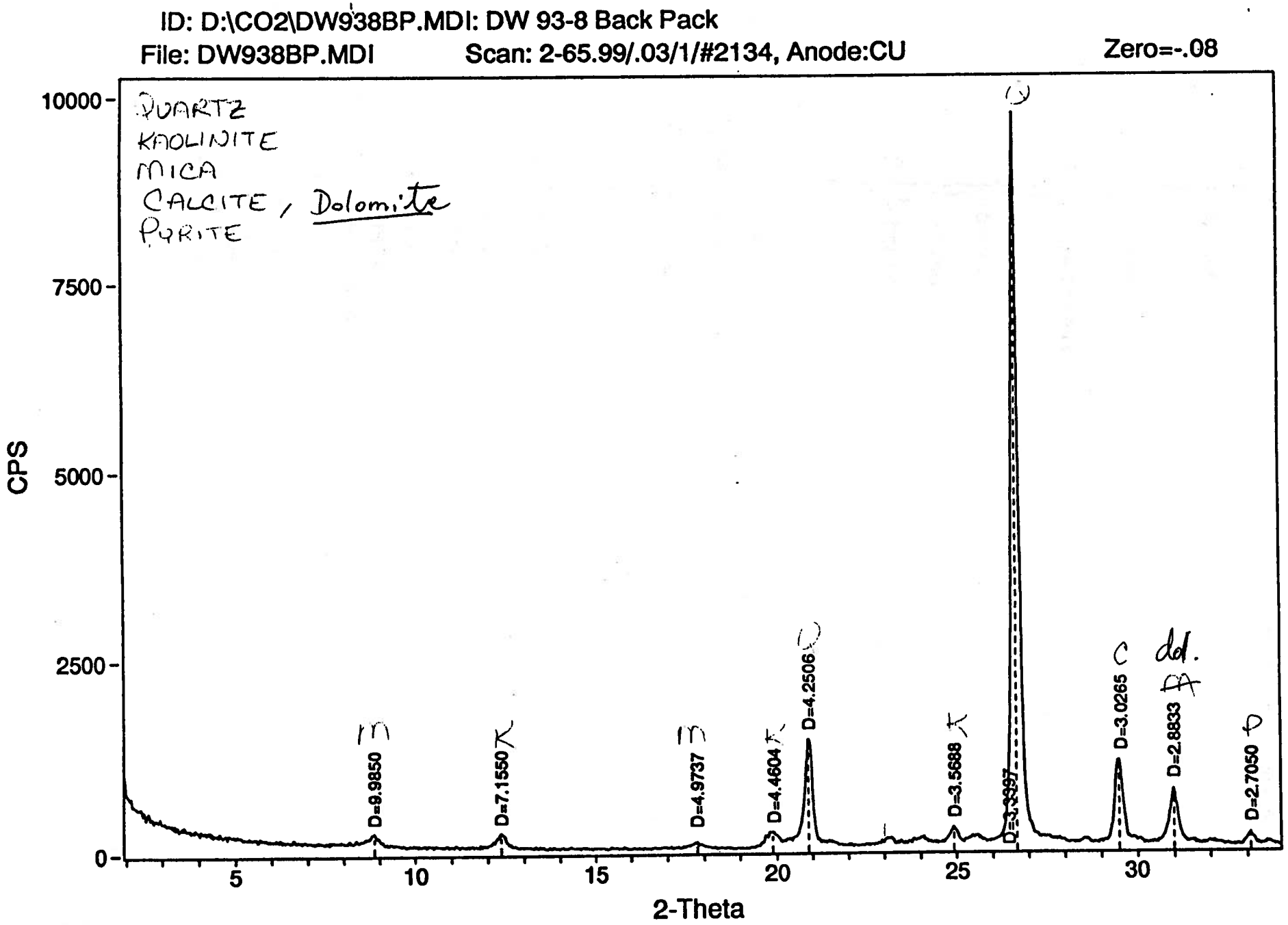
ID: D:\CO2\DW938BP.MDI: DW 93-8 Back Pack
File: DW938BP.MDI
Scan: 2-65.99/.03/1/#2134, Anode:CU
Zero=-.08
QUARTZ
KAOLINITE
MICA
CALCITE, Dolomite
PYRITE
CPS
10000
7500
5000
2500
0
5
10
15
20
25
30
2-Theta
D=9.9850
D=7.1550
D=4.9737
D=4.4604
D=4.2506
D=3.5688
D=3.3397
D=3.0265
D=2.8833
D=2.7050

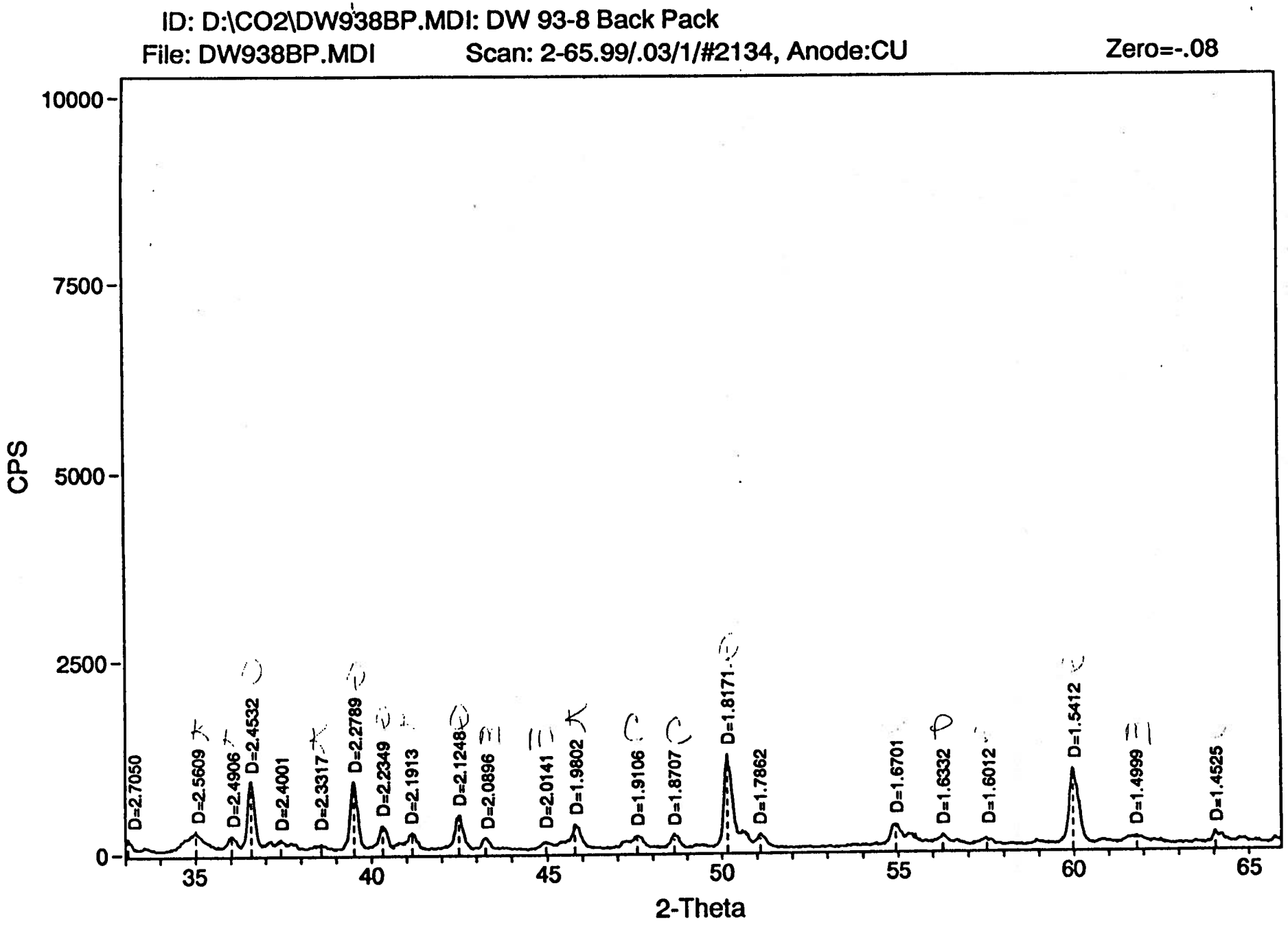
ID: D:\CO2\DW938BP.MDI: DW 93-8 Back Pack
File: DW938BP.MDI
Scan: 2-65.99/.03/1/#2134, Anode:CU
Zero=-.08
CPS
10000
7500
5000
2500
0
35
40
45
50
55
60
65
2-Theta
D=2.7050
D=2.5609
D=2.4906
D=2.4532
D=2.4001
D=2.3317
D=2.2789
D=2.2349
D=2.1913
D=2.1248
D=2.0896
D=2.0141
D=1.9802
D=1.9106
D=1.8707
D=1.8171
D=1.7862
D=1.6701
D=1.6332
D=1.6012
D=1.5412
D=1.4999
D=1.4525

Jade: Peak Listing — Fri Nov 05 1993 @11:01am

File: DW939BP.MDI> D:\CO2\DW939BP.MDI: DW 93-9 Back Pack

Scan Parameters:		Search Parameters:
Radiation = CU_1.540598		Filter length(pts) = 15
Scan Range = 2 - 65.99		Noise level(sigmas) = 4.5
Step Size = .03		Intensity cutoff(%) = .5-100
Count Time = 1 sec.		2-Theta Zero (degs) = 0

	Peak-Position		Centroid-Position		Peak & Area are without Bkgrd					
#	2Theta	d	2Theta	d	Bkgrd	Peak	I%	Area	I%	FWHM*
1:	12.352	7.1599	12.352	7.1601	72	71	0.4	327	0.2	0.124
2:	19.881	4.4622	19.899	4.4582	50	130	0.7	1537	1.1	0.319
3:	20.927	4.2415	20.906	4.2458	55	3046	16.1	24254	17.2	0.215
4:	23.176	3.8348	23.162	3.8371	64	104	0.5	779	0.6	0.202
5:	26.691	3.3372	26.694	3.3368	118	18960	100.0	140820	100.0	0.201
6:	29.598	3.0157	29.579	3.0176	49	4370	23.0	28990	20.6	0.179
7:	31.038	2.8790	31.019	2.8807	41	738	3.9	6623	4.7	0.242
8:	35.030	2.5595	35.018	2.5604	51	122	0.6	1765	1.3	0.391
9:	36.619	2.4520	36.614	2.4523	58	809	4.3	6955	4.9	0.232
10:	39.532	2.2778	39.545	2.2770	58	1090	5.7	8531	6.1	0.211
11:	40.370	2.2324	40.367	2.2326	56	593	3.1	4736	3.4	0.216
12:	41.211	2.1888	41.210	2.1888	56	116	0.6	1075	0.8	0.250
13:	42.531	2.1239	42.535	2.1236	52	1206	6.4	9817	7.0	0.220
14:	43.282	2.0887	43.290	2.0883	50	131	0.7	1155	0.8	0.238
15:	45.860	1.9771	45.858	1.9772	49	497	2.6	4391	3.1	0.239
16:	47.662	1.9065	47.656	1.9067	52	190	1.0	1802	1.3	0.256
17:	48.652	1.8700	48.668	1.8694	53	185	1.0	1593	1.1	0.232
18:	50.184	1.8164	50.213	1.8155	51	2662	14.0	22990	16.3	0.233
19:	51.142	1.7846	51.147	1.7845	45	153	0.8	1614	1.1	0.285
20:	54.952	1.6696	54.968	1.6691	55	451	2.4	4506	3.2	0.270
21:	55.429	1.6563	55.415	1.6567	50	189	1.0	1969	1.4	0.281
22:	60.021	1.5401	60.036	1.5398	59	1155	6.1	11583	8.2	0.271
23:	61.162	1.5141	61.161	1.5141	50	86	0.5	1494	1.1	0.469
24:	64.102	1.4515	64.118	1.4512	51	192	1.0	1646	1.2	0.231

* Intensity values are based on counts per second.

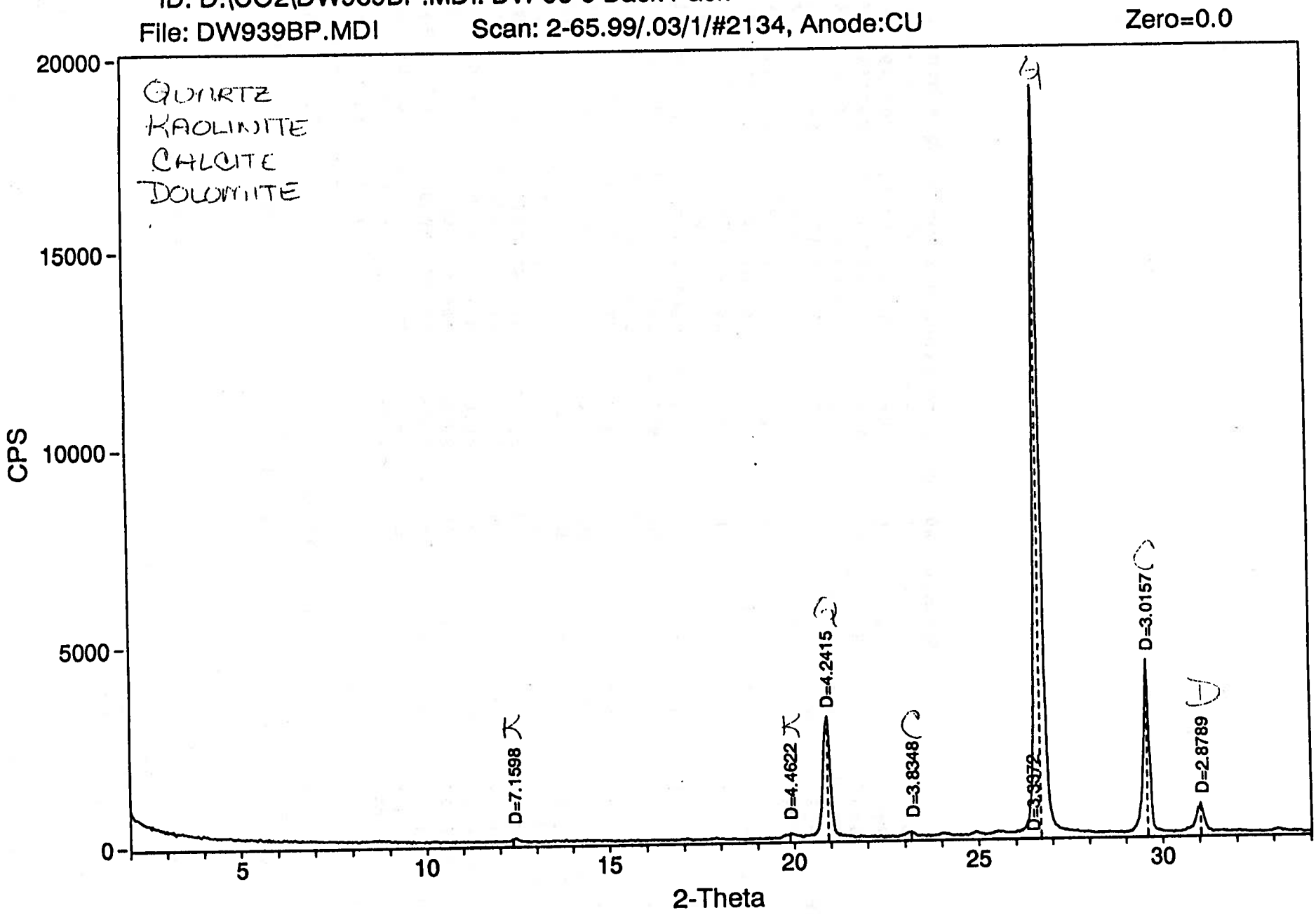
ID: D:\CO2\DW939BP.MDI: DW 93-9 Back Pack
File: DW939BP.MDI
Scan: 2-65.99/.03/1/#2134, Anode:CU
Zero=0.0
QUARTZ
KAOLINITE
CALCITE
DOLOMITE
CPS
20000
15000
10000
5000
0
5
10
15
20
25
30
2-Theta
D=7.1598
D=4.4622
D=4.2415
D=3.8348
D=3.3372
D=3.0157
D=2.8789

81-T1

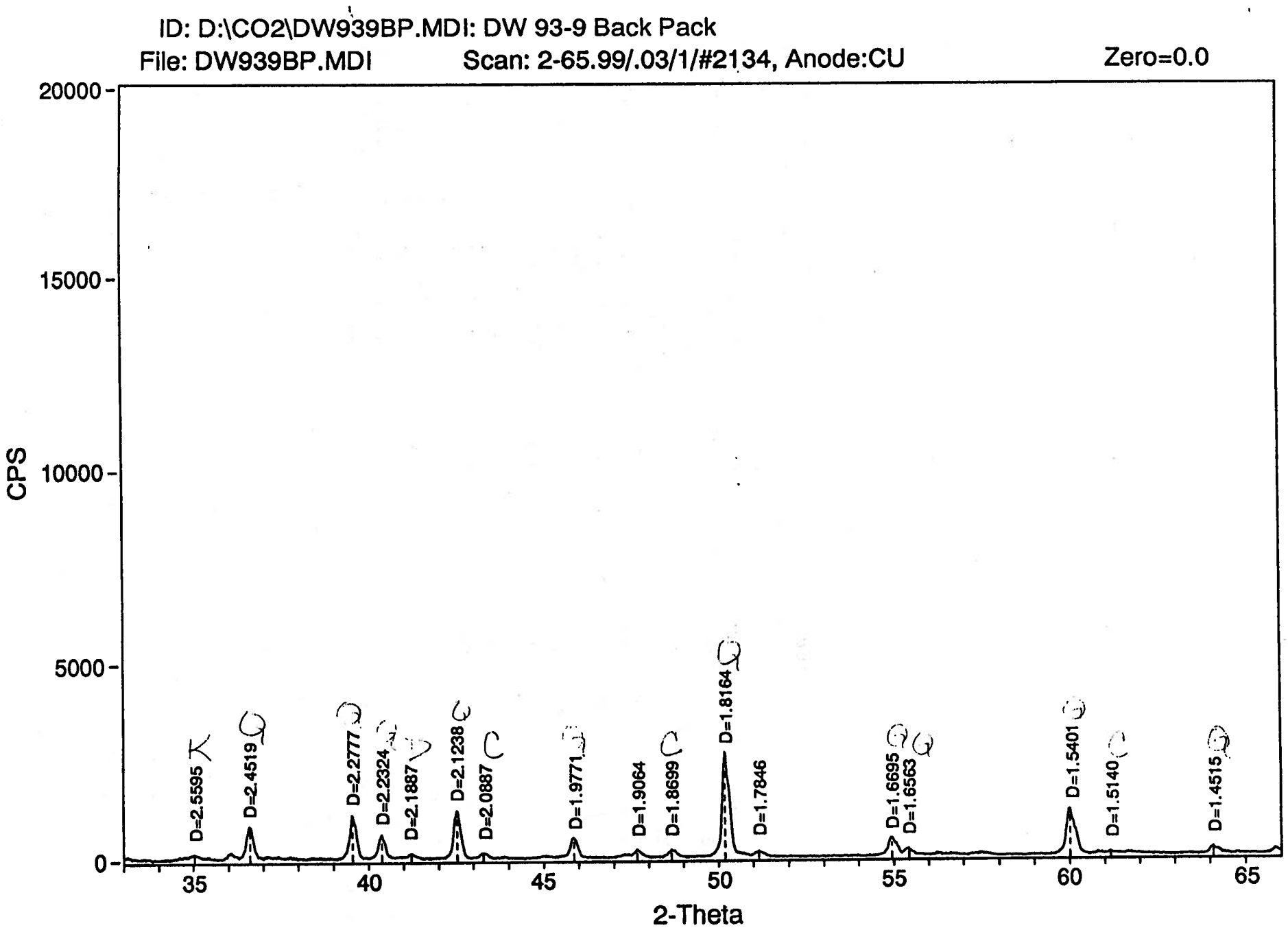
ID: D:\CO2\DW939BP.MDI: DW 93-9 Back Pack
File: DW939BP.MDI
Scan: 2-65.99/.03/1/#2134, Anode:CU
Zero=0.0
CPS
20000
15000
10000
5000
0
35
40
45
50
55
60
65
2-Theta
D=2.5595
D=2.4519
D=2.2777
D=2.2324
D=2.1887
D=2.1238
D=2.0887
D=1.9771
D=1.9064
D=1.8699
D=1.8164
D=1.7846
D=1.6695
D=1.6563
D=1.5401
D=1.5140
D=1.4515

II-19

Jade: Peak Listing — Thu Nov 04 1993 @3:47pm

File: DW9313BP.SAV> D:\CO2\DW9313BP.MDI: DW 93-13 Back Pack

Scan Parameters:		Search Parameters:
Radiation = CU_1.540598		Filter length(pts) = 15
Scan Range = 2 - 65.99		Noise level(sigmas) = 4.5
Step Size = .03		Intensity cutoff(%) = .5-100
Count Time = 1 sec.		2-Theta Zero (degs) = 0

	Peak-Position		Centroid-Position		Peak & Area are without Bkgrd					
#	2Theta	d	2Theta	d	Bkgrd	Peak	I%	Area	I%	FWHM*
1:	12.291	7.1953	12.278	7.2027	87	279	1.5	3507	2.7	0.339
2:	20.837	4.2596	20.817	4.2637	80	3415	18.9	34143	25.9	0.270
3:	24.861	3.5785	24.880	3.5759	153	417	2.3	4425	3.4	0.287
4:	26.627	3.3450	26.608	3.3474	50	18060	100.0	131726	100.0	0.197
5:	34.944	2.5656	34.979	2.5631	62	191	1.1	2413	1.8	0.341
6:	35.901	2.4994	35.886	2.5004	66	194	1.1	5898	4.5	0.821
7:	36.501	2.4597	36.506	2.4594	76	1214	6.7	11076	8.4	0.246
8:	37.730	2.3824	37.734	2.3821	82	95	0.5	754	0.6	0.214
9:	38.479	2.3377	38.482	2.3375	76	230	1.3	4083	3.1	0.479
10:	39.441	2.2828	39.438	2.2830	73	1010	5.6	8701	6.6	0.233
11:	40.280	2.2372	40.274	2.2375	66	602	3.3	4722	3.6	0.212
12:	42.440	2.1282	42.438	2.1283	53	950	5.3	7500	5.7	0.213
13:	45.799	1.9796	45.783	1.9803	58	607	3.4	5613	4.3	0.250
14:	50.122	1.8185	50.140	1.8179	55	2002	11.1	16506	12.5	0.223
15:	54.863	1.6721	54.887	1.6714	66	514	2.8	6522	5.0	0.343
16:	55.341	1.6588	55.336	1.6589	68	296	1.6	4165	3.2	0.380
17:	59.933	1.5422	59.958	1.5416	51	1720	9.5	14938	11.3	0.234
18:	62.245	1.4903	62.287	1.4894	52	163	0.9	1914	1.5	0.317
19:	64.041	1.4528	64.054	1.4525	56	169	0.9	1774	1.3	0.283

* Intensity values are based on counts per second.

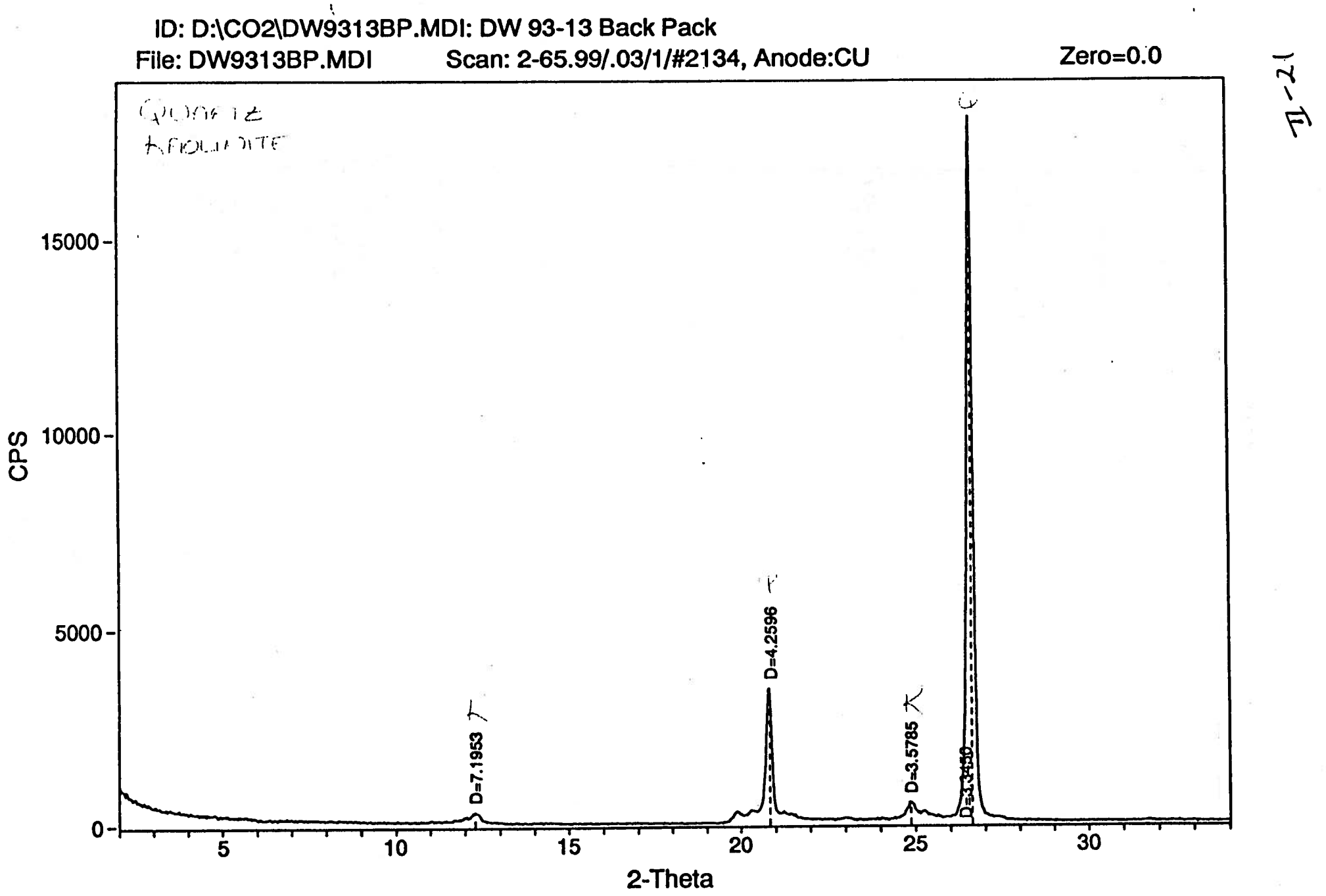
ID: D:\CO2\DW9313BP.MDI: DW 93-13 Back Pack
File: DW9313BP.MDI
Scan: 2-65.99/.03/1/#2134, Anode:CU
Zero=0.0
CALCITE
ARAGONITE
15000
10000
5000
0
CPS
D=7.1953
D=4.2596
D=3.5785
D=3.2450
5
10
15
20
25
30
2-Theta

ID: D:\CO2\DW9313BP.MDI: DW 93-13 Back Pack

File: DW9313BP.MDI Scan: 2-65.99/.03/1/#2134, Anode:CU Zero=0.0

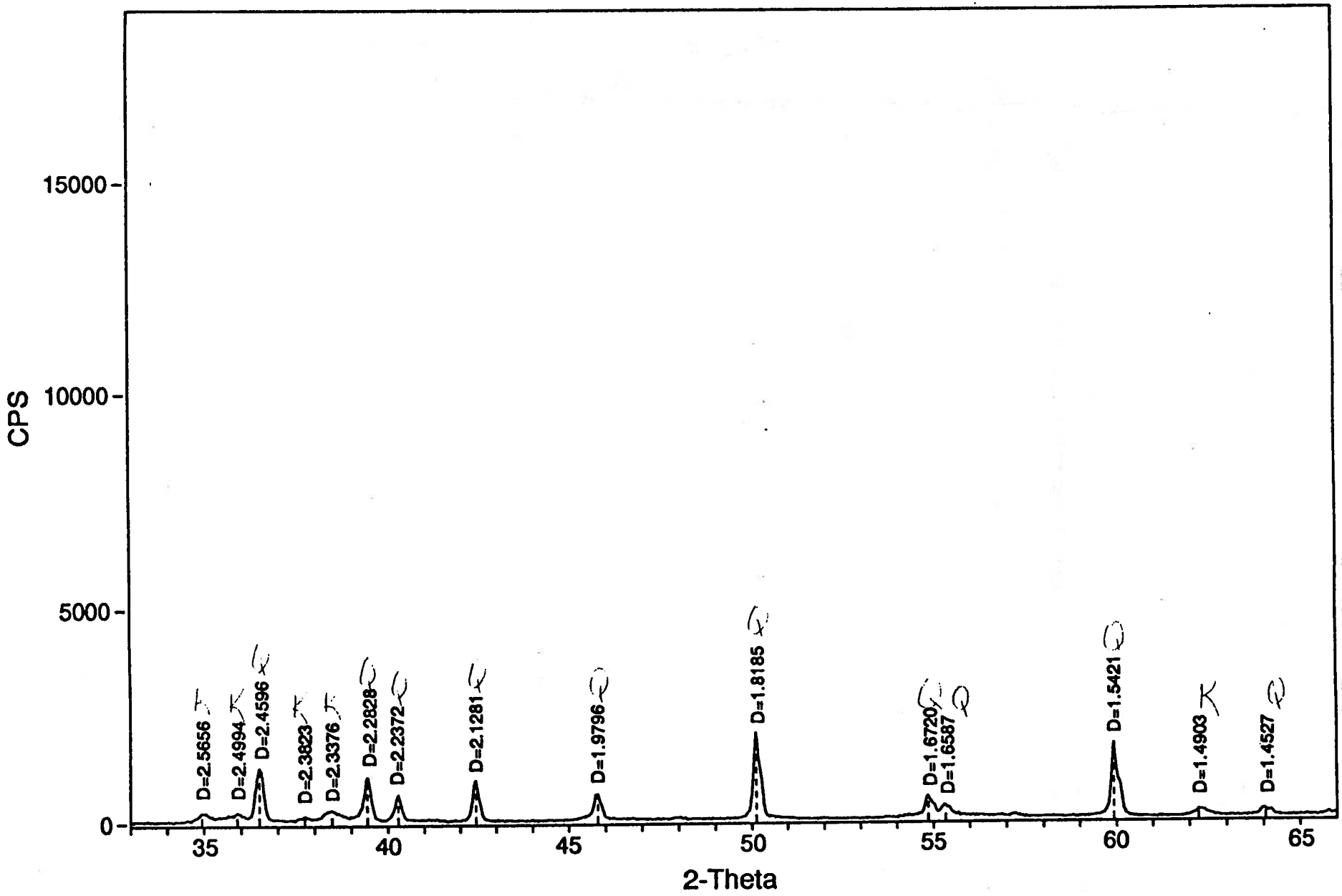

APPENDIX III

XRD Traces of Autoclave Experiment Powders

Jade: Peak Listing — Thu Mar 24 1994 @11:10am

File: AL4711PR.SAV> D:\OTHERUSE\BRIAN\AL4711PR.MDI: Albite & Sand 4711 Pre-Run Bulk

Scan Parameters:
Radiation = CU_1.540598
Scan Range = 2 - 65.99
Step Size = .03
Count Time = 1 sec.

Search Parameters:
Filter length(pts) = 9
Noise level(sigmas) = 3.5
Intensity cutoff(%) = .5-100
2-Theta Zero (degs) = 0

	Peak-Position		Centroid-Position		Peak & Area are without Bkgrd					
#	2Theta	d	2Theta	d	Bkgrd	Peak	I%	Area	I%	FWHM*
1:	13.819	6.4033	13.816	6.4047	107	329	3.5	3336	3.3	0.274
2:	20.784	4.2704	20.803	4.2666	50	372	3.9	3694	3.7	0.268
3:	21.952	4.0457	21.959	4.0445	51	199	2.1	1752	1.7	0.238
4:	23.024	3.8597	23.008	3.8624	64	134	1.4	709	0.7	0.143
5:	23.718	3.7483	23.722	3.7476	62	332	3.5	4645	4.6	0.378
6:	24.258	3.6661	24.245	3.6681	59	1104	11.7	9473	9.4	0.232
7:	25.491	3.4915	25.499	3.4905	66	188	2.0	1667	1.7	0.239
8:	26.627	3.3450	26.615	3.3466	76	2240	23.7	24968	24.9	0.301
9:	27.979	3.1864	27.967	3.1877	64	9439	100.0	100474	100.0	0.287
10:	29.723	3.0034	29.737	3.0020	63	179	1.9	1182	1.2	0.178
11:	30.349	2.9427	30.351	2.9426	57	348	3.7	3753	3.7	0.291
12:	31.403	2.8463	31.414	2.8454	53	527	5.6	5453	5.4	0.279
13:	35.298	2.5407	35.291	2.5412	55	97	1.0	1644	1.6	0.458
14:	36.585	2.4542	36.563	2.4556	45	183	1.9	2629	2.6	0.388
15:	37.581	2.3914	37.588	2.3910	42	330	3.5	3369	3.4	0.276
16:	39.500	2.2796	39.495	2.2798	42	159	1.7	1873	1.9	0.318
17:	40.279	2.2373	40.279	2.2372	43	82	0.9	579	0.6	0.191
18:	42.381	2.1310	42.387	2.1307	40	238	2.5	3125	3.1	0.355
19:	44.720	2.0249	44.724	2.0247	36	58	0.6	630	0.6	0.293
20:	45.589	1.9882	45.594	1.9881	37	273	2.9	4156	4.1	0.411
21:	46.822	1.9387	46.836	1.9382	39	62	0.7	527	0.5	0.229
22:	48.320	1.8821	48.322	1.8820	45	67	0.7	628	0.6	0.253
23:	49.820	1.8288	49.823	1.8287	38	415	4.4	7318	7.3	0.476
24:	50.723	1.7984	50.733	1.7981	42	196	2.1	3026	3.0	0.417
25:	51.287	1.7799	51.284	1.7800	41	90	1.0	979	1.0	0.294
26:	52.370	1.7456	52.387	1.7451	39	67	0.7	844	0.8	0.340
27:	53.179	1.7210	53.177	1.7210	40	277	2.9	2959	2.9	0.288
28:	55.277	1.6605	55.279	1.6605	37	101	1.1	1447	1.4	0.387
29:	57.744	1.5953	57.757	1.5950	39	81	0.9	901	0.9	0.300
30:	58.757	1.5702	58.739	1.5706	42	211	2.2	2543	2.5	0.325
31:	59.961	1.5415	59.974	1.5412	46	312	3.3	4012	4.0	0.347
32:	63.775	1.4582	63.814	1.4574	51	1839	19.5	22189	22.1	0.326

* Intensity values are based on counts per second.

III-1

ID: D:\OTHERUSE\BRIAN\AL4711PR.MDI: Albite & Sand 4711 Pre-Run Bulk

File: AL4711PR.MDI Scan: 2-65.99/.03/1/#2134, Anode:CU Zero=0.0

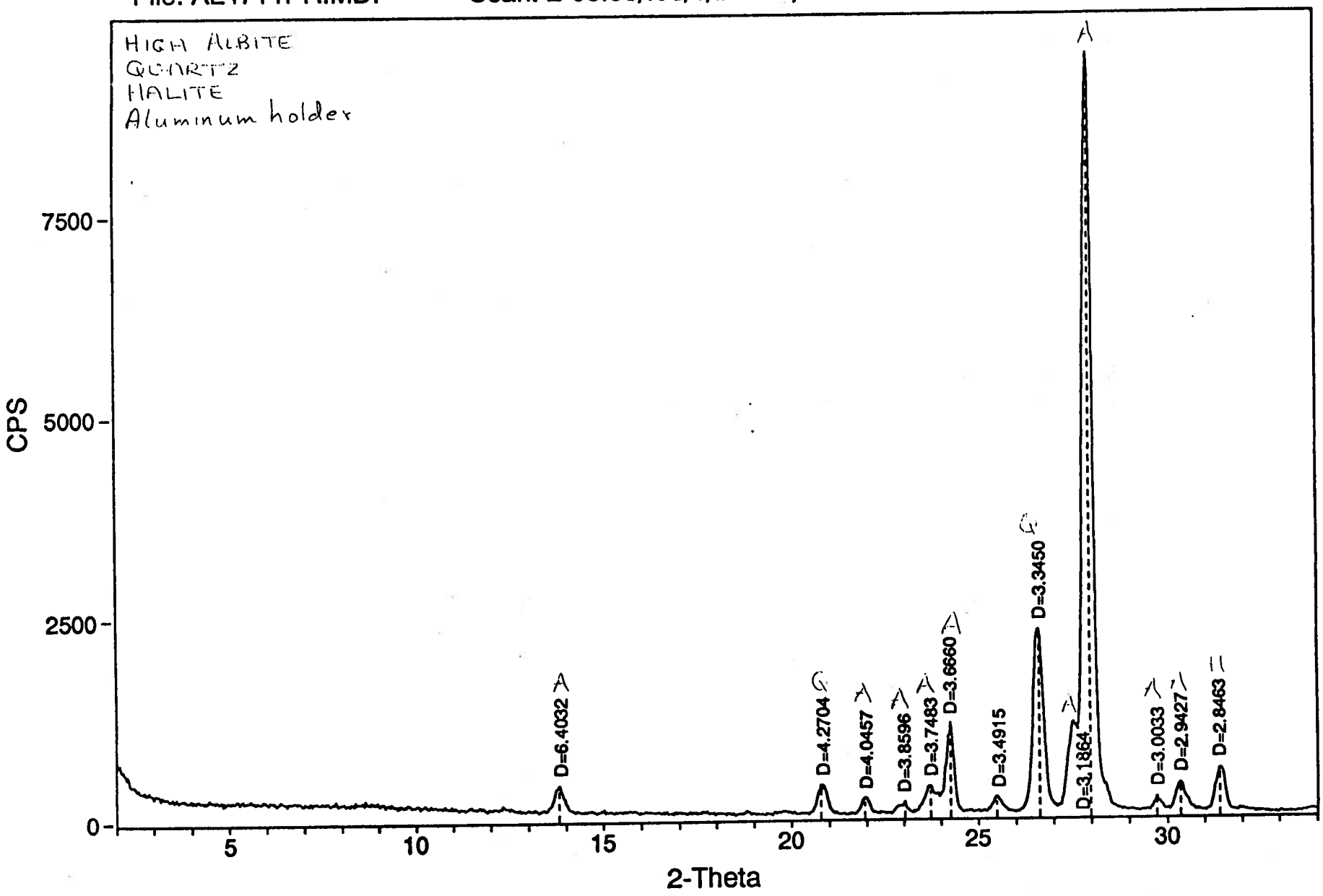

ID: D:\OTHERUSE\BRIAN\AL4711PR.MDI: Albite & Sand 4711 Pre-Run Bulk
File: AL4711PR.MDI Scan: 2-65.99/.03/1/#2134, Anode:CU Zero=0.0

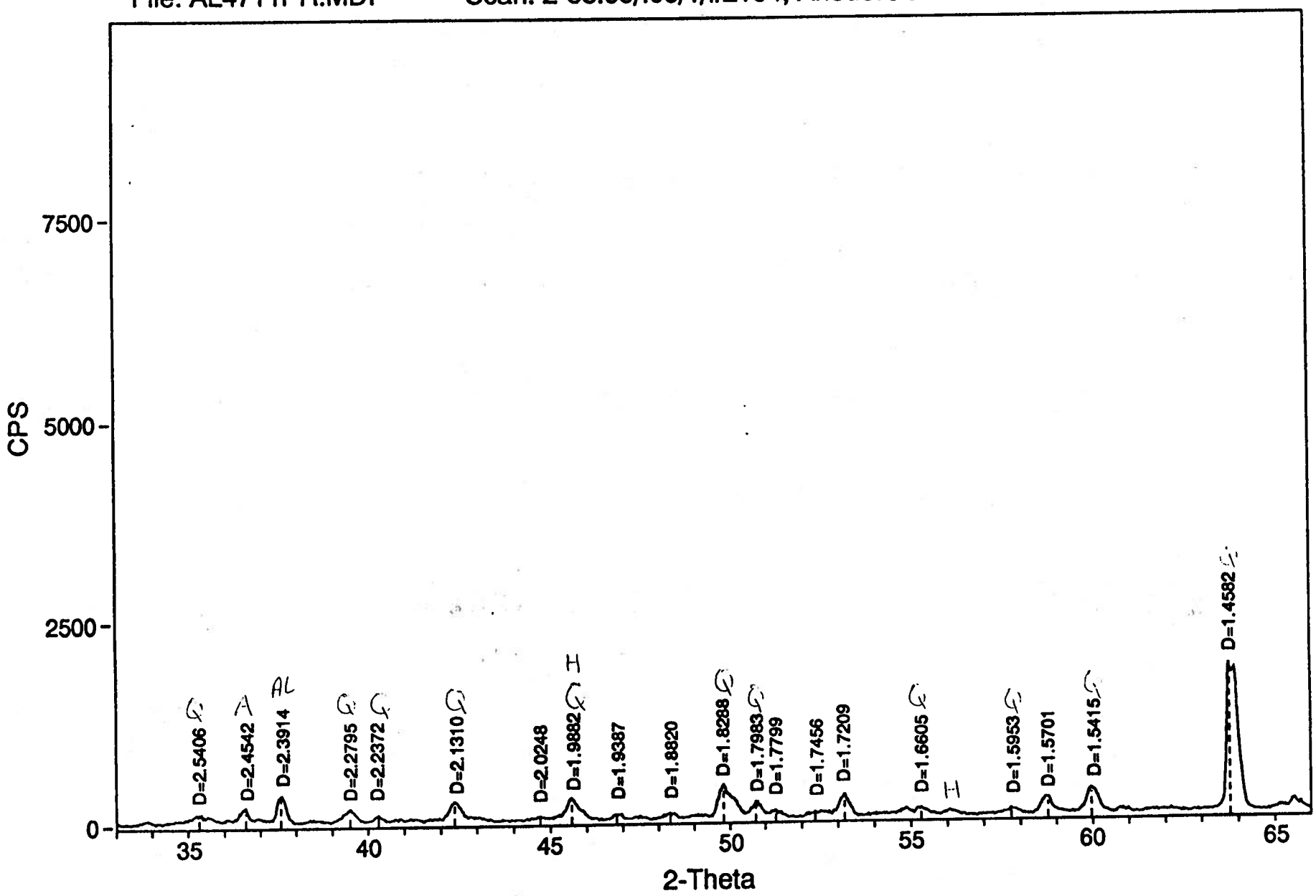

Jade: Peak Listing — Thu Mar 24 1994 @11:07am

File: 4711POST.SAV> D:\OTHERUSE\BRIAN\4711POST.MDI: 4711 Post Bulk Back Pack

Scan Parameters:		Search Parameters:	
Radiation	= CU_1.540598	Filter length(pts)	= 9
Scan Range	= 2 - 65.99	Noise level(sigmas)	= 3.5
Step Size	= .03	Intensity cutoff(%)	= .5-100
Count Time	= 1 sec.	2-Theta Zero (degs)	= 0

	Peak-Position		Centroid-Position		Peak & Area are without Bkgrd					
#	2Theta	d	2Theta	d	Bkgrd	Peak	I%	Area	I%	FWHM*
1:	13.850	6.3886	13.850	6.3890	163	197	4.0	2277	3.6	0.312
2:	20.784	4.2705	20.804	4.2664	90	310	6.3	2788	4.5	0.243
3:	21.952	4.0457	21.960	4.0443	68	224	4.6	2059	3.3	0.248
4:	22.823	3.8932	22.846	3.8894	63	264	5.4	2024	3.2	0.207
5:	23.543	3.7758	23.572	3.7712	62	231	4.7	2134	3.4	0.249
6:	24.291	3.6612	24.286	3.6619	59	168	3.4	2330	3.7	0.374
7:	25.490	3.4916	25.499	3.4904	59	80	1.6	856	1.4	0.289
8:	26.573	3.3517	26.585	3.3502	60	1870	38.0	20810	33.3	0.300
9:	27.981	3.1862	27.977	3.1866	50	4916	100.0	62535	100.0	0.343
10:	29.805	2.9952	29.791	2.9966	48	92	1.9	721	1.2	0.212
11:	30.352	2.9425	30.363	2.9414	44	396	8.1	3735	6.0	0.255
12:	31.434	2.8437	31.438	2.8433	42	290	5.9	3475	5.6	0.324
13:	35.328	2.5386	35.322	2.5390	43	58	1.2	343	0.5	0.160
14:	36.529	2.4579	36.521	2.4584	47	195	4.0	2153	3.4	0.298
15:	39.470	2.2812	39.465	2.2815	40	118	2.4	1113	1.8	0.255
16:	40.221	2.2403	40.231	2.2398	45	95	1.9	846	1.4	0.240
17:	41.239	2.1873	41.244	2.1871	44	47	1.0	387	0.6	0.222
18:	41.780	2.1603	41.778	2.1604	39	71	1.4	753	1.2	0.286
19:	42.322	2.1339	42.336	2.1332	42	295	6.0	4720	7.5	0.432
20:	42.863	2.1082	42.865	2.1081	40	65	1.3	754	1.2	0.313
21:	44.964	2.0144	44.977	2.0138	32	61	1.2	640	1.0	0.283
22:	45.622	1.9869	45.640	1.9861	32	114	2.3	2119	3.4	0.502
23:	48.175	1.8874	48.204	1.8863	32	95	1.9	890	1.4	0.253
24:	50.120	1.8186	50.113	1.8188	41	368	7.5	6314	10.1	0.463
25:	50.661	1.8004	50.668	1.8002	44	155	3.2	1706	2.7	0.297
26:	51.380	1.7769	51.376	1.7771	49	403	8.2	3933	6.3	0.264
27:	52.700	1.7355	52.696	1.7356	49	229	4.7	2738	4.4	0.323
28:	53.151	1.7218	53.150	1.7219	49	103	2.1	1040	1.7	0.273
29:	54.014	1.6963	54.007	1.6965	49	53	1.1	319	0.5	0.163
30:	55.285	1.6603	55.314	1.6595	41	323	6.6	3382	5.4	0.283
31:	57.503	1.6014	57.516	1.6011	37	137	2.8	1392	2.2	0.274
32:	58.760	1.5701	58.756	1.5702	41	171	3.5	1963	3.1	0.310
33:	59.988	1.5409	59.987	1.5409	44	156	3.2	2261	3.6	0.391
34:	60.830	1.5215	60.830	1.5216	41	103	2.1	1934	3.1	0.507
35:	61.675	1.5027	61.686	1.5025	58	94	1.9	644	1.0	0.185
36:	63.831	1.4571	63.828	1.4571	40	148	3.0	2181	3.5	0.398

* Intensity values are based on counts per second.

III-4

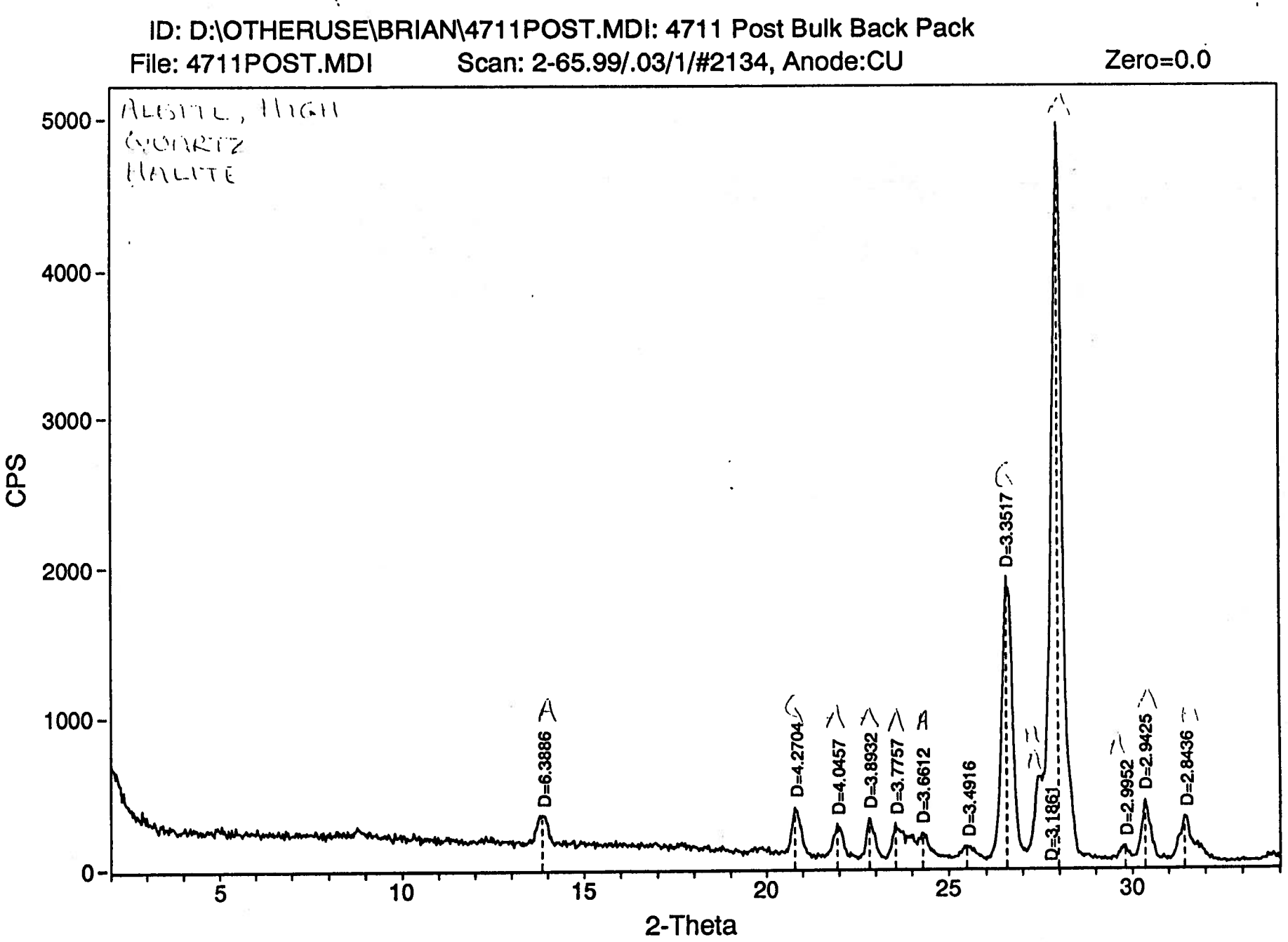
ID: D:\OTHERUSE\BRIAN\4711POST.MDI: 4711 Post Bulk Back Pack
File: 4711POST.MDI
Scan: 2-65.99/.03/1/#2134, Anode:CU
Zero=0.0
ALBITE, HIGH
QUARTZ
HALITE
CPS
2-Theta
D=6.3886
D=4.2704
D=4.0457
D=3.8932
D=3.7757
D=3.6612
D=3.4916
D=3.3517
D=3.1861
D=2.9952
D=2.9425
D=2.8436

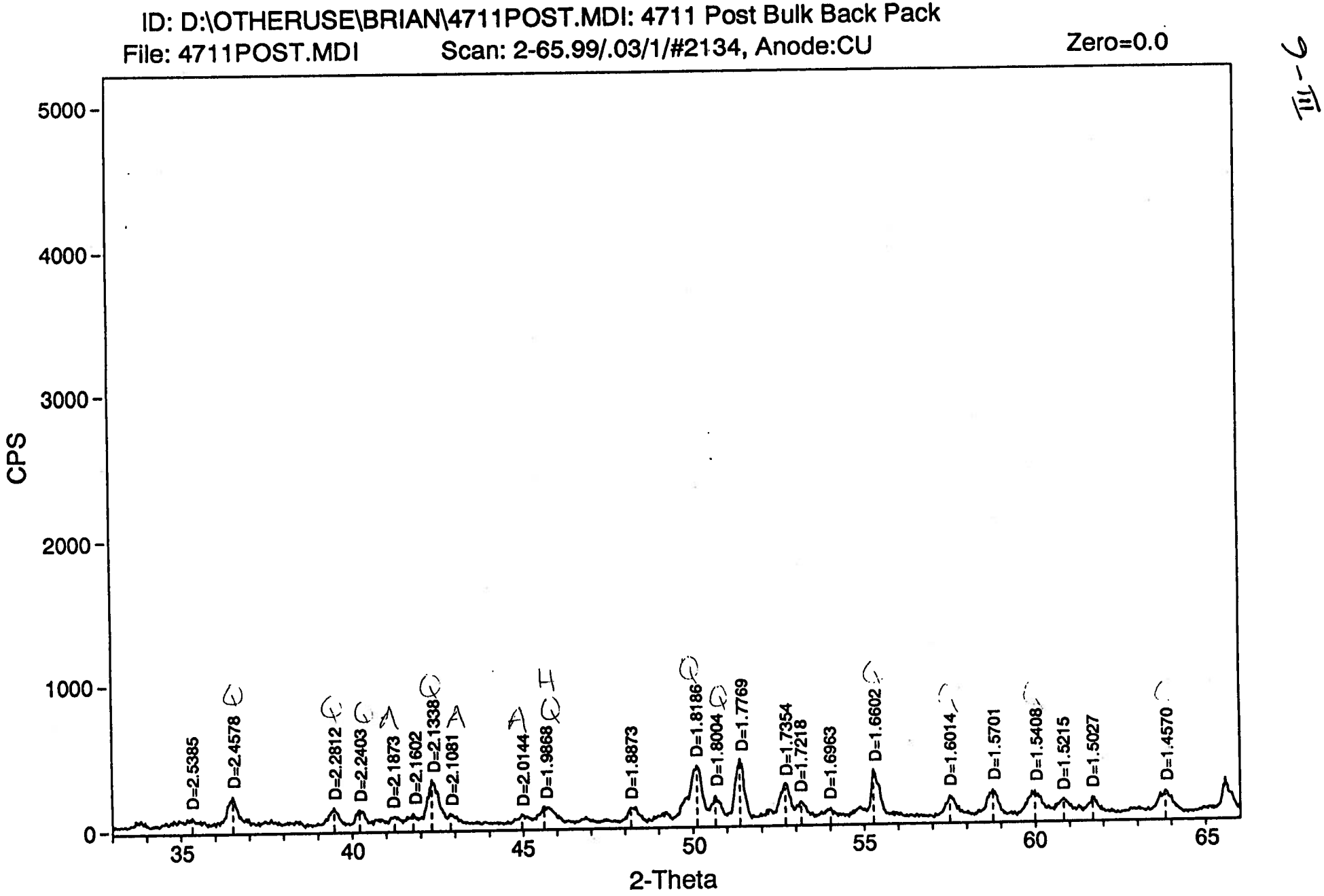
ID: D:\OTHERUSE\BRIAN\4711POST.MDI: 4711 Post Bulk Back Pack
File: 4711POST.MDI
Scan: 2-65.99/.03/1/#2134, Anode:CU
Zero=0.0
CPS
2-Theta
D=2.5385
D=2.4578
D=2.2812
D=2.2403
D=2.1873
D=2.1602
D=2.1338
D=2.1081
D=2.0144
D=1.9868
D=1.8873
D=1.8186
D=1.8004
D=1.7769
D=1.7354
D=1.7218
D=1.6963
D=1.6602
D=1.6014
D=1.5701
D=1.5408
D=1.5215
D=1.5027
D=1.4570

7-11

Jade: Peak Listing — Thu Mar 24 1994 @11:11am

File: LA4712PR.SAV> D:\OTHERUSE\BRIAN\LA4712PR.MDI: Labradorite & Sand 4712 Pre-Rur

Scan Parameters:		Search Parameters:
Radiation = CU_1.540598		Filter length(pts) = 9
Scan Range = 2 - 65.99		Noise level(sigmas) = 3.5
Step Size = .03		Intensity cutoff(%) = .5-100
Count Time = 1 sec.		2-Theta Zero (degs) = -.08

	Peak-Position		Centroid-Position		Peak & Area are without Bkgrd					
#	2Theta	d	2Theta	d	Bkgrd	Peak	I%	Area	I%	FWHM*
1:	14.037	6.3042	14.013	6.3149	38	96	1.0	699	0.7	0.197
2:	20.909	4.2452	20.902	4.2466	35	403	4.3	4103	4.3	0.275
3:	21.991	4.0386	21.996	4.0378	39	199	2.1	2016	2.1	0.274
4:	22.891	3.8818	22.903	3.8799	38	128	1.4	1068	1.1	0.225
5:	23.787	3.7377	23.774	3.7396	45	319	3.4	2926	3.1	0.248
6:	24.420	3.6421	24.413	3.6432	49	143	1.5	1498	1.6	0.283
7:	25.653	3.4698	25.679	3.4663	61	215	2.3	2060	2.2	0.259
8:	26.670	3.3397	26.673	3.3394	88	2433	25.7	24312	25.7	0.270
9:	28.139	3.1687	28.125	3.1703	66	9470	100.0	94517	100.0	0.269
10:	29.670	3.0085	29.663	3.0092	66	455	4.8	4218	4.5	0.250
11:	30.418	2.9363	30.404	2.9375	57	2201	23.2	19724	20.9	0.242
12:	31.709	2.8196	31.715	2.8191	56	91	1.0	1351	1.4	0.401
13:	35.432	2.5314	35.448	2.5303	36	121	1.3	2269	2.4	0.506
14:	36.598	2.4533	36.596	2.4535	40	220	2.3	2503	2.6	0.307
15:	39.510	2.2790	39.512	2.2789	38	139	1.5	2430	2.6	0.472
16:	42.569	2.1221	42.566	2.1222	37	237	2.5	5359	5.7	0.611
17:	45.752	1.9816	45.758	1.9813	33	137	1.4	1922	2.0	0.379
18:	47.368	1.9176	47.365	1.9178	34	70	0.7	646	0.7	0.249
19:	50.161	1.8172	50.163	1.8171	39	274	2.9	4897	5.2	0.483
20:	50.821	1.7951	50.832	1.7948	39	138	1.5	2114	2.2	0.414
21:	51.510	1.7728	51.514	1.7726	56	111	1.2	745	0.8	0.181
22:	53.159	1.7216	53.157	1.7216	39	571	6.0	6331	6.7	0.299
23:	54.903	1.6710	54.906	1.6708	38	126	1.3	1218	1.3	0.261
24:	60.116	1.5379	60.096	1.5384	39	152	1.6	2057	2.2	0.365
25:	60.931	1.5193	60.935	1.5192	41	85	0.9	809	0.9	0.257
26:	62.160	1.4921	62.161	1.4921	42	71	0.7	945	1.0	0.359
27:	62.880	1.4768	62.888	1.4766	38	125	1.3	1751	1.9	0.378

* Intensity values are based on counts per second.

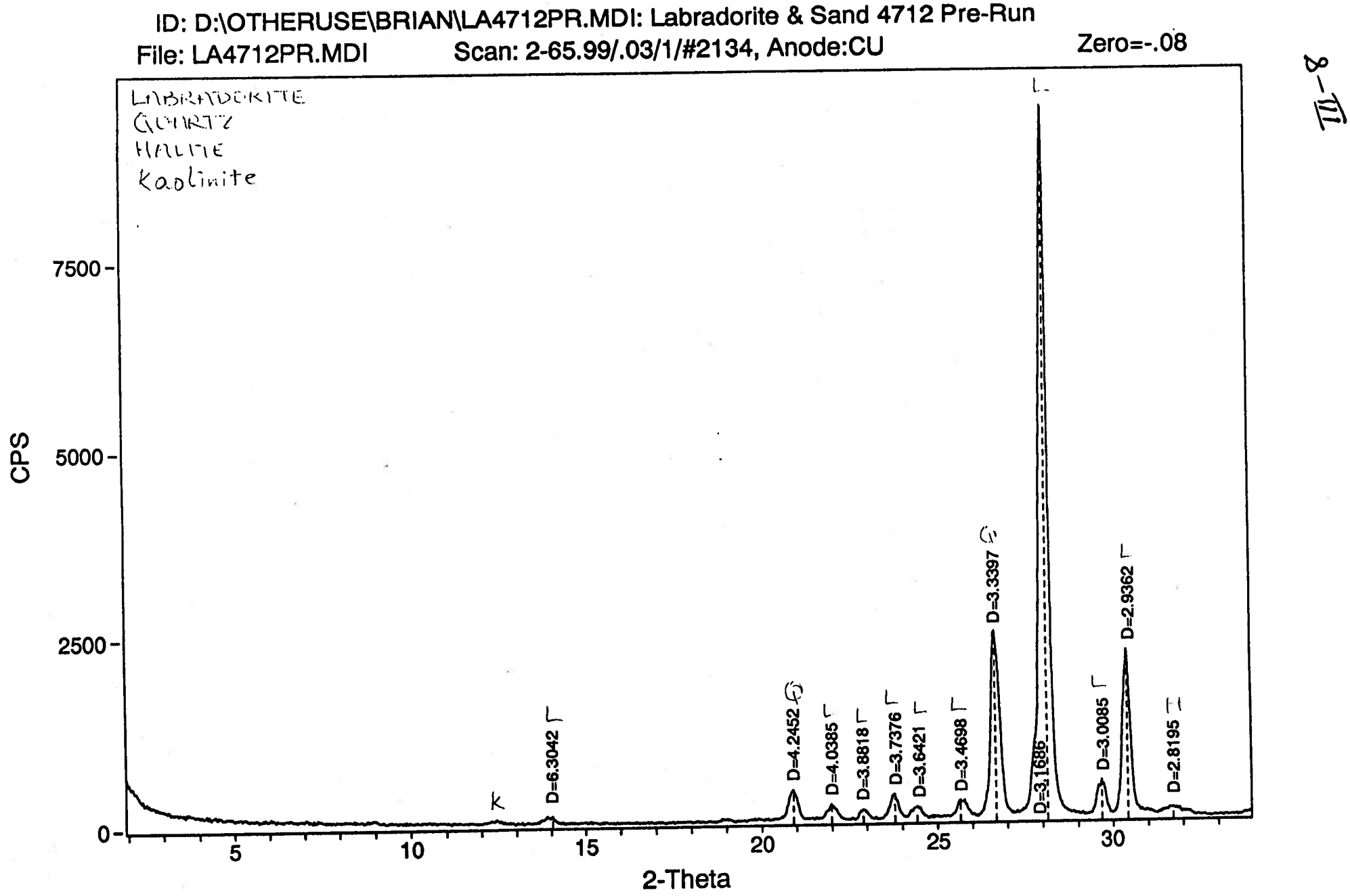
ID: D:\OTHERUSE\BRIAN\LA4712PR.MDI: Labradorite & Sand 4712 Pre-Run
File: LA4712PR.MDI
Scan: 2-65.99/.03/1/#2134, Anode:CU
Zero=-.08
LABRADORITE
QUARTZ
HALITE
Kaolinite
CPS
7500
5000
2500
0
5
10
15
20
25
30
2-Theta
K
D=6.3042
D=4.2452
D=4.0385
D=3.8818
D=3.7376
D=3.6421
D=3.4698
D=3.3397
D=3.1686
D=3.0085
D=2.9362
D=2.8195

8-TII

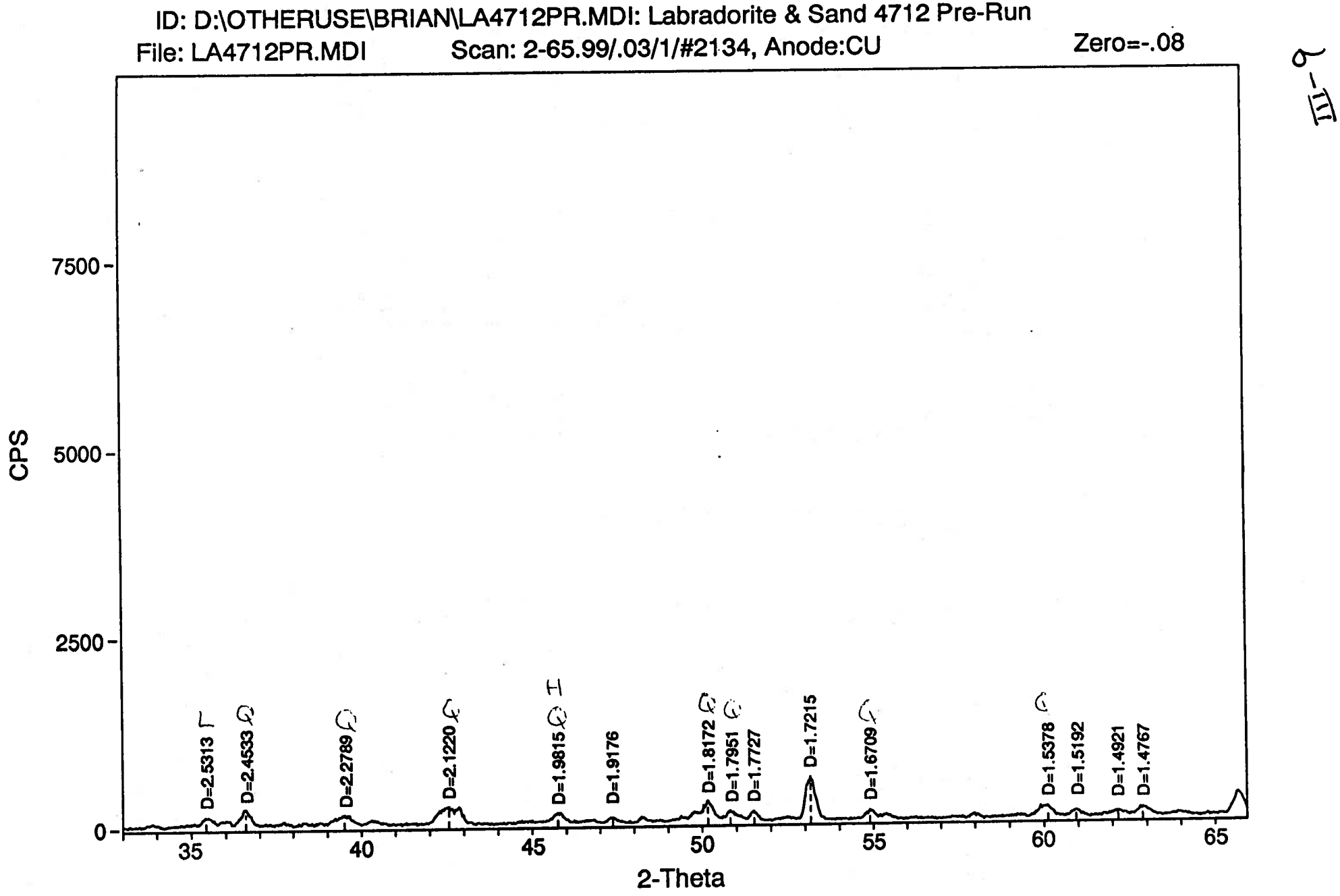
ID: D:\OTHERUSE\BRIAN\LA4712PR.MDI: Labradorite & Sand 4712 Pre-Run
File: LA4712PR.MDI
Scan: 2-65.99/.03/1/#2134, Anode:CU
Zero=-.08
CPS
7500
5000
2500
0
35
40
45
50
55
60
65
2-Theta
D=2.5313
D=2.4533
D=2.2789
D=2.1220
D=1.9815
D=1.9176
D=1.8172
D=1.7951
D=1.7727
D=1.7215
D=1.6709
D=1.5378
D=1.5192
D=1.4921
D=1.4767

9-III

Jade: Peak Listing — Thu Mar 24 1994 @11:08am

File: 4712POST.SAV> D:\OTHERUSE\BRIAN\4712POST.MDI: 4712 Post Bulk Back Pack

Scan Parameters:
Radiation = CU_1.540598
Scan Range = 2 - 65.99
Step Size = .03
Count Time = 1 sec.

Search Parameters:
Filter length(pts) = 9
Noise level(sigmas) = 3.5
Intensity cutoff(%) = .5-100
2-Theta Zero (degs) = 0

	Peak-Position		Centroid-Position		Peak & Area are without Bkgrd					
#	2Theta	d	2Theta	d	Bkgrd	Peak	I%	Area	I%	FWHM*
1:	12.386	7.1404	12.386	7.1404	52	36	1.5	146	0.6	0.109
2:	13.939	6.3484	13.935	6.3500	44	41	1.7	227	1.0	0.149
3:	20.814	4.2644	20.842	4.2587	32	269	11.4	3174	13.6	0.319
4:	22.037	4.0303	22.022	4.0330	36	212	9.0	1751	7.5	0.223
5:	22.965	3.8696	22.953	3.8715	39	95	4.0	563	2.4	0.160
6:	23.718	3.7483	23.713	3.7491	39	286	12.1	3213	13.8	0.303
7:	24.294	3.6608	24.321	3.6568	42	312	13.2	3317	14.2	0.287
8:	25.583	3.4792	25.597	3.4773	50	68	2.9	569	2.4	0.226
9:	26.511	3.3594	26.511	3.3595	59	1107	47.0	10725	46.1	0.262
10:	26.689	3.3374	26.679	3.3386	50	1700	72.2	23282	100.0	0.370
11:	27.772	3.2097	27.782	3.2085	49	1443	61.3	15461	66.4	0.289
12:	28.129	3.1698	28.112	3.1717	49	2355	100.0	22670	97.4	0.260
13:	29.749	3.0008	29.744	3.0012	44	41	1.7	211	0.9	0.139
14:	30.411	2.9369	30.426	2.9355	42	827	35.1	6606	28.4	0.216
15:	31.731	2.8177	31.725	2.8182	35	122	5.2	1662	7.1	0.368
16:	33.773	2.6518	33.775	2.6517	32	89	3.8	930	4.0	0.282
17:	35.424	2.5320	35.434	2.5313	39	65	2.8	1324	5.7	0.550
18:	36.622	2.4518	36.622	2.4518	41	117	5.0	1189	5.1	0.274
19:	37.249	2.4120	37.235	2.4129	40	63	2.7	476	2.0	0.204
20:	39.415	2.2843	39.447	2.2825	37	146	6.2	1329	5.7	0.246
21:	40.312	2.2355	40.319	2.2351	37	73	3.1	642	2.8	0.237
22:	42.289	2.1354	42.291	2.1354	31	224	9.5	3495	15.0	0.421
23:	44.752	2.0235	44.758	2.0232	28	38	1.6	259	1.1	0.184
24:	45.829	1.9784	45.819	1.9788	27	126	5.4	1514	6.5	0.324
25:	48.404	1.8790	48.383	1.8797	32	64	2.7	678	2.9	0.286
26:	49.728	1.8320	49.734	1.8318	41	156	6.6	2623	11.3	0.454
27:	50.178	1.8166	50.163	1.8171	37	242	10.3	4028	17.3	0.449
28:	50.901	1.7925	50.901	1.7925	38	144	6.1	1487	6.4	0.279
29:	51.556	1.7713	51.553	1.7714	46	51	2.2	217	0.9	0.115
30:	52.759	1.7337	52.751	1.7339	37	50	2.1	283	1.2	0.153
31:	53.208	1.7201	53.203	1.7203	37	43	1.8	339	1.5	0.213
32:	54.893	1.6712	54.896	1.6711	34	64	2.7	674	2.9	0.284
33:	55.401	1.6571	55.407	1.6569	32	110	4.7	1135	4.9	0.279
34:	58.225	1.5833	58.225	1.5833	35	37	1.6	131	0.6	0.096
35:	59.961	1.5415	59.954	1.5417	36	154	6.5	2353	10.1	0.413
36:	64.067	1.4523	64.060	1.4524	37	63	2.7	1174	5.0	0.503

* Intensity values are based on counts per second.

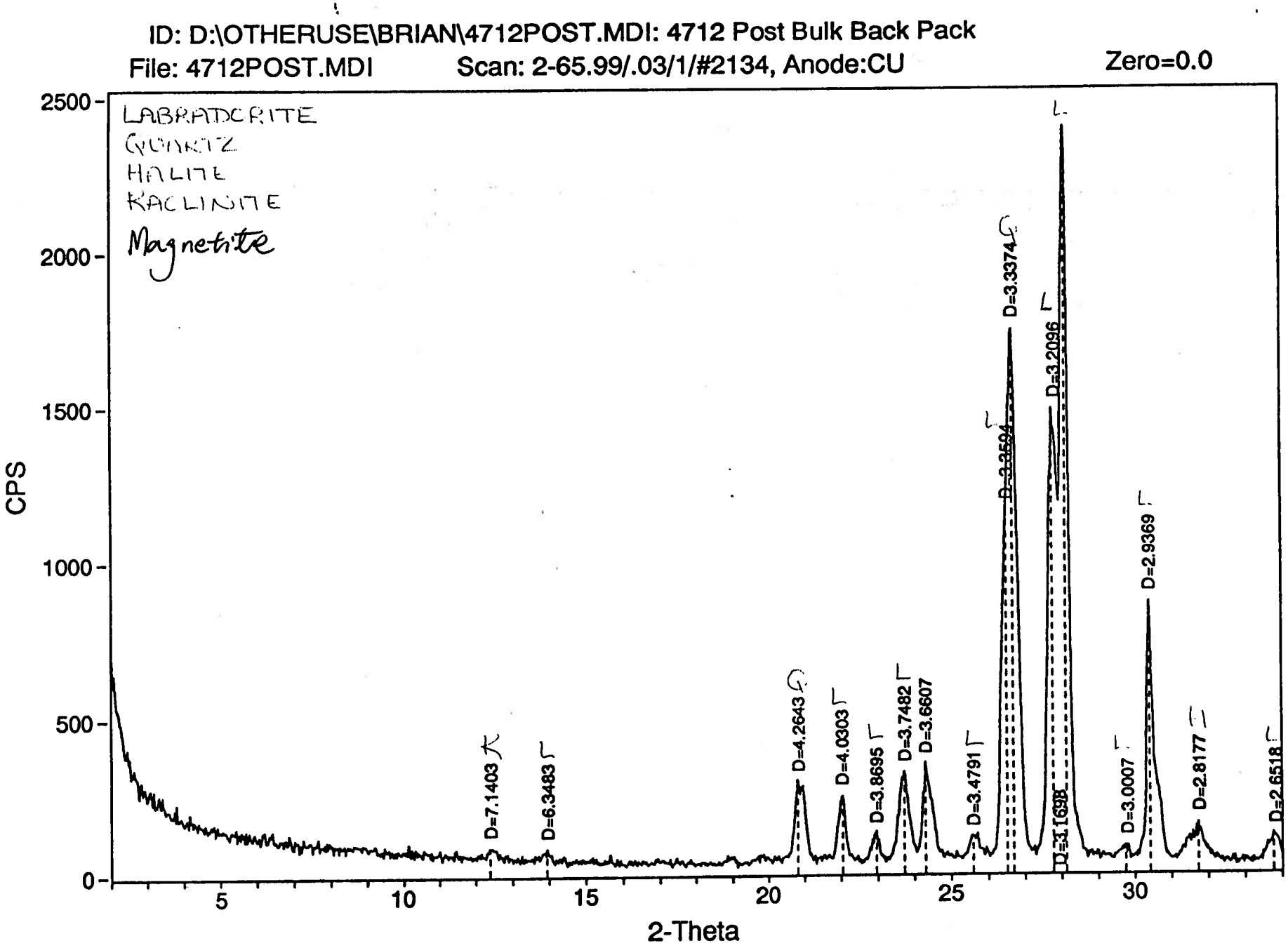
ID: D:\OTHERUSE\BRIAN\4712POST.MDI: 4712 Post Bulk Back Pack
File: 4712POST.MDI
Scan: 2-65.99/.03/1/#2134, Anode:CU
Zero=0.0
LABRADORITE
QUARTZ
HALITE
KAOLINITE
Magnetite
CPS
2-Theta
D=7.1403
D=6.3483
D=4.2643
D=4.0303
D=3.8695
D=3.7482
D=3.6607
D=3.4791
D=3.3374
D=3.2096
D=3.0007
D=2.9369
D=2.8177
D=2.6518

III - 11

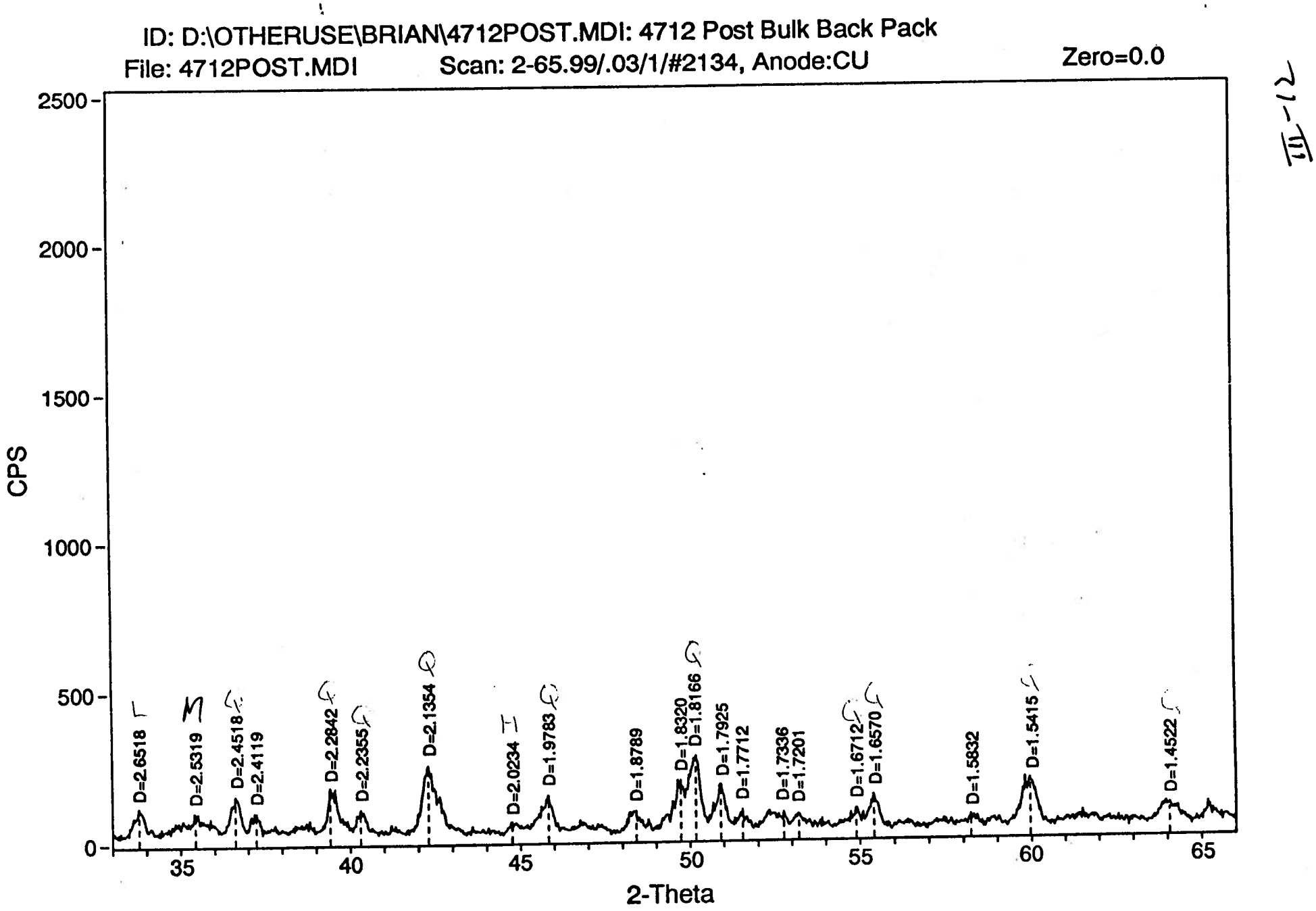
ID: D:\OTHERUSE\BRIAN\4712POST.MDI: 4712 Post Bulk Back Pack
File: 4712POST.MDI
Scan: 2-65.99/.03/1/#2134, Anode:CU
Zero=0.0
CPS
2500
2000
1500
1000
500
0
35
40
45
50
55
60
65
2-Theta
D=2.6518
D=2.5319
D=2.4518
D=2.4119
D=2.2842
D=2.2355
D=2.1354
D=2.0234
D=1.9783
D=1.8789
D=1.8320
D=1.8166
D=1.7925
D=1.7712
D=1.7336
D=1.7201
D=1.6712
D=1.6570
D=1.5832
D=1.5415
D=1.4522

21-111

Jade: Peak Listing — Thu Mar 24 1994 @11:09am

File: 4713PRE.SAV> D:\OTHERUSE\BRIAN\4713PRE.MDI: 4713 Pre-Run Bulk Back Pack

Scan Parameters:		Search Parameters:
Radiation = CU_1.540598		Filter length(pts) = 9
Scan Range = 2 - 65.99		Noise level(sigmas) = 3.5
Step Size = .03		Intensity cutoff(%) = .5-100
Count Time = 1 sec.		2-Theta Zero (degs) = 0

	Peak-Position		Centroid-Position		Peak & Area are without Bkgrd					
#	2Theta	d	2Theta	d	Bkgrd	Peak	I%	Area	I%	FWHM*
1:	12.381	7.1434	12.380	7.1437	48	109	0.8	1004	0.7	0.249
2:	19.762	4.4889	19.779	4.4850	45	105	0.7	1251	0.9	0.322
3:	20.897	4.2476	20.880	4.2510	43	1649	11.6	18095	12.3	0.296
4:	26.659	3.3412	26.656	3.3415	72	14213	100.0	147027	100.0	0.279
5:	27.772	3.2097	27.773	3.2096	73	112	0.8	3079	2.1	0.742
6:	31.880	2.8048	31.895	2.8036	44	72	0.5	795	0.5	0.298
7:	34.913	2.5678	34.914	2.5677	42	123	0.9	2192	1.5	0.481
8:	36.561	2.4558	36.567	2.4554	49	532	3.7	5823	4.0	0.296
9:	39.500	2.2795	39.498	2.2797	42	477	3.4	5174	3.5	0.293
10:	40.283	2.2370	40.299	2.2362	42	272	1.9	3112	2.1	0.309
11:	42.499	2.1254	42.496	2.1255	38	677	4.8	7599	5.2	0.303
12:	45.802	1.9795	45.808	1.9792	30	250	1.8	3374	2.3	0.364
13:	50.152	1.8175	50.161	1.8172	29	770	5.4	10034	6.8	0.352
14:	54.950	1.6696	54.952	1.6696	38	779	5.5	9548	6.5	0.331
15:	60.018	1.5402	60.010	1.5404	39	582	4.1	7653	5.2	0.355
16:	64.099	1.4516	64.089	1.4518	33	101	0.7	1165	0.8	0.311

* Intensity values are based on counts per second.

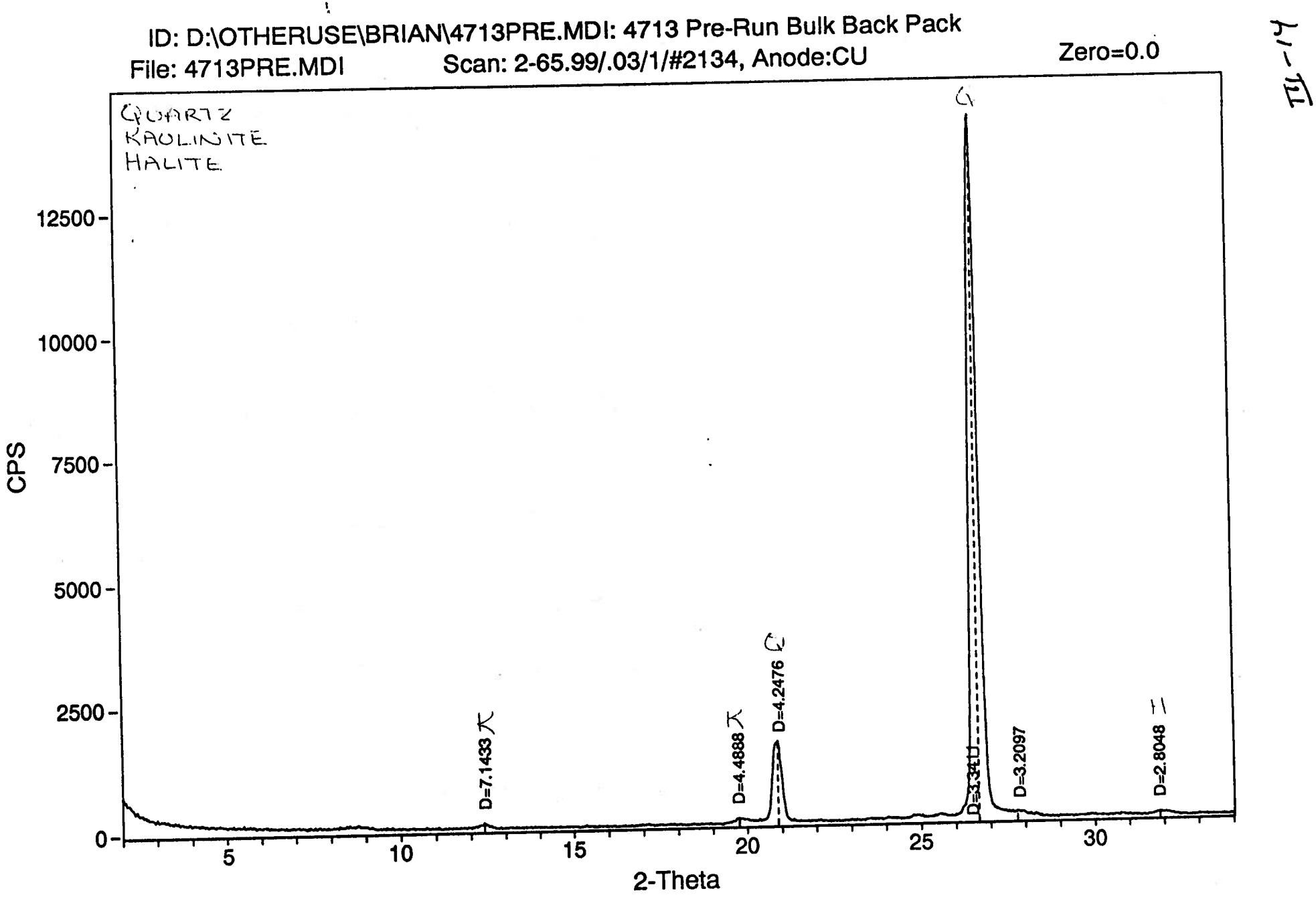
ID: D:\OTHERUSE\BRIAN\4713PRE.MDI: 4713 Pre-Run Bulk Back Pack
File: 4713PRE.MDI
Scan: 2-65.99/.03/1/#2134, Anode:CU
Zero=0.0
QUARTZ
KAOLINITE
HALITE
CPS
12500
10000
7500
5000
2500
0
5
10
15
20
25
30
2-Theta
D=7.1433
D=4.4888
D=4.2476
D=3.3410
D=3.2097
D=2.8048

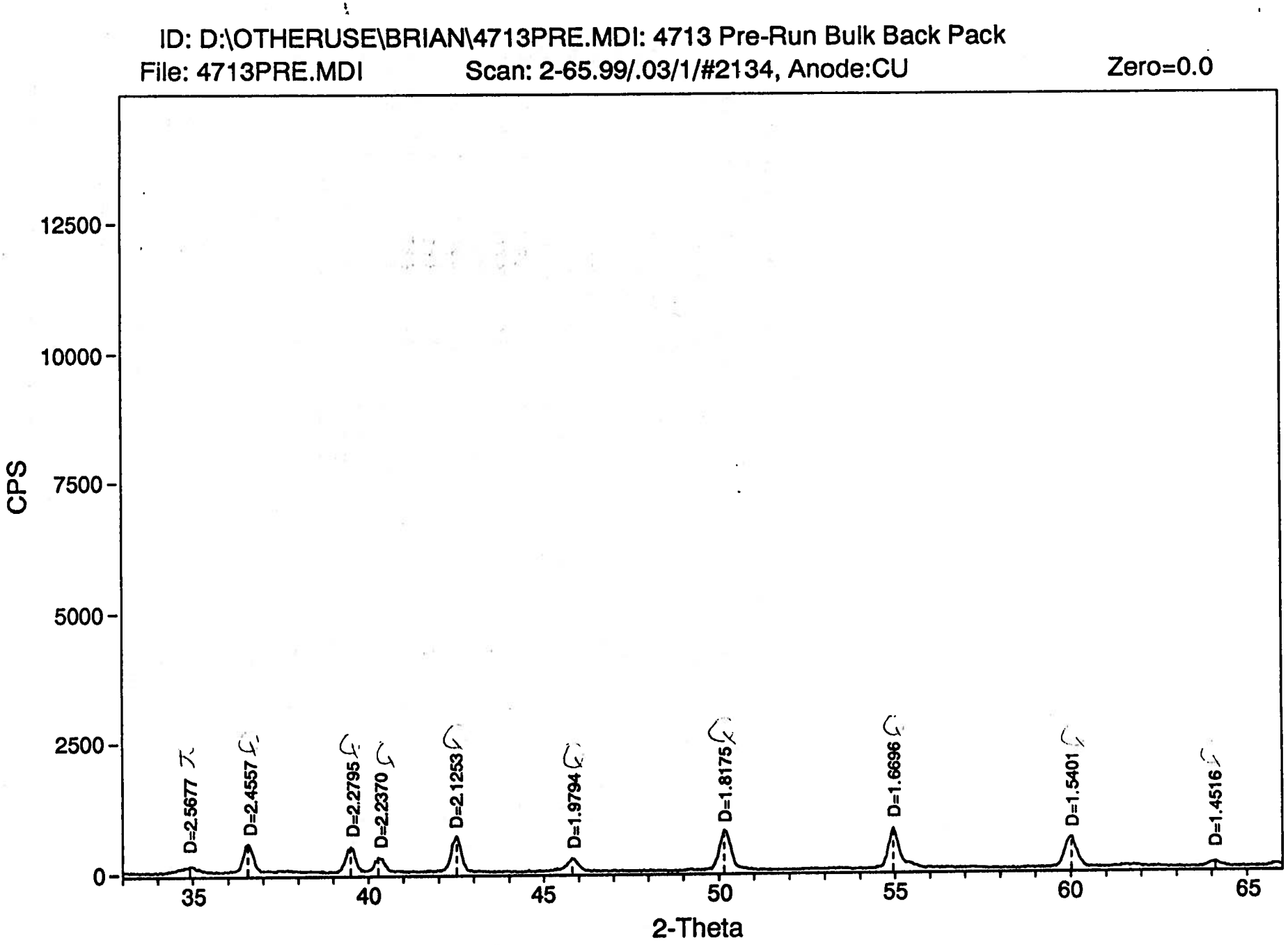
ID: D:\OTHERUSE\BRIAN\4713PRE.MDI: 4713 Pre-Run Bulk Back Pack
File: 4713PRE.MDI
Scan: 2-65.99/.03/1/#2134, Anode:CU
Zero=0.0
CPS
12500
10000
7500
5000
2500
0
35
40
45
50
55
60
65
2-Theta
D=2.5677
D=2.4557
D=2.2795
D=2.2370
D=2.1253
D=1.9794
D=1.8175
D=1.6696
D=1.5401
D=1.4516

Jade: Peak Listing — Thu Mar 24 1994 @11:09am

File: 4713POST.SAV> D:\OTHERUSE\BRIAN\4713POST.MDI: 4713 Post Bulk Back Pack

Scan Parameters:		Search Parameters:
Radiation = CU_1.540598		Filter length(pts) = 9
Scan Range = 2 - 65.99		Noise level(sigmas) = 3.5
Step Size = .03		Intensity cutoff(%) = .5-100
Count Time = 1 sec.		2-Theta Zero (degs) = 0

	Peak-Position		Centroid-Position		Peak & Area are without Bkgrd					
#	2Theta	d	2Theta	d	Bkgrd	Peak	I%	Area	I%	FWHM*
1:	8.720	10.1330	8.723	10.1284	70	67	0.9	691	0.8	0.278
2:	12.350	7.1612	12.356	7.1577	41	72	0.9	731	0.9	0.274
3:	19.821	4.4756	19.824	4.4749	35	111	1.4	1510	1.8	0.367
4:	20.868	4.2533	20.861	4.2547	35	1511	19.6	16550	19.8	0.296
5:	26.659	3.3411	26.653	3.3418	61	7710	100.0	83507	100.0	0.292
6:	27.978	3.1865	27.969	3.1875	58	83	1.1	840	1.0	0.273
7:	32.031	2.7920	32.028	2.7922	41	50	0.6	524	0.6	0.283
8:	34.822	2.5744	34.830	2.5737	35	103	1.3	2011	2.4	0.527
9:	36.532	2.4577	36.541	2.4570	42	528	6.8	5619	6.7	0.287
10:	39.470	2.2812	39.470	2.2812	36	484	6.3	5187	6.2	0.289
11:	40.310	2.2356	40.302	2.2360	40	204	2.6	2201	2.6	0.291
12:	42.470	2.1268	42.467	2.1269	35	450	5.8	5368	6.4	0.322
13:	45.828	1.9784	45.819	1.9788	26	263	3.4	3577	4.3	0.367
14:	50.152	1.8175	50.160	1.8172	26	1015	13.2	12101	14.5	0.322
15:	54.947	1.6697	54.936	1.6700	32	385	5.0	6015	7.2	0.422
16:	60.018	1.5402	60.005	1.5405	39	606	7.9	7799	9.3	0.347
17:	61.696	1.5023	61.695	1.5023	38	44	0.6	457	0.5	0.280
18:	64.013	1.4533	64.020	1.4532	29	95	1.2	1192	1.4	0.339

* Intensity values are based on counts per second.

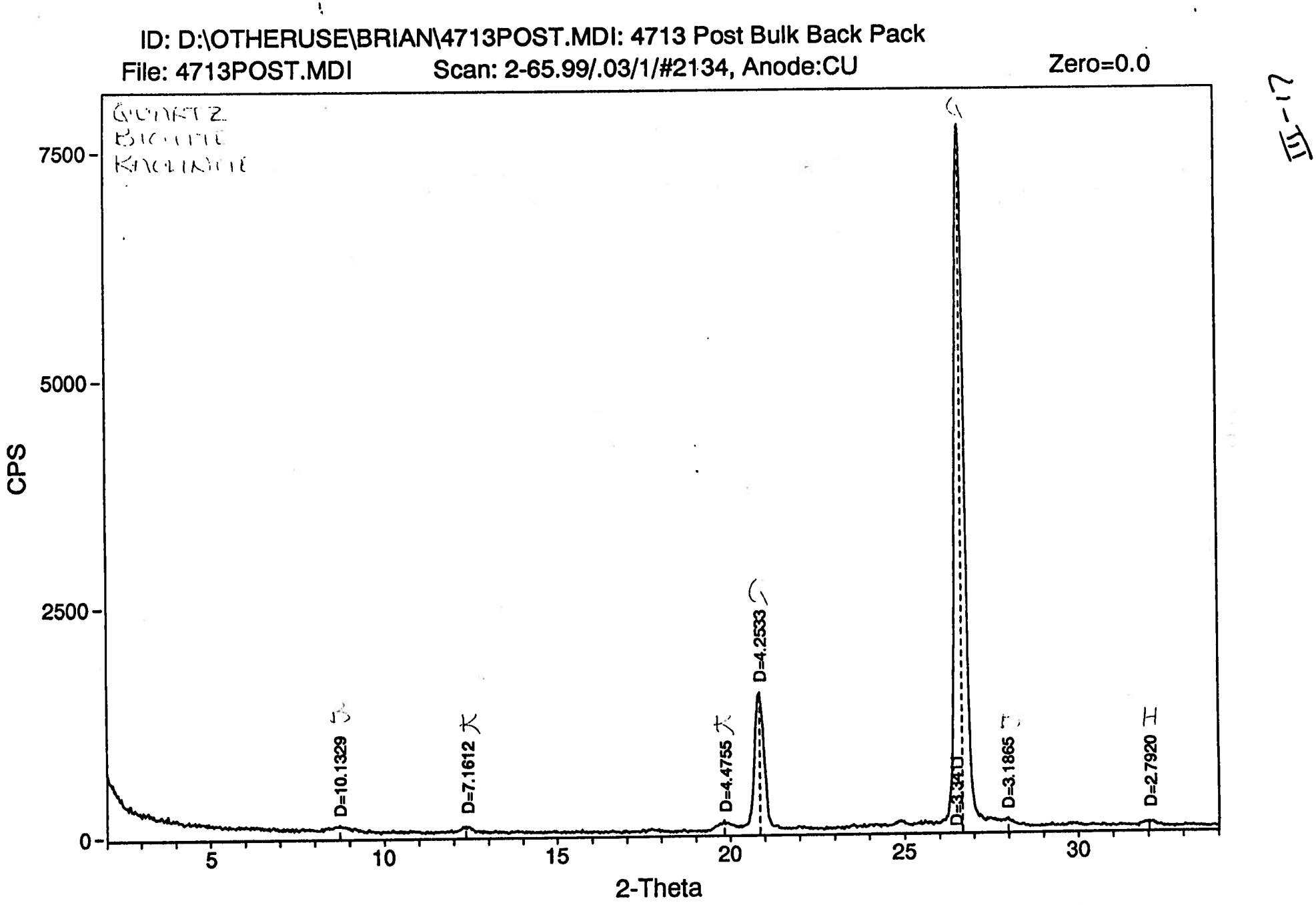
ID: D:\OTHERUSE\BRIAN\4713POST.MDI: 4713 Post Bulk Back Pack
File: 4713POST.MDI
Scan: 2-65.99/.03/1/#2134, Anode:CU
Zero=0.0
QUARTZ
BIOTITE
KAOLINITE
7500
5000
2500
0
CPS
D=10.1329
D=7.1612
D=4.4755
D=4.2533
D=3.3410
D=3.1865
D=2.7920
5
10
15
20
25
30
2-Theta

III-17

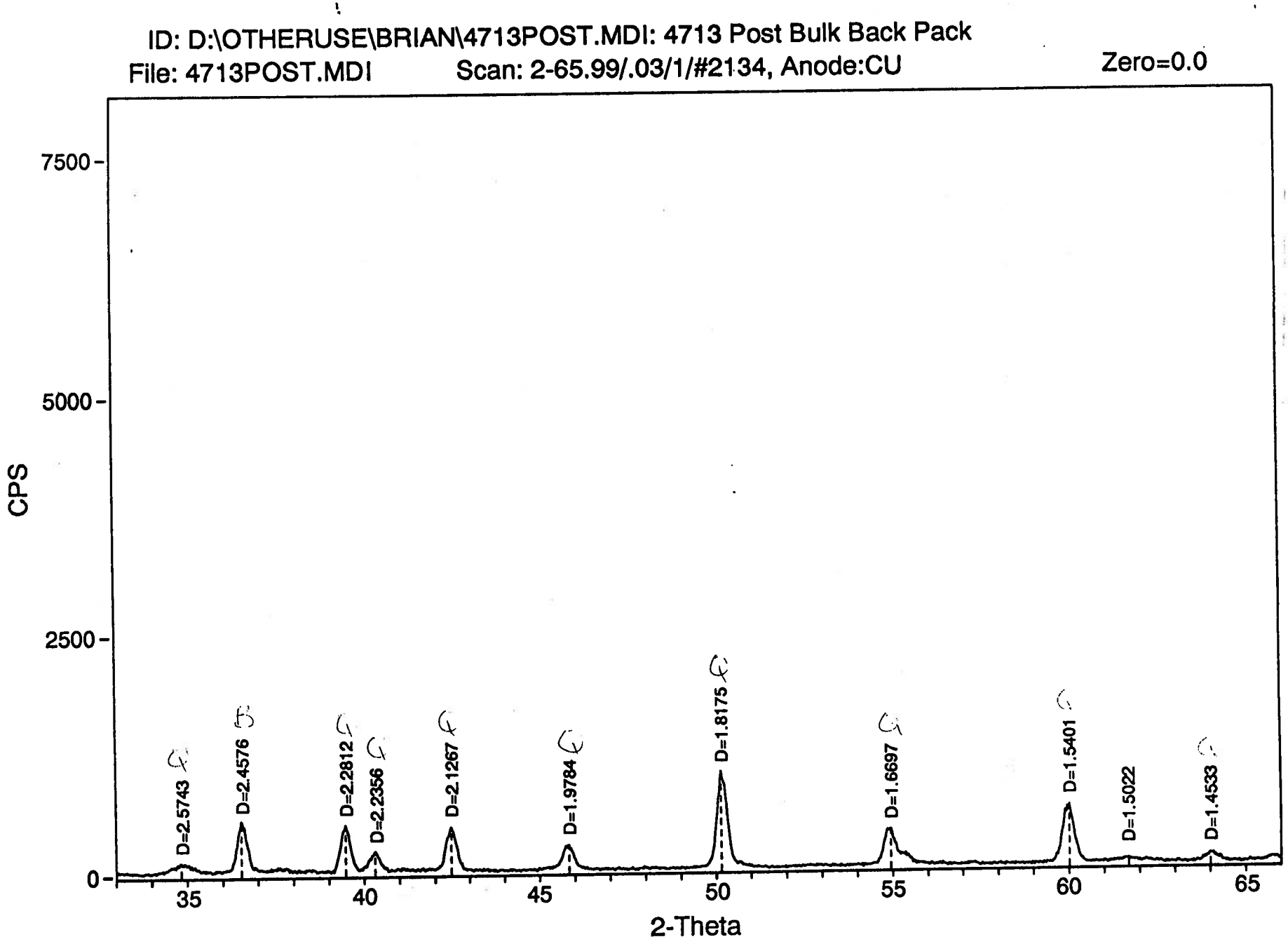
ID: D:\OTHERUSE\BRIAN\4713POST.MDI: 4713 Post Bulk Back Pack
File: 4713POST.MDI
Scan: 2-65.99/.03/1/#2134, Anode:CU
Zero=0.0
7500
5000
2500
0
CPS
D=2.5743
D=2.4576
D=2.2812
D=2.2356
D=2.1267
D=1.9784
D=1.8175
D=1.6697
D=1.5401
D=1.5022
D=1.4533
35
40
45
50
55
60
65
2-Theta

81-TL

Jade: Peak Listing — Thu Mar 24 1994 @11:10am

File: BI4714PR.SAV> D:\OTHERUSE\BRIAN\BI4714PR.MDI: Biotite & Sand 4714 Pre-Run Bul

Scan Parameters:

Radiation = CU_1.540598
Scan Range = 2 - 65.99
Step Size = .03
Count Time = 1 sec.

Search Parameters:

Filter length(pts) = 9
Noise level(sigmas) = 3.5
Intensity cutoff(%) = .5-100
2-Theta Zero (degs) = 0

	Peak-Position		Centroid-Position		Peak & Area are without Bkgrd					
#	2Theta	d	2Theta	d	Bkgrd	Peak	I%	Area	I%	FWHM*
1:	8.689	10.1689	8.684	10.1748	83	4445	56.6	52667	61.5	0.320
2:	20.723	4.2829	20.733	4.2809	36	133	1.7	1398	1.6	0.284
3:	24.197	3.6752	24.187	3.6768	48	72	0.9	952	1.1	0.357
4:	26.541	3.3558	26.548	3.3548	74	7860	100.0	85605	100.0	0.294
5:	28.280	3.1532	28.284	3.1527	80	145	1.8	1540	1.8	0.287
6:	30.499	2.9286	30.504	2.9281	47	151	1.9	2301	2.7	0.411
7:	32.957	2.7156	32.956	2.7157	43	100	1.3	1197	1.4	0.323
8:	34.014	2.6336	34.037	2.6319	44	133	1.7	1103	1.3	0.224
9:	35.719	2.5117	35.717	2.5118	40	739	9.4	7669	9.0	0.280
10:	36.771	2.4423	36.765	2.4426	35	124	1.6	2042	2.4	0.445
11:	39.380	2.2862	39.380	2.2862	26	87	1.1	970	1.1	0.301
12:	40.105	2.2466	40.113	2.2461	26	54	0.7	532	0.6	0.266
13:	41.421	2.1782	41.425	2.1780	26	135	1.7	1661	1.9	0.332
14:	42.377	2.1312	42.359	2.1321	25	73	0.9	651	0.8	0.241
15:	45.111	2.0082	45.116	2.0080	25	1258	16.0	15002	17.5	0.322
16:	50.028	1.8217	50.026	1.8218	22	168	2.1	1720	2.0	0.276
17:	54.801	1.6738	54.810	1.6736	24	494	6.3	7229	8.4	0.395
18:	60.140	1.5374	60.125	1.5377	30	254	3.2	4141	4.8	0.440

* Intensity values are based on counts per second.

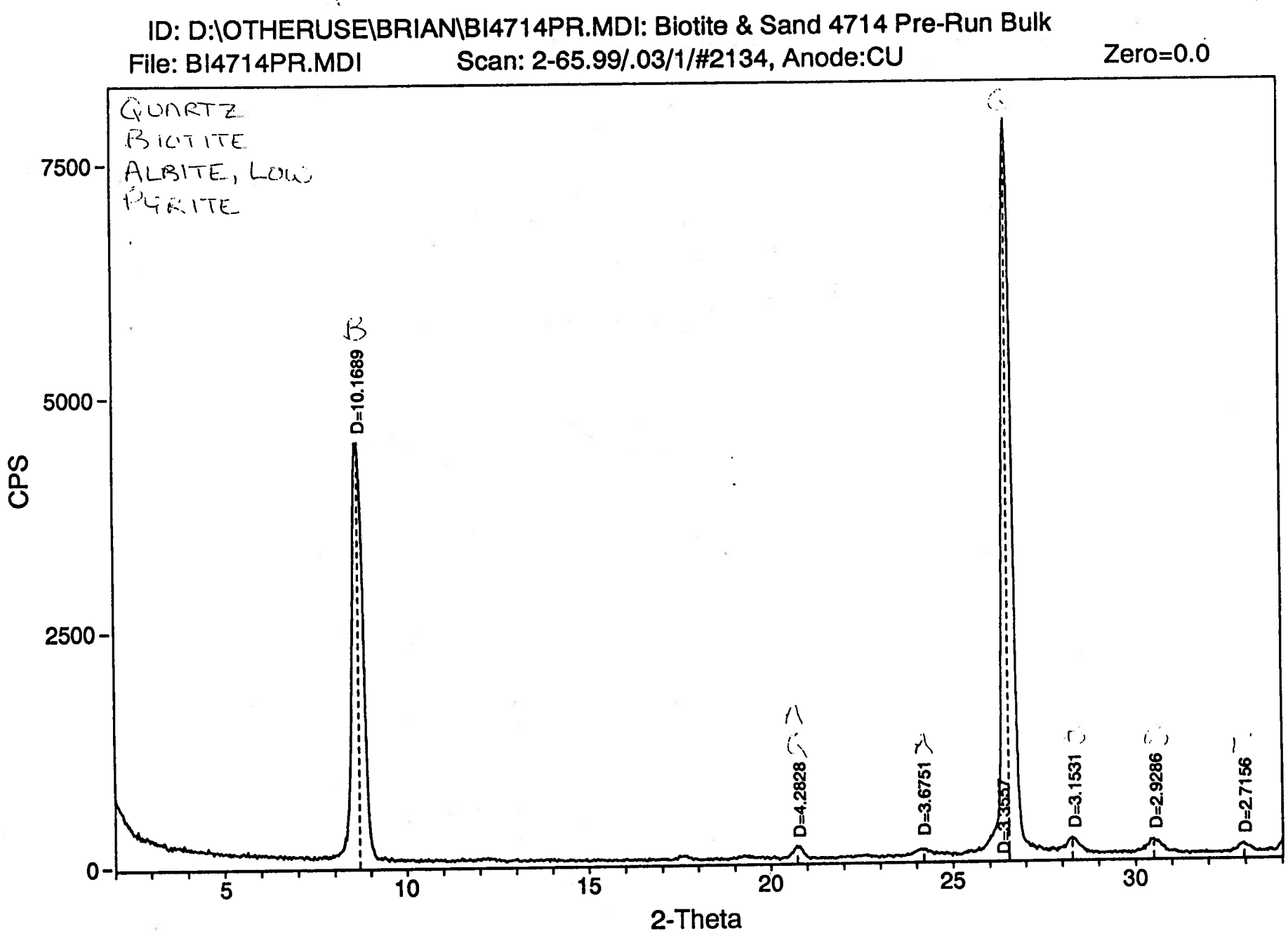
ID: D:\OTHERUSE\BRIAN\BI4714PR.MDI: Biotite & Sand 4714 Pre-Run Bulk
File: BI4714PR.MDI
Scan: 2-65.99/.03/1/#2134, Anode:CU
Zero=0.0
QUARTZ
BIOTITE
ALBITE, LOW
PYRITE
B
D=10.1689
D=4.2828
D=3.6751
D=3.3537
D=3.1531
D=2.9286
D=2.7156
7500
5000
2500
0
CPS
5
10
15
20
25
30
2-Theta

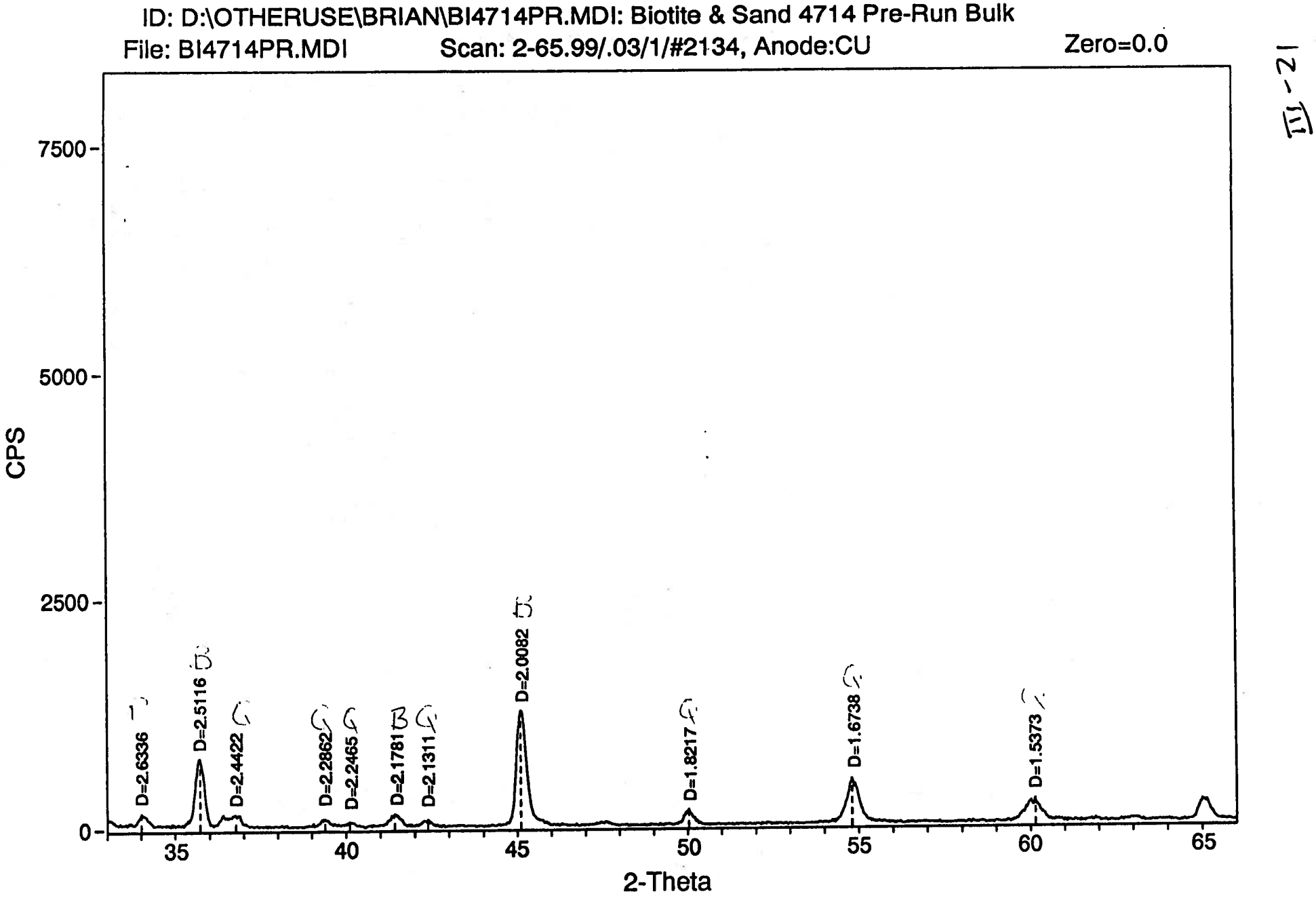
ID: D:\OTHERUSE\BRIAN\BI4714PR.MDI: Biotite & Sand 4714 Pre-Run Bulk
File: BI4714PR.MDI
Scan: 2-65.99/.03/1/#2134, Anode:CU
Zero=0.0
CPS
7500
5000
2500
0
35
40
45
50
55
60
65
2-Theta
D=2.6336
D=2.5116
D=2.4422
D=2.2862
D=2.2465
D=2.1781
D=2.1311
D=2.0082
D=1.8217
D=1.6738
D=1.5373

Jade: Peak Listing — Thu Mar 24 1994 @11:09am

File: 4714POST.SAV> D:\OTHERUSE\BRIAN\4714POST.MDI: 4714 Post Bulk Back Pack

Scan Parameters:
Radiation = CU_1.540598
Scan Range = 2 - 65.99
Step Size = .03
Count Time = 1 sec.

Search Parameters:
Filter length(pts) = 9
Noise level(sigmas) = 3.5
Intensity cutoff(%) = .5-100
2-Theta Zero (degs) = 0

	Peak-Position		Centroid-Position		Peak & Area are without Bkgrd					
#	2Theta	d	2Theta	d	Bkgrd	Peak	I%	Area	I%	FWHM*
1:	8.782	10.0612	8.795	10.0462	72	4410	77.6	50176	78.5	0.307
2:	20.813	4.2645	20.833	4.2605	32	171	3.0	1697	2.7	0.268
3:	24.174	3.6787	24.196	3.6754	41	87	1.5	1090	1.7	0.338
4:	26.688	3.3375	26.676	3.3390	64	5684	100.0	63899	100.0	0.304
5:	28.313	3.1496	28.333	3.1474	63	183	3.2	2270	3.6	0.335
6:	30.648	2.9147	30.646	2.9149	39	187	3.3	2832	4.4	0.409
7:	33.053	2.7079	33.064	2.7070	40	98	1.7	1128	1.8	0.311
8:	34.160	2.6227	34.163	2.6224	38	181	3.2	2039	3.2	0.304
9:	35.839	2.5036	35.831	2.5041	34	524	9.2	5835	9.1	0.301
10:	36.833	2.4383	36.843	2.4376	30	165	2.9	2365	3.7	0.387
11:	39.412	2.2844	39.432	2.2833	25	53	0.9	815	1.3	0.415
12:	40.220	2.2404	40.223	2.2402	27	51	0.9	432	0.7	0.229
13:	41.540	2.1722	41.540	2.1722	26	147	2.6	1999	3.1	0.367
14:	42.470	2.1268	42.460	2.1273	23	55	1.0	486	0.8	0.239
15:	45.202	2.0043	45.216	2.0038	23	913	16.1	11340	17.7	0.335
16:	47.749	1.9032	47.731	1.9039	20	45	0.8	494	0.8	0.296
17:	50.151	1.8175	50.153	1.8175	19	165	2.9	1789	2.8	0.293
18:	54.920	1.6705	54.920	1.6705	22	506	8.9	7239	11.3	0.386
19:	60.172	1.5366	60.175	1.5365	27	283	5.0	4832	7.6	0.461
20:	63.081	1.4726	63.078	1.4726	26	41	0.7	541	0.8	0.356

* Intensity values are based on counts per second.

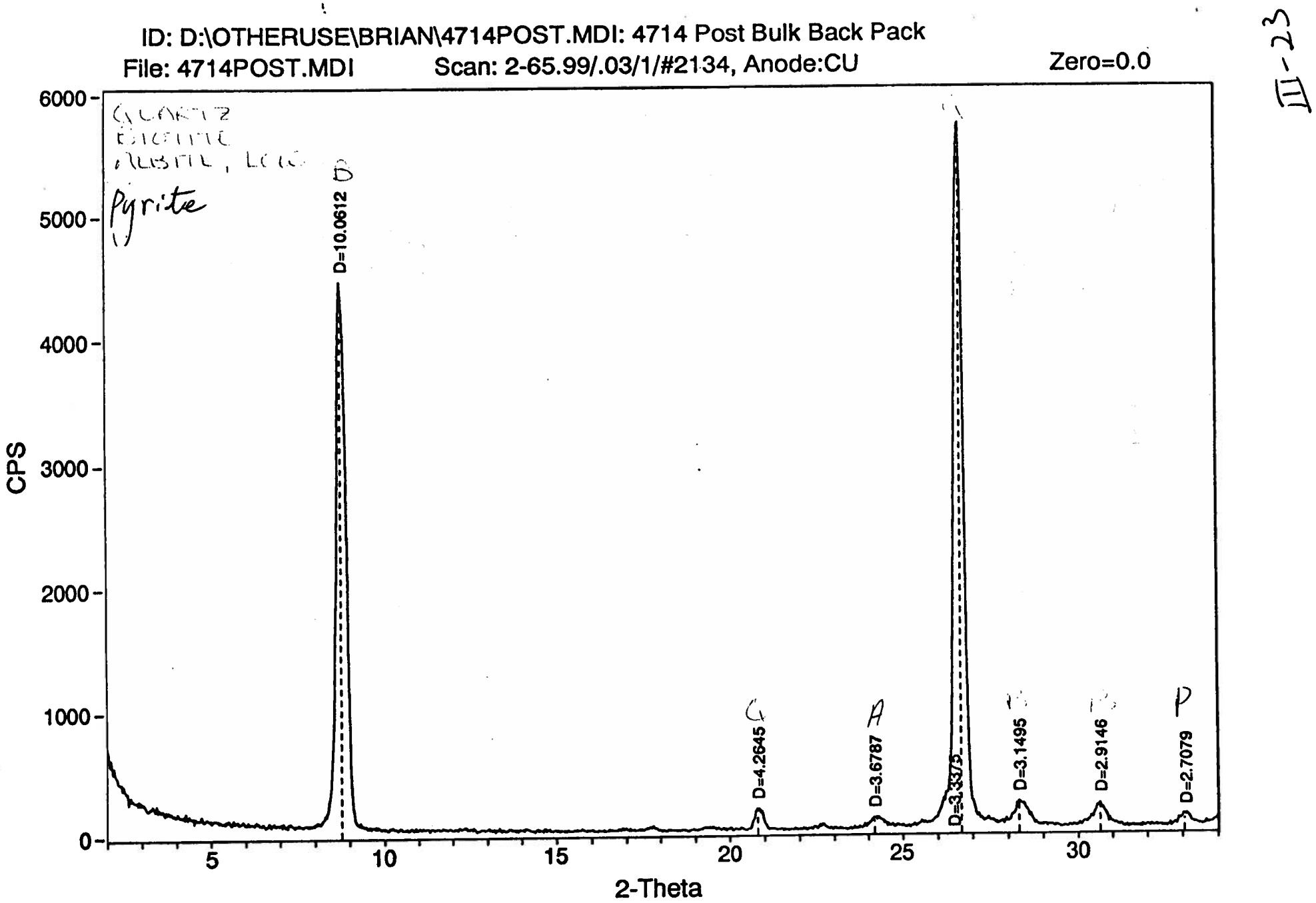
ID: D:\OTHERUSE\BRIAN\4714POST.MDI: 4714 Post Bulk Back Pack
File: 4714POST.MDI
Scan: 2-65.99/.03/1/#2134, Anode:CU
Zero=0.0
QUARTZ
BIOTITE
ALBITE, LOW
Pyrite
D=10.0612
D=4.2645
D=3.6787
D=3.3375
D=3.1495
D=2.9146
D=2.7079
CPS
2-Theta
6000
5000
4000
3000
2000
1000
0
5
10
15
20
25
30

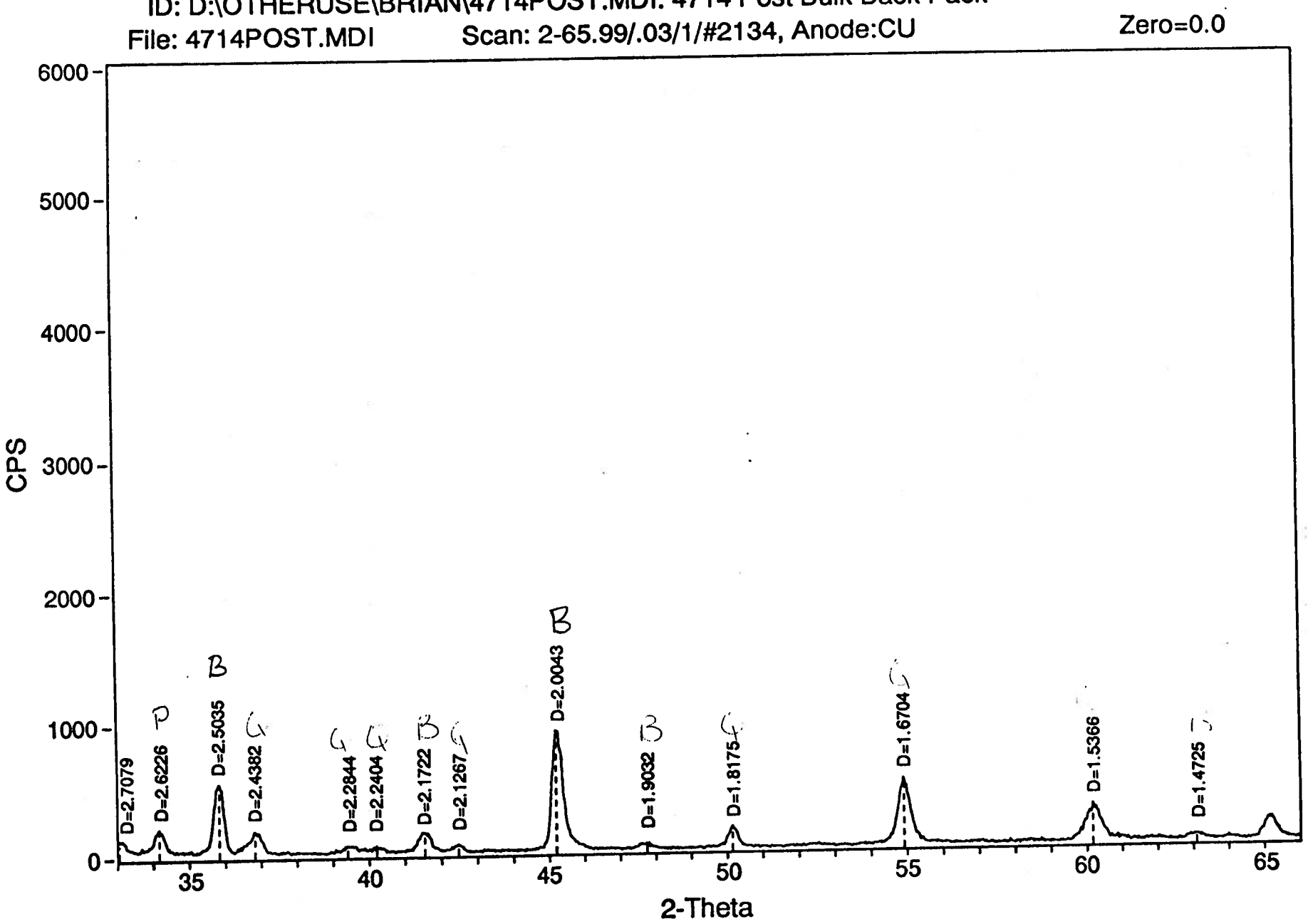
ID: D:\OTHERUSE\BRIAN\4714POST.MDI: 4714 Post Bulk Back Pack
File: 4714POST.MDI
Scan: 2-65.99/.03/1/#2134, Anode:CU
Zero=0.0
CPS
2-Theta
D=2.7079
D=2.6226
D=2.5035
D=2.4382
D=2.2844
D=2.2404
D=2.1722
D=2.1267
D=2.0043
D=1.9032
D=1.8175
D=1.6704
D=1.5366
D=1.4725

Jade: Peak Listing — Thu Mar 24 1994 @11:11am

File: DW931457.SAV> D:\OTHERUSE\BRIAN\DW931457.MDI: DW 93 - 1,4,5,7 Bulk Back Pack

Scan Parameters:		Search Parameters:
Radiation = CU_1.540598	||	Filter length(pts) = 9
Scan Range = 2 - 65.99	||	Noise level(sigmas) = 3.5
Step Size = .03	||	Intensity cutoff(%) = .5-100
Count Time = 1 sec.	||	2-Theta Zero (degs) = 0

	Peak-Position		Centroid-Position		Peak & Area are without Bkgrd					
#	2Theta	d	2Theta	d	Bkgrd	Peak	I%	Area	I%	FWHM*
1:	8.690	10.1675	8.688	10.1701	76	63	1.1	556	0.9	0.238
2:	12.347	7.1629	12.335	7.1698	44	75	1.3	738	1.1	0.266
3:	19.758	4.4899	19.759	4.4896	34	97	1.6	1563	2.4	0.435
4:	20.781	4.2709	20.790	4.2691	36	1122	18.9	12208	19.0	0.294
5:	24.830	3.5830	24.831	3.5828	65	60	1.0	510	0.8	0.229
6:	26.571	3.3519	26.578	3.3511	58	5929	100.0	64403	100.0	0.293
7:	31.997	2.7949	31.981	2.7962	37	55	0.9	622	1.0	0.305
8:	34.852	2.5722	34.849	2.5724	39	114	1.9	2032	3.2	0.481
9:	36.529	2.4578	36.521	2.4583	45	697	11.8	7592	11.8	0.294
10:	39.411	2.2845	39.418	2.2841	39	433	7.3	4249	6.6	0.265
11:	40.222	2.2403	40.230	2.2399	38	221	3.7	2498	3.9	0.305
12:	42.436	2.1284	42.419	2.1292	34	393	6.6	4724	7.3	0.325
13:	45.741	1.9820	45.739	1.9821	28	256	4.3	3177	4.9	0.335
14:	50.091	1.8196	50.090	1.8196	25	734	12.4	9083	14.1	0.334
15:	54.803	1.6737	54.816	1.6734	33	258	4.4	3516	5.5	0.368
16:	59.929	1.5423	59.924	1.5424	32	482	8.1	6458	10.0	0.362
17:	64.009	1.4534	64.008	1.4535	28	101	1.7	1205	1.9	0.322

* Intensity values are based on counts per second.

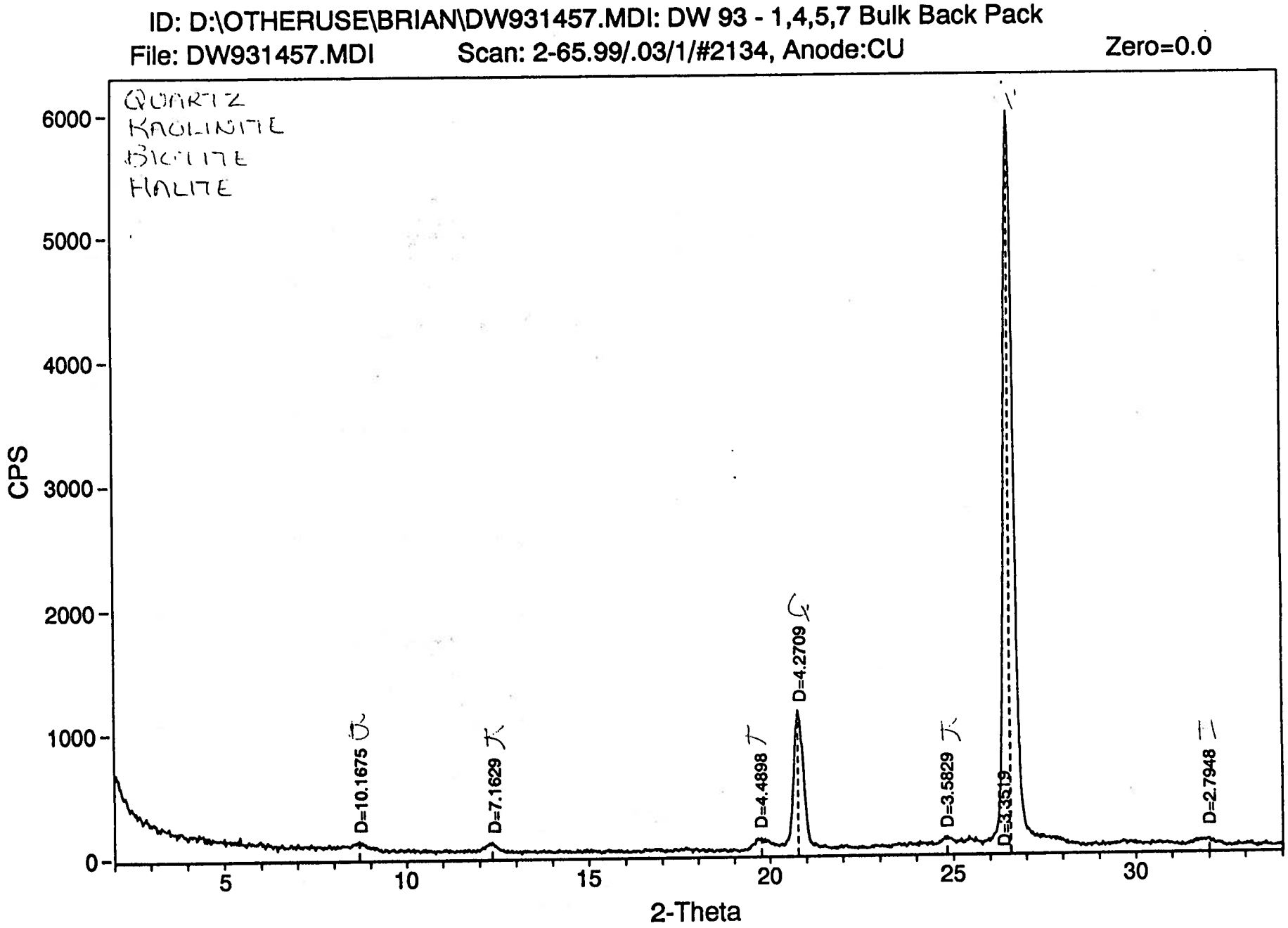
ID: D:\OTHERUSE\BRIAN\DW931457.MDI: DW 93 - 1,4,5,7 Bulk Back Pack
File: DW931457.MDI
Scan: 2-65.99/.03/1/#2134, Anode:CU
Zero=0.0
QUARTZ
KAOLINITE
BIOTITE
HALITE
CPS
2-Theta
D=10.1675
D=7.1629
D=4.4898
D=4.2709
D=3.5829
D=3.3519
D=2.7948

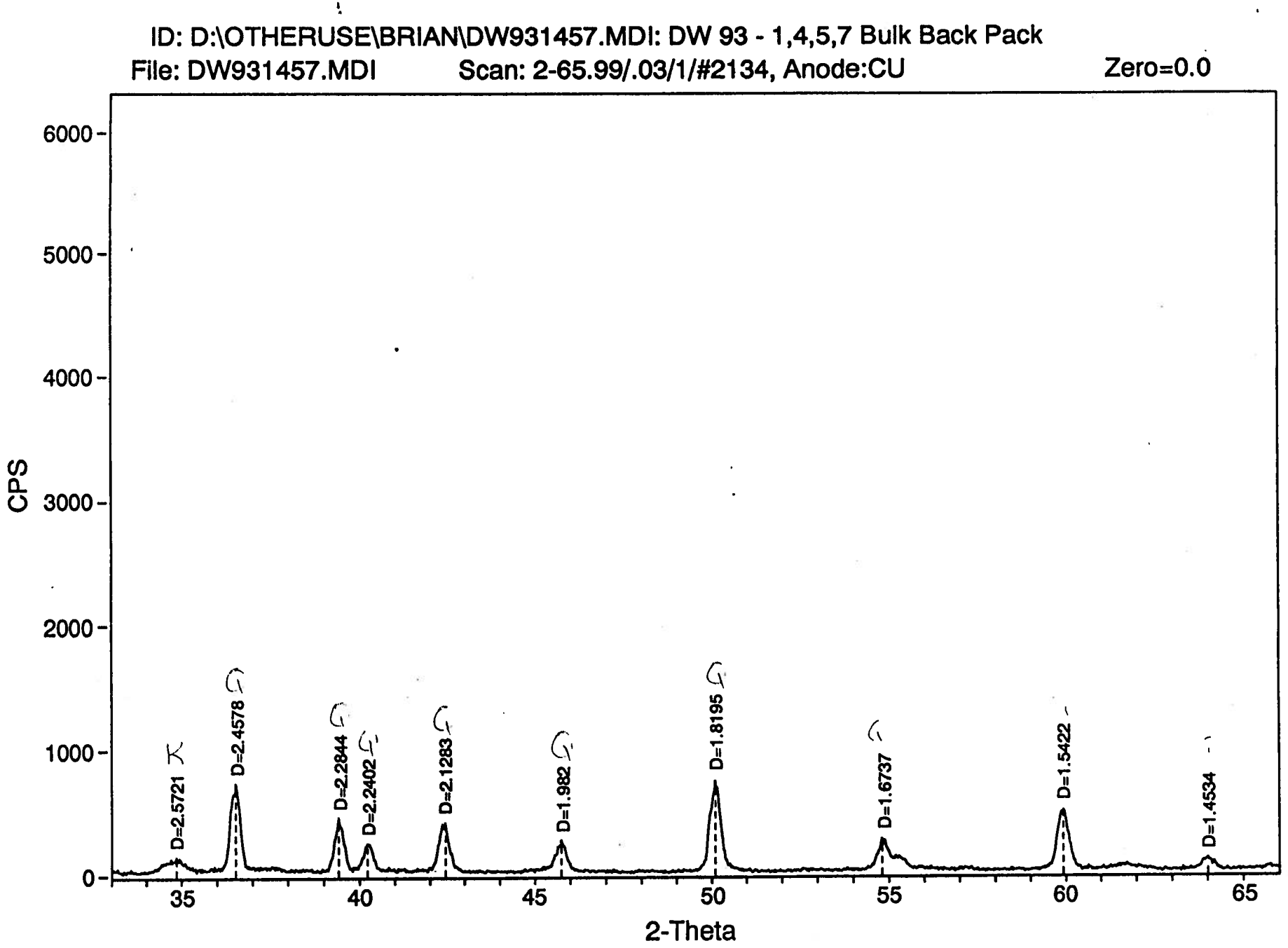
ID: D:\OTHERUSE\BRIAN\DW931457.MDI: DW 93 - 1,4,5,7 Bulk Back Pack
File: DW931457.MDI
Scan: 2-65.99/.03/1/#2134, Anode:CU
Zero=0.0
CPS
6000
5000
4000
3000
2000
1000
0
D=2.5721
D=2.4578
D=2.2844
D=2.2402
D=2.1283
D=1.982
D=1.8195
D=1.6737
D=1.5422
D=1.4534
35
40
45
50
55
60
65
2-Theta

APPENDIX IV

Rate Law Derivation

REACTION KINETICS APPROACH

Mass Action Rate Law:

Premise (Based on the theory of elementary reactions): Assume reaction rate, R, is proportional to the "concentration" of the reactants raised to the power of their stoichiometry.

Empirical Rules for Formulating Reaction

1. For silicates form of rate law varys over three pH regions: acid, neutral and basic. In these cases express the rate law as the sum of three different reactions if sufficient data exists. Otherwise use the form of the reaction for the pH range of the data

2. Always configure a reaction so that hydronium or hydroxyl power is zero or unity. This is based on experiment where power ranges between 0 and 2.

3. Always write as a hydration reaction.

4. Split the reaction into forward (+) and backward (-) rates and write the rate law for R_+ and R_- using the rate constants k_+ (= dissolution rate constant) and k_- (= precipitation rate constant).

5. The concentration of the mineral is expressed as surface area, A, and is assumed to contribute equally to the forward and backward reactions.

6. Sum R_+ and R_- for each reaction to get total rate, R, for each reaction.

7. Use the relation that: $K_{eq} = k_+/k_-$ to get rid of one of the rate constants in the total rate equation

8. Collect terms so that activities of ions can be replaced by the saturation state or Ω where

$$\Omega = IAP/K_{eq}$$

9. Final rate equation for a silicate reaction should only involve Ω, surface area, the proton, hydroxide ion or activity of water, and the rate constant. Note in the case of carbonates CO_2 also becomes important.

10. The total rate law for the dissolution, precipitation of a mineral is just the sum of the rate laws for each "elementary" reaction.

Example 1 (R for a single "elementary" Silicate reaction)

K-feldspar in the acid region:

$$\text{K-feldspar} + H^+ + H_2O = K^+ + Al(OH)_3 + 3SiO_2$$

Forward Reaction Rate $R_+ = k_+A[H^+][H_2O] = k_+A[H^+]$

note: $[H_2O]$ is 1 and is usually dropped.

Backward Reaction Rate $R_- = k_-A[K^+][Al(OH)_3][SiO_2]^3$

Net Reaction Rate $R = R_+ - R_- = A(k_+[H^+]-k_-[K^+][Al(OH)_3][SiO_2]^3)$

multiply by $(k_+[H^+]/k_+[H^+])$ $R = k_+[H^+]A(1-[K^+][Al(OH)_3][SiO_2]^3/[H^+]K_{eq})$

substituting for $[K^+][Al(OH)_3][SiO_2]^3/[H^+] = IAP$

$R = k_+[H^+]A(1-\Omega)$

The form of this equation is easily generalized to the left side of the dissolution reaction. All the aqueous ions on the left side of the reaction will appear to their stoichiometric power in the rate equation. All the ions on the right side of the reaction will dissapear into the Ω term. Consequently the rate law can easily be written from a quick inspection of the reaction equation.

Example 2 (R for three "elementary" carbonate reactions)

1. $\text{Calcite} = Ca^{++} + CO_3^{=}$
2. $\text{Calcite} + H^+ = Ca^{++} + HCO_3^-$
3. $\text{Calcite} + H_2CO_3 = Ca^{++} + 2\ HCO_3^-$

$R_{1+} = Ak_{1+}$

$R_{2+} = Ak_{2+}[H^+]$

$R_{3+} = Ak_{3+}[H_2CO_3]$

$R_+ = R_{1+} + R_{2+} + R_{3+} = A(k_{1+} + k_{2+}[H^+) + k_{3+}[H_2CO_3])$

This is Plummers rate equation for high undersaturation (i.e. far from equilibrium where the back reaction is not important).

The total rate of any one of the three reactions, can be simply written by inspection - as for example:

$R_2 = Ak_{2+}[H^+](1-\Omega)$

The value of K_{eq} depends on both the reaction stoichiometry and the aqueous species chosen to formulate the dissolution reaction. However Ω is a ratio and is not as sensitive. Ω for a mineral phase of fixed stoichiometry, depends on the reaction stoichiometry (i.e if the reaction is multiplied by any factor, Ω will change). Ω does not depend on the aqueous species used to form the reaction because the species are all related through homogeneous equilibria. That is Ω is an identical value at any instance in time for all three reactions providing the reaction is written involving only one molecule of the mineral phase.

Therefore the total rate for calcite dissolution/precipitation can simply be written as the sum of the rates of all three reactions:

$R = R_1 + R_2 + R_3 = A(k_{1+} + k_{2+}[H^+) + k_{3+}[H_2CO_3])(1-\Omega)$

Relating the rate constant to the aqueous solution where it dominates, the rate equation becomes:

$R = R_{neutral} + R_{acid} + R_{CarbonDioxide} = A(k_{n+} + k_{a+}[H^+) + k_{CD+}[H_2CO_3])(1-\Omega)$

where n=neutral, a=acid and CD = CO_2

Example 3 (Form of R for acid/neutral/base silicate reactions)

Three forms of the rate law are used for silicate reactions in the absence of detailed information.

$R_{acid} = k_{a+}[H^+]A(1-\Omega)$

$R_{neutral} = k_{n+}A(1-\Omega)$

$R_{base} = k_{b+}[OH^-]A(1-\Omega)$

$R = R_{acid} + R_{neutral} + R_{base} = (k_{a+}[H^+] + k_{n+} + k_{b+}[OH^-])A(1-\Omega)$

The paucity of rate constants hampers using the correct rate equation for the conditions of interest. The most common dissolution experimental data is interpreted as being fit to a rate equation of zero order or, $R_{neutral}$, where the rate is constant far from equilibium (i.e. Ω is << 0) by the above approach. Fortunately because Ω is independent of the aqueous s[ecies used to formulate the reaction, it doesn't matter what set of species we use to calculate Ω. We only have to deal with one dissolution reaction per mineral. Consequently the following approach may be used: Ω is calculated using a reaction involving the bare ions. A table may be built up giving the stoichiometry of the bare ions dissolution reaction for the mineral, the equilibrium constant - K_{eq}, and the rate constants - k_a, k_n, k_b, k_{CD}, etc. The dissolution reaction is used to keep track of the mass balance between the ions transferred by the breakdown of the mineral and vica versa. The rate law is used to keep track of the velocity with which it occurs.

Rate Constants:

The rate constant, k, is given in a number of different units and is dependent on the units of the rate, R. For the way the rate laws are formulated here, R is in moles per m^2 per second. To change to cm^2, divide by 10,000; to change to hours, multiply by 3600; to change to days, multiply by 86,400; to change to years, multiply by 31,557,600.

Arrhenius Equation for Temperature Variation of the Rate Constants:

$k = Ae^{-E/RT}$

where A is the pre-exponential factor (not to be confused with surface area) and E is the activation energy. A and E are normally assumed to be independent of temperature.

If this is true then the Arrhenius equation can be reduced to the form:

$\log(k) = B + C/T$

where B = A & C = E/2.303R

and a plot of log(k) vs 1/T will be a straight line.

Additional terms may be added to get a better fit. For example in Helgeson et al., 1984:

$$\log(k) = B + C/T + D.\log(T)$$

APPENDIX V

Rate Constants

Table A. Rate Constants at 25°C (unless noted) for a Variety of Minerals

Mineral	Reference	25°C $\log (k_{H+})\ a_{H+}^{x}$	25°C $\log (k_{n+})$	25°C $\log (k_{CO2+})\ P_{CO_2}^{z}$	25°C $\log (k_{OH+})\ a_{OH^-}^{z}$
K-Feldspar	Sverdrup, 1990	-9.5, x=0.5	-12.3	-11.6, z=0.6	-11.2, y=0.3
	Helgeson et al., 1984	-8.66, $x=^{1.0}$	-11.52		
	Busenberg & Clemency, 1976		-12.3		
Albite	Sverdrup, 1990	-9.5, x=0.5	-11.8	-10.6to-11.5, z=0.6	-9.9, y=0.3
	Helgeson et al., 1984	-8.73, x=1.0	-11.5	---	-14.6, y=-0.4
	Chou & Wallest, 1985		-11.8		
	Holdren & Berner, 1979		-11.4		
	Knauss & Wollery, 1986		-12.4		
Labradorite	Sverdrup, 1990	-8.75, x=0.5	-11.7	< -11.6, z=0.6	-
Anorthite	Sverdrup, 1990	-5.8, x=1.0	-11.9	-11.6	-9.7, y=0.3
	Fleer, 1982		-8.6		
Quartz	Sverdrup, 1990	-9.7, x=0.33	-11.6	---	-8.8, y=0.3
	Rimstidt & Barnes, 1980		-13.4		
	Knauss & Wollery, 1988		-13.4		
Gibbsite	Sverdrup, 1990	-7.5, x=1.0	-11.5	---	-7.2, y=0.6
	Nagy & Lasaga, 1992		-9.34 @ 80°C		

K
1-

Mineral	Reference	25°C log $(k_{H+})\ a_{H+}^{x}$	25°C log (k_{n+})	25°C log $(k_{CO2+})\ P_{CO_2}^{z}$	25°C log $(k_{OH+})\ a_{OH^-}^{z}$
Biotite	Sverdrup, 1990	-9.3, x=0.6	< -12.3	< -11.7	---
	Acker & Bricker, 1992	x=-0.34	-11.4		
Muscovite	Sverdrup, 1990	-9.7, x=0.6	<-13.2	-11.6	-10.7, y=0.3
	Knauss & Wollery, 1989	-10.7, x=-0.37 @ 70°C	-12.6 @ 70°C		-14.1, y=0.22 @ 70°C
	Lin & Clemency, 1981		-13.06		
Chlorite	Sverdrup, 1990	-7.7, x=0.7	< -11.6	---	---
Glauconite	Sverdrup, 1990	-4.8, x=0.7	---	---	---
Kaolinite	Sverdrup, 1990	-8.4, x=0.7	-12.5	---	---
	Carroll & Walther, 1990		-13.0		
	Naggy et al., 1990		-11.9 @ 80°C		
Calcite	Chou, Garrels & Wollast, 1989	-0.05, x=1.0	-6.19	-3.30, z=1.0	
	Plummeg, Wigley & Parkhurst, 1978	-0.29, x=1.0	-5.93	-3.46, z=1.0	
Dolomite	Chou, Garrels & Wollast, 1989	-2.59, x=0.75	7.66	-4.00, z=0.75	
(Sedimentary)	Busenberg & Plummer, 1982	-3.19, x=0.5	-7.53	-5.11, z=0.5	
(Hydrothermal)	Busenberg & Plummer, 1982	-3.76, x=0.5	-8.61	-5.36, z=0.5	
Magnesite	Chou, Garrels & Wollast, 1989	-4.60, x=1.0	-9.35	-5.22, z=1.0	

Table B. Rate Constants at 54°C for a Variety of Minerals

Minerals	Reference	54°C $\log (k_{H+}) a_{H^+}^{x}$	54°C $\log (k_{n+})$	54°C $\log (k_{CO2+}) P_{CO_2}^{z}$	54°C $\log (k_{OH-}) a_{OH^-}^{y}$
K-Feldspar	Sverdrup, 1990	-8.47	-11.76		
	Helgeson et al., 1984	-7.38, x=1.0	-10.93		
	Busenberg & Clemency, 1976				
Albite	Sverdrup, 1990	-8.50	-11.01	-10.51	-8.98
	Helgeson et al., 1984	-7.35, x=1.0			
	Chou & Wollast, 1985				
	Holdren & Berner, 1979				
	Knauss & Wollery, 1986				
Labradorite	Sverdrup, 1990				
Anorthite	Sverdrup, 1990	-5.26	-11.04		
	Fleer, 1982		-10.24		
Quartz	Sverdrup, 1990	-8.54			-7.84
	Rimstidt & Barnes, 1980		-12.20		
	Knauss & Wollery, 1988		-11.99		
Gibbsite	Sverdrup, 1990	-6.57	-10.44		-6.55

Minerals	Reference	54°C $\log (k_{H+}) a^{x}_{H^+}$	54°C $\log (k_{n+})$	54°C $\log (k_{CO2,+}) P^{z}_{CO_2}$	54°C $\log (k_{OH-}) a^{y}_{OH^-}$
Biotite	Sverdrup, 1990		< - 11.16		
	Acker & Bricker/Fleer		-10.49		
Muscovite	Sverdrup, 1990				
	Knauss & Wollery, 1989				
	Lin & Clemency, 1981				
Chlorite	Sverdrup, 1990	-6.36			
Glauconite	Sverdrup, 1990	-3.52			
Kaolinite	Sverdrup, 1990	-7.85	-11.42		
	Carroll & Walther, 1990				
	Nagy et al., 1990				
Calcite	Chou et al., 1989				
	Plummer et al, 1978	-0.16	-5.83	-2.82	
Dolomite	Chou et al., 1989				
(Sedimentary)	Busenburg & Plummer, 1982	-2.63	-6.73	-4.57	
(Hydrothermal)	Busenburg & Plummer, 1982	-2.88	-7.13	-4.67	
Magnesite	Chou et al, 1989				

Table C. Rate Constants at 105°C for a Variety of Minerals

Mineral	Reference	105° C $\log (k_{H+}) a^{x}_{H^+}$	105° C $\log (k_{n+})$	105° C $\log (k_{CO2+}) P^{z}_{CO_2}$	105° C $\log (k_{OH-}) a^{y}_{OH^-}$
K-Feldspar	Sverdrup, 1990	-7.05	-11.00		
	Helgeson et al., 1984	-5.61, x=1.0	-10.11		
	Busenburg &Clem.,1976				
Albite	Sverdrup, 1990	-7.11	-9.92	-9.81	-7.70
	Helgeson et al., 1984	-5.43, x=1.0			
	Chou & Wollast, 1985				
	Holdren & Berner, 1979				
	Knauss & Wollery, 1986				
Labradorite	Sverdrup, 1990				
Anorthite	Sverdrup, 1990		-9.86		
	Fleer, 1982	-4.50	-7.93		
Quartz	Sverdrup, 1990	-6.94			-6.51
	Rimstidt & Barnes, 1980		-10.59		
	Knauss & Wollery, 1988		-10.02		
Gibbsite	Sverdrup, 1990	-5.28	8.98		-5.64

Mineral	Reference	105° C $\log (k_{H+}) a_{H^+}^{x}$	105° C $\log (k_{n+})$	105° C $\log (k_{CO2+}) P_{CO_2}^{z}$	105° C $\log (k_{OH+}) a_{OH^-}^{y}$
Biotite	Sverdrup, 1990		< -8.58		
	Acker & Bricker/Fleer		-9.23		
Muscovite	Sverdrup, 1990				
	Knauss & Wollery, 1989				
	Lin & Clemency, 1981				
Chlorite	Sverdrup, 1990	-4.49			
Glauconite	Sverdrup, 1990	-1.75			
Kaolinite	Sverdrup, 1990	-5.69	-9.94		
	Carroll & Walther, 1990				
	Nagy et al., 1990				
Calcite	Chou et al., 1989				
	Plummer et al.,1989	+0.02	-5.70	-1.92	
Dolomite	Chou et al., 1989				
	Busenburg&Plum., 1982	-1.85	-5.61	-3.83	
	Busenburg&Plum., 1982	-1.66	-5.08	-3.69	
Magnesite	Chou et al., 1989				

Table D. Equations for Temperature Variation of Rate Constants of Minerals

Mineral	Reference	$\log (k_{H^+})a^{x}_{H^+}$	$\log (k_{n+})$	$\log (k_{CO2+})P^{z}_{CO_2}$	$\log (k_{OH^+})a^{y}_{OH^-}$
K-Feldspar	Sverdrup, 1990	2.067 - 3447/T	-6.166 - 1828/T		
	Helgeson et al., 1984	2.8 - 4152/T + logT x=1	-7.8 - 1847/T + log T		
	Busenberg & Clemency, 1976				
Albite	Sverdrup, 1990	1.769 - 3358/T	-2.914 - 2648/T	-5.374 - 1676/T	0.493 - 3097/T
	Helgeson et al., 1984	3.9 - 4502/T + logT x=1			
	Chou & Wollast, 1985				
	Holdren & Berner, 1979				
Labradorite	Sverdrup, 1990				
Anorthite	Sverdrup, 1990	0.334 - 1828/T	-6.853 - 5588/T		
	Fleer, 1982		*-2.261 - 2872/T		
Quartz	Sverdrup, 1990	3.339 - 3886/T			2.031 - 3228/T
	Rimstidt & Barnes, 1980		1.174 - 4158/T - 0.002028 T		
	Knauss & Wollery, 1988		2.583 - 4764/T		
Gibbsite	Sverdrup, 1990	3.016 - 3134/T	0.418 - 3551/T		0.161 - 2194/T
Biotite	Sverdrup, 1990		0.546 - 3828/T		
	Acker & Bricker/Fleer		-1.135 - 3059/T (Ea from Fleer)		